

***INSTITUTO TECNOLÓGICO DE AERONÁUTICA***



Fernanda Muzzio Almirão

Friction characterization of geosynthetic interfaces through  
inclined plane experiment

*Trabalho de Graduação*  
2009

***Civil***

FERNANDA MUZZIO ALMIRÃO

**Friction characterization of geosynthetic interfaces  
through inclined plane experiment**

Orientador  
Prof<sup>a</sup>. Dr. Delma Vidal (ITA)

**DIVISÃO DE ENGENHARIA CIVIL**

SÃO JOSÉ DOS CAMPOS  
COMANDO-GERAL DE TECNOLOGIA AEROESPACIAL  
INSTITUTO TECNOLÓGICO DE AERONÁUTICA

2009

**Dados Internacionais de Catalogação-na-Publicação (CIP)**  
**Divisão de Informação e Documentação**

Almirão, Fernanda Muzzio

Friction characterization of geosynthetic interfaces through inclined plane experiment / Fernanda Muzzio Almirão.

São José dos Campos, 2009.

171f.

Trabalho de Graduação – Divisão de Engenharia Civil – Instituto Tecnológico de Aeronáutica, 2009.  
Orientador: Prof. Dr. Delma Vidal.

1. Coeficientes de atrito. 2. Geossintéticos. 3. Revestimento. 4. Talude. I. Comando-Geral de Tecnologia Aeroespacial. Instituto Tecnológico de Aeronáutica. Divisão de Engenharia Civil. II. Friction characterization of geosynthetic interfaces through inclined plane experiment

**REFERÊNCIA BIBLIOGRÁFICA**

ALMIRÃO, Fernanda Muzzio. **Friction characterization of geosynthetic interfaces through inclined plane experiment**, 2009. 171f. Trabalho de Conclusão de Curso. (Graduação) – Instituto Tecnológico de Aeronáutica, São José dos Campos.

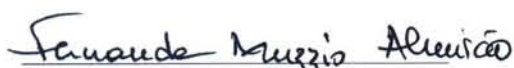
**CESSÃO DE DIREITOS**

NOME DOS AUTORES: Fernanda Muzzio Almirão

TÍTULO DO TRABALHO: Friction characterization of geosynthetic interfaces through inclined plane experiment

TIPO DO TRABALHO/ANO: Graduação / 2009

É concedida ao Instituto Tecnológico de Aeronáutica permissão para reproduzir cópias deste trabalho de graduação e para emprestar ou vender cópias somente para propósitos acadêmicos e científicos. O autor reserva outros direitos de publicação e nenhuma parte desta monografia de graduação pode ser reproduzida sem a autorização do autor.



Fernanda Muzzio Almirão

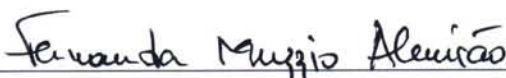
R. H8A, 106

CTA – São José dos Campos – SP

12228-460

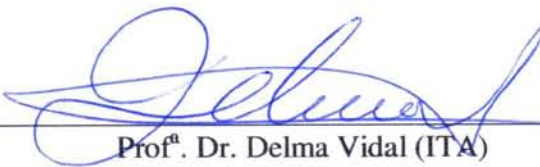
**FRICTION CHARACTERIZATION OF GEOSYNTHETIC INTERFACES THROUGH  
INCLINED PLANE EXPERIMENT**

Essa publicação foi aceita como Relatório Final de Trabalho de Graduação



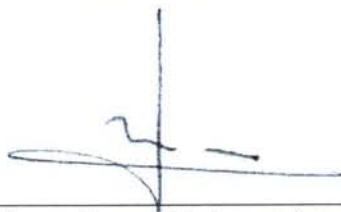
---

Fernanda Muzzio Almirão  
Autora



---

Prof. Dr. Delma Vidal (ITA)  
Orientadora



---

Prof. Dr. Jean-Pierre Gourc (Université Joseph Fourier)  
Co-orientador



---

Prof. Dr. Eliseu Lucena Neto  
Coordenador do Curso de Engenharia Civil

São José dos Campos, 20 de novembro de 2009

To my friend, Carina Furusho,  
who offered me one of the greatest opportunities  
of my life: the internship at MIT

*Fernanda Muzzio Almirão*

## ACKNOWLEDGEMENTS

Many people deserve thanks for making my undergraduate experience at ITA so wonderful:

My advisor, Prof. Delma Vidal, for her reliable guidance and clarification of important issues encountered during this work.

My co-adviser, Prof. Jean-Pierre Gourc, who promptly accepted my internship at LTHE, guided my research and was really patient with my French abilities.

Dr. Laurent Briançon, who has taught me a lot about the inclined plane experiment.

The Fundação Estudar, for funding my internship abroad.

My professors from ITA, for helping a sometimes clueless student to survive at graduate school.

My counselor professor, for being present since the beginning of ITA.

The Thor Experience, for presenting me a new perspective in life.

André Okamoto, for inspiring me even during the toughest moments.

My roommates, for supporting and encouraging me throughout my five years at ITA.

My co-workers at LTHE, for teaching me French and helping me to adapt to life abroad.

My friends, for making me smile all the time.

My brother and sisters, who have become my best friends in life.

My step father, who always believed in my aspirations, and have always given me the best examples.

My father, who saved me during the hardest weeks at ITA, sweetening my life with candies and cakes.

And finally, my Mother, who supported and listened to all my complaints and difficulties, never letting me give it up and always illuminating my heart and mind.

You all inspired me more than you know.

“I have a dream, a fantasy  
To help me through reality  
And my destination  
makes it worth the while  
Pushing through the darkness  
still another mile”

*Lisa Stokke, I Have a Dream*

## Resumo

A pesquisa tem como objetivo comparar resultados obtidos através de ensaios realizados com dois dispositivos de plano inclinado. O primeiro plano testado foi dimensionado de acordo com a ISO12957-2:2005 e, além da análise prevista pela norma, foram realizadas a análise de força e a análise conjunta. Na análise de força, é medido o esforço necessário para segurar a caixa superior durante a inclinação do plano. Já a análise conjunta é uma junção da tomada de valores do deslocamento da caixa superior seguida pela análise de força. O segundo plano a ser utilizado possui dimensões inferiores às prescritas em norma, porém viabiliza a análise do comportamento dinâmico das interfaces. Os parâmetros obtidos neste ensaio são os ângulos de atrito estático ( $\Phi_0$  e  $\Phi_{50}$ ) e o ângulo de atrito dinâmico ( $\Phi^{\text{lim}}$ ). O foco do trabalho é verificar se ambos os planos fornecem parâmetros equivalentes para caracterizar as interfaces geossintético-geossintético.

## **Abstract**

The purpose of this research is to compare the test results found with two inclined plane apparatus. The first plane tested was developed according to ISO12957-2: 2005 and, besides the analysis prescribed by this standard, it was performed the force and combined analyses. In force analysis, it is measured the force required to hold the upper box during the inclination of the plane. The combined analysis includes both standard and force analysis. The second plane to be tested has smaller dimensions than the ones prescribed by the standard however it enables the study of the dynamic behavior of interfaces. The parameters obtained in this test are the static friction angles ( $\Phi_0$  and  $\Phi_{50}$ ) and the dynamic friction angle ( $\Phi^{\text{lim}}$ ). The focus of the work is to evaluate whether both planes provide equivalent parameters to characterize the geosynthetic-geosynthetic interfaces.

## TABLE OF FIGURES

Figure 2.1 – Bandeirantes landfill, Sao Paulo, Brazil (brasil-virtual.net) .....	23
Figure 2.2 – Construction of landfill in Itaquaquecetuba, Sao Paulo, Brazil (brasil-virtual.net).....	23
Figure 2.3 – Solid waste containment system with high geosynthetic utilization (Koerner, 1997).....	24
Figure 2.4 - Winneshiek Co. Landfill Commission, Decorah. Cap cover construction stage of a landfill construction. (www.jbholland.net).....	25
Figure 2.5 – Geosynthetic liner installation of a landfill construction. (www.cpengeers.com).....	25
Figure 2.6 – Geosynthetic liner of a landfill construction. (www.cpengeers.com).....	25
Figure 2.7 – Single clay liner (Koerner, 1997).....	26
Figure 2.8 - Single geomembrane liner (Koerner, 1997) .....	26
Figure 2.9 – Double-composite liner (with geosynthetic clay liner) and geonet (Koerner, 1997).....	27
Figure 2.10 – Double-composite liner (with geosynthetic clay liner), geonet and geocomposite (Koerner, 1997) .....	27
Figure 2.11 – Image of the region where the slide occurred (REYES RAMIREZ ET AL., 2003).....	29
Figure 2.12 – Sketch of the rupture, lateral view of the slope.....	29
Figure 3.1 – Different mechanisms of slides: (a) sudden sliding; (b) jerky sliding; (c) gradual sliding	33
Figure 3.2 – Pictures of GLS being installed (KOERNER, 1997).....	36
Figure 3.3 – Pictures of GLS being installed (KOERNER, 1997).....	37
Figure 3.4 – Example of wind-damaged geomembrane (KOERNER, 1997) .....	37
Figure 3.5 – Example of wind-damaged geomembrane (KOERNER, 1997) .....	37
Figure 4.1 - Large dimension inclined plane.....	40
Figure 4.2 - Sketch of the large dimension inclined plane.....	41
Figure 4.3 – Upper box dispositive.....	41
Figure 4.4 - Load transfer toward guides and geosynthetics.....	42
Figure 4.5 - Geosynthetic attachment disposal .....	42
Figure 4.6 – Configuration examples for each case of analysis.....	44
Figure 4.7 – Sketch of the combined analysis mechanism.....	44
Figure 4.8 - Free body diagram for standard procedure.....	45
Figure 4.9 - Balance of efforts for force analysis.....	46
Figure 4.10 – Determination of the linear function $f_r(\beta)$ .....	47
Figure 4.11 – Small dimension inclined plane .....	48
Figure 4.12 - Sketch of the small dimension inclined plane .....	49
Figure 4.13 – Mobile plate dispositive of the small inclined plane.....	49
Figure 4.14 - Load transfer to geosynthetics .....	50
Figure 4.15 – Body diagram for small dimension apparatus.....	51
Figure 4.16 – Configuration examples for the guidance system.....	53
Figure 4.17 – Mobile plate on configuration type $\beta$ .....	54
Figure 4.18 – Mobile plate on configuration type $\gamma$ .....	54
Figure 4.19 – Geotextiles used for trials. ....	55
Figure 4.20 - Geomembranes used for trials. ....	55
Figure 4.21 – Model of identification of performed tests .....	57
Figure 4.22 - Inclined plane test result A 17-I. Interface tested: HB x PVC.....	60
Figure 4.23 – Inclined plane test result A 17-I. Interface tested: HB x PVC.....	61
Figure 4.24 - Inclined plane test result B 73-III (combined analysis procedure). Interface tested: HB-PVC.....	62
Figure 4.25 - Inclined plane test result B 73-III (combined analysis procedure). Interface tested: HB-PVC.....	63
Figure 4.26 - Inclined plane test result B 44-I (force analysis procedure). Interface tested: PVC-PVC.....	63
Figure 5.1 – Curve Displacement vs. Inclination of interface Rnnp-PVC, series A6, guidance systems $\alpha$ , tested with the small dimension inclined plane.....	65
Figure 5.2 – Curve Displacement vs. Inclination of interface Rnnp-PVC, series B40, B41 and B43, tested with the standard dimension inclined plane.....	67

Figure 5.3 – Curve Lambda vs. Inclination of interface Rnnp-PVC, series B40 and B41, tested with the standardized dimension inclined plane. ....	67
Figure 5.4 – Curve Lambda vs. Inclination of interface Rnnp-PVC, series B43, tested with the standard dimension inclined plane. ....	68
Figure 5.5– Curve Displacement vs. Inclination of interface HB-PVC, series A8, A9, A17 and A29, tested with the small dimension inclined plane.....	71
Figure 5.6 – Curve Lambda vs. Inclination of interface HB-PVC, series B73, tested with the standardized inclined plane. ....	72
Figure 5.7 – Curve Displacement vs. Inclination of interface HB-PVC, series B73, tested with the standardized inclined plane. ....	72
Figure 5.8 – Curve Displacement vs. Inclination of interface nnp40-PVC, series A13, tested with the small dimension inclined plane. ....	73
Figure 5.9 – Curve Lambda vs. Inclination of interface nnp40-PVC, series B74, tested with the standardized dimension inclined plane. ....	75
Figure 5.10 – Curve Displacement vs. Inclination of interface nnp40-PVC, series B74, tested with the standardized dimension inclined plane. ....	75
Figure 5.11 – Curve Displacement vs. Inclination of interface nnp40-PVC, series A13, tested with the standardized dimension inclined plane. ....	76
Figure 5.12 – Curve Displacement vs. Inclination of interface nnp40-PVC, series B74, tested with the standardized dimension inclined plane. ....	77
Figure 5.13 – Curve Displacement vs. Inclination of interface Rnnp-PP, series A32, tested with the small dimension inclined plane.....	78
Figure 5.14 – Curve Lambda vs. Inclination of interface Rnnp-PP, series B80, tested with the standardized dimension inclined plane. ....	79
Figure 5.15 – Curve Displacement vs. Inclination of interface Rnnp-PP, series B80, tested with the standardized dimension inclined plane. ....	79
Figure 5.16 – Curve Displacement vs. Inclination of interface nnpC-PP, series A25 & 26, tested with the small dimension inclined plane. ....	80
Figure 5.17 – Curve Displacement vs. Inclination of interface nnpC-PP, series B82, tested with the standardized dimension inclined plane. ....	81
Figure 5.18 – Curve Lambda vs. Inclination of interface nnpC-PP, series B82, tested with the standardized dimension inclined plane. ....	82
Figure 5.19 - Curve Displacement vs. Inclination of interface Rnnp-HDPE, series A31, tested with small dimension inclined plane. ....	83
Figure 5.20 - Curve Displacement vs. Inclination of interface Rnnp-HDPE, series B45, tested with the standardized dimension inclined plane. ....	84
Figure 5.21 – Curve Displacement vs. Inclination of interface HB-HDPE, series A21, tested with the small dimension inclined plane.....	85
Figure 5.22 – Curve Displacement vs. Inclination of interface HB-HDPE, series A24, tested with the small dimension inclined plane.....	86
Figure 5.23 – Curve Lambda vs. Inclination of interface HB-HDPE, series B75 and B81, tested with the standardized dimension inclined plane.....	87
Figure 5.24 – Curve Displacement vs. Inclination of interface HB-HDPE, series B75 and B81, tested with the standardized inclined plane. ....	87
Figure 5.25 – Sketch of the planes A and B attachment disposal of the geomembranes lower layer. (top view).....	89
Figure 5.26 – Curve Displacement vs. Inclination of interface nnp40-EPDM, series A14 & 15, tested with the small dimension inclined plane.....	90
Figure 5.27 – Curve Lambda vs. Inclination of interface nnp40-EPDM, series A52 and A53, tested with the standardized inclined plane. ....	90
Figure 5.28 – Curve Displacement vs. Inclination of interface nnp40-EPDM, series A52 and A53, tested with the standardized inclined plane. ....	91
Figure 5.29 - Dynamic results of interface Rnnp x HDPE, series A31, guidance system $\delta$ .....	93
Figure 5.30 - Test results of interface Rnnp x HDPE, series B45.....	94

Figure 5.31 - Dynamic results of interface HB-HDPE, series A21, guidance system $\delta$ .....	95
Figure 5.32 - Dynamic results of interface HB x HDPE, series A24, guidance system $\delta$ .....	95
Figure 5.33 - Dynamic results of interface Rnnp x PVC, series A30, guide system type $\delta$ .....	97
Figure 5.34 - Dynamic results of interface nnp40 x HDPE, series A22 and A23, guidance system $\delta$	101
Figure 5.35 – Graphic <i>Lambda vs. Inclination</i> , interface Rnnp x PVC .....	104
Figure 5.36 – Graphic <i>Lambda vs. Inclination</i> , interface PVC x PVC .....	104
Figure I.1 – Graphic Displacement vs. Inclination .....	115
Figure I.2 – Graphic Displacement vs. Inclination .....	116
Figure I.3 – Graphic Displacement vs. Inclination .....	117
Figure I.4 – Graphic Displacement vs. Inclination .....	118
Figure I.5 – Graphic Displacement vs. Inclination .....	119
Figure I.6 – Graphics Displacement vs. Time, Velocity vs. Time, Acceleration vs. Time.....	119
Figure I.7 – Graphic Displacement vs. Time .....	120
Figure I.8 – Graphic Displacement vs. Inclination .....	121
Figure I.9 – Graphics Displacement vs. Time, Velocity vs. Time, Acceleration vs. Time.....	121
Figure I.10 – Graphic Displacement vs. Inclination .....	122
Figure I.11 – Graphics Displacement vs. Time, Velocity vs. Time, Acceleration vs. Time.....	122
Figure I.12 – Graphic Displacement vs. Inclination .....	123
Figure I.13 – Graphic Displacement vs. Inclination .....	124
Figure I.14 – Graphic Displacement vs. Inclination .....	125
Figure I.15 – Graphics Displacement vs. Time, Velocity vs. Time, Acceleration vs. Time.....	125
Figure I.16 – Graphic Displacement vs. Inclination .....	126
Figure I.17 – Graphic Displacement vs. Inclination .....	127
Figure I.18 – Graphic Displacement vs. Inclination .....	128
Figure I.19 – Graphics Displacement vs. Time, Velocity vs. Time, Acceleration vs. Time.....	128
Figure I.20 – Graphic Displacement vs. Inclination .....	129
Figure I.21 – Graphics Displacement vs. Time, Velocity vs. Time, Acceleration vs. Time.....	129
Figure I.22 – Graphic Displacement vs. Inclination .....	130
Figure I.23 – Graphics Displacement vs. Time, Velocity vs. Time, Acceleration vs. Time.....	130
Figure I.24 – Graphic Displacement vs. Inclination .....	131
Figure I.25 – Graphics Displacement vs. Time, Velocity vs. Time, Acceleration vs. Time.....	131
Figure I.26 – Graphic Displacement vs. Inclination .....	132
Figure I.27 – Graphics Displacement vs. Time, Velocity vs. Time, Acceleration vs. Time.....	132
Figure I.28 – Graphic Displacement vs. Inclination .....	133
Figure I.29 – Graphics Displacement vs. Time, Velocity vs. Time, Acceleration vs. Time.....	133
Figure I.30 – Graphic Displacement vs. Inclination .....	134
Figure I.31 – Graphics Displacement vs. Time, Velocity vs. Time, Acceleration vs. Time.....	134
Figure I.32 – Graphic Displacement vs. Inclination .....	135
Figure I.33 – Graphics Displacement vs. Time, Velocity vs. Time, Acceleration vs. Time.....	135
Figure I.34 – Graphic Displacement vs. Inclination .....	136
Figure I.35 – Graphics Displacement vs. Time, Velocity vs. Time, Acceleration vs. Time.....	136
Figure I.36 – Graphic Displacement vs. Inclination .....	137
Figure I.37 – Graphics Displacement vs. Time, Velocity vs. Time, Acceleration vs. Time .....	137
Figure I.38 – Graphic Displacement vs. Inclination .....	138
Figure I.39 – Graphics Displacement vs. Time, Velocity vs. Time, Acceleration vs. Time.....	138
Figure I.40 – Graphic Displacement vs. Inclination .....	139
Figure I.41 – Graphic Displacement vs. Inclination .....	140
Figure I.42 – Graphics Displacement vs. Time, Velocity vs. Time, Acceleration vs. Time.....	140

Figure II.1 – Graphic Lambda vs. Inclination.....	142
Figure II.2 – Graphic Lambda vs. Inclination.....	143
Figure II.3 – Graphic Displacement vs. Inclination.....	143
Figure II.4 – Graphic Lambda vs. Inclination.....	144
Figure II.5 – Graphic Displacement vs. Inclination.....	144
Figure II.6 – Graphic Lambda vs. Inclination.....	145
Figure II.7 – Graphic Displacement vs. Inclination.....	145
Figure II.8 – Graphic Lambda vs. Inclination.....	146
Figure II.9 – Graphic Displacement vs. Inclination.....	146
Figure II.10 – Graphic Lambda vs. Inclination.....	147
Figure II.11 – Graphic Displacement vs. Inclination.....	147
Figure II.12 – Graphic Lambda vs. Inclination.....	148
Figure II.13 – Graphic Displacement vs. Inclination.....	148
Figure II.14 – Graphic Lambda vs. Inclination.....	149
Figure II.15 – Graphic Displacement vs. Inclination.....	149
Figure II.16 – Graphic Lambda vs. Inclination.....	150
Figure II.17 – Graphic Displacement vs. Inclination.....	150
Figure II.18 – Graphic Lambda vs. Inclination.....	151
Figure II.19 – Graphic Displacement vs. Inclination.....	151
Figure II.20 – Graphic Lambda vs. Inclination.....	152
Figure II.21 – Graphic Displacement vs. Inclination.....	152

## NOTATIONS

$\beta$	Inclined plane angle
$\beta_{\text{Stand}}$	Plane inclination correspondent to the standard displacement
$\beta_0$	Inclination angle of the plane correspondent to the static limit equilibrium
$\beta_s$	Inclination angle on non-stabilized sliding
$\beta_{50}$	Inclination of the plane correspondent to a displacement of 50 mm
$u$	Relative displacement
$u_B$	Relative displacement of the upper box
$u_G$	Relative displacement of the geosynthetics layers
$u_{50}$	Displacement equals to 50 mm
$F$	Force required to hold back the upper box
$T_{\text{Sensor}}$	Traction force due to the displacement's sensor
$fr(\beta)$	Force to hold back the empty upper box correspondent to inclination $\beta$
$\lambda$	Function representing the friction behavior
$\gamma$	Acceleration of the plate during instant $t$
$g$	Gravity
$W_s$	Weight of soil contained in the upper box
$W_T$	Total weight of the mobile plate
$m_T$	Total mass of the plate
$\Phi$	Friction angle of the interface
$\Phi_{\text{gg}}$	Threshold angle of friction related to the beginning of the non-stabilized sliding for an interface geosynthetic-geosynthetic
$\Phi^{\text{Static}}$	Friction angle of the interface determined through static analysis
$\Phi^{\text{Dyn}}$	Friction angle of the interface determined through dynamic analysis
$\Phi_0$	Friction angle correspondent to a box's displacement of 5 mm.
$\Phi_{50}$	Friction angle correspondent to a box's displacement of 50 mm.
$\Phi_{\text{peak}}$	First peak value of function $\lambda$ shown on curve <i>Lambda vs. Inclination</i>
$\Phi_{\text{peak};I}$	First peak value of function $\lambda$ shown on curve <i>Lambda vs. Inclination</i> for the first test of a series
$\Phi^{\text{lim}}$	Dynamic friction angle
$\Phi_{\text{res}}$	Residual friction angle
$\Phi_{0,A}$	Friction angle correspondent to a box's displacement of 5 mm, determined using plane A
$\Phi_{50,A}$	Friction angle correspondent to a box's displacement of 50 mm, determined using plane A
$\Phi_{0,B}$	Friction angle correspondent to a box's displacement of 5 mm, determined using plane B
$\Phi_{50,B}$	Friction angle correspondent to a box's displacement of 50 mm, determined using plane B

## ABBREVIATIONS

<b>Rnnp</b>	Geotextile Nonwoven Needle Punched reinforced with PET wires
<b>nnp40</b>	Geotextile Nonwoven Needle Punched
<b>nnpC</b>	Geotextile Nonwoven Needle Punched calandered
<b>HB</b>	Geotextile Nonwoven Heat-Bounded
<b>PVC</b>	Geomembrane Polyvynil Chloride
<b>HDPE</b>	Geomembrane High Density Polyethylene
<b>EPDM</b>	Geomembrane Ethylene Propylene Diene Monomer
<b>PP</b>	Geomembrane Polypropylene
<b>Dyn1</b>	Test type dyn1
<b>Dyn2</b>	Test type dyn 2
<b>GBR-P</b>	Polymeric geosynthetic barrier
<b>GBR-C</b>	Clay geosynthetic barriers
<b>GBR-B</b>	Bituminous geosynthetic barrier
<b>CCL</b>	compacted clay layers
<b>GMB</b>	Geomembrane (Polymeric geosynthetic barrier)
<b>GTX</b>	Geotextile
<b>GEC</b>	Geocomposite for erosion control
<b>GLS</b>	Geosynthetic lining systems
<b>GTr</b>	Reinforcement nonwoven needle punched geotextile
<b>GS</b>	Geospacer
<b>GMpp</b>	Polypropylene geomembrane
<b>GMhdpe</b>	High density polyethylene geomembrane
<b>Plane A</b>	Small dimension inclined plane
<b>Plane B</b>	Standardized inclined plane
<b>l</b>	Length
<b>w</b>	Width
<b>h</b>	Height
<b>Type <math>\alpha</math></b>	Guidance test type presented in Figure 4.16
<b>Type <math>\beta</math></b>	Guidance test type presented in Figure 4.16
<b>Type <math>\gamma</math></b>	Guidance test type presented in Figure 4.16
<b>Type <math>\delta</math></b>	Guidance test type presented in Figure 4.16

## TABLE OF CONTENTS

<b>1</b>	<b>INTRODUCTION .....</b>	<b>18</b>
<b>2</b>	<b>GEOSYNTHETICS .....</b>	<b>21</b>
2.1	Introduction.....	21
2.2	Application on Landfills .....	22
2.3	Concept of Liner Systems.....	26
2.4	Products (Geotextiles, Geomembranes and others).....	27
2.5	Site case (detention basin) .....	28
<b>3</b>	<b>PARAMETERS OF INTERFACE.....</b>	<b>30</b>
3.1	Introduction.....	30
3.2	Conventional Tests .....	31
3.2.1	Shear test (ISO12957-1:2005).....	31
3.2.2	Inclined plane (ISO 12957-2:2005).....	31
3.3	Characteristics observed in literature.....	33
3.3.1	Characteristics of slide behavior.....	33
3.3.2	Critics to ISO 12957-2.....	34
3.3.3	Use of inclined plane of large dimensions .....	34
3.3.4	Use of inclined plane of small dimensions.....	35
3.3.5	Influence of the plane inclination rate .....	38
3.3.6	Friction angle results .....	39
<b>4</b>	<b>STUDY OF FRICTION BEHAVIOR – EXPERIMENT DETAILS .....</b>	<b>40</b>
4.1	Introduction.....	40
4.2	Large dimension apparatus (B).....	40
4.2.1	Description of the apparatus .....	40
4.2.2	Test analysis .....	43
4.2.3	Standard Analysis .....	44
4.2.4	Force Analysis .....	45
4.2.5	Combined Analysis .....	46
4.2.6	Test details.....	46
4.3	Small dimension apparatus (A).....	48
4.3.1	Description of the apparatus .....	48
4.3.2	Test analysis .....	50
4.3.3	Test details.....	52
4.4	Geosynthetics.....	54
4.5	Sensors .....	56
4.6	Notation for tests.....	56

4.7	Interfaces tested .....	57
4.8	Procedure for calculation of parameters .....	59
4.8.1	Introduction .....	59
4.8.2	Inclined plane A.....	60
4.8.3	Inclined plane B.....	62
<b>5</b>	<b>TEST RESULTS.....</b>	<b>64</b>
5.1	Introduction.....	64
5.2	Static Analysis .....	64
5.2.1	Introduction .....	64
5.2.2	Interface Rnp-PVC .....	65
5.2.3	Interface HB-PVC .....	70
5.2.4	Interface nnp40-PVC.....	73
5.2.5	Interface Rnp-PP .....	77
5.2.6	Interface nnpC-PP .....	80
5.2.7	Interface Rnp-HDPE.....	82
5.2.8	Interface HB-HDPE.....	84
5.2.9	Interface nnp40-EPDM.....	88
5.3	Dynamic Analysis.....	91
5.3.1	Introduction .....	91
5.3.2	Interface Rnp-HDPE.....	92
5.3.3	Interface HB-HDPE.....	94
5.3.4	Interface nnpC-PP .....	96
5.3.5	Interface Rnp-PVC .....	97
5.3.6	Interface HB-PVC .....	98
5.3.7	Interface nnp40-PVC.....	99
5.3.8	Interface nnp40-HDPE .....	100
5.3.9	Interface nnpC-HDPE.....	101
5.4	Summary of results .....	101
<b>6</b>	<b>CONCLUSIONS .....</b>	<b>109</b>
	<b>REFERENCES .....</b>	<b>112</b>
	<b>APPENDIX I.....</b>	<b>114</b>
	<b>APPENDIX II .....</b>	<b>141</b>
	<b>ANNEX A.....</b>	<b>153</b>

# 1 INTRODUCTION

Over the years, engineering solutions involving the implementation of geosynthetic materials have grown enormously. With the emerging variety of materials, it has become possible to explore new applications, design models and methods related to these products.

One of the main points concerning the study of geosynthetics is the friction characterization of interfaces soil-geosynthetic and geosynthetic-geosynthetic. This type of analysis is very important to optimize construction solutions such as slope liner systems, very common on landfills and basin detention, for instance.

Direct shear box and inclined plane experiments are two standard tests (ISO 12957 Part 1 and 2, 2005) recommended for characterization of interfaces friction behavior, each one presenting its specifications and peculiarities.

Many authors have presented articles and thesis wherein they have made tests with a great diversity of interfaces and using the inclined plane apparatus. They have developed new methods to augment the parameters and conditions of analysis such as improving the inclined plane systems to perform hydraulic tests and measuring new parameters such as force, instead of displacement (BRIANÇON, 2001). Other tests have been performed to try to extend the use of the inclined plane from a static experiment to a dynamic one (REYES RAMIREZ, 2003).

All these tests have been made in order to develop the inclined plane experiment from a traditional index test to a performance oriented test which would collaborate in a deeper study of how the interfaces behave in slope liner systems. The experiment procedure explained in ISO 12957-2:2005 dictates a unique moment when it is possible to determine the interface friction angle: when the upper box reaches a displacement equals to 50 mm.

Regarding previous studies of the inclined plane, Reyes Ramirez (2003) performed significant modifications to mold the experiment for dynamic analysis. These changes mainly in a reduction of the interface contact surface in comparison with the dimensions prescribed in ISO 12957-2:2005. Despite the alterations of dimensions, there is no study of how the reduction of contact surface impacts the standard results.

Reyes Ramirez (2003) validated the values obtained with his modified plane (small dimension inclined plane) comparing it with results achieved using the direct shear box. He did not directly compare the results to the standardized inclined plane. That is why one of the objectives of the present work is to assess if these physical modifications affect the standardized inclined plane results.

Only contrasting their results with the direct shear box, Reyes Ramirez & Gourc (2003) criticized the standard affirming that the use of conventional friction angles for assessing stability of geosynthetic liners in slope is non-conservative. Also, they suggested a revision of the old version of ISO 12957-2:2005.

The argument for the critic is based on the behavior presented by a few interfaces geosynthetic-geosynthetic that showed a gradual slide instead of the traditional sudden slide (typical for sand-geosynthetic interfaces). This behavior may advance the non-stabilized sliding moment and the determination of the friction angle for displacement equals to 50 mm may become inappropriate.

Based on the great possibility of interfaces available to be tested nowadays, and on the diversity of results that could be found, it is easy to believe that the simple index value suggested by the standard is outdated.

Hence, the objective of this work is to validate the results of the small dimension inclined plane comparing it directly with results made with standard test apparatus and therefore, evaluate whether the standard indeed needs an actualization.

This work was possible due to the collaboration of Instituto Tecnológico de Aeronáutica, Sao Jose dos Campos, Brazil and Université Joseph Fourier, Grenoble, France. The research was made during an internship program offered by Laboratoire d'étude des Transferts en Hydrologie et Environnement and together with Dr. Laurent Briançon and Dr. Jean-Pierre Gourc.

The report is divided into six chapters. In chapter 2 it is discussed the application of geosynthetics (in particular at landfills) and a few definitions involving these products. Also is presented a site case where the friction characterization was required. Chapter 3 presents a discussion of what exists in literature concerning the inclined plane experiment. Chapter 4 includes the specifications of the planes used for tests, description of test, calculation and

analysis procedures and characterization of interfaces utilized. Chapter 5 presents the test results of the experiment and finally chapter 6 comprises recommendations and conclusions regarding the test results.

## 2 GEOSYNTHETICS

### 2.1 Introduction

In accordance with ISO 10318:2005, geosynthetic is a term used to describe a product in which at least one of its components is made from a synthetic or natural polymer. In addition, they are available in three ranges of forms such as a sheet, a strip or a three-dimensional structure.

Also in accordance with ISO 10318:2005, geosynthetics are used in contact with soil or other materials in geotechnical and civil engineering applications.

Separation, reinforcement, filtration, drainage and containment are primarily functions of geosynthetic applications that are very common in civil engineering. These products can be used in sectors such as:

- Transportation ( Roads & railways)
- Rockfall protection (Stabilization barriers and embankments)
- Water and waste (Dams & water tanks; landfills)
- Coastal (Breakwaters & offshore reefs)
- Erosion Control
- Hydraulic Structures
- Geotechnical (Gabion walls, reinforced slopes and panel wall systems)
- Mining (Dump structures and rock barriers)
- Golf and turf (Bunkers and ponds)

Over the years, different geosynthetic products have been manufactured to suit construction needs and to replace traditional materials. Clay geosynthetic barriers (GBR-C), for instance, have replaced or significantly reduced the thickness of compacted clay layers (CCL) used to create impermeable layers for landfills. ([www.maccaferri.co.nz](http://www.maccaferri.co.nz))

Since the focus of this work is the characterization of interfaces friction behavior in systems composed by superposed geosynthetics, and the most complex form of application of these kinds of systems is on landfills, this chapter focus on the application of geosynthetics in

landfills. Here, it is also presented the definition of barriers of geosynthetics and a study of one site case (detention basin).

## **2.2 Application on Landfills**

The primary function of the landfill is to protect the environment controlling hazardous leachates generated by the decomposing waste. In modern landfills, the waste is contained by a liner system. As a result, the main functions of the liner system are to isolate the landfill contents from the environment and to protect the soil and ground water from pollution (waste).

They are designed using a range of geosynthetic products that provide advantages over traditional materials in terms of performance, design, efficiency and cost. Geomembranes (usually HDPE and PP) and clay geosynthetic barriers are quoted as being used on barriers to move the leachates from the base of landfills and barriers to prevent additional water from penetrating the waste basin. In addition, geocomposite drains and protection geotextiles are cited in conjunction with barriers to form the lining system. ([www.maccaferri.co.nz](http://www.maccaferri.co.nz))

A landfill construction model can be described into 11 main phases: (VIDAL, 2002)

- 1- Land is excavated.
- 2- A compacted clay and synthetic liner are added. This liner prevents contaminants from seeping into the groundwater.
- 3- A protection layer is installed.
- 4- A leachate collection system is installed, usually composed by a coarse granular material and a filtering element (an opened woven geotextile).
- 5- The landfill is opened and solid waste is deposited.
- 6- After the landfill is filled to capacity, a drainage layer for gas collection is placed
- 7- Installation of a protection layer
- 8- Installation of a cover geosynthetic or clay liner
- 9- Installation of a rain water collection system composed by a drainage geocomposite or a granular drain protected by a geotextile filter
- 10- A final stabilizing soil layer is placed.
- 11- Grass and other short rooted plants are planted. These plants will prevent erosion of the landfill surface.

Figure 2.1 to Figure 2.6 show pictures of geosynthetic installation in a landfill and construction details of a solid waste containment system with high geosynthetic utilization proposed by Koerner (1998).



**Figure 2.1 – Bandeirantes landfill, Sao Paulo, Brazil (brasil-virtual.net)**



**Figure 2.2 – Construction of landfill in Itaquaquecetuba, Sao Paulo, Brazil (brasil-virtual.net)**

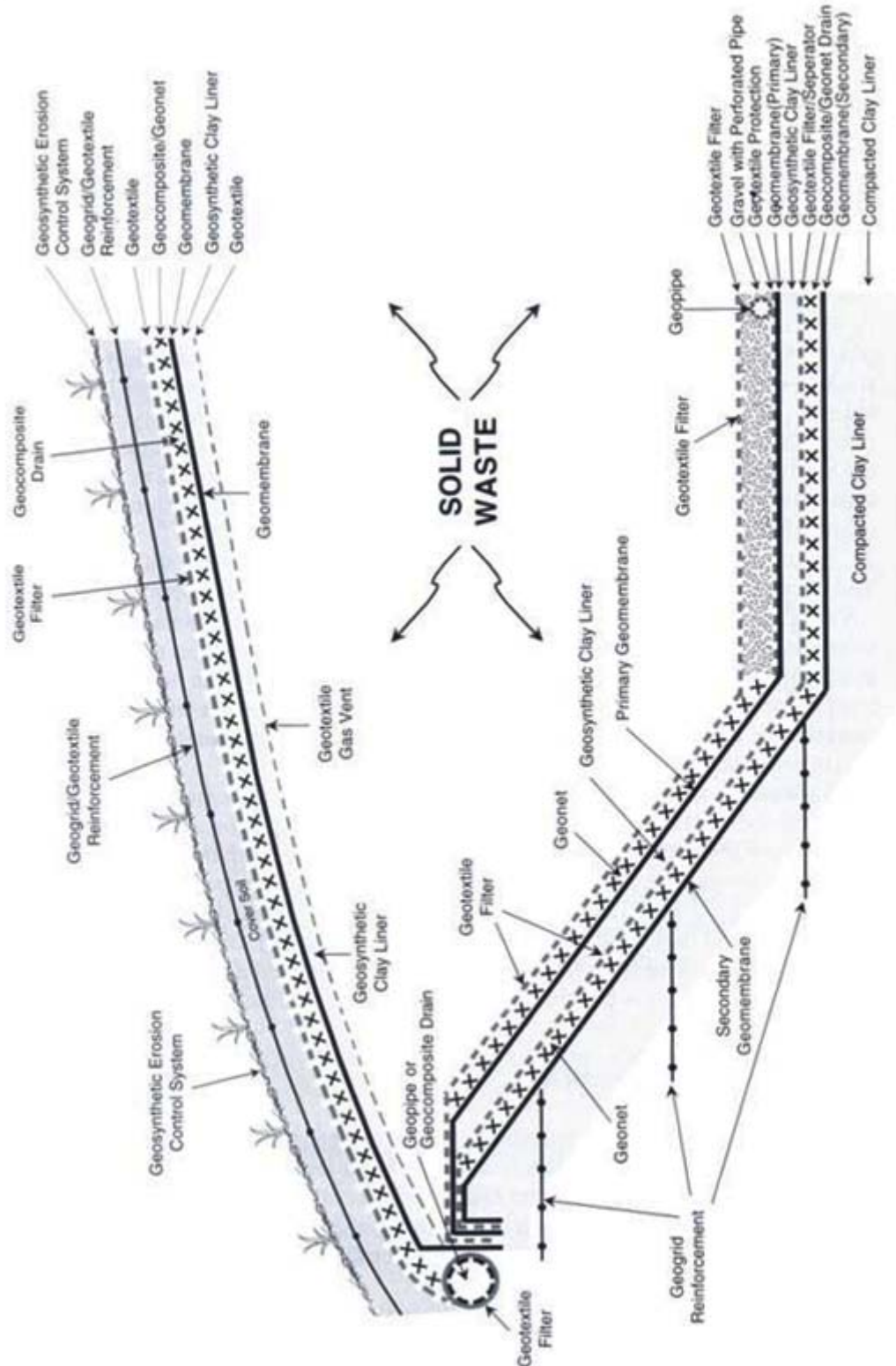


Figure 2.3 – Solid waste containment system with high geosynthetic utilization (Koerner, 1997)



**Figure 2.4 - Winneshiek Co. Landfill Commission, Decorah. Cap cover construction stage of a landfill construction. ([www.jbholland.net](http://www.jbholland.net))**



**Figure 2.5 – Geosynthetic liner installation of a landfill construction. ([www.cpengeers.com](http://www.cpengeers.com))**



**Figure 2.6 – Geosynthetic liner of a landfill construction. ([www.cpengeers.com](http://www.cpengeers.com))**

## 2.3 Concept of Liner Systems

A liner system is a system composed by superposed geosynthetics. It can be of three types:

- **Single Liner** - when made of a single barrier (e.g. geomembrane);
- **Composite Liner** - when composed of two or more barriers (e.g. geomembrane and compacted clay) juxtaposed and acting jointly in the entire length of the system;
- **Double Liner** - when consisting of two barriers (usually geomembranes) with an interposed draining system.

A few examples of liner systems are presented in Figure 2.7, Figure 2.8, Figure 2.9 and Figure 2.10.

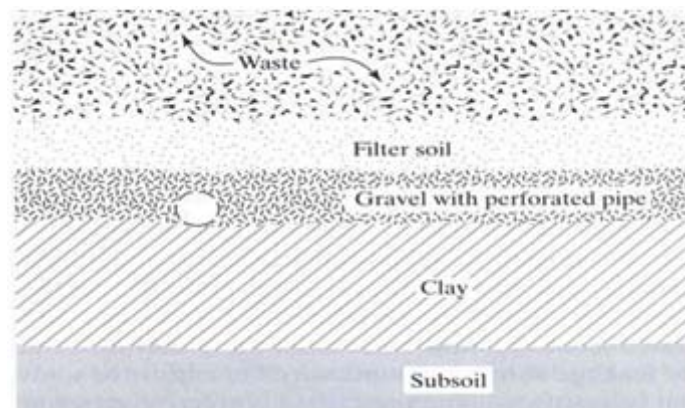


Figure 2.7 – Single clay liner (Koerner, 1997)

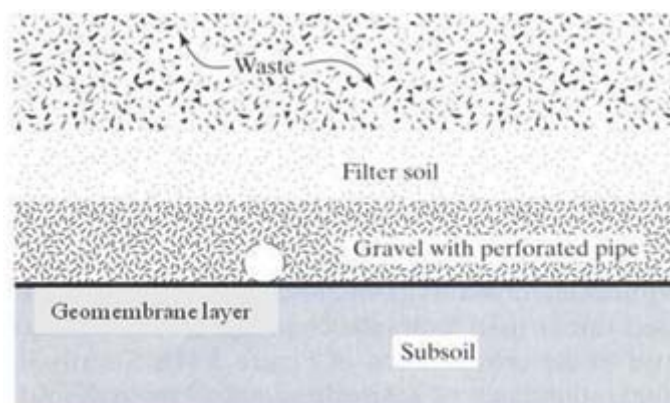


Figure 2.8 - Single geomembrane liner (Koerner, 1997)

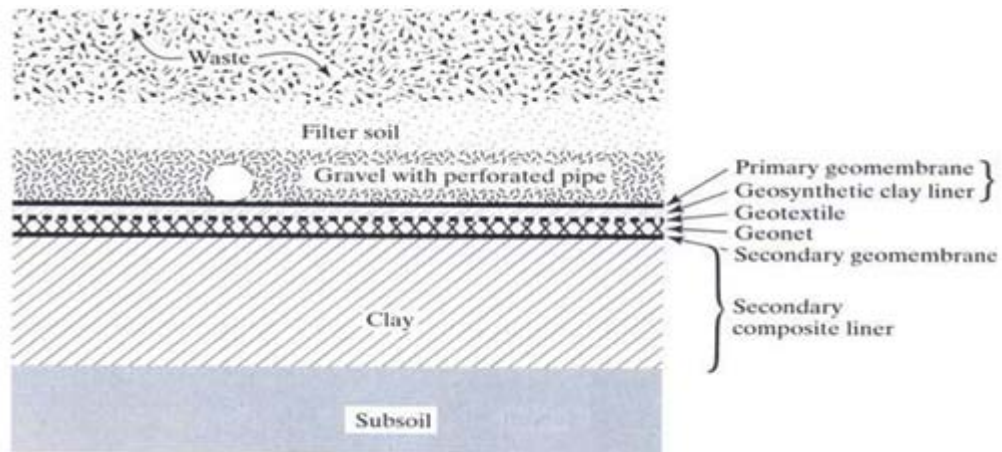


Figure 2.9 – Double-composite liner (with geosynthetic clay liner) and geonet (Koerner, 1997)

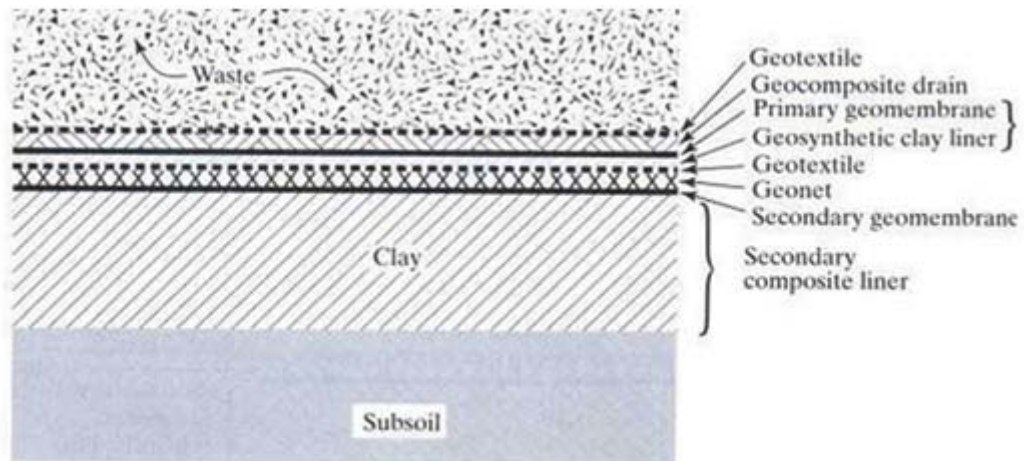


Figure 2.10 – Double-composite liner (with geosynthetic clay liner), geonet and geocomposite (Koerner, 1997)

## 2.4 Products (Geotextiles, Geomembranes and others)

As presented on ISO 10318:2005, the geosynthetic term includes four main categories (geotextiles, geotextile related product, geosynthetic barriers and geocomposites), which are defined as follows:

- **Geotextile:** planar, permeable and polymeric (synthetic or natural) textile material, which may be nonwoven, knitted or woven.

- **Geotextile-related product:** planar, permeable and polymeric (synthetic or natural) material, which does not comply with the definition of a geotextile. They can be separated into six categories: geogrids, geonets, geomats, geocells, geospacers, and geostrips.
- **Geosynthetic barrier:** low-permeability geosynthetic material, used with the purpose of reducing or preventing the flow of fluid through the construction. They are divided into three groups:
  - **Polymeric geosynthetic barrier (GBR-P):** factory-assembled structure of geosynthetic materials in the form of a sheet which acts as a barrier.
  - **Clay geosynthetic barrier (GBR-C):** factory-assembled structure of geosynthetic materials in the form of a sheet which acts as a barrier.
  - **Bituminous geosynthetic barrier (GBR-B):** factory-assembled structure of geosynthetic materials in the form of a sheet which acts as a barrier
- **Geocomposite:** manufactured, assembled material using at least one geosynthetic product among the components.

Formerly, the polymeric geosynthetic barrier was known as geomembranes (GMB), and, in this work, it will be referred with this oldest terminology.

## 2.5 Site case (detention basin)

Reyes Ramirez et al. (2003) discussed factors that could result on the sliding of the liner system cover in the slope of a detention basin that was observed just after the execution of the liner system.

The liner system in question was composed of a clay geosynthetic barrier (GBR-C), as the liner element, and a geocomposite for erosion control (GEC), made with a woven geotextile sewed to a geomat. The vegetal layer was deposited over the GEC without compaction (Figure 2.12).

The problem noticed was that the geocomposite for erosion control slid over the GBR-C followed by a woven geotextile rupture (Figure 2.11). Many justifications were raised to

determine the reason for this problem, and one of them, consisted of checking whether the inclination of the slope was equivalent to the friction angle of the interfaces on the liner system. It was also studied the friction behavior of the interface regarding the dynamic analysis (this study will be better explained on Chapter 4).



**Figure 2.11 – Image of the region where the slide occurred (REYES RAMIREZ ET AL., 2003)**

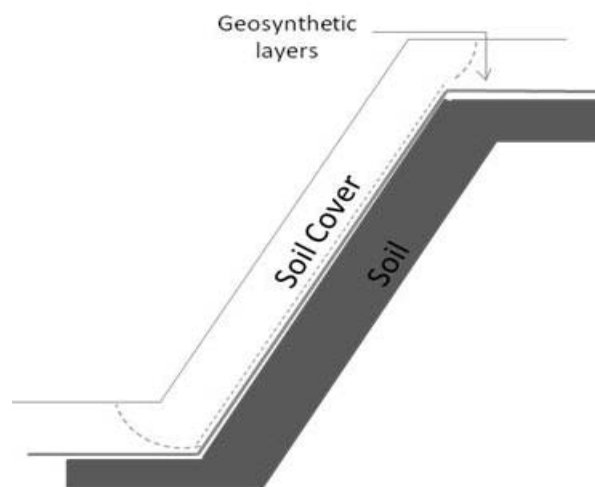


**Figure 2.12 – Sketch of the rupture, lateral view of the slope.**

To solve this stability problem and to study the critical conditions of the interfaces, normally, it is adopted the inclined plane experiment.

### 3 PARAMETERS OF INTERFACE

#### 3.1 Introduction

Geosynthetic lining systems (GLS) are composed by geosynthetics of different nature usually covered by a cap of soil, which is placed to provide protection for the geosynthetic system. Between the soil cover and the geomembrane layer, a geotextile can be positioned to ensure the protection of the system. This geotextile have many functions. For instance, it can protect the geomembrane during the placement of the soil cover and the service of the structure or can also contribute for making the soil cover stable. (BRIANÇON ET AL., 2002)

The coverage soil layer is usually equivalent to a (low) normal stress, not superior to 15 kPa.

As pointed out by Koerner (2007), on circumstances where a lined slope is covered with soil, a stability calculation should be made to asses the potential for sliding failure of the soil barrier layer. He exemplified situation as:

- Landfill liners with leachate collection sand or gravel above them, until such time that the solid waste acts as passive resistance restraint;
- Surface impoundment liners where the cover soil is placed over the geomembrane to shield it from degradation (ultraviolet light, heat degeneration and equipment damage);
- Landfill covers that have topsoil and protection soil placed over the geomembrane.

Since the preferential failure planes of the GLS are generally located at the interfaces of this geosynthetic materials it is necessary to study the friction angles between the different geosynthetics that compose the layers and also between geosynthetics and soil.

The most famous experiments for this kind of study analysis are the direct shear box and the inclined plane. Many authors have already made comparisons between this two types of test results claiming that the inclined plane is best suited for low stress conditions ( $< 10$  kPa) while the shear boxes are better fitted to normal stresses higher than 50 kPa (BRIANÇON ET AL., 2002, REYES RAMIREZ, 2003).

Reyes Ramirez (2003) strengthened the idea that the inclined plane is most recommended in these cases because it is easier to simulate the different stages of the construction of a thin soil layer which would be equivalent to normal stresses under 5 kPa.

## **3.2 Conventional Tests**

### **3.2.1 Shear test (ISO12957-1:2005)**

ISO 12957-1:2005 describes a method of determining the friction characteristics of geosynthetics and related products in contact with standardized sand, i.e. sand with a specified density and moisture content, under normal stress and at a constant rate of displacement, using a direct shear apparatus. The procedure can also be used for testing geosynthetic barriers.

The shear test is composed of two semi boxes, one above the other, which can be filled with soil. Between these boxes, it can be placed the sample of geotextile. Typically, the inferior box is fixed, and the other one can slide above the contact surface in only one direction. There are two possible configurations described in ISO 12957-1:2005 to set the experiment, one with a constant surface of contact and other with a decreasing surface of contact.

The main information presented on the international standard concerns the application of normal and shear efforts. First, the normal stress does not decrease during the test, it remains constant. Second, the normal stress applied is higher than 50 kPa. And finally, the shear stress is applied through a box displacement at a constant rate of 1 mm/min.

### **3.2.2 Inclined plane (ISO 12957-2:2005)**

ISO 12957-2:2005 describes a method of determining the friction characteristics of geosynthetics (geotextiles and geotextile-related products, geosynthetic barriers), in contact with soils, at low normal stress, using an inclined plane apparatus. Among the many points discussed, the most relevant ones are shown as follows. The inclined plane apparatus will be better detailed in Chapter 4.

The method was primarily intended as a performance test to be used with site-specific soils, but it may also be used as an index test with standard sand.

The friction angle of the interface soil-geosynthetic is determined by measuring the inclination angle of the apparatus in which a box filled with soil (with the possibility of additional charges) has slid 50 mm.

Variants in relation to the test described in the standard can be used to measure the friction characteristics of geosynthetics in non-standard conditions:

- a) A second layer of geosynthetic can be attached to the upper box to measure the friction of a geomembrane over a geosynthetic;
- b) The values of normal stress different from those of the standard can be applied to simulate a more realistic condition of the site.

The normal force must be applied by any method to obtain a regular distribution of the normal stress on the entire surface of the specimen. The normal force applied must be such that the normal stress is equal to  $(5.0 \pm 0.1)$  kPa.

The plane must be set with a mechanism for raising the plane slowly, at a constant speed of  $(3.0 \pm 0.5)^\circ/\text{min}$ .

The geosynthetic (lower layer) must be fixed to the inclined plane apparatus to limit any relative movement between the layer and the plane. The techniques previewed are sewing or gluing, rough support to increase the coefficient of friction, or anchoring the layer outside the contact area.

Regarding to the dimensions of the apparatus, the standard prescribes minimum dimensions for both upper (length,  $l = 300$  mm, and width,  $w = 300$  mm) and lower ( $l = 400$  mm,  $w = 325$  mm) box.

As a final point, repetitions of the test must be performed using new samples. Any other test made on different sides of the sample or in a different direction should be made using new samples.

### 3.3 Characteristics observed in literature

#### 3.3.1 Characteristics of slide behavior

Gourc and Reyes Ramirez (2004) divided the upper box slide behavior into three characteristic phases:

- **Phase 1 (Static phase):** upper box practically immobile (displacement of the box equals to zero) over the inclined plane until reaching an angle  $\beta_0$ .
- **Phase 2 (Transitory phase):** for an increasing value of inclination higher than  $\beta_0$ , upper box moves gradually downwards.
- **Phase 3 (Non-stabilized sliding phase):** upper box undergoes non-stabilized sliding at an increasing speed, even if plane inclination is held constant to  $\beta_s$ .

Where,  $\beta_0$  was defined as the plane inclination angle correspondent to the static limit equilibrium, and  $\beta_s$  stands for inclination angle on non-stabilized sliding.

As indicated by Reyes Ramirez and Gourc (2003), Phase 2 may be of three types: (Figure 3.1)

- 1) **Sudden sliding:** abrupt displacement of the upper box under non-stabilized sliding with a nearly non-existent Phase 2 ( $\beta_0 = \beta_s$ );
- 2) **Jerky sliding:** displacement  $u$  increasing in a stick-slip fashion; and
- 3) **Gradual sliding:** displacement  $u$  progressively increases with inclination  $\beta$ .

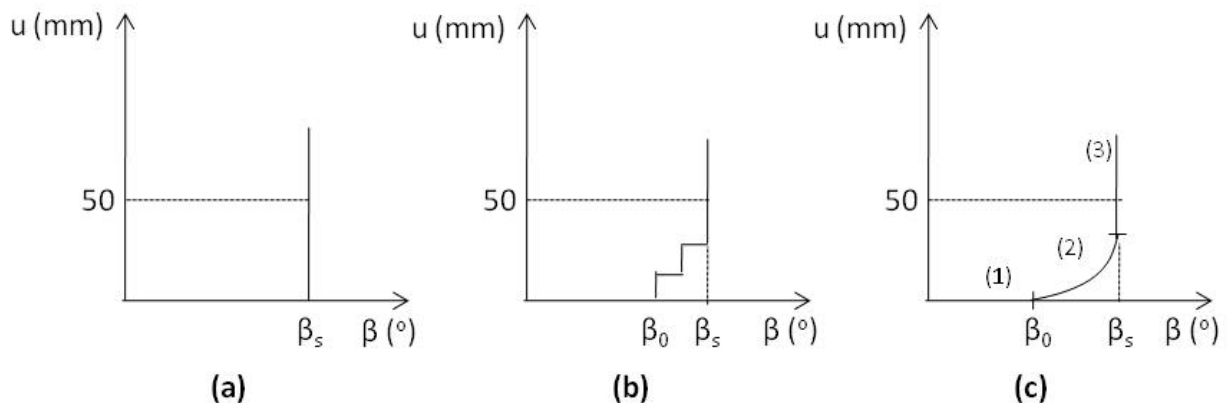


Figure 3.1 – Different mechanisms of slides: (a) sudden sliding; (b) jerky sliding; (c) gradual sliding

### 3.3.2 Critics to ISO 12957-2

Gourc & Reyes Ramirez (2004) noticed that the non-stabilized sliding (Phase 3) often happened for plane displacement values smaller than the standard value 50 mm. Consequently, it was questioned how to define the threshold displacement corresponding to the standard angle of friction of the interface geosynthetic-geosynthetic.

Also, they strengthened the idea that some interface dynamic friction behavior may be entirely different from static one due to the influence of the displacement rate (modification of contact conditions) and the material damage (linked to the sliding displacement). As a result they proposed one modified inclined plane test that would be capable of simulating conditions to characterize the interface friction on phase 3.

### 3.3.3 Use of inclined plane of large dimensions

Briançon et al. (2002) performed a study on slope stability of geosynthetic lining systems and investigated interfaces subjected to low vertical stress using the large dimensions inclined plane apparatus (one of the apparatus that was used at the present work). The interfaces were tested between nonwoven needle-punched geotextiles and geomembranes and a few results reached are shown in Table 3.1.

**Table 3.1 - Friction angle test results found using inclined plane experiment. (BRIANÇON ET AL., 2002)**

Interface	Friction angle
Reinforcement nonwoven needle-punched geotextile – Polypropylene geomembrane	16-17°
Reinforcement nonwoven needle-punched geotextile – HDPE geomembrane	14-15°

Also, Briançon et al. (2002) implemented and validated a new test procedure (force test) for inclined plane experiment. The force test was set to measure the force required to hold back the upper box during the inclination of the plane.

The comparison between force and displacement test results made by these authors showed that the maximum difference between the values measured by these two types of tests was inferior to 2° in all tested cases. This difference was similar to the accuracy of the results they found for the displacement test type (ISO 12957-2 prescribed test type).

### 3.3.4 Use of inclined plane of small dimensions

Reyes Ramirez & Gourc (2003) published a paper with important aspects regarding tests using the small dimension inclined plane. The tests were made under a normal stress of 5.7 kPa and with three types of interfaces:

1. Reinforcement nonwoven needle punched geotextile (GTr) - geospacer (GS),
2. Polypropylene geomembrane (GMpp) – GS, and
3. High density polyethylene geomembrane (GMhdpe)- GS.

On their publication, they analyze the threshold angle of friction related to the beginning of the non-stabilized sliding for an interface geosynthetic-geosynthetic, defined as  $\Phi_{gg}$ .

Besides the traditional tests, two new analyses were performed.

- An abrasion analysis consisted of testing the same geomembrane sample several times; and
- A creep test consisted of raising the inclined plane, with the upper plate in a fixed position, up to an angle  $\beta$  smaller than the non-stabilized angle  $\beta_s$ . The upper plate is then released and the evolution of displacement (u), at a fixed angle of inclination, is observed.

#### (a) Abrasion analysis

Reyes Ramirez & Gourc (2003) performed a few abrasion analysis using GMhdpe-GS and GMpp-GS, making five successive inclined plane tests in each sample. Their conclusions:

- GMhdpe interface showed that the angle of friction can be slightly increased with the growth of cumulative displacement. This augment was more significant for the three first tests, becoming less pronounced for the last two. Finally, a “brittle” behavior was observed for all five tests performed with the same sample.
- The results for the GMpp demonstrated its sensitivity to abrasion. The angle relative to the sliding initialization was practically the same for all tests, but the behavior of the curve after this angle was no longer comparable.

In the article, it was recommended to avoid the use of a same sample more than once, being tolerated cumulative sliding length of 100 mm since it did not show a significant modification in the behavior of both interfaces tested. As observed for interface GMpp-GS, cumulative displacement equal or bigger than 500 mm could heavily affect the interface frictional behavior.

These authors also highlighted that cumulative displacement variations may correspond to actual field conditions, becoming necessary to properly considerate the abrasion. According to them, often on site, the geosynthetics are laid on a slope without first being stretched or thermal dilation problems can generate geomembrane waves. In these cases, the installation of a granular cover layer on the slope induces relative displacements at the geosynthetic-geosynthetic interfaces that are easily capable of exceeding 500 mm for points far from the anchorage till the top of the slope.

Kroener (1998) exhibited a few pictures that give support to previous statement (Figure 3.2, to Figure 3.5). In addition, he pointed out the problem of wind uplift during the execution of the geomembrane layers (Figure 3.4 and Figure 3.5) that can also induce relative displacements higher than 500mm. To avoid wind damaged he recommends the use of sandbags to hold the deployed geomembrane in position until the final cover is placed.

The results found by Reyes Ramirez & Gourc (2003) give an idea of what to expect from this interfaces in terms of abrasion. Though it is important to be aware that these materials could present sensitivity related to abrasion, it is not possible to affirm that GMhdpe and GMpp will present the same behavior when in touch with other materials different from geospacers.



**Figure 3.2 – Pictures of GLS being installed (KOERNER, 1997)**



**Figure 3.3 – Pictures of GLS being installed (KOERNER, 1997)**



**Figure 3.4 – Example of wind-damaged geomembrane (KOERNER, 1997)**



**Figure 3.5 – Example of wind-damaged geomembrane (KOERNER, 1997)**

## **(b) Creep Test**

The tests in interfaces GMhpde-GS and GMpp-GS revealed that the analysis of inclined plane diagram *Displacement (u) vs. Inclination ( $\beta$ )* serves to distinguish the behavior of these two interfaces. GMhpde exhibits sudden non-stabilized sliding, whereas the GMpp sliding is quite gradual.

The different behavior of the geomembranes before reaching the sliding threshold angle led to the performance of a creep test.

The results for this type of test showed that a non-stabilized sliding may be obtained for inclination  $\beta < \beta_s$  in interfaces showing gradual sliding (e.g. GMpp-GS). Consequently, considerations of the threshold value of friction angle  $\Phi_{gg}$  in a design process can not be supposedly conservative.

In summary, the article recommended the examination in detail of the sliding phase prior to reaching the threshold value  $\beta_s$  of non-stabilized sliding. It is believed that the friction behavior interpretation offered by ISO12957-2 is incomplete for geosynthetic-geosynthetic interfaces, since  $\Phi_{gg}$  is the only value currently included for design.

### **3.3.5 Influence of the plane inclination rate**

Reyes Ramirez (2003), with the inclined plane of small dimensions and with respect to the raising rate of the plane, affirmed that the tilting rate of the plane (between  $0.5^\circ/\text{min}$  and  $3.0^\circ/\text{min}$ ) does not interfere in the determination of the static friction angle of geosynthetic-geosynthetic interfaces. However, a slow raising rate ( $1^\circ/\text{min}$ ) contributed to overestimate the angle of non-stabilized slide.

Briançon (2001) studied the influence of the plane inclination rate in the results of large dimension apparatus, using three different velocities. From the results it was inferred that the inclination velocity of the plane changes with the interface tested. For this reason he reinforced the importance to fix this parameter. The author affirmed that the velocity prescribed of  $(3.0 \pm 0.5)^\circ/\text{min}$ , the same adopted by ISO 12957-2:2005, does not allow some analysis as deformation and development of stress in geosynthetics. Consequently, he adopted one velocity inferior than the standardized:  $(0.5 \pm 0.2)^\circ/\text{min}$ .

### 3.3.6 Friction angle results

Several authors have already performed tests using inclined plane experiments but not all of them used the same interfaces. Koutsourais & Sprague (1991 apud BRIANÇON, 2001) made tests using nonwoven needle-punched geotextiles; PVC and HDPE geomembranes. His results are shown on Table 3.3 and the details of the inclined plane are shown in Table 3.2.

**Table 3.2 – Inclined plane details used by Koutsourais & Sprague (1991, apud BRIANÇON, 2001)**

Type of upper box	Raising velocity (°/min)	Contact surface (m x m)
Plate	1.5±0.5	0.051 x 0.152

**Table 3.3 - Friction angle test results found using inclined plane experiment. Koutsourais & Sprague (1991, apud BRIANÇON, 2001)**

<b>Interface</b>	<b>Friction angle</b>
Nonwoven needle-punched geotextile - PVC geomembrane	22°
Nonwoven needle-punched geotextile - HDPE geomembrane	19°

## 4 STUDY OF FRICTION BEHAVIOR – EXPERIMENT DETAILS

### 4.1 Introduction

At this chapter, two inclined planes used in this work are presented and detailed. The first is the inclined plane of large dimensions (plane B) that is the same plane used by Briançon (2001) and it is in accordance with ISO 12975-2:2005. The second is the inclined plane of small dimensions (plane A) that was developed and tested by Reyes Ramirez (2003). This chapter also comprises the procedures of tests and analysis of results, besides it mentions the interfaces studied, its characteristics and the sensors used.

### 4.2 Large dimension apparatus (B)

#### 4.2.1 Description of the apparatus

Relative to the use of inclined planes to determine friction characteristics of geosynthetic-geosynthetic interfaces, the large dimension apparatus is in accordance with ISO 12957-2 (2005) and it is recommended to conduct tests on geosynthetic samples of large dimensions (BRIANÇON ET AL., 2002). Figure 4.1 and Figure 4.2 illustrates plane B.



Figure 4.1 - Large dimension inclined plane.

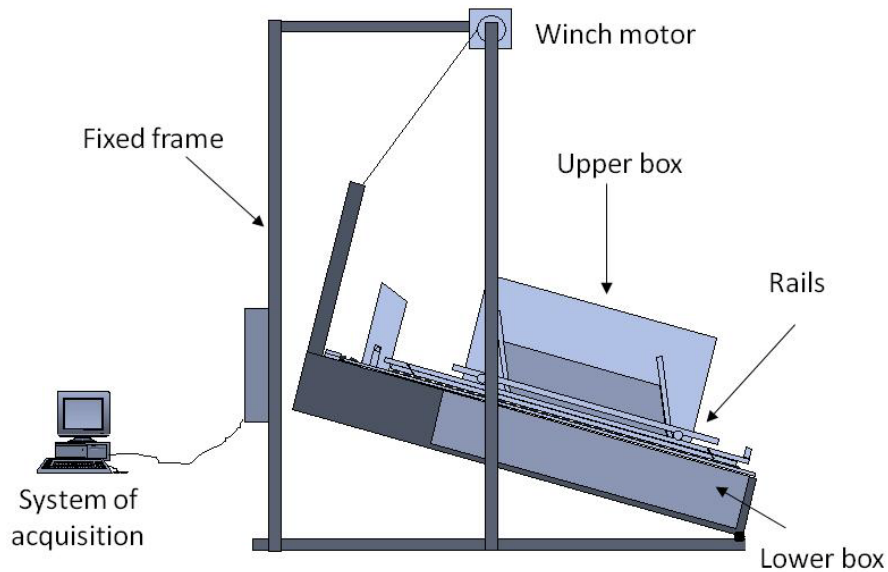


**Figure 4.2 - Sketch of the large dimension inclined plane.**

The device is composed of a tilting lower box ( $l = 2.0$  m,  $w = 1.2$  m and  $h = 0.3$  m) and a mobile upper box ( $l = 1.0$  m,  $w = 1.0$  m and  $h = 0.5$  m). The two boxes can be filled with soil although, in this experiment, the lower box will remain empty.

As showed in Figure 4.3, the upper box is composed of a metallic chassis that supports two fixed lateral walls and two inclinable walls. The box is fitted with a system of wheels and can move along rails installed on each side of the rigid base (lower box).

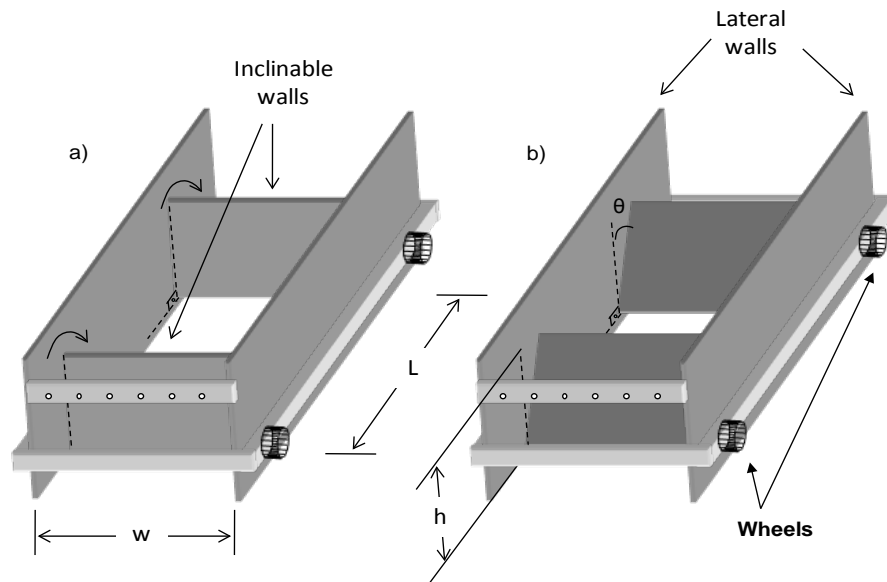


**Figure 4.3 – Upper box dispositive. Case a: no walls inclination. Case b: walls inclined of  $\theta$ .**

The dispositive was designed so that the rail system supports the upper box empty weight and, the geosynthetic layer support the weight of the soil inside the box (Figure 4.4).

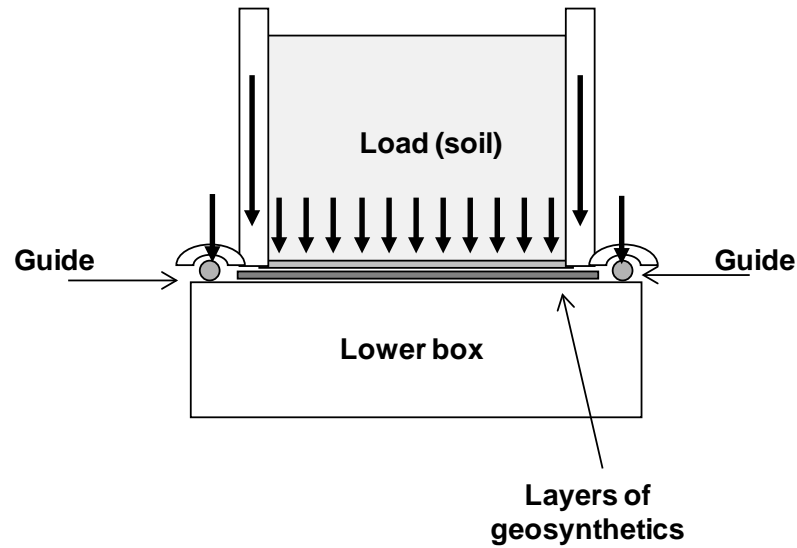


**Figure 4.4 - Load transfer toward guides and geosynthetics**

The geosynthetics are placed between the two boxes in two different arrangements (assuming the two layers disposal of geosynthetics). The first layer, considered here as a geomembrane, is glued using adhesive tapes at the top of the lower box and is also stapled to it. The second layer (geotextile) can be placed over the geomembrane (Figure 4.5 - a) or can be attached to the front of the upper box (Figure 4.5 - b). In test results, only trials made using disposal type b will be analyzed.

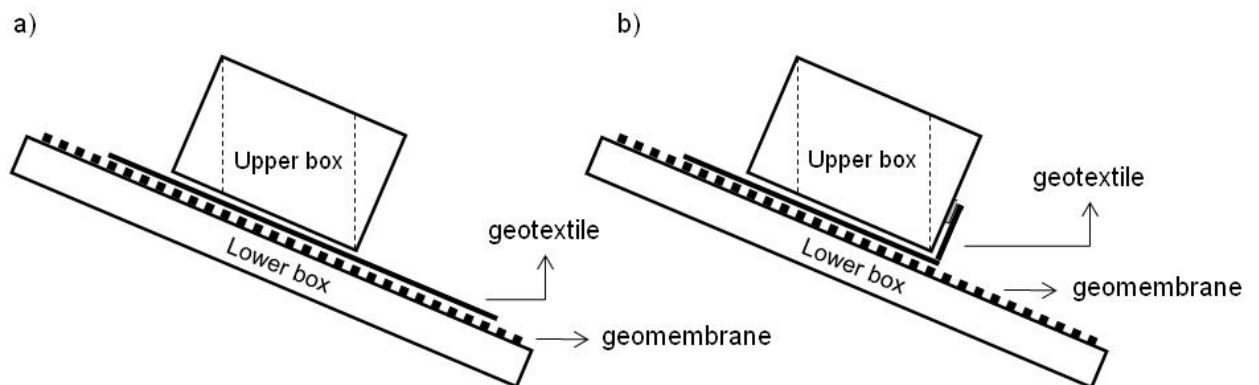


**Figure 4.5 - Geosynthetic attachment disposal**

The lifting mechanism of the inclined plane is composed of a motorized winch that raises the plane with variable controlled speeds (0.5–3.5 °/min). Despite of the range of velocities, the experiment was set for a fixed rate of 2°/min but due to some problems with the system, the actual rate was approximately equal to 1.3°/min.

### 4.2.2 Test analysis

According to Briançon (2001), different test procedures could be carried out with this apparatus in dry or hydraulic conditions. Focusing on dry conditions, three test analyses were adopted.

- 1) **Standard analysis.** In accordance with ISO 12957-2, the displacement of the upper box ( $u_B$ ) is measured while the plane is inclined.
- 2) **Force analysis.** It is measured the force required to hold back the upper box ( $F$ ) during the inclination of the plane.
- 3) **Combined analysis.** Both force and displacement are measured. The dispositive is set so the force required to hold back the box is taken only after the upper box has slid 50 mm. In such conditions, the upper box slides at least 50 mm without being retained and ISO 12957-2 is respected.

As the plane is inclined, it is possible to measure:

- 1) the displacements variations of the upper box ( $u_B$ ),
- 2) the displacements variations of the geosynthetic layers ( $u_G$ ),
- 3) the force required to hold back the upper box ( $F$ ), and
- 4) the plane's angle of inclination ( $\beta$ ).

Figure 4.6 illustrates the sensors configuration during each case of analysis and depending on the attachment disposal of the upper geosynthetic. In the standard analysis, case a, the displacement of the upper box is measured. In the standard analysis, case b, the displacements of the geotextile and the upper box are measured. Since the geotextile is not tied to the box, it is possible to occur a displacement between the upper box and the geotextile. To monitor this compartment the displacement of the box ( $u_B$ ) is taken but, in this case, the main measure is indeed  $u_G$ . For both force and combined analysis, the configuration of sensors is similar except for the length of the cable attached to the force sensor. In combined analysis, this cable must be equal or greater than 50 mm (Figure 4.7).

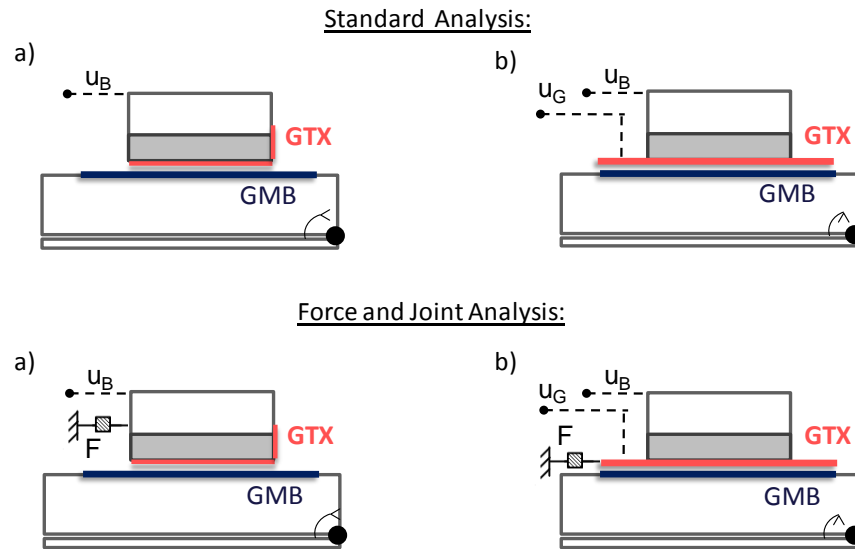


**Figure 4.6 – Configuration examples for each case of analysis. In the standard analysis, the upper box is free to slide, in the force and combined analysis, the upper box is held by the dynamometer’s cable.**

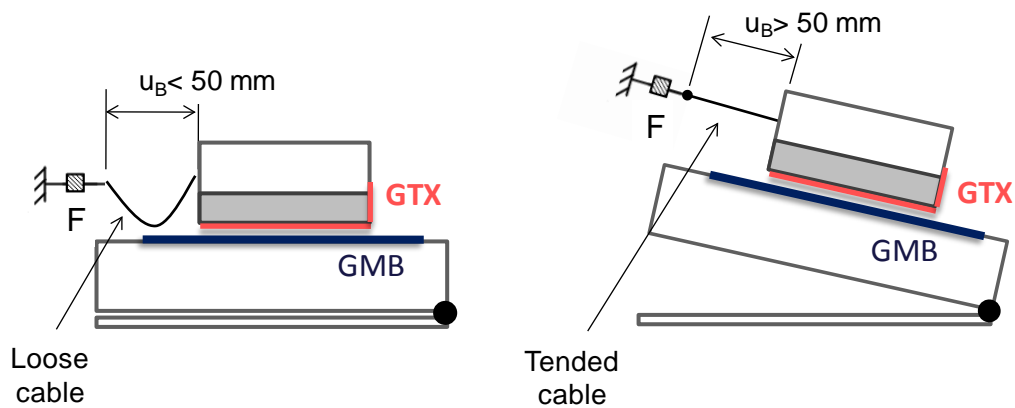


**Figure 4.7 – Sketch of the combined analysis mechanism.**

### 4.2.3 Standard Analysis

This test provides the inclination of the plane angle corresponding to the slide movement between the geosynthetic layers and enables the calculation of the interface friction angle. Figure 4.8 presents the free body diagram for the standard procedure.

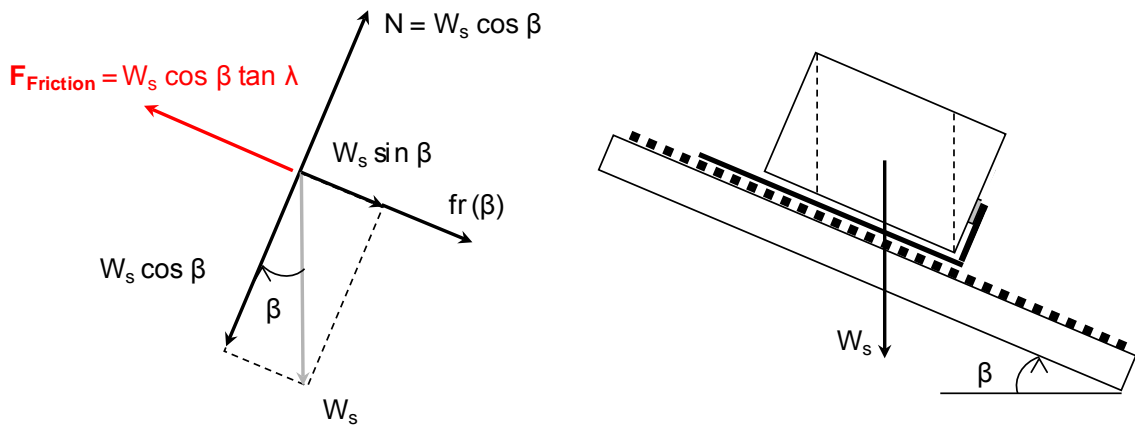


Figure 4.8 - Free body diagram for standard procedure

The friction angle is calculated considering (Figure 4.8):

$$W_s \sin \beta + fr(\beta) = W_s \cos \beta \tan \beta \quad (4.1)$$

$$\tan \lambda = [W_s \sin \beta + fr(\beta)] / (W_s \cos \beta) \quad (4.2)$$

Where  $\lambda$  is considered a function representing the friction behavior and can be determined in the function of inclination  $\beta$ . The friction angle of the interface will be named  $\Phi$ .

Equation (4.2) was written regarding a static analysis and taking into account the weight of the soil contained in the upper box ( $W_s$ ), the plane inclination angle ( $\beta$ ) and the force to hold back the empty upper box ( $fr(\beta)$ ).

#### 4.2.4 Force Analysis

In this test, the dynamometer is connected to the upper box and is attached to a fix point on the inclined plane. The goal is to measure the force required to hold back the upper box during the plane inclination.

The analysis of the body diagram (Figure 4.9) for the tested interfaces leads to Equation 4.3, the same equation found by Briançon (2001).

$$\tan \lambda = \frac{W_s \sin \beta + fr(\beta) - F}{W_s \cos \beta} \quad (4.3)$$

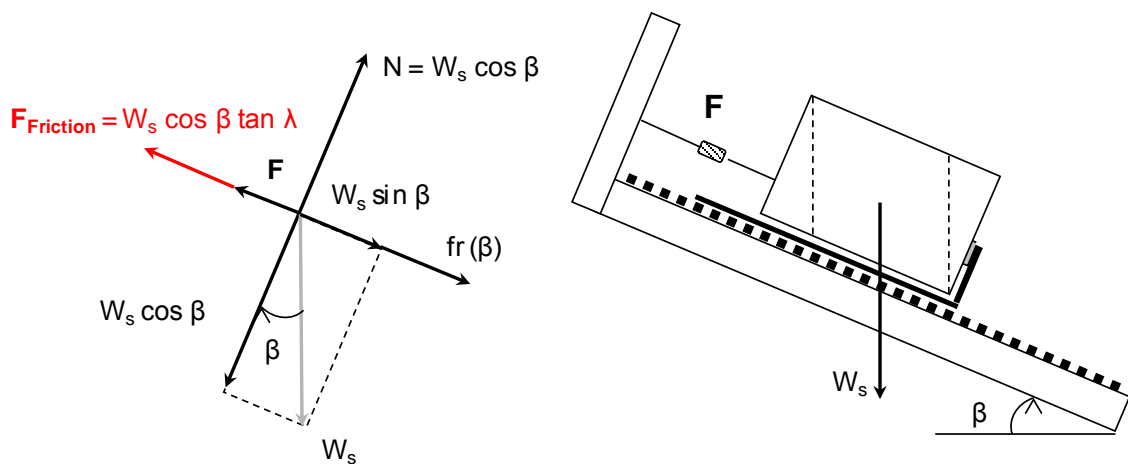


Figure 4.9 - Balance of efforts for force analysis.

#### 4.2.5 Combined Analysis

In this test, both force and displacement sensors are connected. At the beginning of the experiment, the force sensor is set so that the upper box can slide freely at least 50 mm before being retained. Hence, Equation 4.3 is applied to this test considering the force  $F$  null for displacements below 50 mm (Equation 4.2).

#### 4.2.6 Test details

According to Equations 4.2 and 4.3, in order to calculate the friction angle, it is necessary to determine the force required to hold back the empty box ( $fr(\beta)$ ). As mentioned before, it was supposed that the rails support the weight of the empty box and, the geosynthetics layers support the weight of soil.

To determine how function  $fr$  varies with the inclination angle  $\beta$ , it was performed a reference test using the analysis of force. Following, a function  $fr(\beta)$  was calculated and it was assumed that this relation would remain the same in each test subsequently performed (Figure 4.10).

The upper box was filled with sand to assure a normal stress of, approximately, 5 kPa. The incertitude in determining the mass of soil was not ideal (approximately 10% of weight of soil). This is due to the procedure adopted for measurement. The sand was placed in a bag and the conjunct sand plus the bag were weighted. The sand was then removed from the bag and thrown into the upper box. During this procedure a certain amount of sand was lost. Also, during trials, a small amount of sand escaped from the upper box.

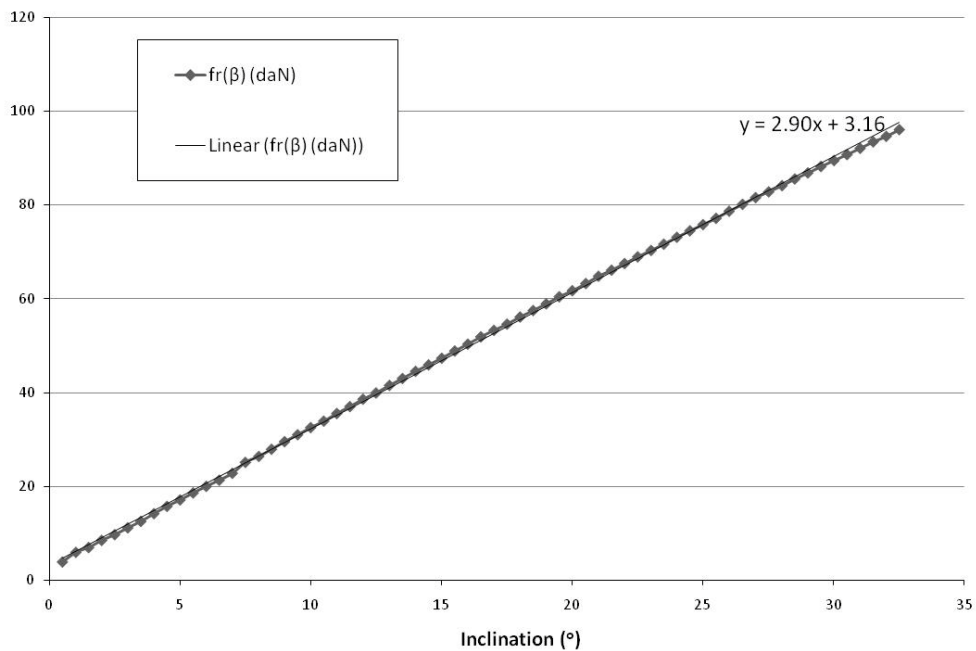


**Figure 4.10 – Determination of the linear function  $fr(\beta)$**

Regarding the use of sand, it was not controlled the compaction, the particles gradation, or the humidity of the material. The soil was uniformly distributed inside the box till filling it up to an average height of 30 cm, which was equivalent to 500 kg, approximately.

Though it was not possible to quantitatively estimate it, the use of sand can interfere in the friction behavior of the geotextile beneath it, especially in those less tick ones.

During the inclination of the plane, the component of weight force acting on the geosynthetic layer is reduced. In this context, and to make sure that the greatest part of the soil weight is transferred to the geosynthetic layer when the box slide begins, the walls of the upper box were adjusted for each interface case studied. As a result of this adjustment, Equations 4.2 and 4.3 become more realistic, since it was assumed a perfect transfer of efforts from the sand to the geosynthetic layer.

In addition, it has not been considered the effects of the movement of the sand inside the box during the experiment and the resulting differences of pressure on the layers beneath the soil.

Parameters such as temperature and humidity of air were not considered on tests. This consideration did not considerably affect the results because the interfaces tested involved only geosynthetics. For further tests, it is recommended to take note of these parameters. If

the study involved interfaces between soil-geosynthetics, parameters such as temperature and relative humidity would have a major weight.

As a final consideration, the procedure to measure the parameter  $\Phi_{\text{peak}}$  is not ideal. The problem is with the cable that holds back the upper box. For both force and combined analysis, in the beginning of the plane inclination, the cable is not stretched. Consequently, the box is able to slide a bit and then be held by the cable, which can affect the values measured by the dynamometer at the breaking moment.

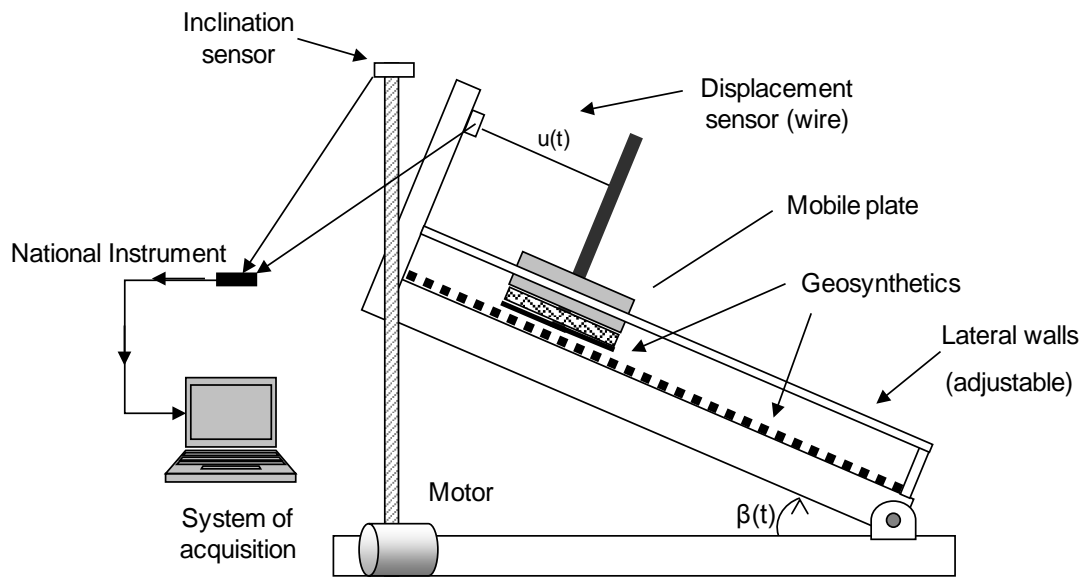
### 4.3 Small dimension apparatus (A)

#### 4.3.1 Description of the apparatus

The small dimension inclined plane (Figure 4.11 and Figure 4.12) was developed to study the behavior of geosynthetics layers on slope and through dynamic conditions (REYES RAMIREZ, 2003). In this context, a few adaptations were implemented on this inclined plane.

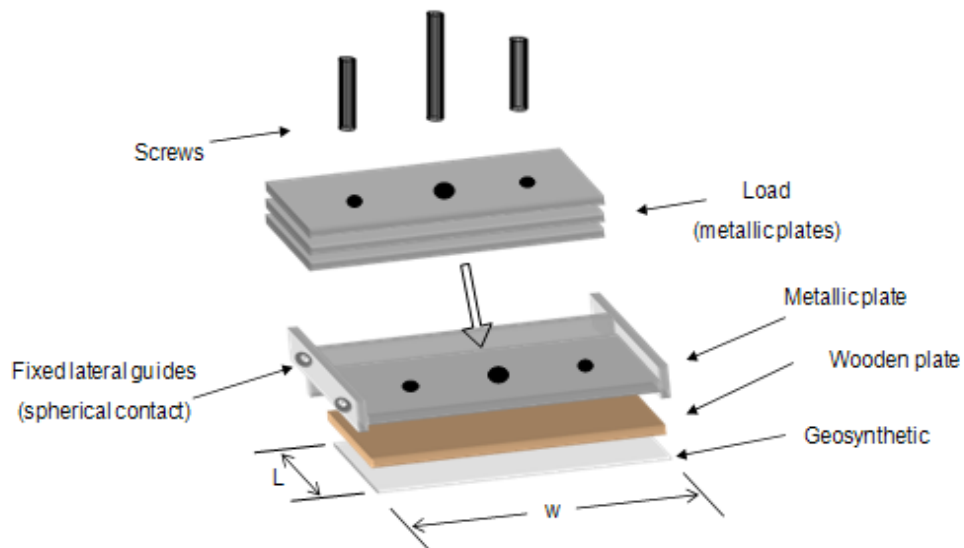


Figure 4.11 – Small dimension inclined plane



**Figure 4.12 - Sketch of the small dimension inclined plane**

For instance, the dimension of the upper and lower boxes was modified in order to increase the displacement length on the slope direction (GOURC AND REYES RAMIREZ, 2004). Also, the geosynthetic-geosynthetic interface case analysis was simplified. The upper box filled with soil was replaced by a mobile plate dispositive (Figure 4.13).



**Figure 4.13 – Mobile plate dispositive of the small inclined plane.**

The mobile plate is composed of a geosynthetic sample glued on a wooden plate ( $l = 180$  mm and  $w = 700$  mm), a metallic plate with fixed lateral guides and three loads of metallic plates (Figure 4.14). In total, the mobile plate weighs  $(62 \pm 1)$  kg.

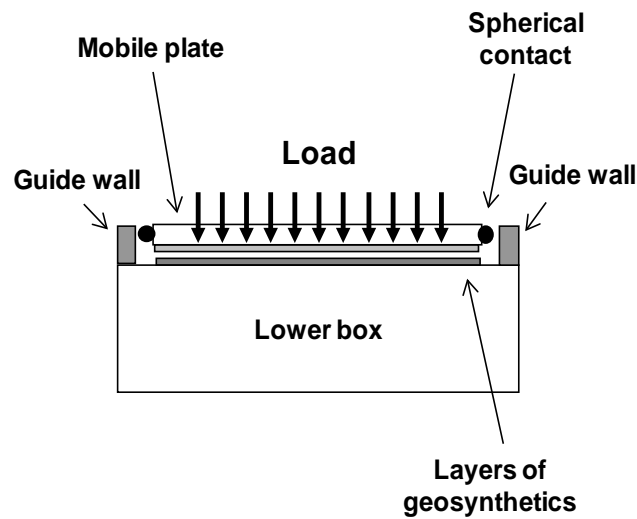


**Figure 4.14 - Load transfer to geosynthetics**

Theoretically, the configuration of lateral guides and the spherical contact enables a total transmission of normal stress to the geosynthetic interface and ensures a non deviated displacement in relation to the slope. Also, the guidance system is assumed without friction.

The dimensions of the lower box are 1.3 m in length ( $l$ ), and 0.8 m in width ( $w$ ), and the geosynthetic layer (geomembrane) can be attached to it trough anchoring grips.

The climb velocity of the plane can be controlled and varies between  $0.5-4.0^\circ/\text{min}$ . The experiment was set for a fixed rate of  $2^\circ/\text{min}$  but due to some problems with the system, the actual rate varied between  $1.1$  and  $1.4^\circ/\text{min}$ .

As a final point, the recording rate of the system of acquisition could be chosen (it was frequently used  $0.1$  s).

### **4.3.2 Test analysis**

According to Reyes Ramirez (2003), two types of tests were defined to determine the characteristic friction angles.

- 1) **Test dyn 1:** the displacement of the plate is measured during the plane inclination ( $\beta$ ) till  $\beta$  was equivalent to  $\beta_s$ .
- 2) **Test dyn 2:** the upper plate is held immobile till the plane reaches a fixed angle greater than  $\beta_s$ , then the plate is loosed free to slide at a fixed inclination angle.

Where, parameter  $\beta_s$  stands for the angle of inclination on non-stabilized sliding. This parameter characterizes the beginning of the uniformly accelerated movement, proposed by Reyes Ramirez & Gourc (2003).

Both types of tests require a dynamic analysis of efforts. As a result, the analysis of the free body diagram shown in Figure 4.15 leads to

$$\tan \Phi = \frac{(m_T g \sin \beta - m_T \gamma - T_{\text{Sensor}})}{m_T g \cos \beta} \quad (4.4)$$

With  $W_T$  standing for total weight of the mobile plate,  $\beta$  for inclination angle of the plane,  $\Phi$  for friction angle,  $\gamma$  for acceleration of the plate during instant  $t$ ,  $g$  for acceleration due to gravity,  $T_{\text{Sensor}}$  for traction force due to the displacement sensor and  $m_T$  for the total mass of the plate. This equation was deduced in accordance with Reyes Ramirez (2003).

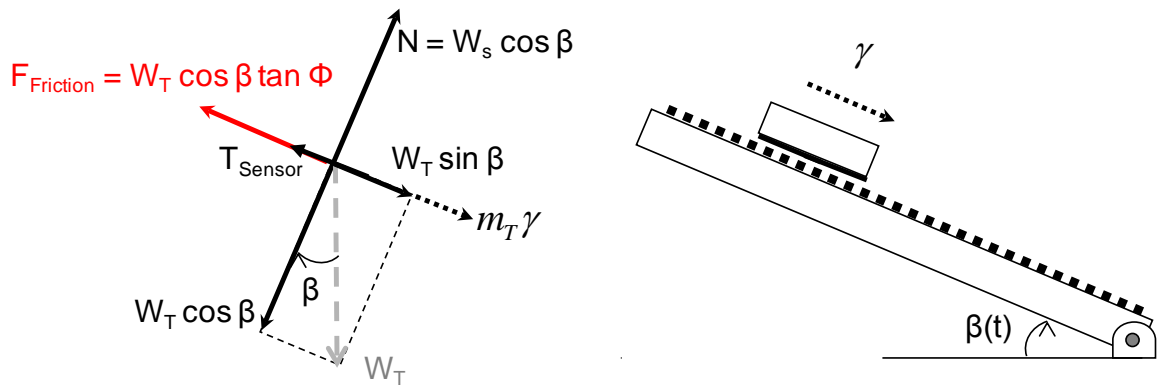


Figure 4.15 – Body diagram for small dimension apparatus

It was assumed that, since the lateral contact of the superior box is a simple ball contact, there is no friction due to the guidance system. Also, the acceleration is assumed parallel to the inclined plane slope and, for inclination angles  $\beta$  smaller or equal to  $\beta_s$ , the acceleration ( $\gamma$ ) is supposed to be null. (REYES RAMIREZ, 2003)

According to the manufacture of the displacement sensor,  $T_{\text{Sensor}}$  is equal to 6.7 N. However, the analysis of Equation 4.4 for a  $\beta$  interval between  $0^\circ$  and  $45^\circ$  leads to the conclusion that  $T_{\text{Sensor}}$  can be neglected.

Hence, the resulting equation from active effort analysis and for  $\beta$  equal or inferior to  $\beta_s$  is reduced to Equation 4.5, a static interpretation.

$$\tan \Phi^{\text{Static}} = \tan \beta \quad (4.5)$$

For  $\beta$  higher than  $\beta_s$  and considering that the upper box reaches a *uniformly accelerated movement*, Equation 4.4 is simplified to:

$$\tan \Phi^{\text{Dyn}} = \tan \beta - \gamma / g \cos \beta \quad (4.6)$$

In this context, in test type Dyn 1, Equation 4.5 is used to determine the friction angle  $\Phi_0$  and  $\Phi_{50}$ . Equation 4.6 is used to determine  $\Phi^{\text{lim}}$  in tests dyn 1 and dyn 2.

To standardize the values chosen for  $\Phi_0$ , and in accordance with the definition presented by Gourc and Reyes Ramirez, 2004, this angle was considered correspondent to a box displacement of 5 mm. In addition, angle  $\Phi_{50}$  is the friction angle corresponding to the box relative displacement of 50 mm.

### 4.3.3 Test details

During the performance of the tests using this inclined plane, some difficulties were encountered, especially regarding the guidance system. For example, the adjustment of the lateral walls was tricky, the walls were rusty and damaged; and the fixed lateral guides were no longer parallel. For this reasons, the consideration adopted (guides without friction) has often became inappropriate. As the mobile plate moved, the plate deviated from the main slope, the spherical contacts often shocked the plane lateral walls and the movement was slowed down. Consequently, the determination of the velocity and acceleration was significantly affected.

Along the trials, four types of guidance system (Figure 4.16) were used to try to minimize the guide friction:

- Type  $\alpha$ : corresponds to the original system and presented the setbacks explained.

- Type  $\beta$ : two spherical balls (right ones) were removed. This feature does not ensure the alignment of displacement and the plane main slope but, whenever the box did not touch the guides, the determination of velocity and acceleration was not compromised. (Figure 4.17)
- Type  $\gamma$ : two spherical balls and one lateral wall (on the right side) were removed. Similar to type  $\beta$  but with a bigger distance between the guide and the wall.
- Type  $\delta$ : similar to type  $\alpha$  except for the spherical contacts. In this case the contacts can be regulated to compensate the non-parallelism of the fixed lateral guide. (Figure 4.18)

The recommended configuration was the last one to be implemented: type  $\delta$ .

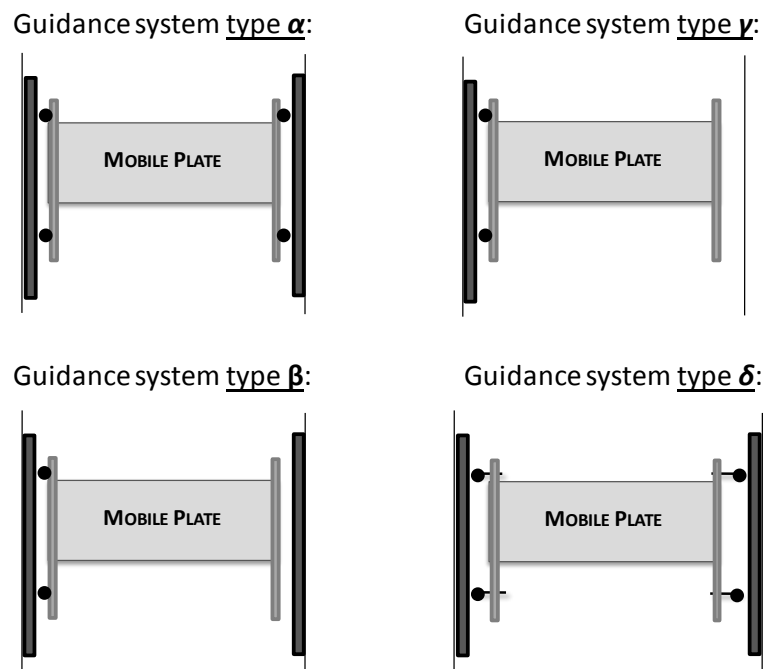


Figure 4.16 – Configuration examples for the guidance system

It is important to note that any of these features interferes on the determination of  $\Phi_0$  and  $\Phi_{50}$ . The movement of the mobile plate was only affected after a displacement of approximately 100 mm.

Finally, to compensate the rustiness and damage on lateral walls, a thin layer of grease was applied on it.

Parameters such as temperature and humidity of the environment were not taken into account. The gravity was supposed equal to  $9.8 \text{ m/s}^2$  for dynamic calculation.



**Figure 4.17 – Mobile plate on configuration type  $\beta$**



**Figure 4.18 – Mobile plate on configuration type  $\gamma$**

#### **4.4 Geosynthetics**

The material used for the trials are shown in Table 4.1 and Table 4.2. More details and specifications are in Annex A, in Figure 4.19 and in Figure 4.20.

**Table 4.1 – Geosynthetics characterization.**

Geotextiles	Notation	Thickness (mm)
Nonwoven Needle Punched reinforced with PET wires biaxial PEC 75/75	Rnp	2.6
Nonwoven Needle Punched for protection, surface density of $40 \text{ g/m}^2$	nnp40	3.4
Nonwoven Needle Punched and calandered Geodren	nnpC	1.4
Nonwoven Heat-Bounded SF56	HB	0.57

**Table 4.2 – Geosynthetics characterization.**

Geomembranes	Notation	Thickness (mm)
High Density Polyethylene	HDPE	1.5
Polyvinyl Chloride	PVC	1.5
Polypropylene	PP	1.0
Ethylene Propylene Diene Monomer	EPDM	1.2

As a final point, the geotextiles were positioned for tests on their longitudinal direction.

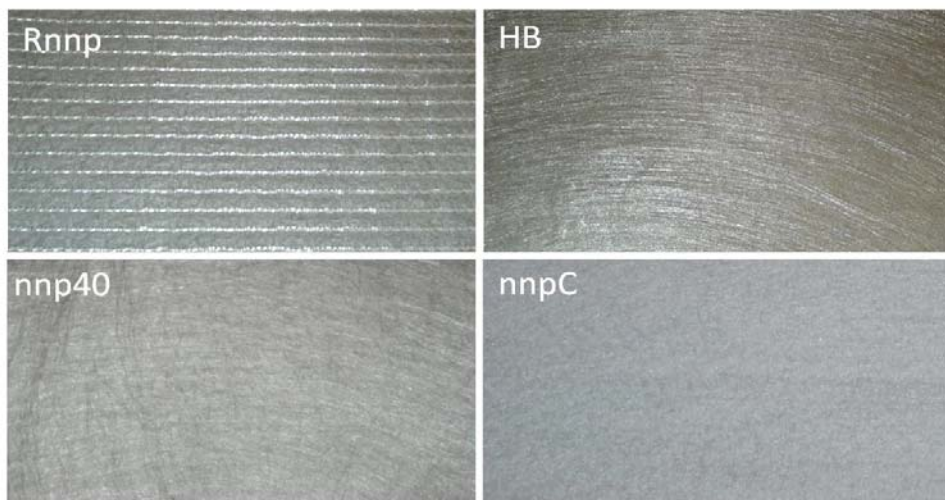


**Figure 4.19 – Geotextiles used for trials.**

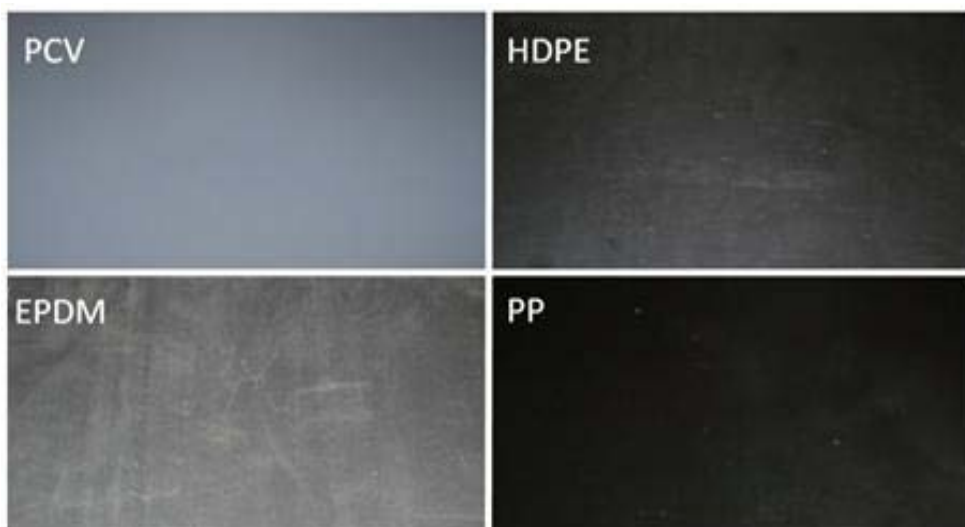


**Figure 4.20 - Geomembranes used for trials.**

## 4.5 Sensors

Table 4.3 and Table 4.4 give the specifications of the sensor used in each type of inclined plane.

**Table 4.3 - Information about the sensors used on inclined plane A.**

<i>Inclined Plane A</i>		
<b>Sensors</b>	<b>Type</b>	<b>Model</b>
Displacement	Unimeasure Position Transducer	PA-60
Inclination	HL Planar Technik Inclinometer	NS-45/V
System of acquisition	National Instruments USB	16 inputs

**Table 4.4 - Information about the sensors used on inclined plane B.**

<i>Inclined Plane B</i>		
<b>Sensors</b>	<b>Type</b>	<b>Model</b>
Force	GEFRAN	TU K 5C
Displacement	GEFRAN LVDT	PCM275E
Displacement	SCAIME	PT1MA-20-UP-420E
Inclination	Sensorex	42724

## 4.6 Notation for tests

Each test was identified as showed in Figure 4.21.

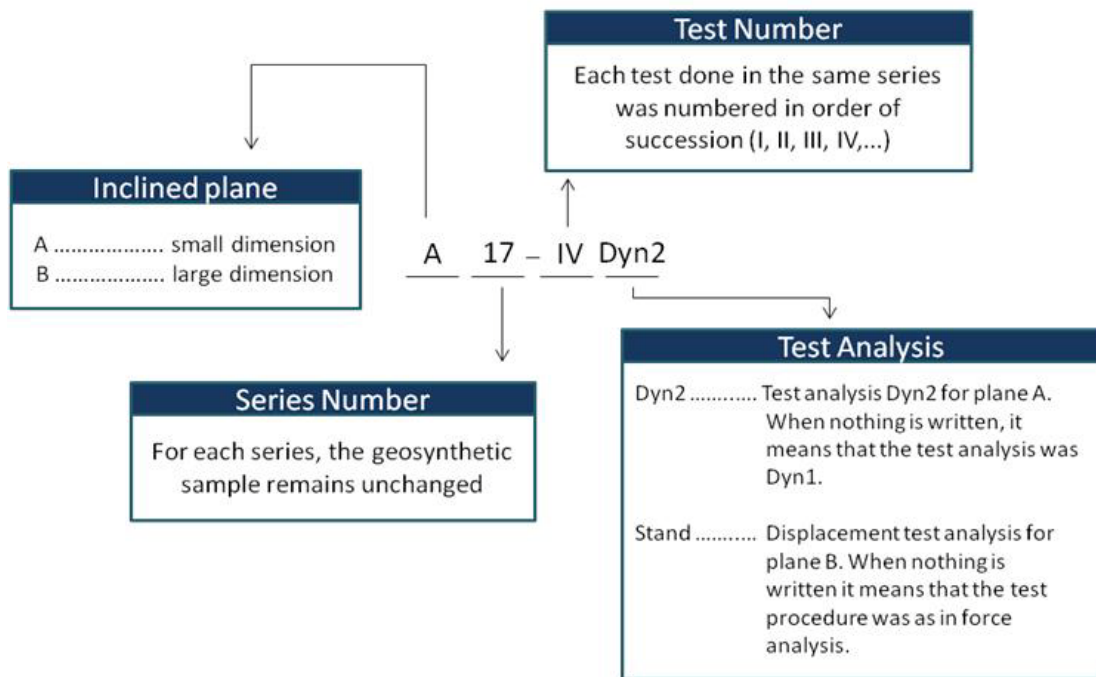


Figure 4.21 – Model of identification of performed tests

## 4.7 Interfaces tested

In total, 10 types of interfaces were studied resulting in 182 tests performed (Table 4.5 and Table 4.6). Due to the time schedule, it was not possible to test all interfaces in both planes.

The interfaces were composed by a geotextile on the upper geosynthetic layer and a geomembrane on the lower layer, except for one series performed in dispositive B, between two PVC geomembranes. For each series of tests, it was used the same sample of geomembrane and geotextile.

In Table 4.5, “guides type” is in accordance with Figure 4.16. The column “materials details” were classified as *New*, *Reused* and *Reverse Side*. This classification qualifies the lower geomembrane initial conditions in each correspondent series. It is important to highlight that, due to some setbacks, the condition of reused and reverse side were necessary though they were not ideal. Also, the geomembranes reused or tested with the reverse side were in good visual conditions.

**Table 4.5 – Interfaces’ details for tests made with inclined plane A.**

Series	Interface tested	Guides Type	Materials Details	Number of tests	
				Dyn 1	Dyn 2
1	Rnnp x PVC	$\alpha$	New	4	0
2	Rnnp x PVC	$\alpha$	New	4	0
3	Rnnp x PEDM	$\alpha$	New	4	0
4	Rnnp x HDPE	$\alpha$	New	4	3
5	Rnnp x HDPE	$\alpha$	Reverse side	1	3
6	Rnnp x PVC	$\alpha$	Reverse side	2	3
7	Rnnp x PEDM	$\alpha$	Reverse side	0	6
8	HB x PVC	$\alpha$	New	3	2
9	HB x PVC	$\alpha$	New	3	2
10	nnp40 x PVC	$\alpha$	New	3	3
11	nnp40 x PVC	$\alpha$	New	3	2
13	nnp40 x PVC	$\beta$	Reused	3	2
14	nnp40 x EPDM	$\beta$	New	1	0
15	nnp40 x EPDM	$\beta$	New	3	2
16	nnp40 x PVC	$\beta$	New	4	2
17	HB x PVC	$\gamma$	Reused	3	2
18	nnp40 x PVC	$\gamma$	Reused	0	1
20	nnp40 x PVC	$\delta$	Reused	3	1
21	HB x HDPE	$\delta$	New	3	2
22	nnp40 x HDPE	$\delta$	New	3	2
23	nnp40 x HDPE	$\delta$	New	3	2
24	HB x HDPE	$\delta$	New	3	2
25	nnpC x PP	$\delta$	New	1	0
26	nnpC x PP	$\delta$	New	1	0
27	nnpC x PP	$\delta$	New	0	1
28	nnpC x HDPE	$\delta$	New	3	2
29	HB x PVC	$\delta$	New	2	2
30	Rnnp x PVC	$\delta$	New	3	2
31	Rnnp x HDPE	$\delta$	New	2	2
32	Rnnp x PP	$\delta$	New	2	0
33	Rnnp x PP	$\delta$	New	0	2
34	HB x PP	$\delta$	New	3	0
35	HB x PP	$\delta$	New	1	0
36	HB x PP	$\delta$	New	0	1
37	HB x PP	$\delta$	New	0	1

In column “number of tests”, it was specified the amount of trials made in each series, and if it was in condition Dyn1 or Dyn2. For all tests, the Dyn1 test was the first one to be performed and then the Dyn2 was used.

In Table 4.6, the “wall inclination” corresponds to the angle  $\theta$  showed in Figure 4.3; “attachment” corresponds to the configurations showed in Figure 4.5; and the “number of tests” corresponds to the number of tests made for each series and for each sort of analysis (standard, force or combined).

**Table 4.6 – Interface details for tests made with inclined plane B.**

Series	Interface tested	Weight of soil (kg)	Wall inclination ( $^{\circ}$ )	Attachment	Number of tests		
					Force	Displacement	Combined
40	Rnnp x PVC	375	0	b	5	2	-
41	Rnnp x PVC	502	25	a	3	0	-
42	Rnnp x PVC	521	25	a	5	0	-
43	Rnnp x PVC	518	25	b	3	1	-
44	PVC x PVC	516	25	a	5	1	-
45	Rnnp x HDPE	519	25	b	4	1	-
46	Rnnp x HDPE	517	25	b	3	1	-
52	nnp40 x EPDM	508	18	b	-	-	1
53	nnp40 x EPDM	508	18	b	-	-	1
73	HP x PVC	484	20	b	-	-	3
74	nnp40 x PVC	484	20	b	-	-	3
75	HB x HDPE	482	20	b	-	-	3
80	Rnpp x PP	480	20	b	-	-	4
81	HB x HDPE	476	20	b	-	-	3
82	nnpC x PP	476	20	b	-	-	3

## 4.8 Procedure for calculation of parameters

### 4.8.1 Introduction

To study the friction characteristics of a geosynthetic-geosynthetic interface, a few parameters must be determinate on each inclined plane experiment. The parameters are:

- $\Phi_{50}$ ,  $\Phi_0$  and  $\Phi^{\text{lim}}$ , for inclined plane A; and

- $\Phi_{50}$ ,  $\Phi_0$ ,  $\Phi_{peak}$  and  $\Phi_{res}$ , for inclined plane B.

Using test results from interfaces HB-PVC and PVC-PVC, each angle calculation is explained as follows.

## 4.8.2 Inclined plane A

### 4.8.2.1 Determination of $\Phi_{50}$

With the results obtained on inclined plane A, it is possible to determine  $\Phi_{50}$  by plotting the curve *Displacement vs. Inclination*.

Accordingly to Equation 4.5,  $\Phi_{50} = \beta_{Stand}$ , the plane inclination for a relative displacement of 50 mm ( $u_{50}$ ). As a result  $\Phi_{50}$  is found directly from the graph showed in Figure 4.22

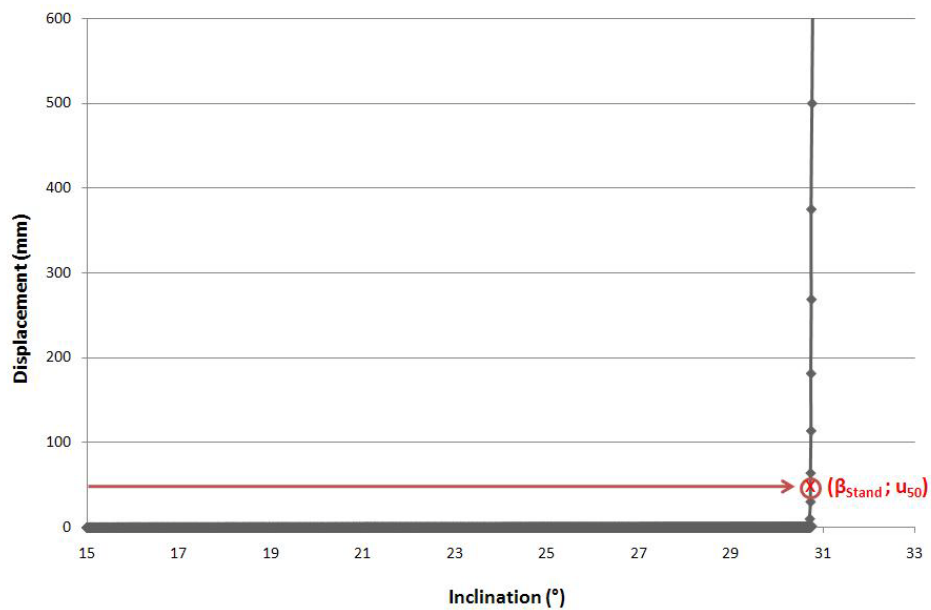


Figure 4.22 - Inclined plane test result A 17-I. Interface tested: HB x PVC.

### 4.8.2.2 Determination of $\Phi_0$

The procedure to calculate  $\Phi_0$  is similar to  $\Phi_{50}$  but with  $\beta = \beta_0$ ; where  $\beta_0$  was standardized as the plane inclination correspondent to the upper box displacement of 5 mm (beginning of the sliding movement).

### 4.8.2.3 Determination of $\Phi^{lim}$

For the entire trial made on inclined plane A, displacement was recorded as a function of time and for every 0.1 s. The diagrams in Figure 4.23 represent the evolution of the box displacement ( $u$ ) against time. From the curve *Displacement vs. Time*, it was deduced the displacement rate diagram  $v(t)$ , plotted in the same figure.

Gourc and Reyes Ramirez (2004) observed that the displacement curves consistently showed a quasi-linear period of the displacement rate as a function of the time, beginning at time  $t_i$  and lasting until  $t_{max}$ . According to their observation, this period is preceded by an intermediate period: from the beginning of the test ( $t = 0$ ), corresponding to a period where the upper box did not move, up to instant  $t_i$ , where displacement  $u$  is equal to  $u_i$ .

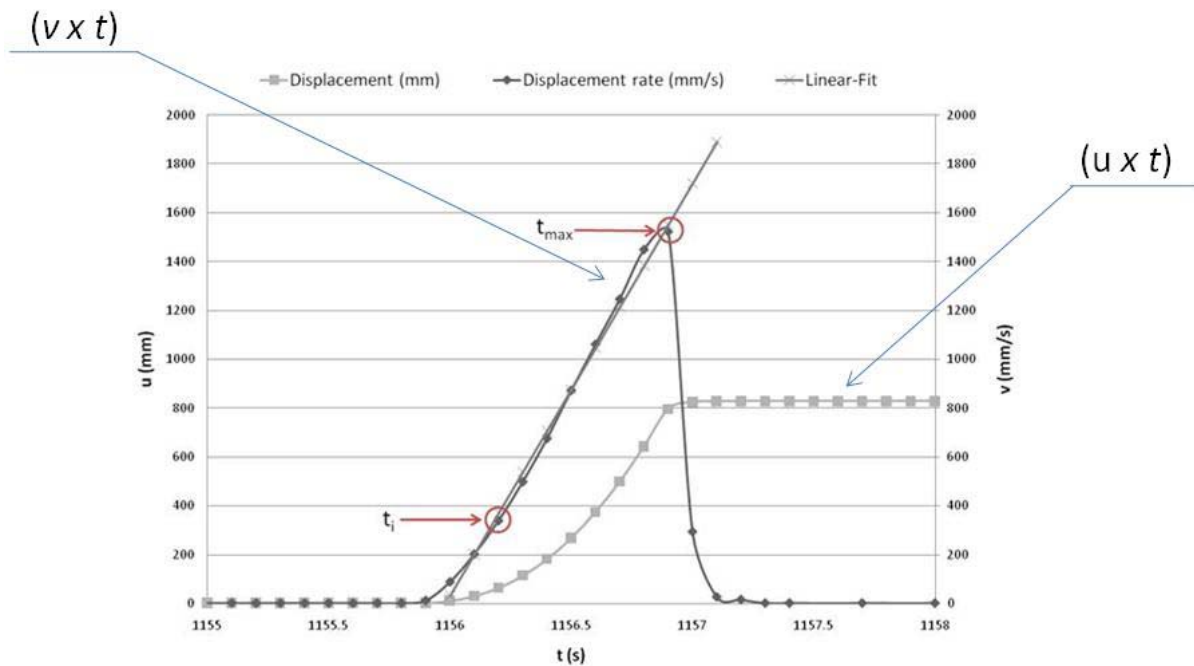


Figure 4.23 – Inclined plane test result A 17-I. Interface tested: HB x PVC.

From the displacement rate curve is possible to fit a straight curve for interval  $[t_i, t_{max}]$ . The slope of the line is equivalent to the box acceleration.

Considering Equation 4.6 and with  $\beta = \beta(t_{max})$ ,  $g = 9.81 \text{ m/s}^2$  and  $\gamma$  determined graphically, angle  $\Phi^{lim}$  is calculated.

### 4.8.3 Inclined plane B

#### 4.8.3.1 Determination of $\Phi_{50}$

With results obtained with inclined plane B (except for force analysis procedure), it is possible to determine  $\Phi_{50}$  by plotting the curve *Displacement x Inclination* (Figure 4.24).

For both displacement and combined analysis, Equation 4.2 is used to determine  $\Phi_{50}$ . From the graphic in Figure 4.24,  $\beta_{\text{Stand}}$  is found and so  $\lambda(\beta_{\text{Stand}}) = \Phi_{50}$  can be calculated.

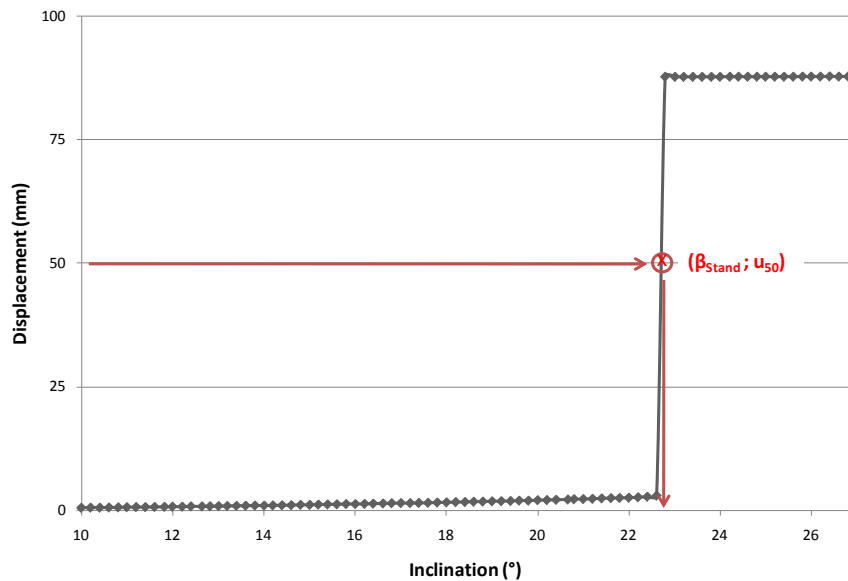


Figure 4.24 - Inclined plane test result B 73-III (combined analysis procedure). Interface tested: HB-PVC.

#### 4.8.3.2 Determination of $\Phi_0$

The procedure for calculating  $\Phi_0$  is similar to  $\Phi_{50}$  but for  $\beta = \beta_0$ ; where  $\beta_0$  was standardized as the plane inclination corresponding to the upper box displacement of 5 mm (beginning of the sliding movement).

#### 4.8.3.3 Determination of $\Phi_{\text{peak}}$

With the same test results displaced in Figure 4.24, function  $\lambda(\beta)$  is plotted (Figure 4.25).

The angle  $\Phi_{\text{peak}}$  is the first peak value of function  $\lambda$  shown in the curve *Lambda vs. Inclination*.

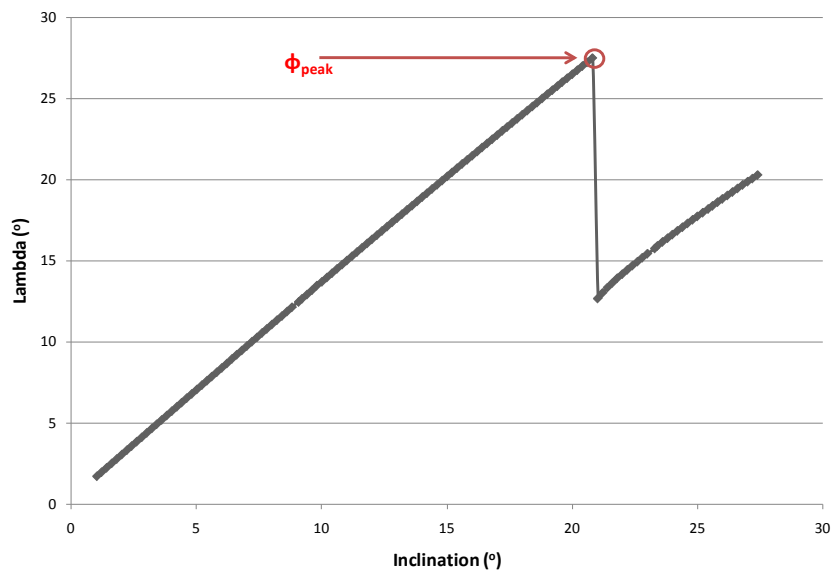


Figure 4.25 - Inclined plane test result B 73-III (combined analysis procedure). Interface tested: HB-PVC.

#### 4.8.3.4 Determination of $\Phi_{res}$

A few interfaces presented a typical behavior for the curves *Lambda vs. Inclination*. After reaching the peak value  $\Phi_{peak}$ , the function  $\lambda$  decreases with plane inclination up to a constant value (Figure 4.26). When  $\lambda(\beta)$  reaches this constant value for an inclination  $\beta$  greater than the  $\beta_{peak}$ , the term residual friction angle ( $\Phi_{res}$ ) will be applied. Numerically,  $\Phi_{res}$  is the average of  $\lambda$  values on the level.

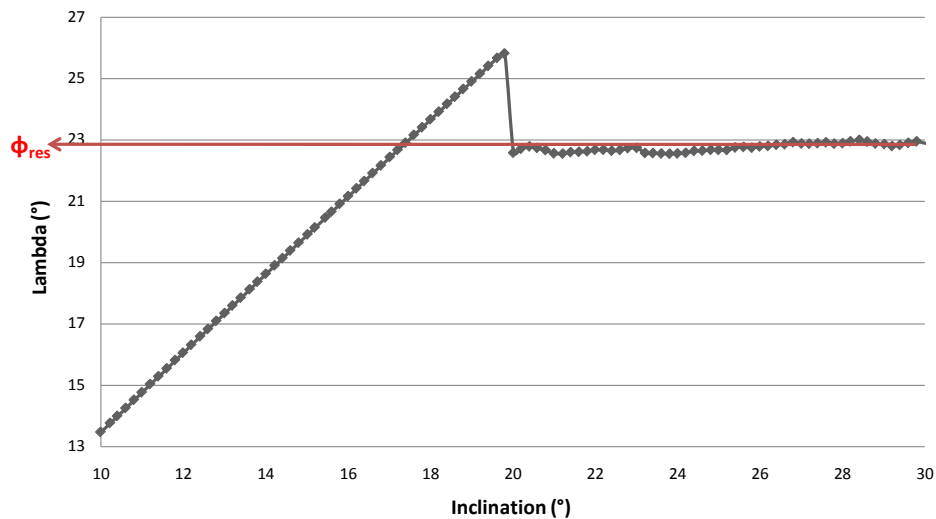


Figure 4.26 - Inclined plane test result B 44-I (force analysis procedure). Interface tested: PVC-PVC.

## 5 TEST RESULTS

### 5.1 Introduction

The tests results were divided into two distinct analyses: static and dynamic. In the static analysis, parameters such as  $\Phi_0$ ,  $\Phi_{50}$  and  $\Phi_{\text{peak}}$  were compared. The goal was to analyze whether these parameters were similar or not. In the dynamic analysis, angles  $\Phi^{\text{lim}}$  and  $\Phi_{\text{res}}$  were presented and compared.

At the end of this chapter, a summary of results is presented noting whether or not both planes can provide equivalent parameter results. Also, it is compared the dynamic with static value results.

It is important to emphasize that not all tests made with the interfaces showed in Table 4.5 and Table 4.6 offered plausible results due to difficulties and a certain amount of them were discarded. The difficulties were mostly because of the guidance system of inclined plane A. For static results, the system of guidance did not interfere in the determination of the characteristic parameters because, in none of the cases, the upper box touched the guidance lateral before a displacement of 100 mm. For dynamic analysis, however, this interference was visually discernible (during monitoring of the tests) and also graphically, despite of a noticeable change of the sliding speed.

### 5.2 Static Analysis

#### 5.2.1 Introduction

In this section, the static angles  $\Phi_0$  and  $\Phi_{50}$  found using inclined plane A are compared with  $\Phi_0$ ,  $\Phi_{50}$  and  $\Phi_{\text{peak}}$  determined using inclined plane B. Also, it is analyzed whether the interfaces presents a gradual or sudden slide behavior.

The series that are going to be analyzed in this section are in Table 5.1.

**Table 5.1 – Series of interfaces studied for the static analysis.**

<b>Interface</b>	<b>Plane A</b>	<b>Plane B</b>
<b>Rnp x PVC</b>	6, 30	40, 41, 43
<b>HB x PVC</b>	8, 9, 17, 29	73
<b>nnp40 x PVC</b>	10, 11, 13, 16, 20	74
<b>Rnp x PP</b>	32, 33	80
<b>nnpC x PP</b>	25, 26, 27	82
<b>Rnp x HDPE</b>	31	45
<b>HB x HDPE</b>	21, 24	75, 81
<b>nnp40 x EPDM</b>	14, 15	52, 53

### 5.2.2 Interface Rnp-PVC

Series A6 and A30 were performed using the inclined plane of small dimensions and with interface Rnp-PVC (Nonwoven needle punched reinforced with PET fibres and Polyvinyl Chloride). These series, represented in Figure 5.1, indicate the occurrence of a sudden slide behavior.

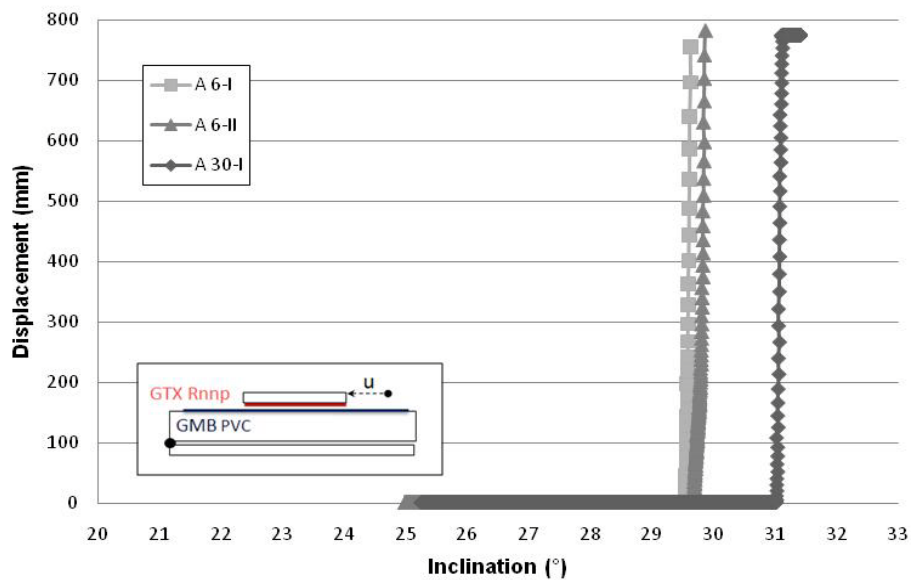


**Figure 5.1 – Curve Displacement vs. Inclination of interface Rnp-PVC, series A6, guidance systems  $\alpha$ , tested with the small dimension inclined plane.**

As shown in Figure 5.1, curves A6-I and A6-II are almost overlapping. This suggests that interface Rnp-PVC is not sensitive to abrasion, at least for a sample used twice. Unfortunately, due to lack of material and time frame, this statement was not possible to be

verified properly. It is recommended, for further tests, a deeper study of abrasion of this interface. In present analysis, test result of A6-II will be considerate valid, despite of the recommendation of ISO 12957-2:2005 to avoid repetition of samples.

The analysis of curves showed in Figure 5.1 led to the values of friction angles shown in Table 5.2. In this case,  $\Phi_0$  could be considerate equal to  $\Phi_{50}$  for each test, resulting in an average value of  $(30 \pm 1)^\circ$ .

Finally, it is important to recall that the series A6 was performed with the system of guidance  $\alpha$  while the series A30 was performed with system  $\delta$ .

**Table 5.2 – Values of friction angles  $\Phi_0$  and  $\Phi_{50}$ , series A6, interface Rnnp-PVC.**

<b>Test A</b>	$\Phi_0$ ( $^\circ$ )	$\Phi_{50}$ ( $^\circ$ )
<b>6 - I</b>	30	30
<b>6 - II</b>	30	30
<b>30 - I</b>	31	31

With the standardized inclined plane, three series were performed: B40, B41 and B43. Series B40 comprises four tests, B41 comprises three and B43, four.

The analysis of the graphic in Figure 5.2 indicates a sudden slide behavior just as for tests results made with plane A.

Tests B40-III, B41-I and II and B43-II and III was set to perform a force analysis but presented an initial displacement of 10 mm. This displacement happened because the rope that held the dynamometer was not completely stretched at the beginning of the experiment. For other tests that will be analyzed ahead, this same problem occurred. Hence, all trials set for a force analysis were, indeed, made in the configurations of a combined analysis.

Test B43-I was intentionally set with the rope free to stretch more than 100 mm. The upper box slipped three times at different moments revealing two big levels (stick slip pattern), the first starting at  $20^\circ$  and the second one starting around  $25^\circ$ . Remarkably,  $\beta$  equals to  $25^\circ$  is the initial slide angle of test B43-II and III. This result exemplified a jerky slide behavior but is unclear if all other first tests of a series present the same behavior because the data acquisition were ended as soon as the upper box stop sliding.

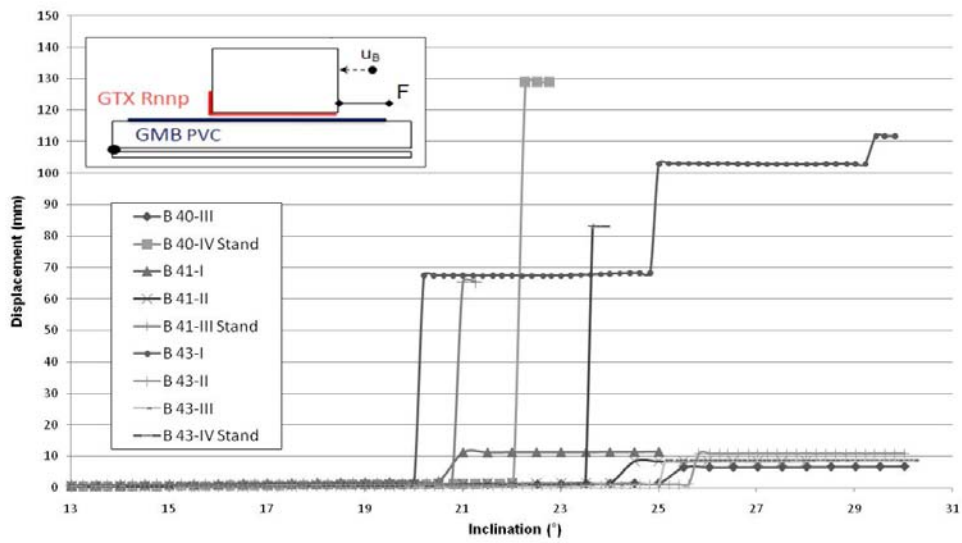


Figure 5.2 – Curve Displacement vs. Inclination of interface Rnnp-PVC, series B40, B41 and B43, tested with the standard dimension inclined plane.

Test B40-I and II are not shown in Figure 5.2, because they were erroneously performed without installing the displacement sensor.

Figure 5.3 and Figure 5.4 show the graphics *Lambda vs. Inclination* for the studied series.

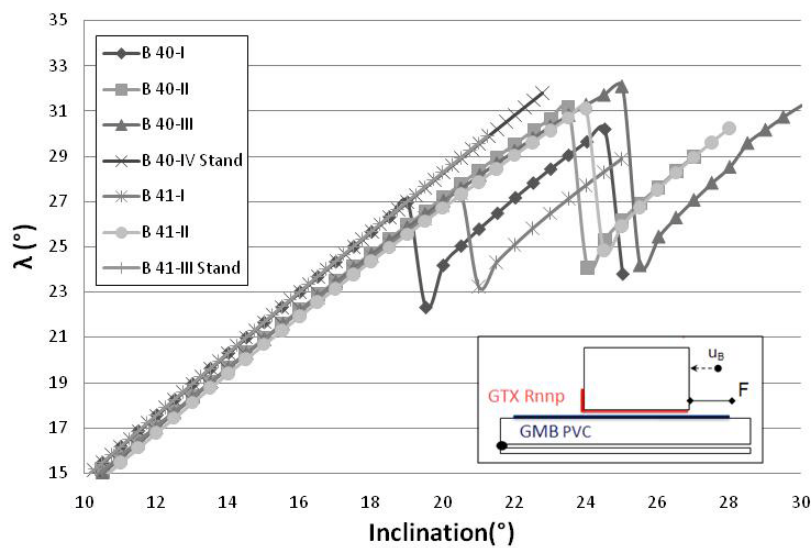
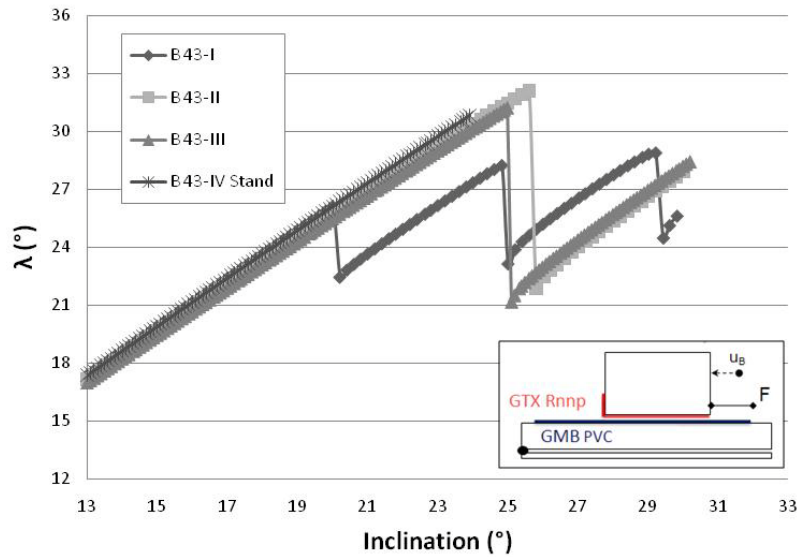


Figure 5.3 – Curve Lambda vs. Inclination of interface Rnnp-PVC, series B40 and B41, tested with the standardized dimension inclined plane.

A peculiar behavior was noticed for all tests made with PVC geomembranes (other tests using this material presented this similar aspect). The first test of a series (with a new sample) presented a reduced static friction angle ( $\Phi_0$ ,  $\Phi_{50}$  and  $\Phi_{peak}$ ) when compared with the other tests of the same series. In other words, after being tested for the first time, there was a gain of

the resistant shear stress and the value of friction values increased. For this reason, the first test of a series will be considered apart.



**Figure 5.4 – Curve Lambda vs. Inclination of interface Rnnp-PVC, series B43, tested with the standard dimension inclined plane.**

Despite of this clear behavior in tests made with plane B, results found from experiments using plane A did not present such feature. This can be justified by the initial condition of geomembrane samples. They were prepared and stored in the laboratory where plane B was installed. But, since the planes were installed in different laboratories, it was necessary to transport the samples from one place to another, which resulted in a different initial condition of friction of the samples.

Table 5.3 presents the first test results of series B40, B41 and B43. Table 5.4 presents the friction angles of other tests of series mentioned before.

**Table 5.3 – Values of friction angle  $\Phi_{peak}$ , tests B40-I, B41-I and B43-I, interface Rnnp-PVC.**

Test	$\Phi_{peak,I}$ (°)
<b>B40-I</b>	27
<b>B41-I</b>	27
<b>B43-I</b>	28

**Table 5.4 – Values of friction angles  $\Phi_0$ ,  $\Phi_{50}$  and  $\Phi_{\text{peak}}$ , series B40, B41 and B43, interface Rnnp-PVC.**

Test	$\Phi_0$ (°)	$\Phi_{50}$ (°)	$\Phi_{\text{peak}}$ (°)
<b>B40-II</b>	-	-	31
<b>B40-III</b>	-	-	32
<b>B40-IV</b>	31	31	-
<b>B41-II</b>	-	-	31
<b>B41-III</b>	29	29	-
<b>B43-II</b>	-	-	32
<b>B43-III</b>	-	-	31
<b>B43-IV</b>	30	30	-

In this case,  $\Phi_0$  could be considered equal to  $\Phi_{50}$  for each test, resulting on an average value of  $(30 \pm 1)^\circ$ . As for  $\Phi_{\text{peak}}$ , its average value was  $(31 \pm 1)^\circ$ . Hence, the correlation can be established:

$$\Phi_{\text{peak},B} > \Phi_{0,B} = \Phi_{50,B} \quad (5.1)$$

Table 5.5 contains the summary results of interface Rnnp-PVC with the average values found for static angles and the number of tests used to calculate this average. It was not taken into account the results of tests B40-I, B41-I and B43-I.

**Table 5.5 – Summary values of friction angles  $\Phi_0$ ,  $\Phi_{50}$  and  $\Phi_{\text{peak}}$ , interface Rnnp-PVC.**

Test	$\Phi_0$ (°)	#	$\Phi_{\text{stand}}$ (°)	#	$\Phi_{\text{peak}}$ (°)	#
<b>A - 6</b>	30	2	30	2	-	-
<b>A - 30</b>	31	1	31	1	-	-
<b>B - 40</b>	30	2	30	2	31	5
<b>B - 43</b>	30	1	30	1	32	3

The values of the friction angles ( $\Phi_0$ ,  $\Phi_{50}$ ,  $\Phi_{\text{peak}}$ ) were very similar and could be written as:

$$\Phi_{\text{peak}} > \Phi_{0,B} = \Phi_{50,B} = \Phi_{0,A} = \Phi_{50,A} \quad (5.2)$$

### 5.2.3 Interface HB-PVC

Four series of tests were performed with interface HB-PVC (Nonwoven Heat-Bounded and Polyvinyl Chloride) and with inclined plane type A. Each of this series consists of three tests “dyn 1” and two tests “dyn2” executed sequentially.

The analysis of the results evidenced the interface sensibility to abrasion. This could be inferred with series A8 (Table 5.6) where every new test accomplished resulted in a reduction of the friction angle values. The same behavior was observed in series A9, A17 and A29.

**Table 5.6 – Values of friction angles  $\Phi_0$  and  $\Phi_{50}$ , series A8, interface HB-PVC, guidance system type  $\alpha$ .**

<b>Test</b>	<b><math>\Phi_0</math> (°)</b>	<b><math>\Phi_{50}</math> (°)</b>
<b>A8-I</b>	33	33
<b>A8-II</b>	28	28
<b>A8-III</b>	27	27

Visually, it was the HB geotextile that suffered most to abrasion. At the end of each experiment, it was noticeable that HB was pretty damaged, presenting a lot of loose wires.

Despite test A17 has being performed using reused sample of PVC the first test of this series did not present such different values of  $\Phi_0$  and  $\Phi_{50}$  which reinforces the supposition above that it was the HB geotextile that suffered the most.

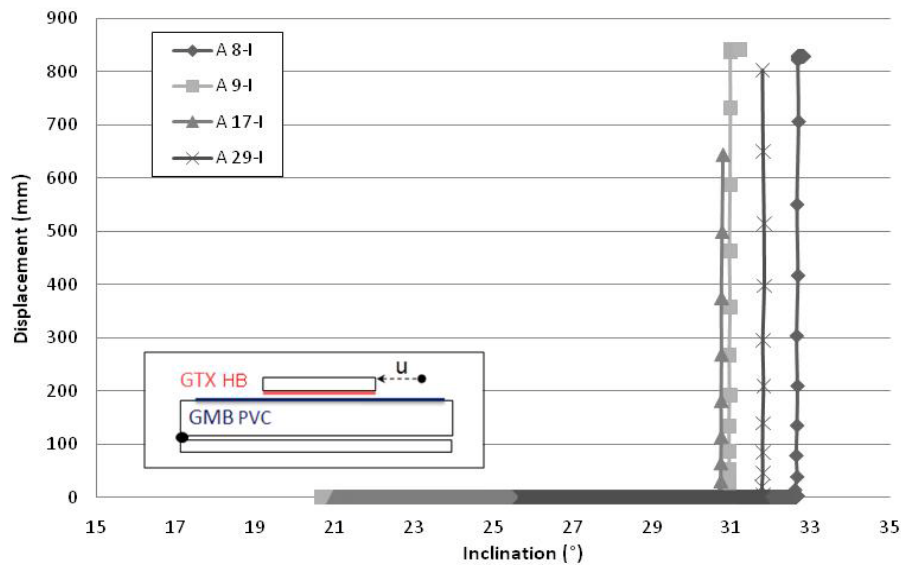
Taking into account the abrasion sensitivity of the interface, only the first test of each series was considered to analysis (Table 5.7).

Figure 5.5 presents the descendent behavior of the upper plate during the inclination of the plane. It is important to recall that series A8 and A9 were tested using guidance system  $\alpha$ , series A17 was tested using guidance system  $\gamma$  and A29 using  $\delta$ .

**Table 5.7 – Values of friction angles  $\Phi_0$  and  $\Phi_{50}$ , series A8, A9, A17 and A29, interface HB-PVC.**

<b>Test</b>	<b><math>\Phi_0</math> (°)</b>	<b><math>\Phi_{50}</math> (°)</b>
<b>A 8-I</b>	33	33
<b>A 9-I</b>	31	31
<b>A 17-I</b>	31	31
<b>A 29-I</b>	32	32

As observed in Figure 5.5, this interface presented a sudden slide movement. Also, the average values for both  $\Phi_0$  and  $\Phi_{50}$  was  $(32 \pm 1)^\circ$ .



**Figure 5.5– Curve Displacement vs. Inclination of interface HB-PVC, series A8, A9, A17 and A29, tested with the small dimension inclined plane.**

Series B73 was performed with interface HB-PVC and with the standardized inclined plane. As exposed in Figure 5.6 and in Table 5.8, tests B73-I and II presented satisfactory results regarding repeatability of values. However, friction values found in B73-III did not match with others in this series presenting higher values for all three angles. Also, this interface showed a gain in the value of friction angle in the third test performed.

For each test, the average values of  $\Phi_0$  and  $\Phi_{\text{peak}}$  is  $(28 \pm 1)^\circ$ , angle  $\Phi_{50}$  presented an average value equals to  $(29 \pm 1)^\circ$ . This value was one degree higher than the others static values because this average was calculated using a smaller number of tests. As a result, this average value is inconclusively when compared to  $\Phi_0$  and  $\Phi_{\text{peak}}$ .

**Table 5.8 – Values of friction angles  $\Phi_0$ ,  $\Phi_{50}$  and  $\Phi_{\text{peak}}$ ; series B73, interface HB-PVC.**

Test	$\Phi_0$ (°)	$\Phi_{50}$ (°)	$\Phi_{\text{peak}}$ (°)
<b>B73-I</b>	28	28	28
<b>B73-II</b>	28	-	28
<b>B73-III</b>	30	30	30

Test B73-II was not set properly, and the upper box free movement was interrupted before the displacement  $u$  has reached 50 mm. For this reason,  $\Phi_{50}$  could not be determined.

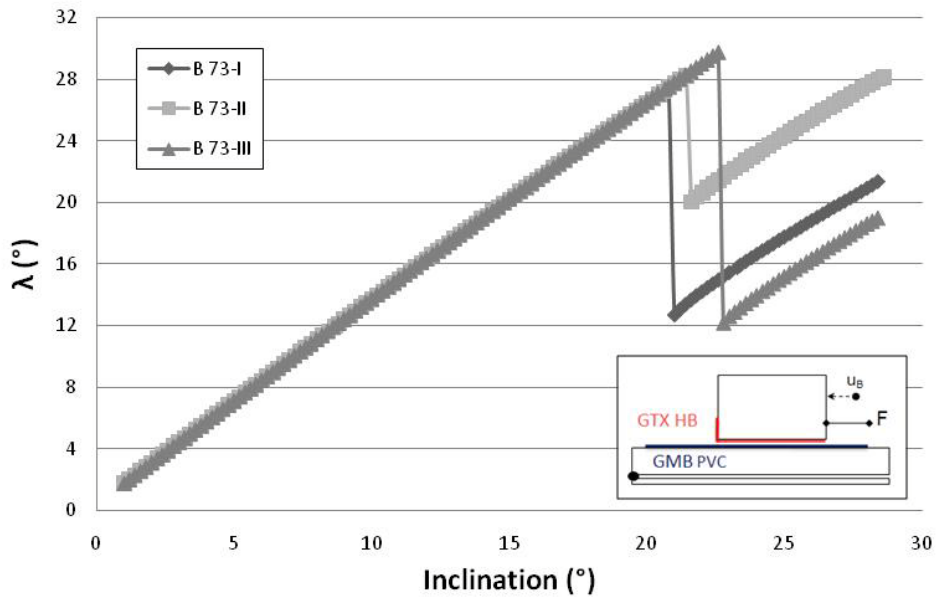


Figure 5.6 – Curve Lambda vs. Inclination of interface HB-PVC, series B73, tested with the standardized inclined plane.

The abrasion was not as evident as in the series executed using the small inclined plane. As for the sudden slide behavior, Figure 5.7 illustrates the same kind for plane A.

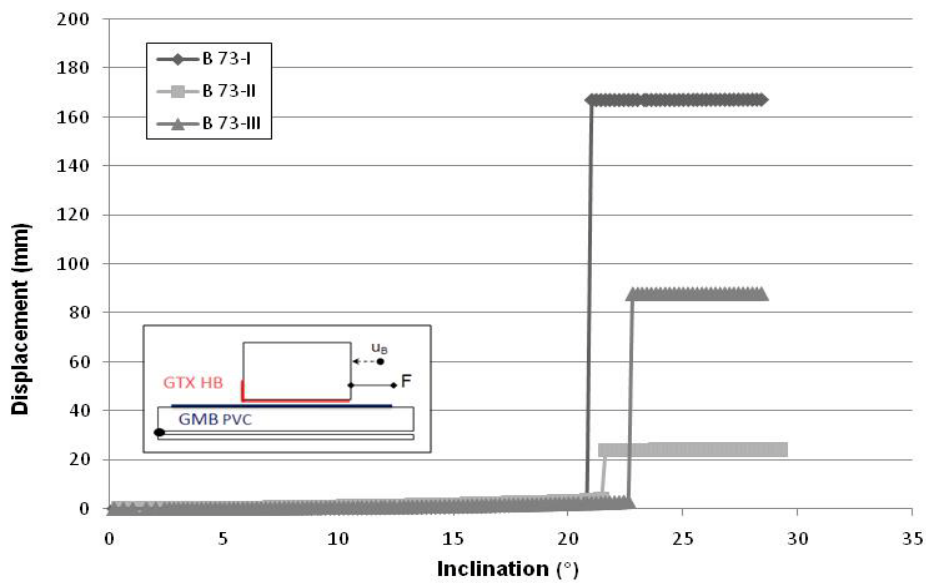


Figure 5.7 – Curve Displacement vs. Inclination of interface HB-PVC, series B73, tested with the standardized inclined plane.

Table 5.9 combines the average values of friction angles found for interface HB-PVC.

Table 5.9 – Summary values of friction angles  $\Phi_0$ ,  $\Phi_{50}$  and  $\Phi_{peak}$ , interface HB-PVC.

Test	$\Phi_0$ (°)	#	$\Phi_{50}$ (°)	#	$\Phi_{peak}$ (°)	#
A - 8	33	1	33	1	-	-
A - 9	31	1	31	1	-	-
A - 17	31	1	31	1	-	-
A - 29	32	1	32	1	-	-
B - 73	28	3	29	2	28	3

The comparison of values found using plane A and B leads to

$$\Phi_{0,A} = \Phi_{50,A} > \Phi_{0,B} = \Phi_{peak} \quad (5.3)$$

#### 5.2.4 Interface nnp40-PVC

Series A10, A11, A13, A16 and A20 were tested using the small dimension apparatus and with interface nnp40-PVC (nonwoven needle punched and Polyvinyl Chloride). Series A13 showed in Figure 5.21 represents the typical behavior of this group of series: good repeatability of the friction angle results (even when reusing samples), low sensibility to abrasion and sudden slide.

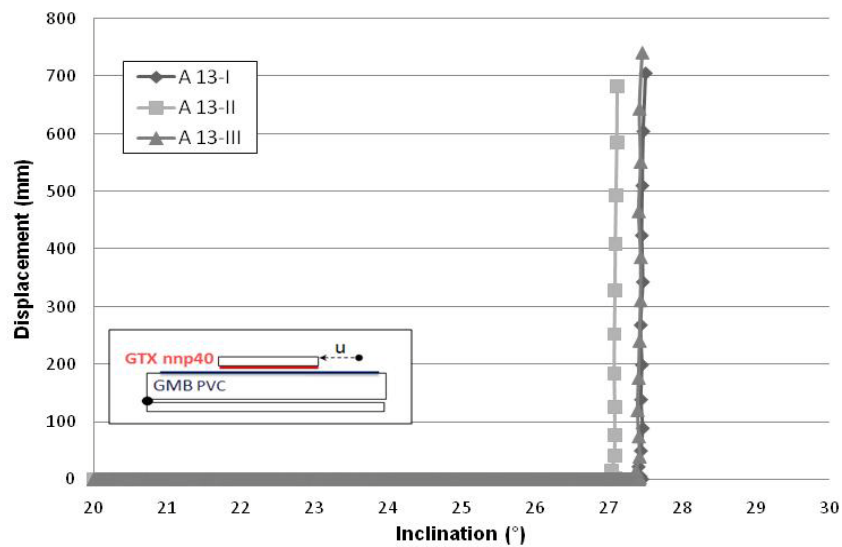


Figure 5.8 – Curve Displacement vs. Inclination of interface nnp40-PVC, series A13, tested with the small dimension inclined plane.

Except for series A20, the tests were performed using the guidance systems types  $\alpha$  and  $\beta$  which implied a few problems. Their behavior after displacement  $u = 300$  mm could not be

taken into account, since after  $u = 300$  mm the upper plate touched the lateral walls and interfered in the descendent movement. However, it was possible to measure friction angles  $\Phi_0$  and  $\Phi_{50}$  as exposed in Table 5.10.

Table 5.10 presents a summary of results found for series A10, A11, A13, A16 and A20. The friction angles  $\Phi_0$  and  $\Phi_{50}$  were equivalent and the average value determined was  $(27 \pm 1)^\circ$ .

Series B74 (Table 5.11) was performed with the standardized apparatus and with the adoption of the combined analysis procedure. Once again the first test was separated from global analysis for presenting reduced values for the friction angles ( $\Phi_0$ ,  $\Phi_{50}$ ,  $\Phi_{\text{peak}}$ ), in this case  $\Phi_{\text{peak}}$  was equal to  $(22 \pm 1)^\circ$ .

Test B74-II was not set properly, and the upper box could not move freely till a displacement  $u$  equals to 50 mm. Consequently,  $\Phi_{50}$  could not be determined.

**Table 5.10 – Summary values of friction angles  $\Phi_0$  and  $\Phi_{50}$ , interface nnp40-PVC, test type A.**

Test	$\Phi_0$ (°)	$\Phi_{50}$ (°)
<b>A10 – I</b>	28	28
<b>A 10 – II</b>	27	27
<b>A 10 – III</b>	27	27
<b>A 11 – I</b>	28	28
<b>A 11 – II</b>	28	28
<b>A 11 – III</b>	27	27
<b>A 13 – I</b>	27	27
<b>A 13 – II</b>	27	27
<b>A 13 – III</b>	27	27
<b>A 16 – I</b>	27	27
<b>A 16 – II</b>	27	27
<b>A 16 - III</b>	28	28
<b>A 20 - I</b>	27	27
<b>A 20 - II</b>	27	27

**Table 5.11 – Values of friction angles  $\Phi_0$ ,  $\Phi_{50}$  and  $\Phi_{\text{peak}}$ , series B74, interface nnp40-PVC.**

Test	$\Phi_0$ (°)	$\Phi_{50}$ (°)	$\Phi_{\text{peak}}$ (°)
<b>B74-II</b>	27	-	27
<b>B74-III</b>	28	28	28

Figure 5.10 and Figure 5.11 illustrate the behavior of the upper box during the inclination of the plane. An exam Figure 5.10 confirms the sudden slide behavior.

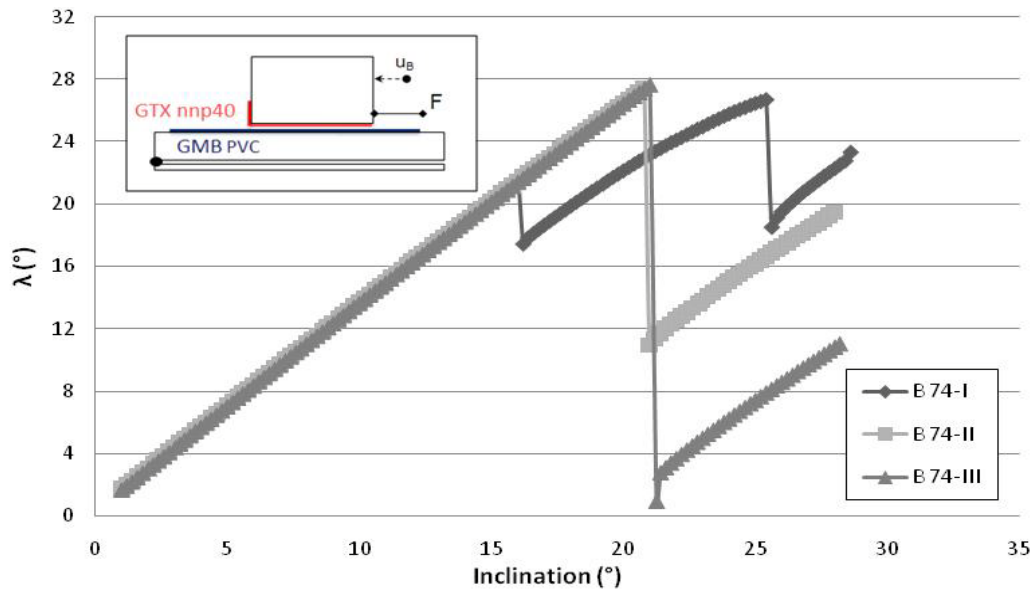


Figure 5.9 – Curve Lambda vs. Inclination of interface nnp40-PVC, series B74, tested with the standardized dimension inclined plane.

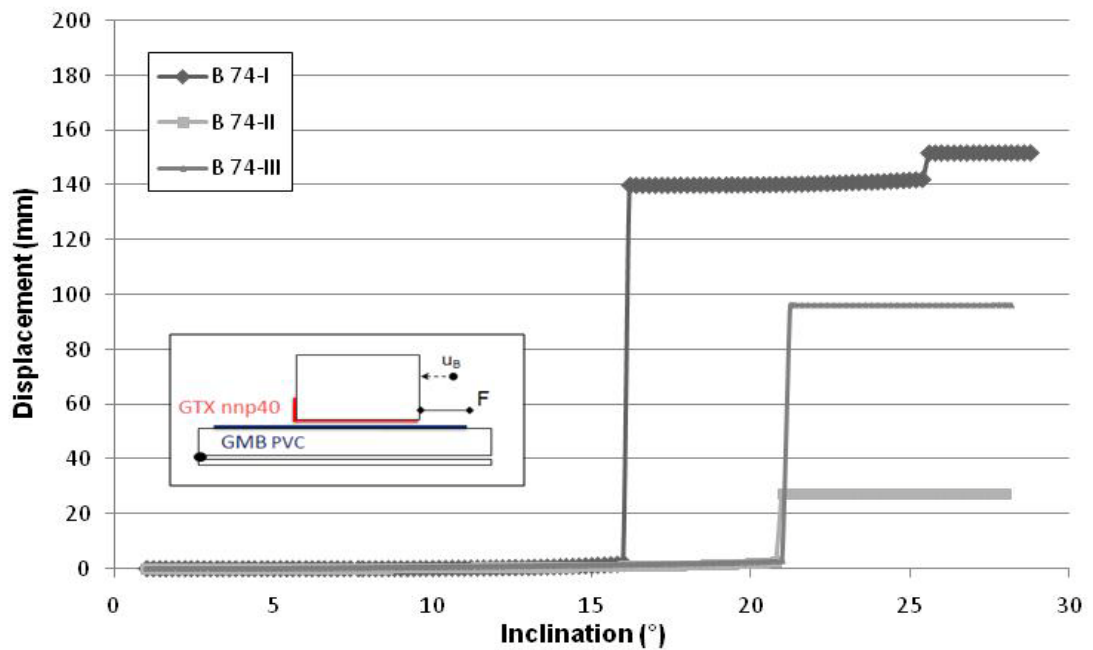


Figure 5.10 – Curve Displacement vs. Inclination of interface nnp40-PVC, series B74, tested with the standardized dimension inclined plane.

Table 5.12 exposes the summary values of friction angles found for interface nnp40-PVC. Its analysis leads to:

$$\Phi_{\text{peak}} = \Phi_{0,B} = \Phi_{50,B} > \Phi_{0,A} = \Phi_{50,A} \quad (5.4)$$

Friction angles determined with the small dimension apparatus were inferior by one degree, which corresponds to the adopted incertitude.

**Table 5.12 – Summary values of friction angles  $\Phi_0$ ,  $\Phi_{50}$  and  $\Phi_{\text{peak}}$ , interface nnp40-PVC.**

Test	$\Phi_0$ (°)	#	$\Phi_{50}$ (°)	#	$\Phi_{\text{peak}}$ (°)	#
A - 10	27	3	27	3	-	-
A - 11	28	3	28	3	-	-
A - 13	27	3	27	3	-	-
A - 16	28	3	28	3	-	-
A - 20	27	2	27	2	-	-
B - 74	28	2	28	1	28	2

A better detailed analysis of the curve *Displacement vs. Inclination* indicates a gradual sliding of the box, that is, the displacement  $u$  progressively increases with inclination  $\beta$ . Since this behavior happened for displacements shorter than 5 mm, this gradual sliding phase will not be considered.

Figure 5.11 and Figure 5.12 correspond to the graphics in Figure 5.9 and Figure 5.10 detailed.

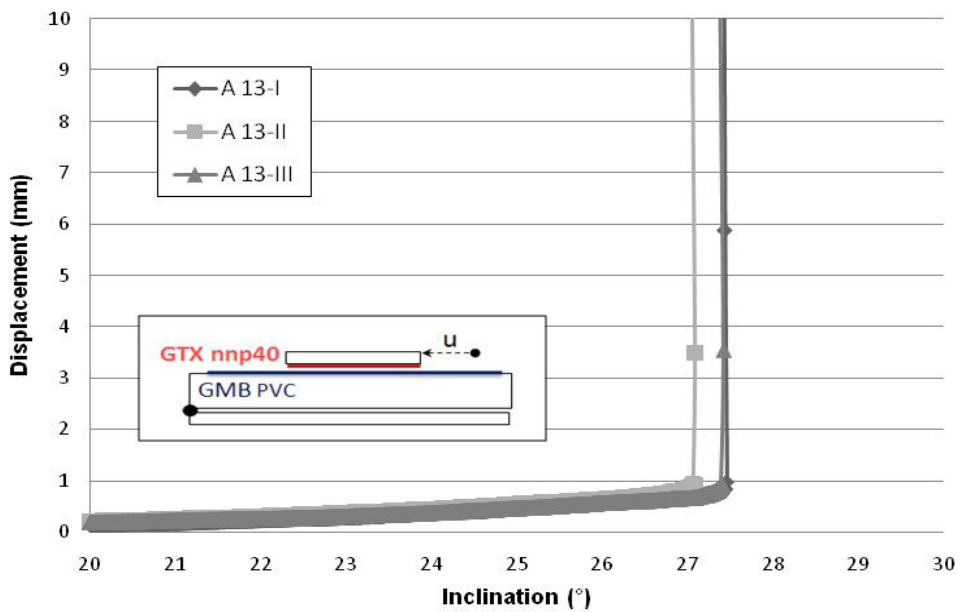


**Figure 5.11 – Curve Displacement vs. Inclination of interface nnp40-PVC, series A13, tested with the standardized dimension inclined plane.**

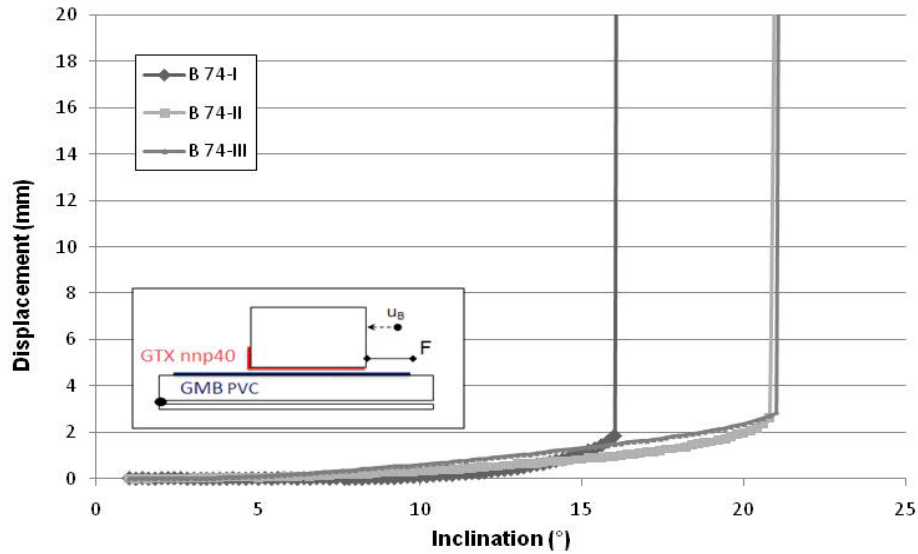


Figure 5.12 – Curve Displacement vs. Inclination of interface nnp40-PVC, series B74, tested with the standardized dimension inclined plane.

### 5.2.5 Interface Rnp-PP

Series A32 was tested using interface Rnp-PP (Nonwoven needle punched reinforced with PET fibres and Polypropylene) and the inclined plane type A. Due to deadline difficulties, it was not possible to execute more tests, though it is highly recommended to do so.

Two sequential trials compose the series A32 although it would have been better to avoid reusing samples of geomembrane PP due to its sensitivity to abrasion.

As presented in Table 5.13 and in Figure 5.13, the difference between the tests was that the gradual slide phase became more pronounced for A32-II. Considering the standard consideration not to reuse the samples, test A32-I was the one chosen for analysis.

In these conditions, the static friction angles  $\Phi_0$  and  $\Phi_{50}$  were both equal to  $(20 \pm 1)^\circ$ , when considering only test A32-I for analysis.

Table 5.13 – Values of friction angles  $\Phi_0$  and  $\Phi_{50}$ , series A32, interface Rnp-PP, guidance system type  $\alpha$ .

Test	$\Phi_0$ (°)	$\Phi_{50}$ (°)
A32-I	20	20
A32-II	18	21

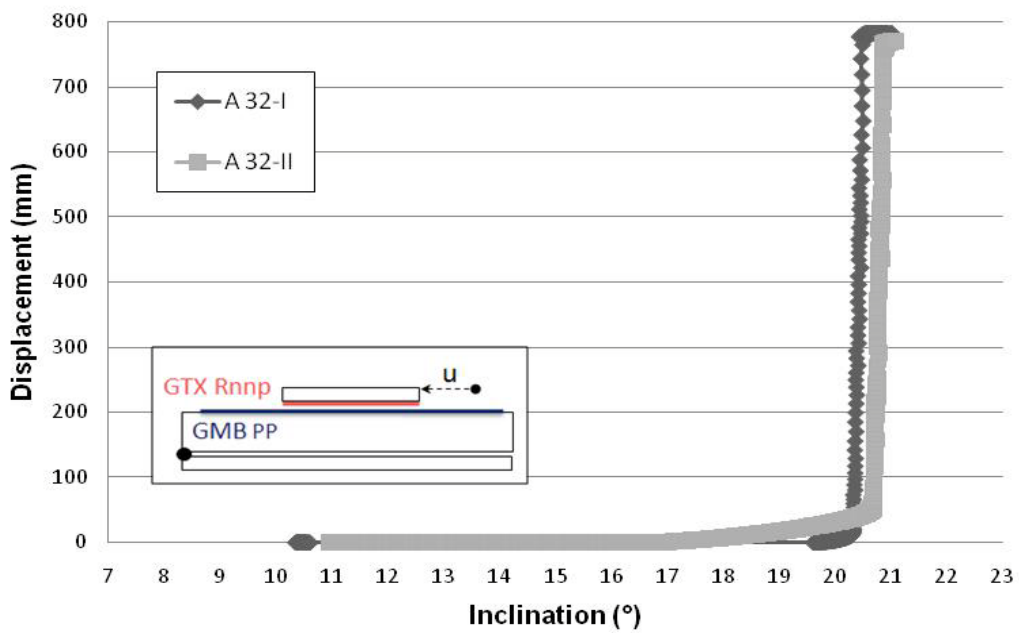


Figure 5.13 – Curve Displacement vs. Inclination of interface Rnnp-PP, series A32, tested with the small dimension inclined plane.

Series B80, tested using the standardized inclined plane, is composed of three sequential tests, presented in Table 5.14.

Table 5.14 – Values of friction angles  $\Phi_0$ ,  $\Phi_{50}$  and  $\Phi_{peak}$ , series B80, interface Rnnp-PP.

Test	$\Phi_0$ (°)	$\Phi_{50}$ (°)	$\Phi_{peak}$ (°)
<b>B80-I</b>	18	18	19
<b>B80-II</b>	18	21	22
<b>B80-III</b>	18	20	22

As illustrated in Figure 5.14, after the peak value of lambda, the curves presented a decay reaching a level path that was the same for the three sequential tests. Also, the peak value of lambda curve was shorter for the first test than for the other test results of the series.

For a best foundation of results, it is recommended to perform other series of tests using this same interface. This way it could be studied whether the path level occurs for the same values even when testing different samples of this same interface. It is also recommended to execute a deeper inspection of the characteristics of this interface in terms of abrasion.

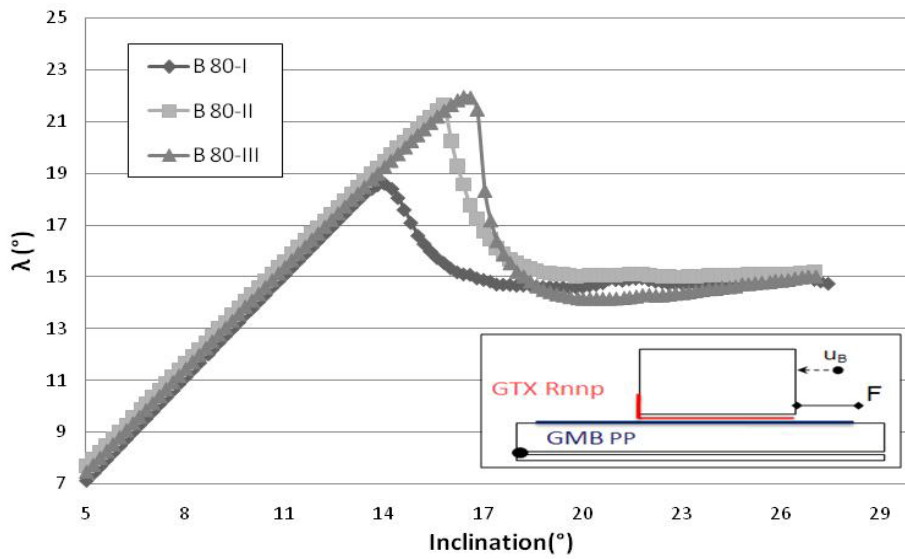


Figure 5.14 – Curve Lambda vs. Inclination of interface Rnnp-PP, series B80, tested with the standardized dimension inclined plane.

In Figure 5.15, the gradual slide is more evident in test B80-II than in B80-I.

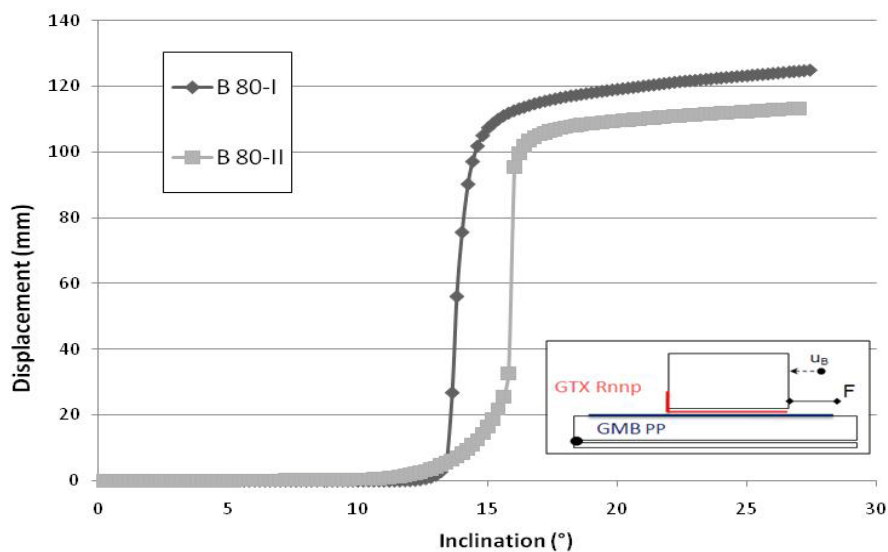


Figure 5.15 – Curve Displacement vs. Inclination of interface Rnnp-PP, series B80, tested with the standardized dimension inclined plane.

Table 5.15 presents the summary of results found in series A32 and B80.

As observed, whenever the gradual behavior happens, the values of friction angles are expected to be related in ascending order ( $\Phi_0 < \Phi_{50} < \Phi_{peak}$ ). In order to discover whether  $\Phi_{50}$  is still a conservative value for friction characterization of the interface, it is recommended the creep test analysis for all interfaces that presented gradual sliding.

Table 5.15 – Summary values of friction angles  $\Phi_0$ ,  $\Phi_{50}$  and  $\Phi_{peak}$ , interface Rnp-PP.

Test	$\Phi_0$ (°)	#	$\Phi_{50}$ (°)	#	$\Phi_{peak}$ (°)	#
A - 32	20	1	20	1	-	-
B - 80	18	3	20	3	22	3

### 5.2.6 Interface nnpC-PP

Series A25, 26 and 27 were made using interface nnpC x PP (nonwoven needle punched calandered and Polypropylene) with small dimension inclined plane. To avoid excessive abrasion of geomembrane PP, it was performed only one test in each of the series.

The series results are presented in Table 5.16 and in the graphic *Displacement vs. Inclination* of Figure 5.16.

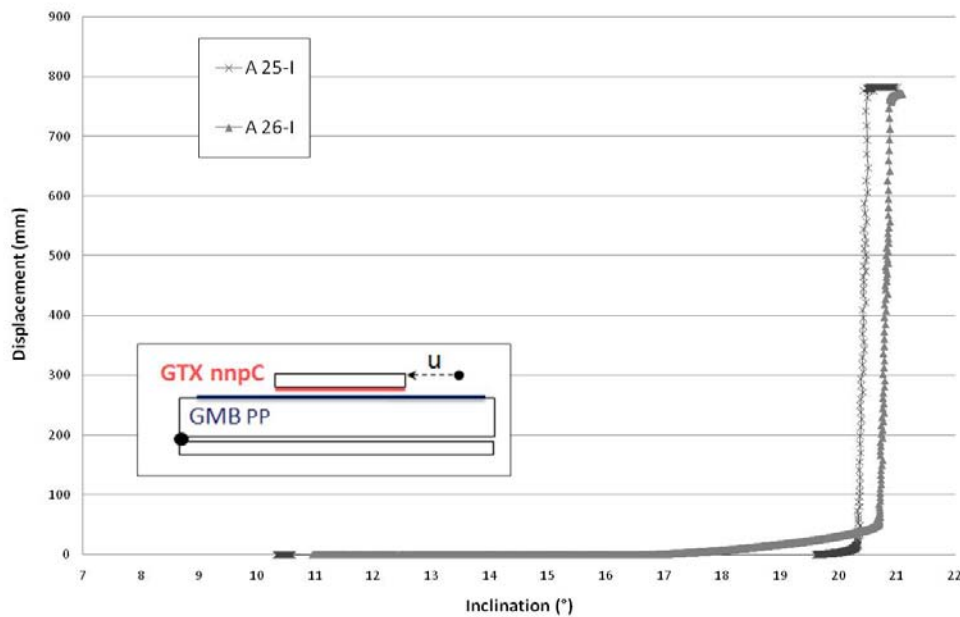


Figure 5.16 – Curve Displacement vs. Inclination of interface nnpC-PP, series A25 & 26, tested with the small dimension inclined plane.

Since test 25-I and 26-I were made with new samples of geomembrane PP it was not possible to observe the interface sensitivity to abrasion.

Table 5.16 – Values of friction angles  $\Phi_0$  and  $\Phi_{50}$ , series A25 & 26, interface nnpC-PP.

Test	$\Phi_0$ (°)	$\Phi_{50}$ (°)
A25-I	15	15
A26-I	15	15

Series B82 was performed using the standardized inclined plane and the friction values are exposed in Table 5.17. Test B82-I was discarded because of errors during the performance of the test.

As noticed for interface Rnnp x PP, interfaces using geomembrane PP may present a gain on the values of the friction angles after being tested by the first time. However, the trials made with series B82 are not conclusively. It seems, by the analysis of Figure 5.17 (*Displacement vs. Inclination*), that this behavior also happens, but it is recommended to perform other series of tests to complete the test made to then, ensure the results found.

**Table 5.17 – Values of friction angles  $\Phi_0$ ,  $\Phi_{50}$  and  $\Phi_{peak}$ , series B82, interface nnpC-PP.**

Test	$\Phi_0$ (°)	$\Phi_{50}$ (°)	$\Phi_{peak}$ (°)
<b>B82-II</b>	12	18	18

Figure 5.17 illustrates the graphic *Displacement vs. Inclination* and Figure 5.18 presents the graphic *Lambda vs. Inclination*.

Regarding the behavior of the interface, at the beginning of the slide it is noticed a gradual slide followed by a sudden slide. (Test B82-II)

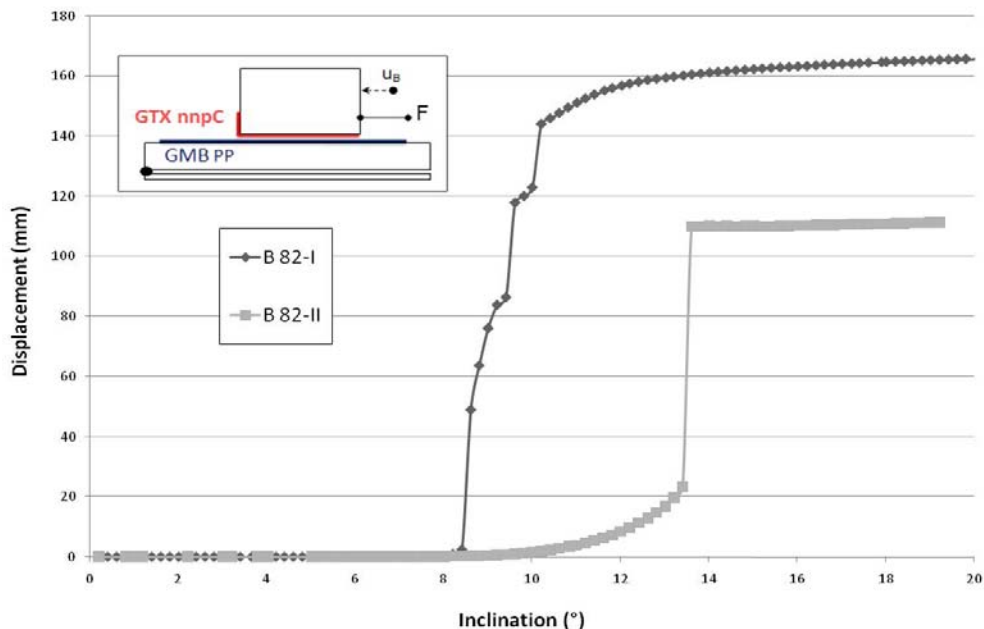


**Figure 5.17 – Curve Displacement vs. Inclination of interface nnpC-PP, series B82, tested with the standardized dimension inclined plane.**

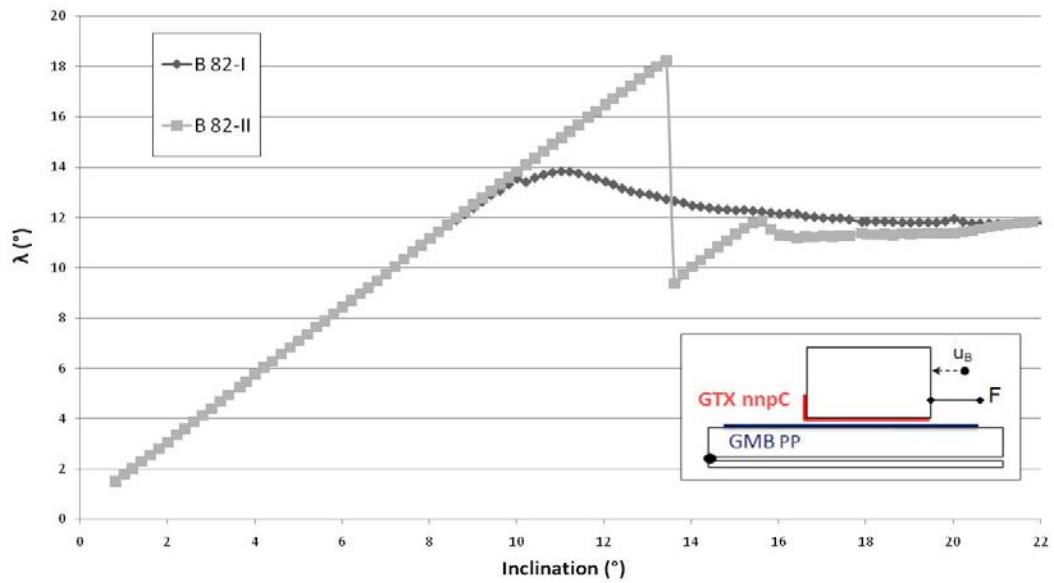


Figure 5.18 – Curve Lambda vs. Inclination of interface nnpC-PP, series B82, tested with the standardized dimension inclined plane.

Table 5.18 shows the summary of average results found for the tests made. For the series using inclined plane A, the average result for both angles  $\Phi_0$  and  $\Phi_{50}$  was equal to  $(15 \pm 1)^\circ$ . As for tests performed with plane B,  $\Phi_0$  was equal to  $(12 \pm 1)^\circ$ ,  $\Phi_{50}$  was equal to  $(18 \pm 1)^\circ$  and  $\Phi_{\text{peak}}$  was equal to  $(18 \pm 1)^\circ$

Table 5.18 – Summary values of friction angles  $\Phi_0$ ,  $\Phi_{50}$  and  $\Phi_{\text{peak}}$ , interface nnpC-PP.

Test	$\Phi_0$ (°)	#	$\Phi_{50}$ (°)	#	$\Phi_{\text{peak}}$ (°)	#
A - 25	15	1	15	1	-	-
A - 26	15	1	15	1	-	-
B - 82	12	1	18	1	18	1

Hence, the results found are correlated in the following order:

$$\Phi_{\text{peak}} = \Phi_{50,B} > \Phi_{50,A} = \Phi_{0,A} > \Phi_{0,B}. \quad (5.5)$$

### 5.2.7 Interface Rnnp-HDPE

Series A31 was performed with interface Rnnp-HDPE (Nonwoven needle punched reinforced with PET wires and High Density Polyethylene) and tested using inclined plane of small dimensions. The static angles found for tests A31-I and II are shown in Table 5.19. Though highly recommended, it was not possible to execute more tests due to deadline difficulties.

Table 5.19 – Values of friction angles  $\Phi_0$  and  $\Phi_{50}$ , series A31, interface Rnnp-HDPE, guidance system  $\delta$ .

Test A	$\Phi_0$ (°)	$\Phi_{50}$ (°)
A31-I	17	17
A31-II	16	16

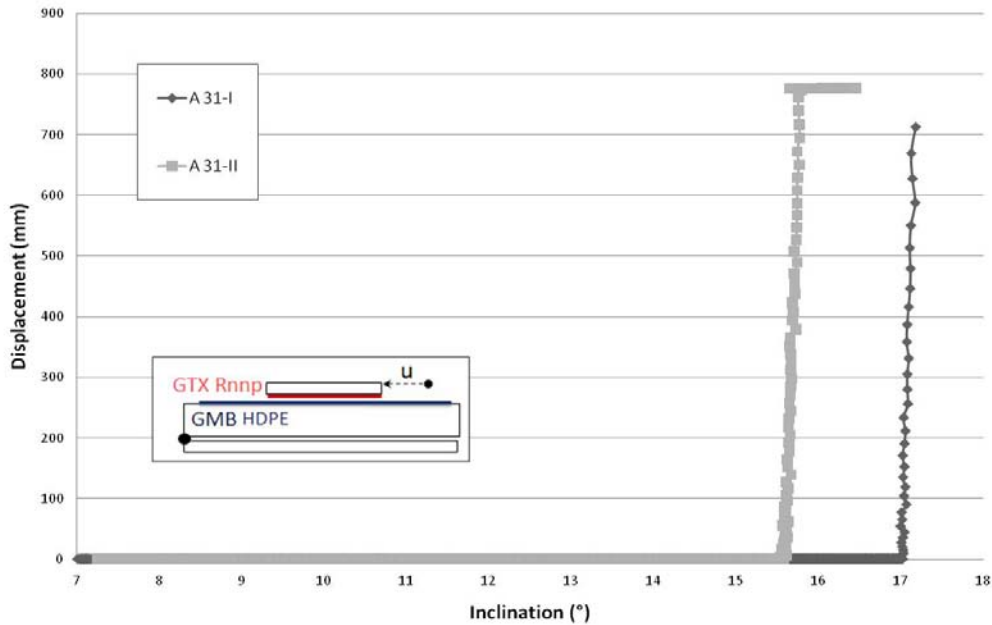


Figure 5.19 - Curve Displacement vs. Inclination of interface Rnnp-HDPE, series A31, tested with small dimension inclined plane.

Series B45 was made using the standardized inclined plane and its static results are shown in Table 5.20. The summary of the average results found for this interface is shown in Table 5.21.

The sensitivity to abrasion can be noticed in series A31 and B45 but must be confirmed through the execution of more trials.

Table 5.20 – Values of friction angles  $\Phi_0$ ,  $\Phi_{50}$ , and  $\Phi_{peak}$ , series B45, interface Rnnp-HDPE.

Test	$\Phi_0$ (°)	$\Phi_{50}$ (°)	$\Phi_{peak}$ (°)
B45-I	-	-	16
B45-II	-	-	12
B45-III	-	-	13
B45-IV	-	-	12
B45-V	12	12	-

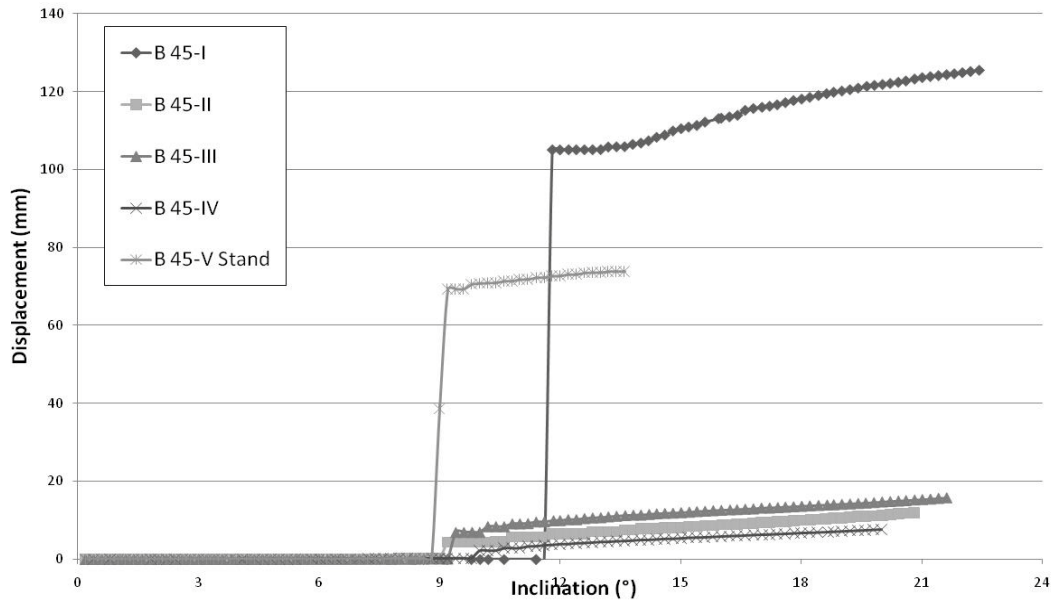


**Figure 5.20 - Curve Displacement vs. Inclination of interface Rnnp-HDPE, series B45, tested with the standardized dimension inclined plane.**

As observed in Figure 5.19 and Figure 5.20, this interface presented a sudden slide behavior.

**Table 5.21 – Summary values of friction angles  $\Phi_0$ ,  $\Phi_{50}$  and  $\Phi_{peak}$ , interface Rnnp-HDPE.**

Test	$\Phi_0$ (°)	#	$\Phi_{50}$ (°)	#	$\Phi_{peak}$ (°)	#
<b>A - 31</b>	16	2	16	2	-	-
<b>B - 45</b>	12	1	12	1	13	4

Hence, the results found are correlated in the following order:

$$\Phi_{0,A} = \Phi_{50,A} > \Phi_{peak} > \Phi_{50,B} = \Phi_{0,B} \quad (5.6)$$

### 5.2.8 Interface HB-HDPE

Interface HB-HDPE (Nonwoven Heat-Bounded and High Density Polyethylene) was used to perform the series A21 and A24. As represented in Figure 5.21 and Figure 5.22, both series presented a sudden slide behavior and, as observed in Table 5.22, the friction angles  $\Phi_0$  and  $\Phi_{50}$  were equal to  $(11 \pm 1)^\circ$ .

Different from the interfaces presented in the topic “abrasion analysis” at chapter 3, interface HB-HDPE did not seem to be that sensible to abrasion. The interface did not present visual damage either. In both series A21 and A24, the variation of the friction angle values was

smaller than one degree, that is, the repeatability of results was appropriated. This time, geotextile HB was not visually damaged.

**Table 5.22 – Values of friction angles  $\Phi_0$  and  $\Phi_{50}$ , series A21 and A24, interface HB-HDPE, guidance system type  $\delta$ .**

Test A	$\Phi_0$ (°)	$\Phi_{50}$ (°)
A21-I	12	12
A21-II	11	11
A21-III	12	12
A24-I	11	11
A24-II	11	11
A24-III	11	11

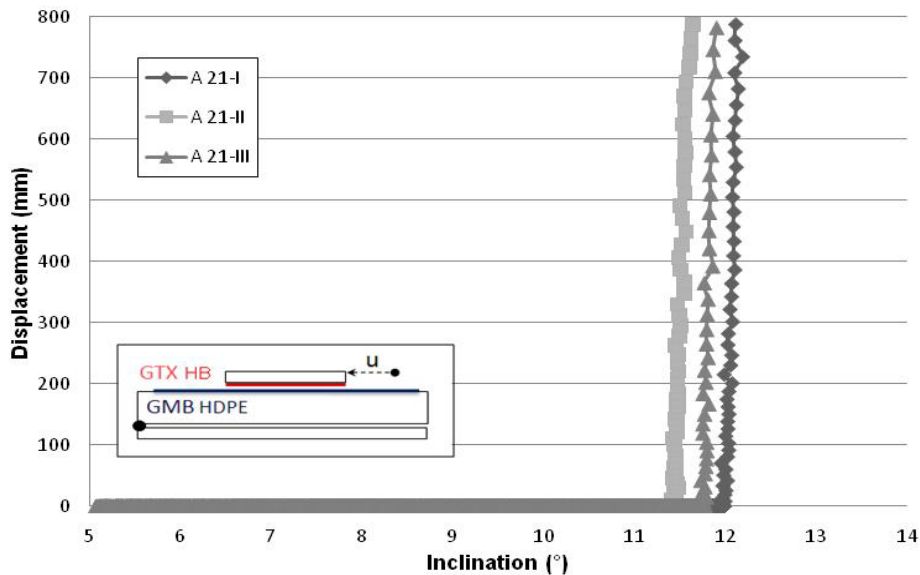


**Figure 5.21 – Curve Displacement vs. Inclination of interface HB-HDPE, series A21, tested with the small dimension inclined plane.**

Tests made using plane B presented a few differences from tests made with plane A. As showed in Table 5.23 and Table 5.24, the values of the friction angle  $\Phi_0$  were no longer equivalent to values of  $\Phi_{50}$ . That can be seeing in Figure 5.24 where it is indicated a gradual slide behavior instead of a sudden one.

In comparison with tests presented before, the shape of graphic (*Lambda vs. Inclination*) in Figure 5.23 has changed, presenting one unique peak followed by a level.

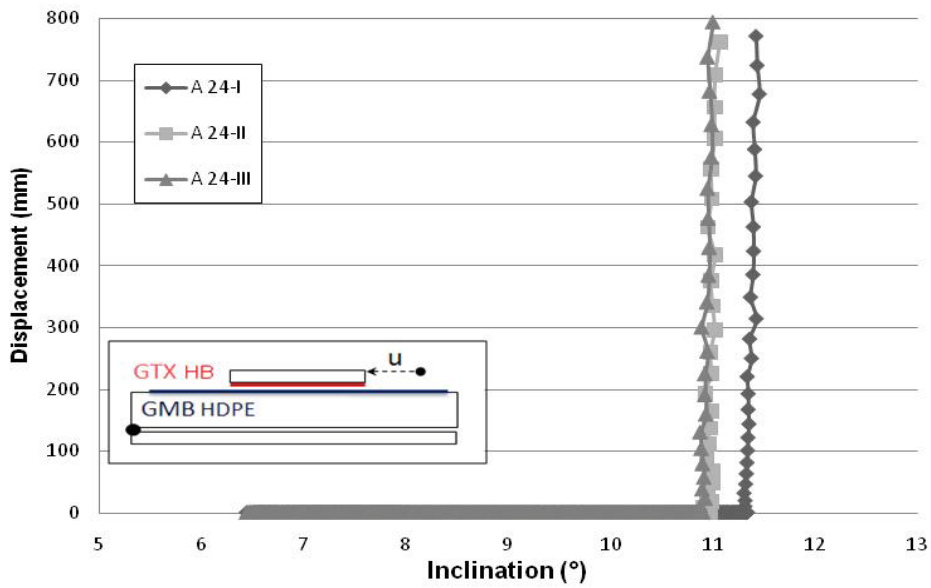


Figure 5.22 – Curve Displacement vs. Inclination of interface HB-HDPE, series A24, tested with the small dimension inclined plane.

For each test of the series B75,  $\Phi_0$  varied at least one degree. Values of  $\Phi_{\text{peak}}$ , though, presented a constant value of  $(17 \pm 1)^\circ$ . Angle  $\Phi_{50}$  could not be determined for test 75-II and III because the apparatus was not set properly and the upper box stop moving before displacement  $u$  has reached 50 mm.

For tests of the series B81,  $\Phi_0$  also varied, this time by two degree. Values of  $\Phi_{50}$  and  $\Phi_{\text{peak}}$  presented a constant value of  $(18 \pm 1)^\circ$ . Comparing the average values of  $\Phi_{50}$  found using planes A and B, it is possible to state that:

$$\Phi_{50, A} < \Phi_{50, B} \quad (5.7)$$

Table 5.23 – Values of friction angles  $\Phi_0$ ,  $\Phi_{50}$  and  $\Phi_{\text{peak}}$ , series B75, interface HB-HDPE.

Test	$\Phi_0$ (°)	$\Phi_{50}$ (°)	$\Phi_{\text{peak}}$ (°)
<b>B75-I</b>	14	16	17
<b>B75-II</b>	16	-	17
<b>B75-III</b>	17	-	17

Table 5.24 – Values of friction angles  $\Phi_0$ ,  $\Phi_{50}$  and  $\Phi_{\text{peak}}$ , series B81, interface HB-HDPE.

Test B	$\Phi_0$ (°)	$\Phi_{50}$ (°)	$\Phi_{\text{peak}}$ (°)
<b>B81-I</b>	15	18	18
<b>B81-II</b>	17	18	18

Between the two series B75 and B81, all curves are practically overlapped till inclination  $\beta$  equals to  $11^\circ$ . After that, they keep presenting similar behavior but the traditional level for series B81 is moved up.

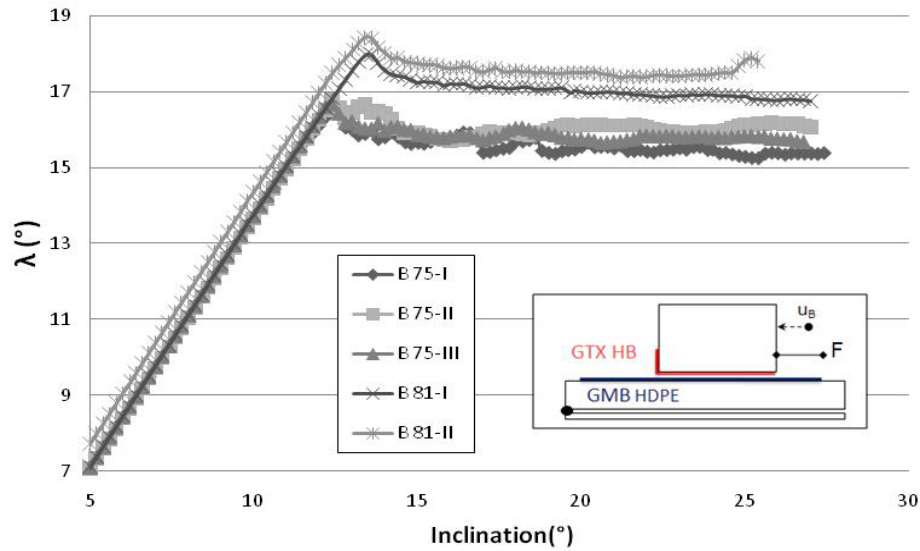


Figure 5.23 – Curve Lambda vs. Inclination of interface HB-HDPE, series B75 and B81, tested with the standardized dimension inclined plane.

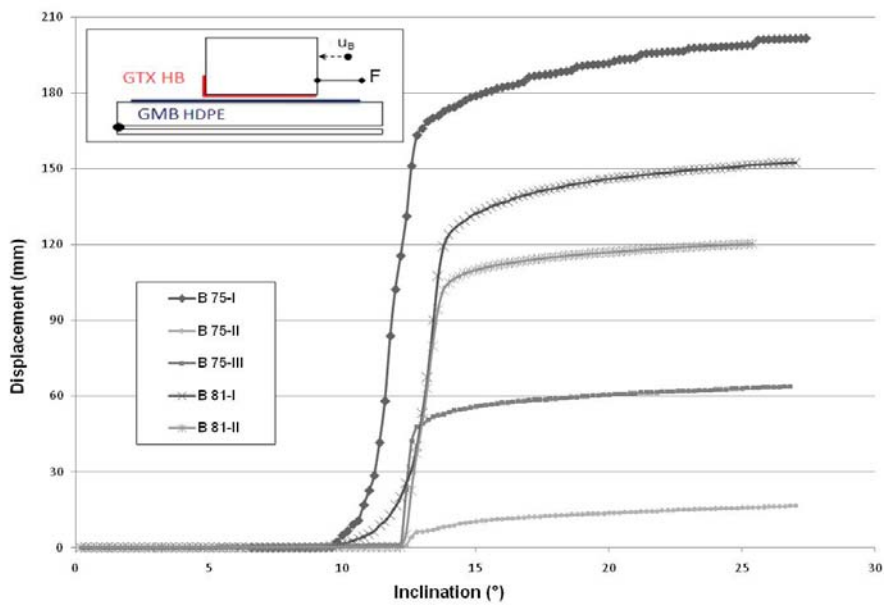


Figure 5.24 – Curve Displacement vs. Inclination of interface HB-HDPE, series B75 and B81, tested with the standardized inclined plane.

Table 5.25 shows the summary of average values of tests performed with interface HB-HDPE.

**Table 5.25 - Summary values of friction angles  $\Phi_0$ ,  $\Phi_{50}$  and  $\Phi_{peak}$ , interface HB-HDPE.**

Test	$\Phi_0$ (°)	#	$\Phi_{50}$ (°)	#	$\Phi_{peak}$ (°)	#
<b>A - 21</b>	12	3	12	3	-	-
<b>A - 24</b>	11	3	11	3	-	-
<b>B - 75</b>	-	-	-	-	17	3
<b>B - 81</b>	-	-	-	-	18	2

The average results for  $\Phi_{0,B}$  and  $\Phi_{50,B}$  were not shown because they presented standard deviations higher than one degree.

### 5.2.9 Interface nnp40-EPDM

Results of series A14 and A15 for interface nnp40-EPDM (Nonwoven Needle Punched and Ethylene Propylene Diene Monomer) are represented in Figure 5.26 and in Table 5.26. As shown in the curve *Displacement vs. Inclination* this interface presents a gradual sliding behavior.

**Table 5.26 – Values of friction angles  $\Phi_0$  and  $\Phi_{50}$ , series A14 & 15, interface nnp40-EPDM.**

Test	$\Phi_0$ (°)	$\Phi_{50}$ (°)
<b>A14-I</b>	20	23
<b>A15-I</b>	24	27
<b>A15-II</b>	23	26
<b>A15-III</b>	23	26

Tests made with inclined plane B are shown in Figure 5.27, Figure 5.28 and in Table 5.27.

The gradual behavior was also evident for tests using plane B. However, the curve *Displacement vs. Inclination* was smoother for tests using plane A. One possible explication for the difference between these curves could be visually noticed. While the upper box was sliding, the EPDM portion located in the frontal region of the upper box was very wave-shaped. This wave-shaped condition was more evident on plane A because: (Figure 5.25)

- The geomembrane EPDM was only attached at the top of the lower box instead of being glued with an adhesive tape and being stapled to it like plane B configuration.

- The configuration of plane A upper plate induced a non-homogenous distribution of the normal stress over the geomembrane surface, resulting in the concentration of efforts in the upper plate frontal border.

These configurations, in addition to the fact that EPDM was very elastic and adherent, caused a more relevant effect for plane A.

The size of the upper box also contributes to the wave-shaped condition. The bigger the surface of contact between the upper box and the geomembrane, the less intense this effect is.

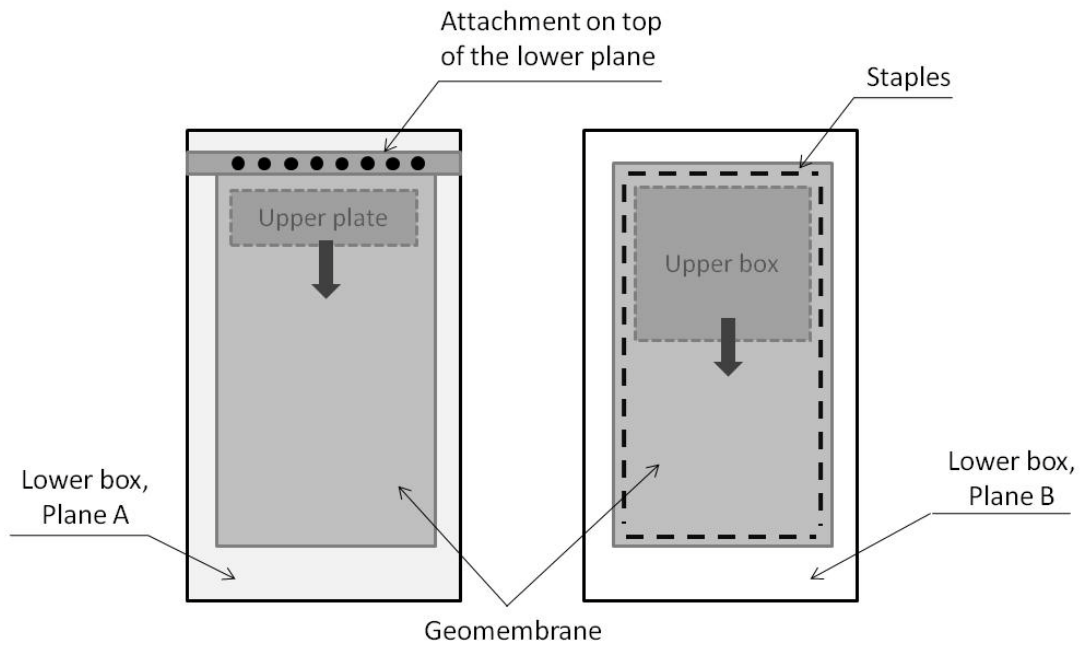


Figure 5.25 – Sketch of the planes A and B attachment disposal of the geomembranes lower layer. (top view)

Regarding the sensitivity to abrasion, for plane A, the curves of series A15 almost overlapped. For plane B, it was not possible to analyze any abrasion features because both tests made were set with new samples of geosynthetic.

Table 5.27 – Values of friction angles  $\Phi_0$ ,  $\Phi_{50}$  and  $\Phi_{peak}$ , series B81, interface HB-HDPE.

Test	$\Phi_0$ (°)	$\Phi_{50}$ (°)	$\Phi_{peak}$ (°)
B52-I	21	22	24
B53-I	23	25	25

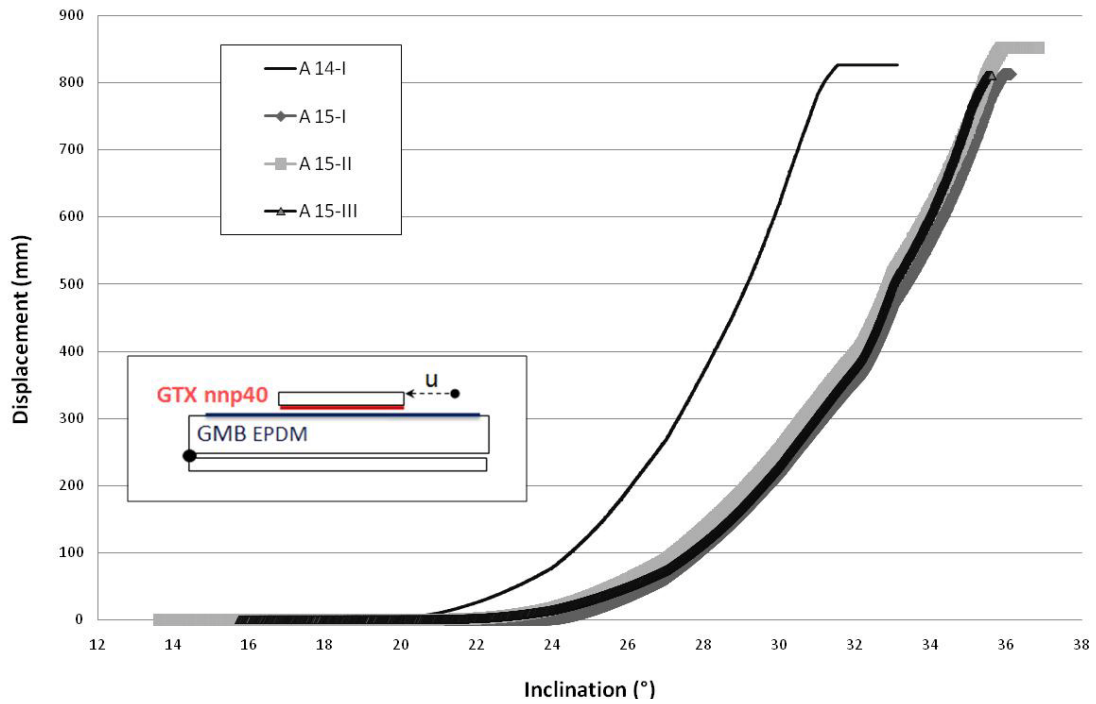


Figure 5.26 – Curve Displacement vs. Inclination of interface nnp40-EPDM, series A14 & 15, tested with the small dimension inclined plane.

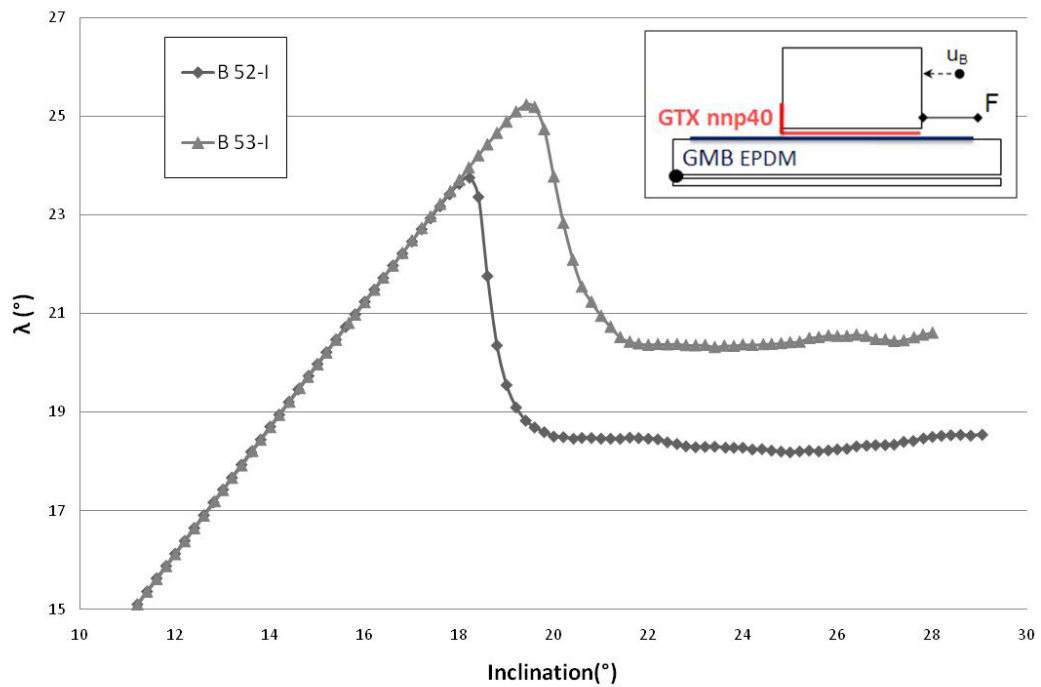
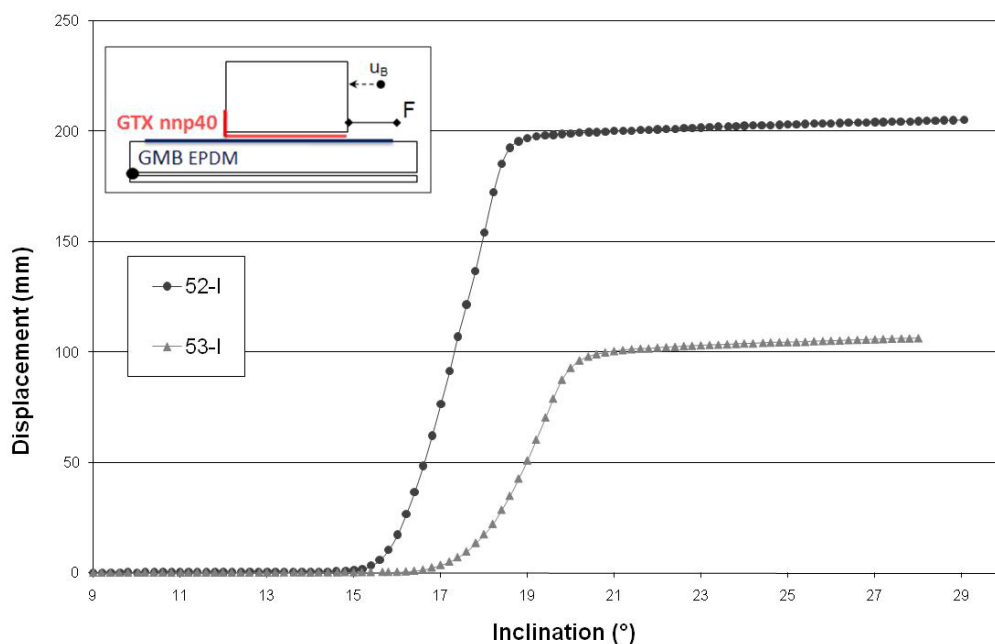


Figure 5.27 – Curve Lambda vs. Inclination of interface nnp40-EPDM, series A52 and A53, tested with the standardized inclined plane.



**Figure 5.28 – Curve Displacement vs. Inclination of interface nnp40-EPDM, series A52 and A53, tested with the standardized inclined plane.**

At last, Table 5.28 shows the summary of average values of tests performed with interface nnp40-EPDM.

**Table 5.28 - Summary values of friction angles  $\Phi_0$ ,  $\Phi_{50}$  and  $\Phi_{peak}$ , interface nnp40-EPDM.**

Test	$\Phi_0$ (°)	#	$\Phi_{50}$ (°)	#	$\Phi_{peak}$ (°)	#
A - 14	20	1	23	1	-	-
A - 15	23	3	26	3	-	-
B - 52	21	1	22	1	24	1
B - 53	23	1	25	1	25	1

As expected whenever the gradual slide occurs, the values of  $\Phi_0$  were inferior to  $\Phi_{50}$ .

## 5.3 Dynamic Analysis

### 5.3.1 Introduction

In this section, the results of dynamic analysis are presented in graphics showing how the displacement, velocity and acceleration vary in time. Each graphic comprises more than one test result and, above each curve there is a title with the identification of the test.

Not all dynamic tests made were successfully, mostly because the upper box from plane A touched the guidance lateral walls during its slide. As a result, the movement of the upper box

was slowed down, jeopardizing the measurement of acceleration. The test analyses were discarded whenever the acceleration was not possible to be calculated because there was not a proper interval of velocity to make the fit-linear.

The dynamic analysis will exposed a comparison between dynamic angle  $\Phi^{lim}$ , from inclined plane A, with angle  $\Phi_{res}$ , from inclined plane B, in order to analyze if they are equivalent or not.

The interfaces tested are presented on Table 5.29.

**Table 5.29 - Series of interfaces studied for the dynamic analysis.**

	<b>Plane A</b>	<b>Plane B</b>
<b>Rnp x HDPE</b>	5, 31	45
<b>HB x HDPE</b>	21, 24	75, 81
<b>nnpC x PP</b>	25, 26, 27	82

The dynamic behavior of other interfaces that did not present a residual behavior was also studied. They are presented at this section (Table 5.30) but no comparison is made with previous results.

**Table 5.30 – Series of interfaces studied for the dynamic analysis.**

	<b>Plane A</b>
<b>Rnp x PVC</b>	6, 30
<b>HB x PVC</b>	8, 9, 17, 29
<b>nnp40 x PVC</b>	10, 11, 13, 20
<b>nnp40 x HDPE</b>	22, 23

### 5.3.2 Interface Rnp-HDPE

Dynamic results of series A31, presented in Figure 5.29 and in Table 5.31, led to a value of  $\Phi^{lim}$  equals to  $(16\pm 1)^\circ$ . Test 31-II was discarded due to problems with the guidance system.

**Table 5.31 - Dynamic results of interface Rnp x HDPE, series A31, guidance system  $\delta$**

<b>Test</b>	<b>A31 - I</b>	<b>A31-III dyn2</b>	<b>A31-IV dyn2</b>
$\gamma$ (mm/s <sup>2</sup> )	178	771	531
$\beta$ (°)	17	21	19
$\Phi^{lim}$ (°)	16	17	16

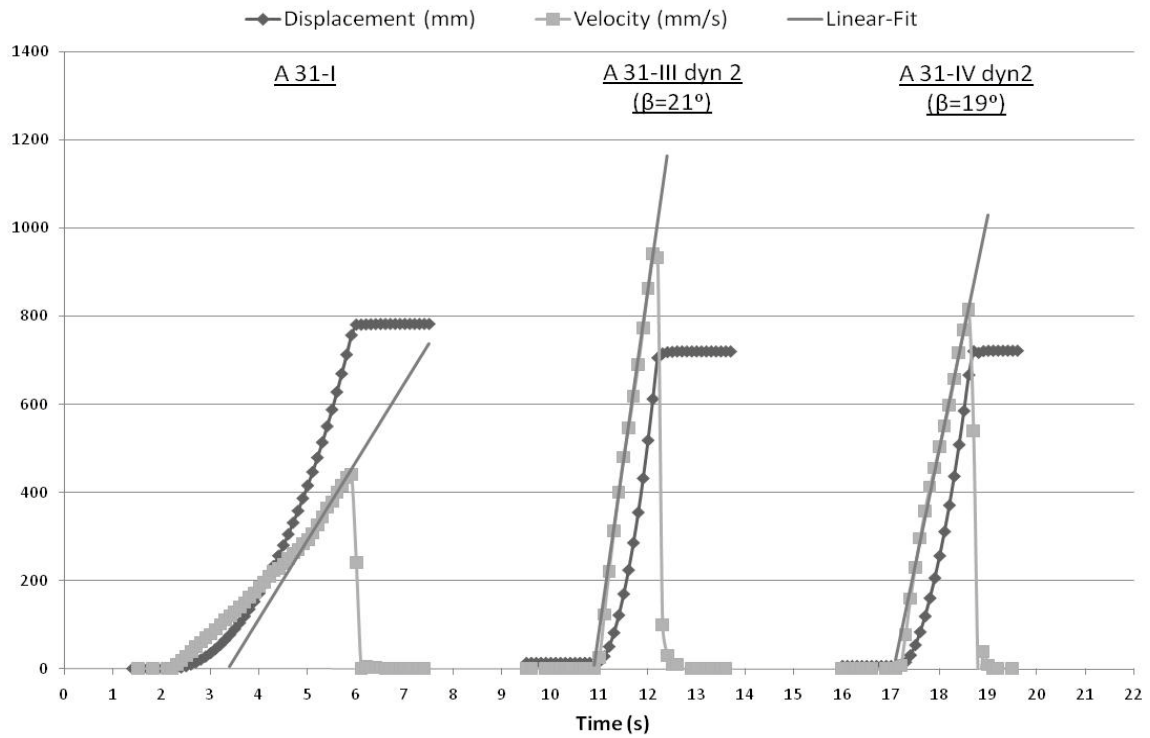


Figure 5.29 - Dynamic results of interface Rnnp x HDPE, series A31, guidance system  $\delta$

The analysis of series B45 is represented in Figure 5.30 and the values found for  $\Phi_{res}$  are in Table 5.32. The average result of  $\Phi_{res}$  is equal to  $(12 \pm 1)^\circ$ .

Table 5.32 - Test results of interface Rnnp x HDPE, series B45

Test	$\Phi_{res}$ ( $^\circ$ )
B45 - I	11
B45 - II	12
B45 - III	11
B45 - IV	12
B45 - V	-

Consequently, the relationship can be written:

$$\Phi^{lim} > \Phi_{res} \quad (5.8)$$

It is highly recommended to perform other series of tests to confirm whether this result can be trust.

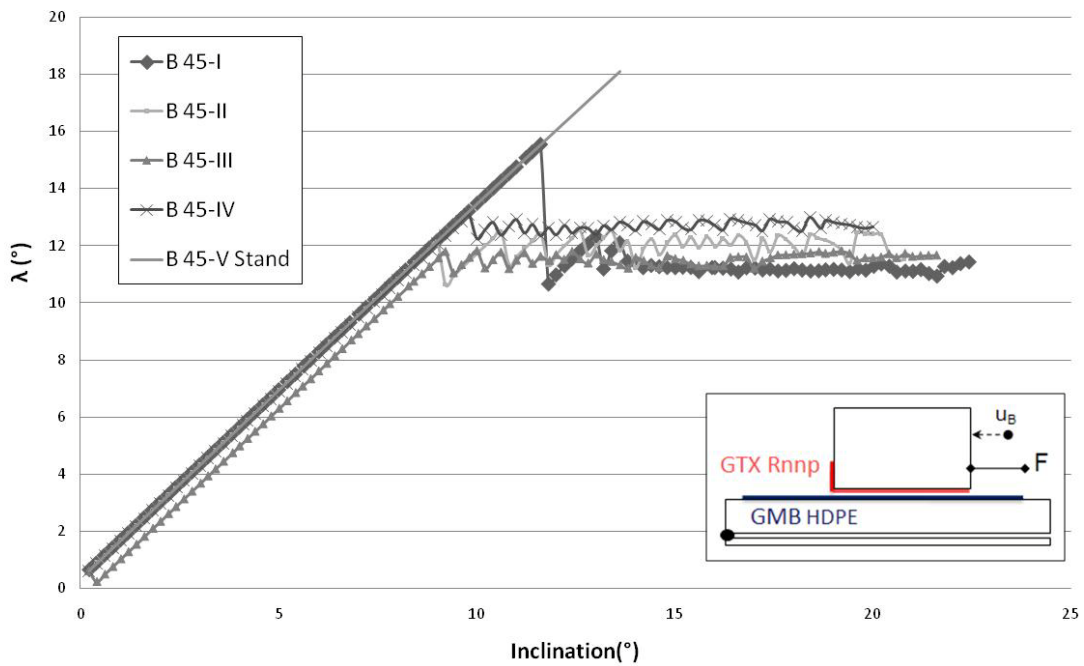


Figure 5.30 - Test results of interface Rnnp x HDPE, series B45

### 5.3.3 Interface HB-HDPE

Dynamic results for series A21 and A24 are showed in Figure 5.31, Figure 5.32, Table 5.33 and Table 5.34.

Table 5.33 - Dynamic results of interface HB-HDPE, series A21, guidance system  $\delta$

Test	A21-I	A21-II	A21-III	A21-IV dyn 2	A21-IV dyn 2
$\gamma$ (mm/s <sup>2</sup> )	84	69	91	1073	737
$\beta$ (°)	12	12	12	18	16
$\Phi^{\text{lim}}$ (°)	12	11	11	12	12

Table 5.34 - Dynamic results of interface HB-HDPE, series A24, guidance system  $\delta$

Test	A24-I	A24-II	A24-III	A24-IV dyn 2	A24-IV dyn 2
$\gamma$ (mm/s <sup>2</sup> )	161	209	219	1006	1025
$\beta$ (°)	11	11	11	16	16
$\Phi^{\text{lim}}$ (°)	10	10	10	10	10

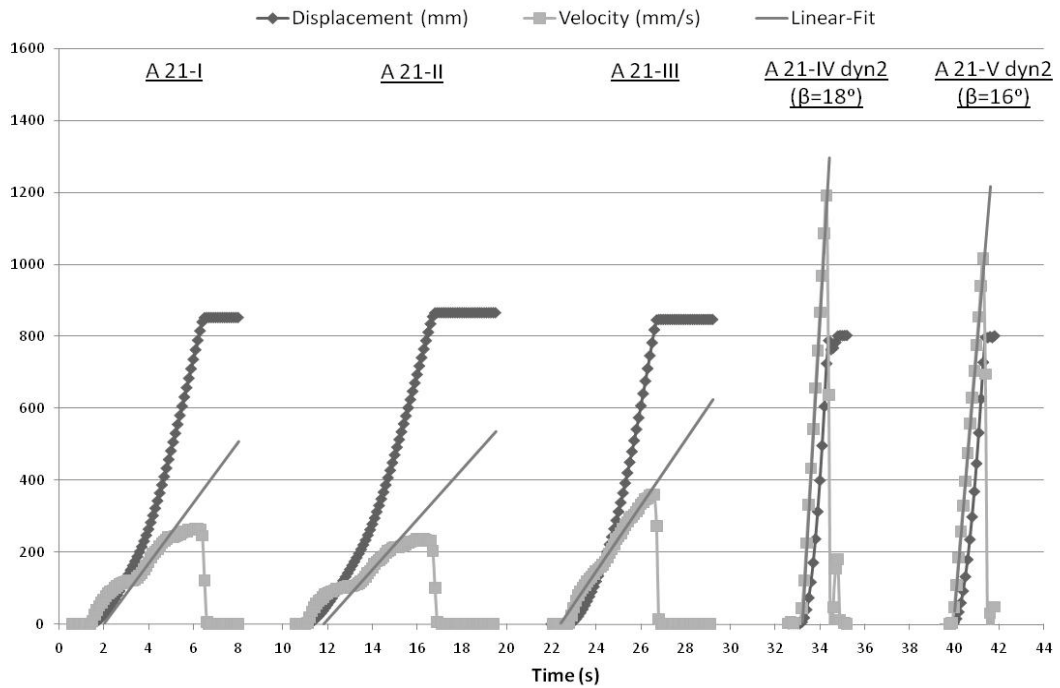


Figure 5.31 - Dynamic results of interface HB-HDPE, series A21, guidance system  $\delta$

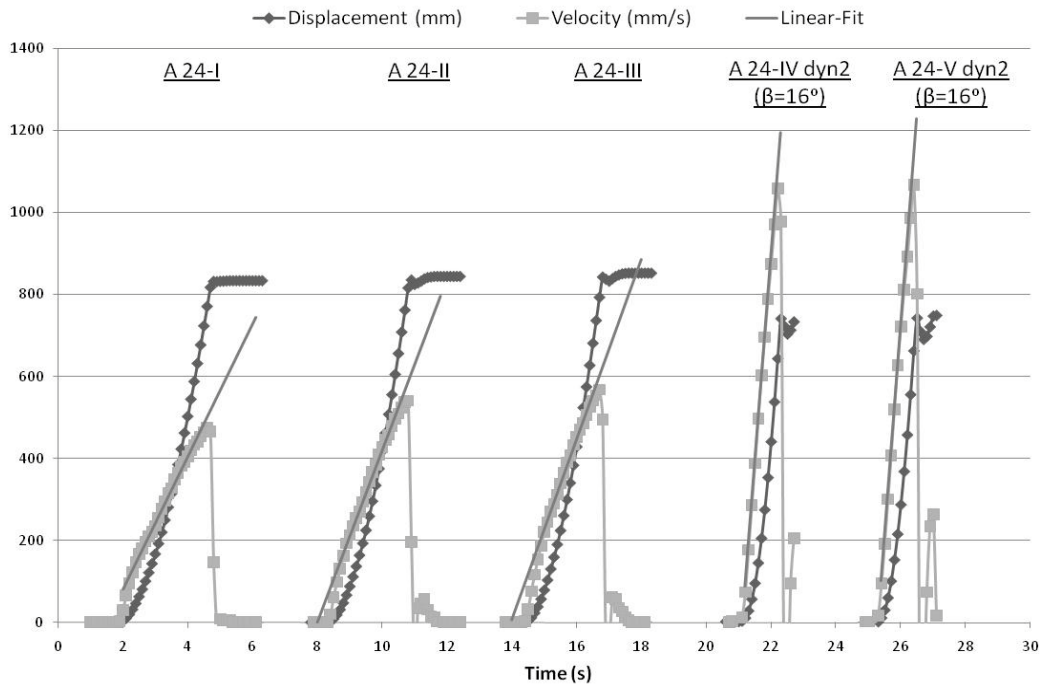


Figure 5.32 - Dynamic results of interface HB x HDPE, series A24, guidance system  $\delta$

The interpretation of the graphics seems more accurate for series A24 where the linear-fit was found using a wider interval. For series A21, the curve of velocity presented points of

inflection that indicated a reduction of the displacement rate. For this reason, the adopted average value of  $\Phi^{\text{lim}}$  was of  $(10 \pm 1)^\circ$ , calculated considering only A24 results.

As expected, for these series it was noticed that the higher the value of  $\beta$ , the faster was the box displacement was.

For trials using plane B, angle  $\Phi_{\text{res}}$  determined is presented in Table 5.35.

**Table 5.35 – Value of angle  $\Phi_{\text{res}}$ , interface HB-HDPE, series B75 and 81, charge of 482 kg and 476 kg, respectively.**

Test	$\Phi_{\text{res}}$ (°)
<b>B75-I</b>	15
<b>B75-II</b>	16
<b>B75-III</b>	16
<b>B81-I</b>	17
<b>B81-II</b>	18

The average results for series  $\Phi_{\text{res}}$  is  $(16 \pm 1)^\circ$  for series B75, and  $(17 \pm 1)^\circ$  for series B81. Because the results of B75 seemed more homogeneous, the chosen average value to characterize the interface was  $(16 \pm 1)^\circ$ . More tests are recommended to guarantee this result.

Comparing the values of  $\Phi^{\text{lim}}$  and  $\Phi_{\text{res}}$ , determined using plane A and B, respectively, it is not possible to assume that they are equivalent. In this case,  $\Phi^{\text{lim}}$  was smaller than  $\Phi_{\text{res}}$ ,

### 5.3.4 Interface nnpC-PP

The dynamic analyses of tests performed with interface nnpC x PP are presented in Table 5.36 and Table 5.37. From these results, the angle  $\Phi^{\text{lim}}$  found was equal to  $(19 \pm 1)^\circ$  while  $\Phi_{\text{res}}$  was equal to  $(11 \pm 1)^\circ$ .

Hence, it can be written that  $\Phi^{\text{lim}}$  is higher than  $\Phi_{\text{res}}$ .

**Table 5.36 - Test results of interface nnpC x PP, test A27-I**

Test	A27-I
$\gamma$ (mm/s <sup>2</sup> )	521
$\beta$ (°)	21
$\Phi^{\text{lim}}$ (°)	19

**Table 5.37 - Test results of interface nnpC x PP, series B82**

Test	$\Phi_{res}$ (°)
<b>B82-I</b>	12
<b>B82-II</b>	11

Tests A25 and A26 were not taken into account for this analysis because they did not have an appropriated interval for the determination of acceleration. As for series A82, only test A82-II was considered for calculation.

The value found for  $\Phi^{lim}$  was higher than the values found for the static angles in tests A25 and A26. This might have happened because the inclination of the plane ( $\beta$ ) stipulated to begin the tests was too high in comparison with static angle  $\Phi_{50}$ . And since this increase of inclination did not result in a large gain in the velocity or acceleration, the value of  $\Phi^{lim}$  remained close to the value of  $\beta$ . For next dyn2 tests, it is recommended to choose a value of  $\beta$  that is approximately  $3^\circ$  higher than  $\Phi_{50}$ , maximum.

Angle  $\Phi^{lim}$  was discarded and additional tests were required.

### 5.3.5 Interface Rnnp-PVC

The dynamic behavior of series A30 is shown in Figure 5.33.

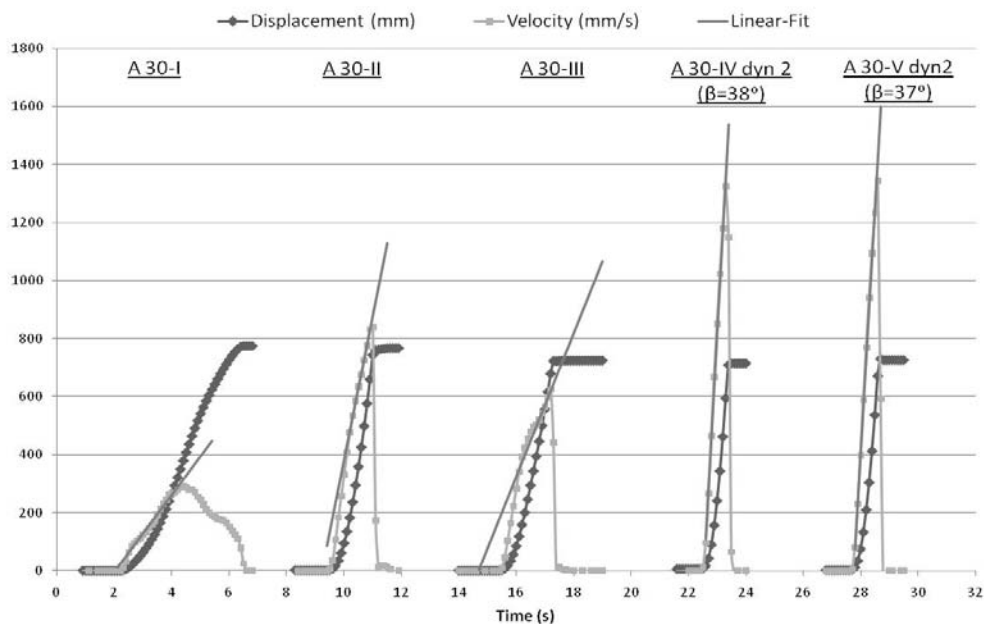


**Figure 5.33 - Dynamic results of interface Rnnp x PVC, series A30, guide system type  $\delta$**

Table 5.38 presents the values found for  $\Phi^{\text{lim}}$  for each test performed on series A30. It is also exhibited the acceleration value extracted from the graphic in Figure 5.33 and the inclination angle ( $\beta$ ) used to calculate  $\Phi^{\text{lim}}$ .

Tests A30-II and III were discarded because the angle  $\beta$  used to calculate  $\Phi^{\text{lim}}$  was higher than expected (a value around  $30^\circ$ ). As a result, considering only A30-I, IV and V, the angle  $\Phi^{\text{lim}}$  was equal to  $(29 \pm 1)^\circ$ .

Series A6 was discarded from this analysis because of problems regarding the guidance system (type  $\alpha$ ).

**Table 5.38 - Dynamic results of interface Rnnp x PVC, series A30, guide system type  $\delta$**

Test	A30-I	A30-II	A30-III	A30-IV dyn 2	A30-V dyn 2
$\gamma$ (mm/s <sup>2</sup> )	132	496	247	1787	1698
$\beta$ (°)	31	35	34	38	37
$\Phi^{\text{lim}}$ (°)	30	33	33	29	28

To better study the effects of acceleration in the determination of  $\Phi^{\text{lim}}$ , it would be better to perform tests of type dyn2 using the same angle  $\beta$ . This would facilitate the analysis and would also increase the credibility of the test result.

As a final point, no value of  $\Phi_{\text{res}}$  was found because the curve *Lambda vs. Inclination* for interface Rnnp x PVC did not present the residual level.

### 5.3.6 Interface HB-PVC

The result of series A8, A9, A17 and A29 are represented, respectively, in Table 5.39, Table 5.40, Table 5.41 and Table 5.42.

Despite the sensitivity to abrasion noticed in the static analysis, the dynamic results presented a good repeatability of  $\Phi^{\text{lim}}$  and this angle was equal to  $(23 \pm 1)^\circ$ .

**Table 5.39 - Dynamic results of interface HB x PVC, series A8, guidance system  $\alpha$**

Test	A8-I	A8-II	A8-III	A8-IV dyn 2	A8-V dyn 2
$\gamma$ (mm/s <sup>2</sup> )	1740	1041	737	1182	898
$\beta$ (°)	33	28	27	29	28
$\Phi^{\text{lim}}$ (°)	23	23	23	23	23

**Table 5.40 - Dynamic results of interface HB x PVC, series A9, guidance system  $\alpha$**

Test	A9-I	A9-II	A9-III	A9-IV dyn 2	A9-V dyn 2
$\gamma$ (mm/s <sup>2</sup> )	1367	1611	1211	1163	1191
$\beta$ (°)	31	32	30	30	30
$\Phi^{\text{lim}}$ (°)	24	23	23	24	24

**Table 5.41 - Dynamic results of interface HB x PVC, series A17, guidance system  $\gamma$ , reused sample of the geomembrane**

Test A	A17-II	A17-III	A17-IV dyn 2	A17-V dyn 2
$\gamma$ (mm/s <sup>2</sup> )	1550	1145	1826	1743
$\beta$ (°)	30	28	33	32
$\Phi^{\text{lim}}$ (°)	21	22	23	23

Test A17-I was discarded because of problems with the guidance system.

**Table 5.42 - Dynamic results of interface HB x PVC, series A29, guidance system  $\delta$**

Test	A29-I	A29-II	A29-III dyn2	A29-IV dyn 2
$\gamma$ (mm/s <sup>2</sup> )	1552	1297	1939	1972
$\beta$ (°)	32	30	35	35
$\Phi^{\text{lim}}$ (°)	24	23	25	25

### 5.3.7 Interface nnp40-PVC

The dynamic behavior of series A13 is showed in Figure I.15, on appendix I. A13-I, II and III correspond to test procedure dyn1, while A13-IV and V correspond to procedure dyn2.

As shown in Table 5.43, the average result for  $\Phi^{\text{lim}}$  presented a good repeatability and the value found was equal to  $(24 \pm 1)^\circ$ .

Table 5.44 presents the dynamic results found for series A18 and A20. The average value determined for  $\Phi^{\text{lim}}$  was also equal to  $(24 \pm 1)^\circ$ .

**Table 5.43 - Dynamic results of interface nnp40 x PVC, series A13, guide system type  $\beta$** 

Test	A13-I	A13-II	A13-III	A13-IV dyn 2	A13-V dyn 2
$\gamma$ (mm/s <sup>2</sup> )	717	571	548	2234	2164
$\beta$ (°)	27	27	27	36	36
$\Phi^{\text{lim}}$ (°)	24	24	24	24	24

**Table 5.44 - Dynamic results of interface nnp40 x PVC, series A18 and A20, guide system type  $\gamma$  and  $\delta$ .**

Test	A18-I dyn2	A20-I	A20-II	A20-III	A20-IV dyn 2
$\gamma$ (mm/s <sup>2</sup> )	1538	414	480	1121	1628
$\beta$ (°)	32	27	27	30	33
$\Phi^{\text{lim}}$ (°)	24	25	24	24	25

### 5.3.8 Interface nnp40-HDPE

The dynamic results for series A22 and A23 presented appropriated values of acceleration only for tests type dyn 2. The curves *Velocity vs. Time* for the dyn1 tests was too irregular to be used to calculate the acceleration. As shown in Figure 5.34, the maximum velocity of the upper box in each test was approximately the same and the liner-fit presented a similar slope. From Table 5.45 it is possible to conclude that  $\Phi^{\text{lim}}$  is equal to  $(13 \pm 1)^\circ$ .

**Table 5.45 - Dynamic results of interface nnp40 x HDPE, series A22 and A23, guidance system  $\delta$** 

Test	A22-IV dyn 2	A22-IV dyn 2	A23-IV dyn 2	A23-IV dyn 2
$\gamma$ (mm/s <sup>2</sup> )	612	605	706	711
$\beta$ (°)	17	17	17	17
$\Phi^{\text{lim}}$ (°)	13	13	13	13

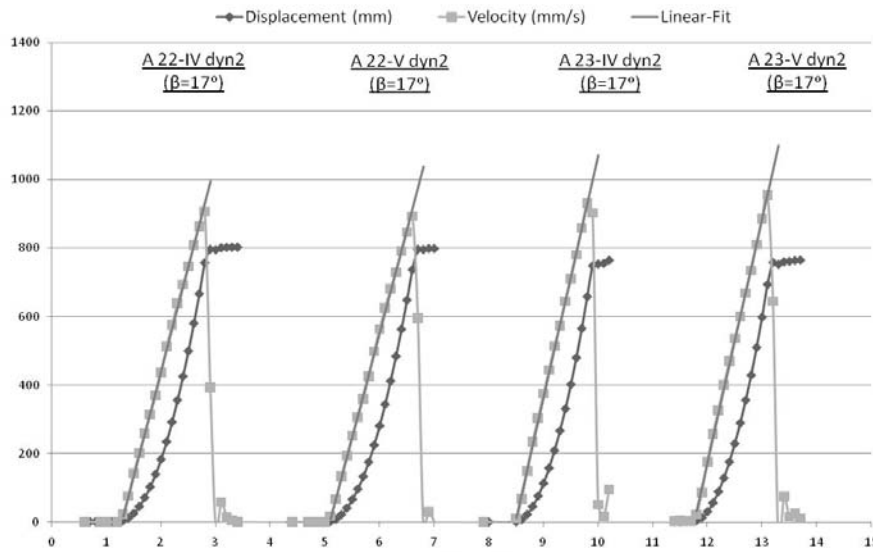


Figure 5.34 - Dynamic results of interface nnp40 x HDPE, series A22 and A23, guidance system  $\delta$

### 5.3.9 Interface nnpC-HDPE

Tests A28-IV and V were performed as dyn2 test types and their results are presented on Table 5.46. The interpretation of the results led to  $\Phi^{\text{lim}}$  equals to  $(15 \pm 1)^\circ$ . It is recommended to execute other series of trials to add credibility to this result.

Table 5.46 - Dynamic results of interface nnpC x HDPE, series A28, guidance system  $\delta$

Test	A28-IV dyn 2	A28-IV dyn 2
$\gamma$ (mm/s <sup>2</sup> )	367	336
$\beta$ (°)	17	17
$\Phi^{\text{lim}}$ (°)	15	15

## 5.4 Summary of results

The results of the static and dynamic analysis of tests using geomembrane PVC are summarized on Table 5.47 to Table 5.49.

**Table 5.47 – Summary of results of interface Rnnp-PVC**

<b>Interface</b>	<b>Rnnp-PVC</b>			
<b>Plane</b>	<b>A</b>		<b>B</b>	
<b>Behavior</b>	Sudden Slide		Sudden Slide (Jearky slide for B43-I)	
<b>Abrasion</b>	Not sensible		Experiment with new samples presented smaller peak friction angle than of reused samples	
$\Phi_0$	$(30 \pm 1)^\circ$	#3	$(30 \pm 1)^\circ$	#3
$\Phi_{50}$	$(30 \pm 1)^\circ$	#3	$(30 \pm 1)^\circ$	#3
$\Phi_{peak}$	-	-	$(31 \pm 1)^\circ$	#5
$\Phi_{peak, I}$	-	-	$(27 \pm 1)^\circ$	#3
<b>Correlation I</b>	$\Phi_{peak} > \Phi_{0,B} = \Phi_{50,B} = \Phi_{0,A} = \Phi_{50,A} > \Phi_{peak, I}$			
$\Phi^{lim}$	$(29 \pm 1)^\circ$	#3	-	
<b>Correlation II</b>	$\Phi_{peak} > \Phi_{0,B} = \Phi_{50,B} = \Phi_{0,A} = \Phi_{50,A} > \Phi^{lim} > \Phi_{peak, I}$			
<b>Conclusion</b>	The static angles calculated using both planes were equivalent			

**Table 5.48 – Summary of results of interface nnp40-PVC**

<b>Interface</b>	<b>nnp40-PVC</b>			
<b>Plane</b>	<b>A</b>		<b>B</b>	
<b>Behavior</b>	Sudden Slide		Sudden Slide	
<b>Abrasion</b>	Not sensible		Experiment with new samples presented smaller peak friction angle then of reused samples	
$\Phi_0$	$(27 \pm 1)^\circ$	#14	$(28 \pm 1)^\circ$	#2
$\Phi_{50}$	$(27 \pm 1)^\circ$	#14	$(28 \pm 1)^\circ$	#1
$\Phi_{peak}$	-	-	$(28 \pm 1)^\circ$	#2
$\Phi_{peak, I}$	-	-	$(22 \pm 1)^\circ$	#1
<b>Correlation I</b>	$\Phi_{peak} = \Phi_{0,B} = \Phi_{50,B} > \Phi_{0,A} = \Phi_{50,A} > \Phi_{peak, I}$			
$\Phi^{lim}$	$(24 \pm 1)^\circ$		-	
<b>Correlation II</b>	$\Phi_{peak} = \Phi_{0,B} = \Phi_{50,B} > \Phi_{0,A} = \Phi_{50,A} > \Phi^{lim} > \Phi_{peak, I}$			
<b>Conclusion</b>	The static angles calculated using both planes can be considerate equivalent due to the incertitude adopted of $1^\circ$ .			

Table 5.49– Summary of results of interface HB-PVC

Interface	HB-PVC			
Plane	A		B	
Behavior	Sudden Slide		Sudden Slide	
Abrasion	Sensible		Not sensible	
$\Phi_0$	$(32 \pm 1)^\circ$	#4	$(28 \pm 1)^\circ$	#3
$\Phi_{50}$	$(32 \pm 1)^\circ$	#4	$(29 \pm 1)^\circ$	#2
$\Phi_{peak}$	-	-	$(28 \pm 1)^\circ$	#3
Correlation I	$\Phi_{0,A} = \Phi_{50,A} > \Phi_{0,B} = \Phi_{peak}$			
$\Phi^{lim}$	$(23 \pm 1)^\circ$		-	
Correlation II	$\Phi_{0,A} = \Phi_{50,A} > \Phi_{0,B} = \Phi_{peak} > \Phi^{lim}$			
Conclusion	The static angles calculated using plane A were bigger than the static angles calculated using plane B			

It is important to recall that the average results of  $\Phi_{0,A}$  and  $\Phi_{50,A}$  for interface HB-PVC were found considering only the tests made with new samples of geosynthetic.

The value of  $\Phi_{50,B}$  was not considered to the correlation analysis in Table 5.49 because in order to determine its average it was used a smaller number of tests than for the other static angles and this difference provoked the disparity among  $\Phi_{0,B}$ ,  $\Phi_{50,B}$  and  $\Phi_{peak}$ . For more details about the determination of these values, check item 5.2.3.

Regarding interfaces composed by geomembrane PVC, it can be stated that:

- For tests made using plane B, the interfaces presented reduced static angles for the tests performed with new samples of geomembrane (HB-PVC was an exception). Angle  $\Phi_{peak,I}$  was smaller than all the other friction values, including  $\Phi^{lim}$ . This interface feature must be better examined in order to avoid misled on project characterization. In this case, the consideration of ISO12957-2 to avoid repetition of samples should be followed.
- Interfaces tested using plane A did not seem sensitive to abrasion, except for interface HB x PVC. As mentioned before, HB suffered most with abrasion than the PVC itself.
- The analysis of tests performed with interfaces composed by PVC geomembranes and using inclined plane B did not present a residual level like interfaces composed by

HDPE or PP. Instead, the graphic *Lambda vs. Inclination* revealed more than one peak value of lambda (Figure 5.35). The only interface tested with PVC that presented a residual level was, curiously, interface PVC-PVC (Figure 5.36).

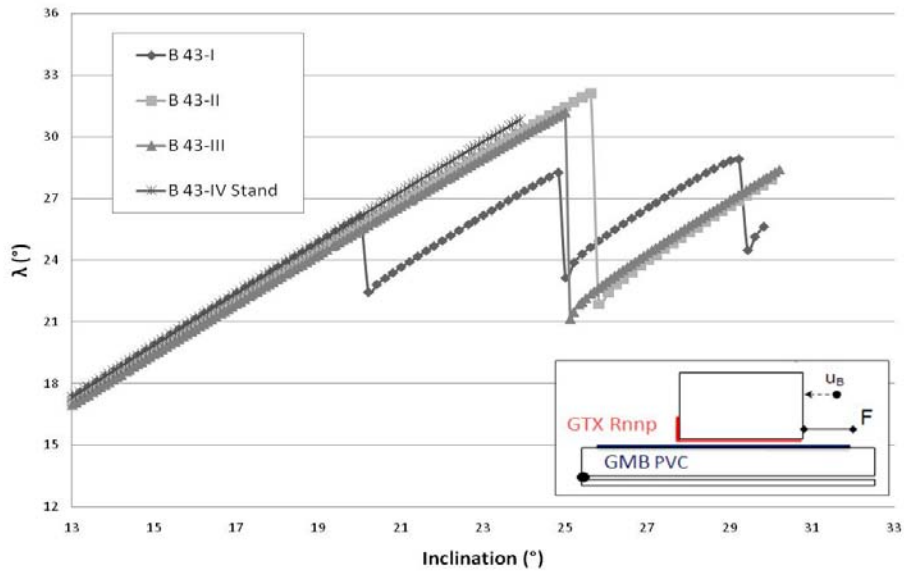


Figure 5.35 – Graphic *Lambda vs. Inclination*, interface Rnnp x PVC

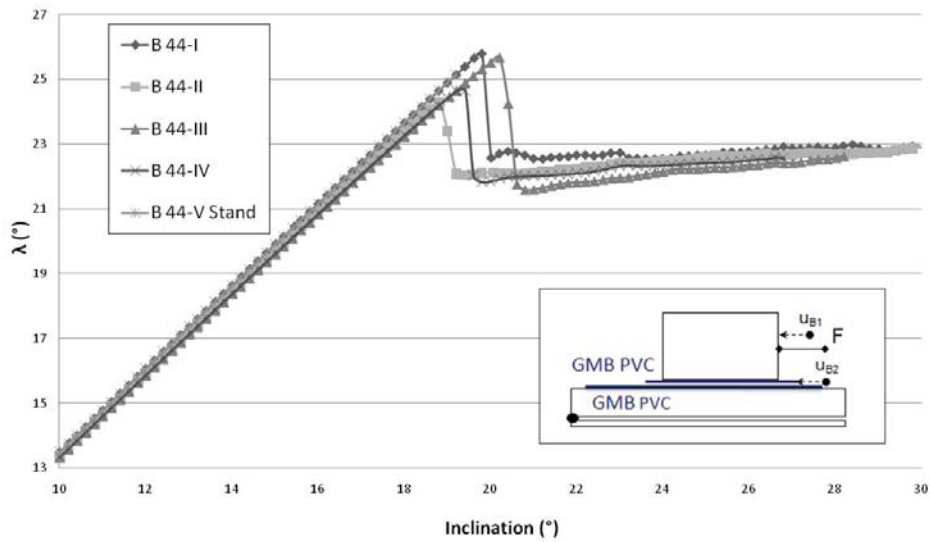


Figure 5.36 – Graphic *Lambda vs. Inclination*, interface PVC x PVC

- The behavior of curve B43-I (Figure 5.35) suggest that a peak value is being repeated periodically. In order to verify if the other tests also present periodical repetitions of the peak value it is recommended to let the experiment last longer, that is, to keep inclining the plane even after the first peak of  $\lambda$  occurs.
- All three interfaces presented the sudden slide behavior

- Angle  $\Phi^{\text{lim}}$  was inferior to the static friction angles, except for  $\Phi_{\text{peak,I}}$ .
- For the results found, interface Rnnp x PVC presented equivalent values for the static angles from plane A and B. Regarding the other, HB x PVC presented higher values for plane A comparing with plane B. Interface nnp40 x PVC presented slightly higher values for plane B than for plane A but, due to the incertitude adopted, they were considered equivalent.

The summary of results of interfaces composed by HDPE is shown in Table 5.50 and Table 5.51.

**Table 5.50 – Summary of results of interface Rnnp-HDPE**

<b>Interface</b>	<b>Rnnp-HDPE</b>			
<b>Plane</b>	<b>A</b>		<b>B</b>	
<b>Behavior</b>	Sudden slide		Sudden slide	
<b>Abrasion</b>	Sensible		Sensible	
$\Phi_0$	$(16 \pm 1)^\circ$	#2	$(12 \pm 1)^\circ$	#1
$\Phi_{50}$	$(16 \pm 1)^\circ$	#2	$(12 \pm 1)^\circ$	#1
$\Phi_{\text{peak}}$	-	-	$(13 \pm 1)^\circ$	#4
<b>Correlation I</b>	$\Phi_{0,A} = \Phi_{50,A} > \Phi_{\text{peak}} = \Phi_{0,B} = \Phi_{50,B}$			
$\Phi^{\text{lim}}$	$(16 \pm 1)^\circ$	#3	-	-
$\Phi_{\text{res}}$	-	-	$(12 \pm 1)^\circ$	#4
<b>Correlation II</b>	$\Phi_{0,A} = \Phi_{50,A} = \Phi^{\text{lim}} > \Phi_{\text{peak}} > \Phi_{0,B} = \Phi_{50,B} = \Phi_{\text{res}}$			
<b>Conclusion</b>	The static angles calculated using plane A were bigger than the static angles calculated using plane B			

Regarding interfaces composed by geomembrane HDPE, it can be state that:

- For interface Rnnp-HDPE, the characteristic angles that were found using planes A and B were very different. Since it was made too few tests with this interface, it is recommended to perform more trials, this time using a bigger sample space.
- All parameters found using interface Rnnp-HDPE and plane A were higher than the parameters found using plane B.
- To better characterize the interfaces study, it should be performed more trials.
- $\Phi_{\text{res}}$  and  $\Phi^{\text{lim}}$  were not equivalent for the tests analyzed. However the tests studied can be supposed inconclusive due to the small amount of tests compared.

Table 5.51 – Summary of results of interface HB-HDPE

Interface	HB-HDPE			
Plane	A		B	
Behavior	Sudden Slide		Gradual Slide	
Abrasion	Not sensible		Not sensible	
$\Phi_0$	$(11 \pm 1)^\circ$	#3	discarded	-
$\Phi_{50}$	$(11 \pm 1)^\circ$	#3	discarded	-
$\Phi_{\text{peak}}$	-	-	$(17 \pm 1)^\circ$	#5
Correlation I	$\Phi_{\text{peak}} > \Phi_{0,A} = \Phi_{50,A}$			
$\Phi^{\text{lim}}$	$(10 \pm 1)^\circ$	#5	-	-
$\Phi_{\text{res}}$	-	-	$(16 \pm 1)^\circ$	#4
Correlation II	$\Phi_{\text{peak}} > \Phi_{\text{res}} > \Phi_{0,A} = \Phi_{50,A} > \Phi^{\text{lim}}$			
Observation	$\Phi_{0,B}$ and $\Phi_{50,B}$ were discarded because the values found presented a large standard deviation			

The summary of results of interfaces composed by PP geomembranes is presented in Table 5.52 and Table 5.53.

Table 5.52 – Summary of results of interface Rnnp-PP

Interface	Rnnp-PP			
Plane	A		B	
Behavior	Gradual slide at the beginning of movement followed by a sudden slide		Gradual slide at the beginning of movement followed by a sudden slide	
Abrasion	Sensible		Sensible	
$\Phi_0$	$(20 \pm 1)^\circ$	#1	$(18 \pm 1)^\circ$	#3
$\Phi_{50}$	$(20 \pm 1)^\circ$	#1	$(20 \pm 1)^\circ$	#3
$\Phi_{\text{peak}}$	-	-	$(22 \pm 1)^\circ$	#3
Correlation II	$\Phi_{\text{peak}} > \Phi_{50,A} = \Phi_{50,B} = \Phi_{0,A} > \Phi_{0,B}$			
Conclusion	The static angle $\Phi_{50,A}$ and $\Phi_{50,B}$ were equivalent			

Table 5.53 – Summary of results of interface nnpC-PP

Interface	nnpC-PP			
Plane	A		B	
Behavior	Gradual slide at the beginning of movement followed by a sudden slide		Gradual slide at the beginning of movement followed by a sudden slide	
Abrasion	-		Experiment with new samples seems to presented smaller peak friction angle than of reused samples	
$\Phi_0$	$(15 \pm 1)^\circ$	#2	$(12 \pm 1)^\circ$	#1
$\Phi_{50}$	$(15 \pm 1)^\circ$	#2	$(18 \pm 1)^\circ$	#1
$\Phi_{peak}$	-	-	$(18 \pm 1)^\circ$	#1
Correlation I	$\Phi_{peak} = \Phi_{50,B} > \Phi_{50,A} = \Phi_{0,A} > \Phi_{0,B}$			
$\Phi^{lim}$	discarted	-	-	-
$\Phi_{res}$	-	-	$(11 \pm 1)^\circ$	#1
Correlation II	$\Phi_{peak} = \Phi_{50,B} > \Phi_{50,A} = \Phi_{0,A} > \Phi_{0,B} > \Phi_{res}$			
Observation	Additional tests are required to confirm the results found with these series studied.			
Conclusion	The static angles calculated using plane A were smaller than the static angles calculated using plane B			

Regarding interfaces composed by geomembrane PP, it can be stated that:

- Tests made using plane B presented the residual level.
- The typical behavior presented was the gradual slide at the beginning of the movement followed by the sudden slide.

The summary of results for interface nnp40 x EPDM is shown on Table 5.54.

Table 5.54 – Summary of results of interface nnp40-EPDM

Interface	nnp40-EPDM	
Plane	A	B
Behavior	Gradual slide	Gradual slide
Abrasion	Sensible	Sensible
Observation	The dynamic analysis was not possible to be analyzed and the average values of the static angles were only determined to each series made. The global average for each inclined plane was not determined.	

Interface nnp40 x EPDM shows that  $\Phi_0$  and  $\Phi_{50}$  can be very different when the interface presents the gradual sliding behavior. For this case, the standard value defined for

displacement equals to 50 mm can result in a non conservative threshold angle  $\Phi_{50}$ . To better analyze whether or not this angles are no longer conservative, the creep test is recommended.

A general overview can be written:

- Angle  $\Phi_{\text{peak}}$  was higher or equal to all the other angles (including for angles calculated using plane A) except for interface Rnnp-HDPE where the static angles estimated using plane A ( $\Phi_{0,A}$ ,  $\Phi_{50,A}$ ) were at least  $3^\circ$  higher than the static angles found using plane B.
- Values of  $\Phi_0$  and  $\Phi_{50}$ , found using the same inclined plane, were equivalent for interfaces that presented sudden slide behavior. Additionally,  $\Phi_{50}$  was higher than  $\Phi_0$  when the gradual behavior happened. As a result,  $\Phi_{50}$  seems to be an appropriate index value to characterize the friction behavior whenever the interface presents a sudden slide behavior. For interfaces presenting gradual slide, the creep test is suggested.
- It was not possible to affirm that all interfaces tested presented equivalent friction results when tested with planes A and B.
- The difficulty in finding a global correlation for the parameters found using both planes indicates that the characterization of the interfaces friction behavior using only plane A over plane B would not always lead to a conservative condition.
- The results found for the dynamic analysis indicate that, to better simulate the field conditions, it is important to consider the parameter  $\Phi^{\text{lim}}$ . For tests studied, all the dynamic angles were inferior to the static angles, except for interface Rnnp-HDPE.
- Generalizations should be avoided regarding the reuse of samples. For PVC interfaces the reuse was not appropriated but for other interfaces, the cumulative displacements on the interfaces better simulated the site conditions.

## 6 CONCLUSIONS

The study of friction characterization is very important for the design of geotechnical projects. The domain of a large amount of data to characterize a slope lining system results in the optimization of values that are better suited to the needs of current engineering projects.

The inclined plane tests have been used to aid this friction characterization and have been applied to study interfaces soil-geosynthetic or geosynthetic-geosynthetic.

This paper focused on the study of interfaces between a geotextile and a geomembrane (GBR-P) in order to compare whether the results reached using the inclined plane of small dimensions were equivalent to results reached with the standardized inclined plane.

The results found indicated that each interface has a peculiar feature that difficult the generalization of results. For interfaces such as Rnnp-PVC, nnp40-PVC and Rnnp-PP, the static angles ( $\Phi_{0,A}$ ,  $\Phi_{50,A}$ ,  $\Phi_{0,B}$ ,  $\Phi_{50,B}$ ) were considered equivalent. For the other interfaces, the static angles from plane A were sometimes higher and sometimes lower than the static angles from plane B.

A lot of adjustments are recommended in order to perform future tests with more accuracy and caution. For tests involving inclined plane A, they are:

- Perform tests using the same guidance system.
- To better study the effects of acceleration on the determination of  $\Phi^{lim}$ , it would be better to perform tests of type dyn2 using the same angle  $\beta$ . This would facilitate the analysis and would also increase the credibility of the test result.
- Better study the sensitivity to abrasion of the interfaces before making trials that use reused samples.
- Perform tests type dyn2 also with new samples of geosynthetics instead of reused samples as made on this work.

For tests involving inclined plane B, they are:

- Use a non elastic rope to hold the upper box on force analysis. The looseness of the rope must be averted in order to avoid the impact in the dynamometer and consequent imprecision of force measurement when the upper box slides.

- The rope pre-tension effort at the beginning of each trial should be defined in order to improve the repeatability of results and to make the analysis even more rigorous. For instance, the pre-tension could be 1% of the maximum effort registered in the dynamometer.

For tests in general:

- Use the same inclination velocity for both planes;
- Take notes of the temperature and humidity of the laboratory during the tests;
- Program trials considering a bigger sample space, with at least 5 series (10 tests) for each inclined plane;
- Study how sensitive the interfaces are to abrasion and how the gradual slide is strengthened with the interface abrasion;
- Run trials of creep test analysis for interfaces that presented gradual sliding;
- Run tests to better analyze the PVC behavior.

The main recommendation is to increase the sample space adopted for the trials. Due to a lot of difficulties involving scarce resources, defects in the guidance system, interference in the system of acquisition and deadline it was not possible to perform the desired amount of tests to obtain appropriated results.

Regarding the theoretical consideration of absence of friction in the guidance system of plane A, the frequent difficulty to perform tests where the upper plate did not touch the lateral walls weakens this consideration. In addition, it was very complicated to adjust the parallelism of the lateral guides. For this reasons, and considering both planes mechanisms of guidance, plane B seems to offer the most reliable system.

The force analysis presents a great advantage when compared with other analysis because it would avoid the problems that arose due to the guidance system. Hence, it would be interesting if ISO12957-2 validated the force analysis procedure.

Plane B has a very laborious procedure to prepare the device since, for each new series, a great amount of sand must be withdraw from the upper box to then be placed again to run next trials. One suggestion to avoid such effort is to reduce the amount of sand used by partially replacing this material for plates of concrete such as performed by Lima Jr. (2000).

It is important to mention that the choice of interfaces that were tested and the sequence of trials to be made were not a decision of the author. Also, the author did not make the trials using the inclined plane B, she just worked with the data and made the analysis. The tests were performed by Dr. Laurent Briançon.

It is very important to separate the concept of an index test analysis and a performance oriented one. The purpose of an index test is to create a reference value based on general analyses that would usually be supplied by manufacturers to guide the designers. These analyses are usually described with parameters and procedures well defined in order to guarantee an accuracy of results no matter who reproduces the trials. The performance oriented tests are a deeper analysis of behaviors. Usually, these tests are made to study more realistic situations and to put together a bigger amount of data besides the index values. The procedure determined by ISO12957-2 illustrates an index test. The dynamic analysis is a performance oriented test.

The most important aspect to be pursued on next researches is to study the appropriated reduction factors to the values found using ISO12957-2 specifications. They will assist the design of safer and optimized lining systems since considerations such as mechanical damage, dynamic analysis and abrasion of surfaces would be in the agenda.

Other special analysis to be recommended is the creep test, highly indicated to study the instability of interfaces that present gradual behavior.

As a final point, to participate in this research was very instructive especially to learn how to deal with the problems generated during the work, how to arrange the schedules of trials, how to prepare the literature review and other aspects that will certainly contribute to the amendment of further researches. There are many aspects that could be improved in this work and, certainly, the researches suggested will help to complement the conclusions achieved.

## REFERENCES

BENVENUTO, C. *Estabilidade de aterros sanitários*. Available at: <<http://brasil-virtual.net/meioambiente/cursos-palestras1.htm>>. Accessed on: November 17<sup>th</sup>, 2009.

BRIANÇON, L. *Stabilité sur pentes des dispositifs geosynthétiques: caractérisation du frottement aux interfaces et applications*. 2001. 178 p. Thesis - Université Bordeaux I, Bordeaux.

BRIANÇON, L.; GIRARD, H.; POULIN, D. Slope Stability of lining systems – experimental modeling of friction at geosynthetic interfaces. *Geotextiles and Geomembranes*, v. 20, 147-172, 2002.

CERENZIO & PANARO. *Solid waste management and construction*. Available at: <<http://www.cpeengineers.com>> Accessed on: October 18<sup>th</sup>, 2009.

VIDAL, D. *Os geossintéticos e suas principais aplicações*. Available at: <<http://civil.ita.br/~delma>>. Accessed on: November 17<sup>th</sup>, 2009.

GOURC, J. P.; REYES RAMIREZ, R. Dynamics-based interpretation of the interface friction test at the inclined plane. *Geosynthetics International*, v.11, No. 6, 439-454, 2004.

INTERNATIONAL STANDARDIZATION ORGANIZATION. *ISO 12957-1:2005: geosynthétiques - détermination des caractéristiques de frottement - Partie 1: essai de cisaillement direct*. European Committee for standardization, Brussels, 2005. 11p.

INTERNATIONAL STANDARDIZATION ORGANIZATION. *ISO 12957-2:2005: geosynthétiques - détermination des caractéristiques de frottement - Partie 2: essai sur plan incliné*. European Committee for standardization, Brussels, 2005. 13p.

INTERNATIONAL STANDARDIZATION ORGANIZATION. *ISO 10318:2005: geosynthetics - terms and definitions*. Brussels, 2005. 36p.

JB HOLLAND CONSTRUCTION INC. *Excavation for landfill*. Available at: <<http://www.jbholland.net/prj4.php>>. Accessed on: October 18<sup>th</sup>, 2009.

KOUTSOURAIS, M. M.; SPRAGUE, C. J. Interfacial friction study of cap and liner components for landfill design. *Geotextiles and Geomembranes*, v.10, p. 531-548, 1991.

KOERNER, Robert M. *Designing with geosynthetics*. 4. ed. Upper Saddle River: Prentice Hall, 1997. 761p.

LIMA JR, N. R. *Estudo da interação entre solo e geossintético em obras de proteção ambiental com o uso do equipamento de Plano Inclinado*. 2000. 148f. Dissertação (Mestrado em Geotecnia) - Departamento de Engenharia Civil, Universidade de Brasília, Brasília/DF.

MACCAFERRI NEW ZEALAND. *Engineering environmental solutions*. Available at: <<http://www.maccaferri.co.nz>>. Accessed on : October 3rd, 2009.

REYES RAMIREZ, R. *Nouveau regard sur l'essai d'interface geosynthetic au Plan Incliné*. 2003. 180p. Thesis, Laboratoire Interdisciplinaire de Recherche Impliquant la Géologie et la Mécanique. University of Grenoble, Grenoble.

REYES RAMIREZ, R.; GOURC, J. P. (2003). Use of inclined plane test in measuring geosynthetic interface friction relationship. *Geosynthetics International*, v. 10, n. 5, p.165–175, 2003.

REYS RAMIRES, R.; GOURC, J. P.; VIDAL, D. Análise de escorregamento no sistema de estanqueidade de uma bacia de detenção. In: SIMPÓSIO BRASILEIRO DE GEOSSINTÉTICOS, 4., 2003, Porto Alegre. *Anais...* São José dos Campos: IGS, 2003. 1 CD-ROM.

## **APPENDIX I**

### **Results of trials using inclined plane A**

---

## Series A-1

**Conditions of test:** guidance system  $\alpha$ , new samples of geosynthetics.

**Observation:** system of acquisition presented interference on the measurement of inclination.

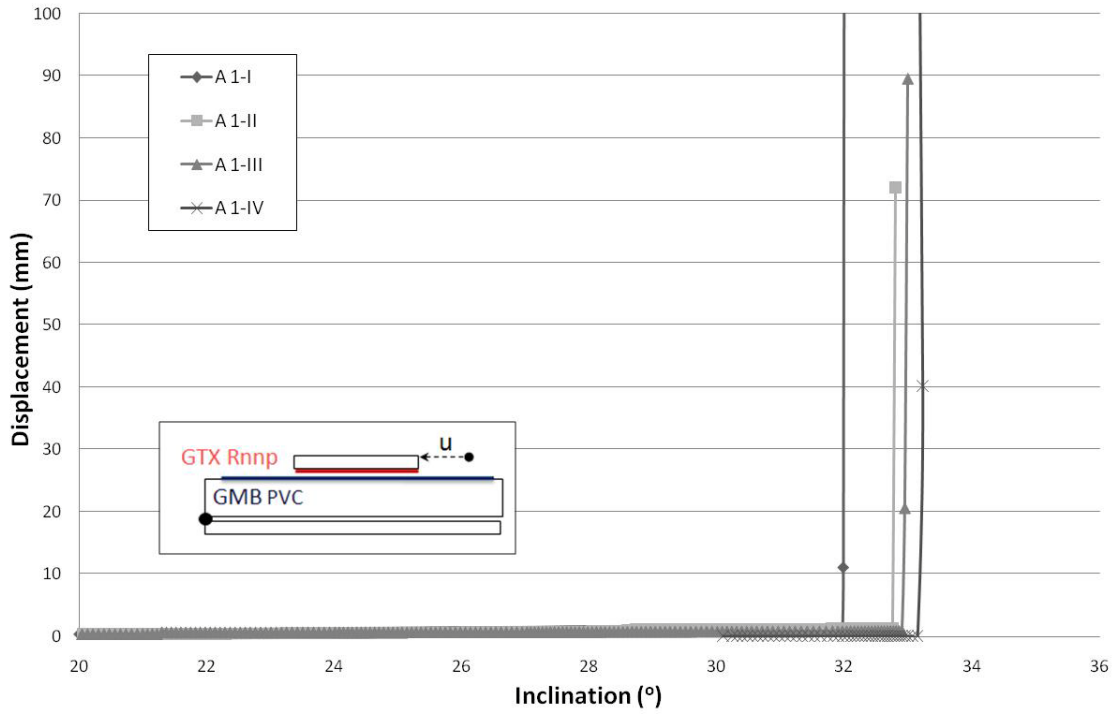


Figure I.1 Graphic *Displacement vs. Inclination*

## Series A-2

**Conditions of test:** guidance system  $\alpha$ , new samples of geosynthetics.

**Observation:** system of acquisition presented interference on the measurement of inclination.

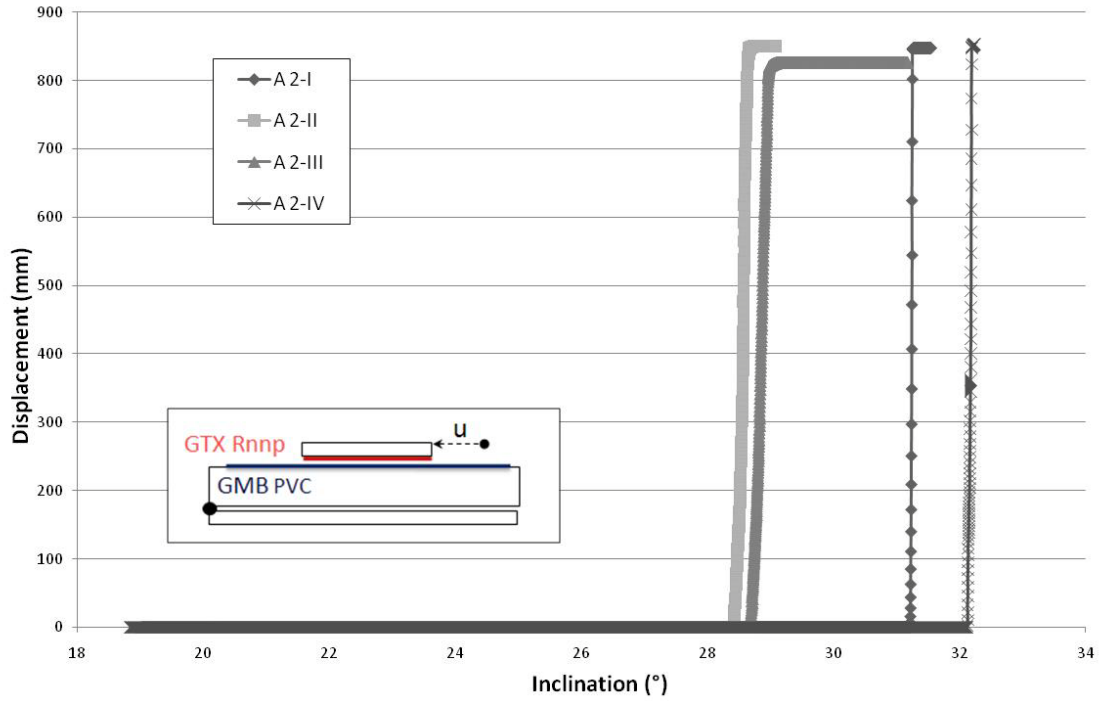
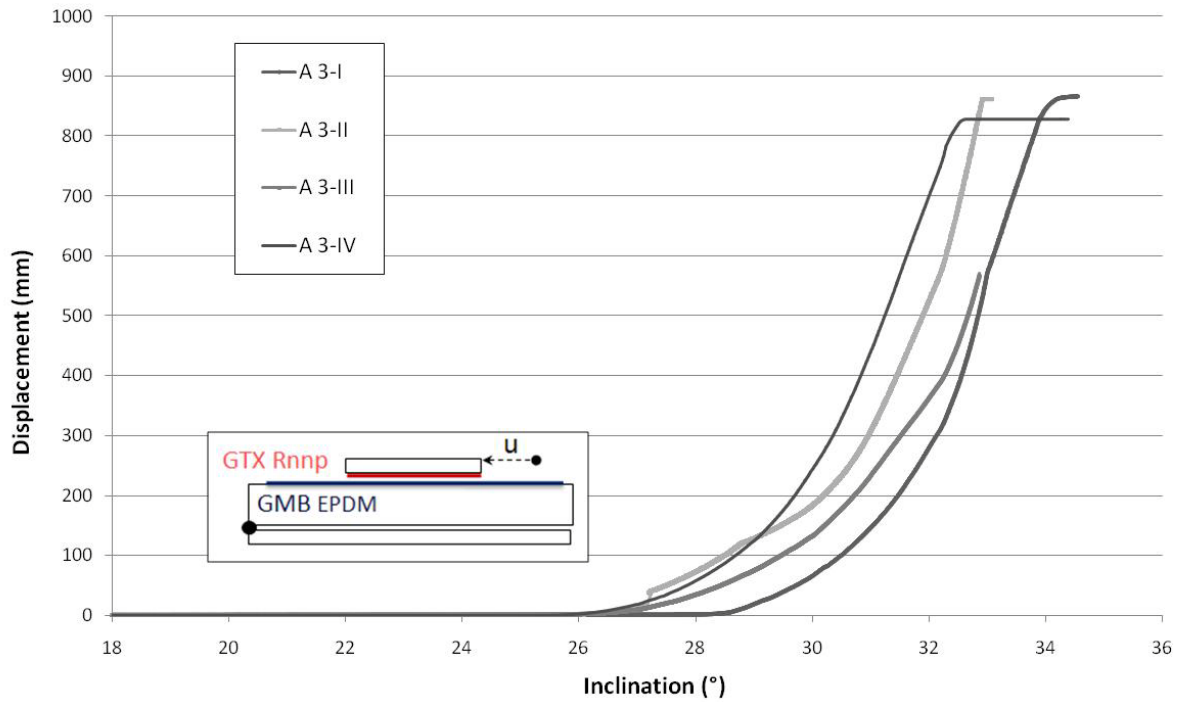


Figure I.2 – Graphic *Displacement vs. Inclination*

### Series A-3

**Conditions of test:** guidance system  $\alpha$ , new samples of geosynthetics.

**Observation:** system of acquisition presented interference on the measurement of inclination.



**Figure I.3 – Graphic Displacement vs. Inclination**

## Series A-4 & 5

**Conditions of series A4:** guidance system  $\alpha$ , new samples of geosynthetics.

**Conditions of series A5:** guidance system  $\alpha$ , reversed side of HDPE sample used on series A4.

### Observations:

- System of acquisition presented interference on the measurement of inclination.
- Visually, sample A5-I presented good conditions: no marks of injury or scratches.

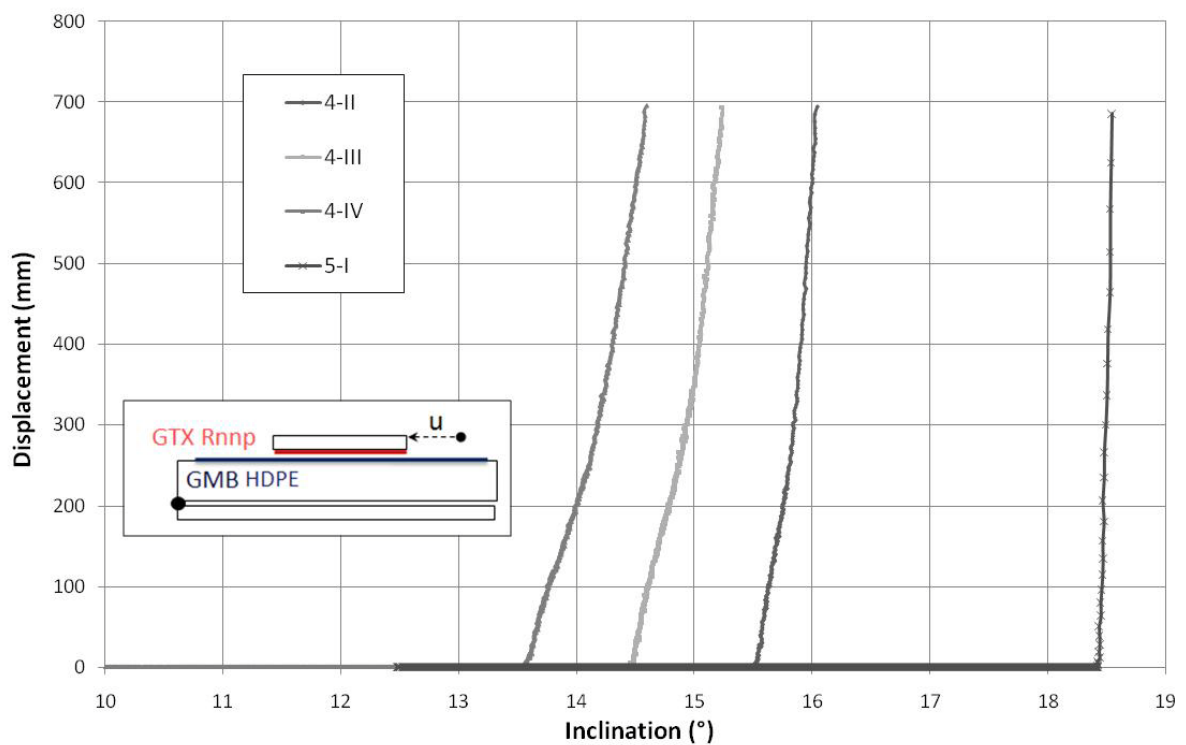


Figure I.4 – Graphic *Displacement vs. Inclination*

## Series A-6

**Conditions of test:** guidance system  $\alpha$ , reversed side of PVC sample used on series A1.

**Observation:**

- System of acquisition presented interference on the measurement of inclination.
- Visually, these sample presented good conditions: no marks of injury or scratches.
- $\beta$  showed in the legend is the inclination of the plane during the entire displacement of the upper box (test dyn2).

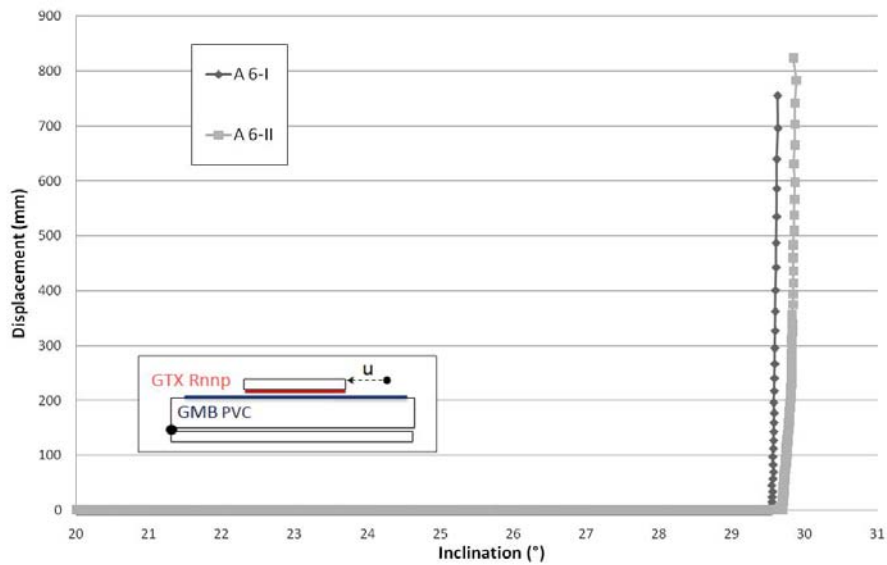


**Figure I.5 – Graphic Displacement vs. Inclination**

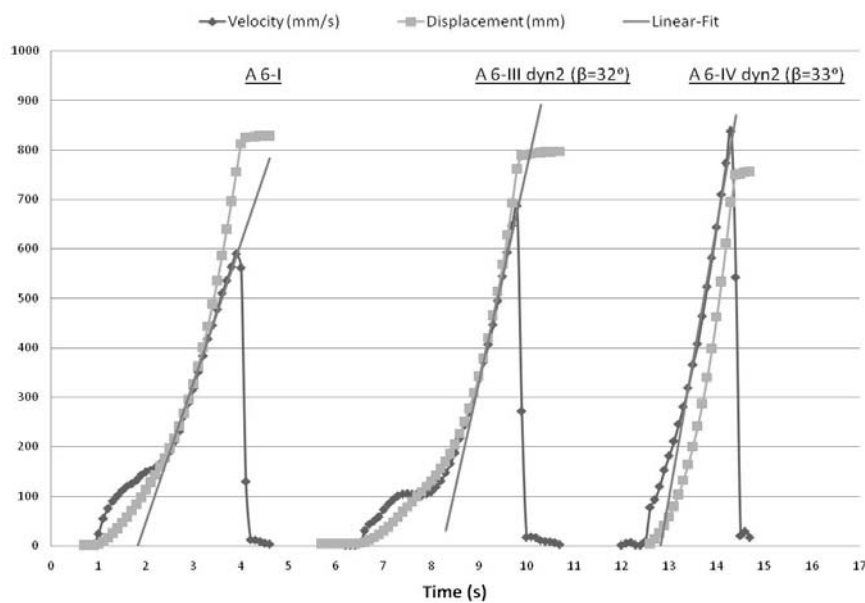


**Figure I.6 – Graphics Displacement vs. Time, Velocity vs. Time, Acceleration vs. Time**

## Series A-7

**Conditions of test:** guidance system  $\alpha$ , reversed side of PEDM sample used on series A3.

### Observations:

- Visually, these sample presented good conditions: no marks of injury or scratches.
- $\beta$  showed in the legend is the inclination of the plane during the entire displacement of the upper box (test dyn2).

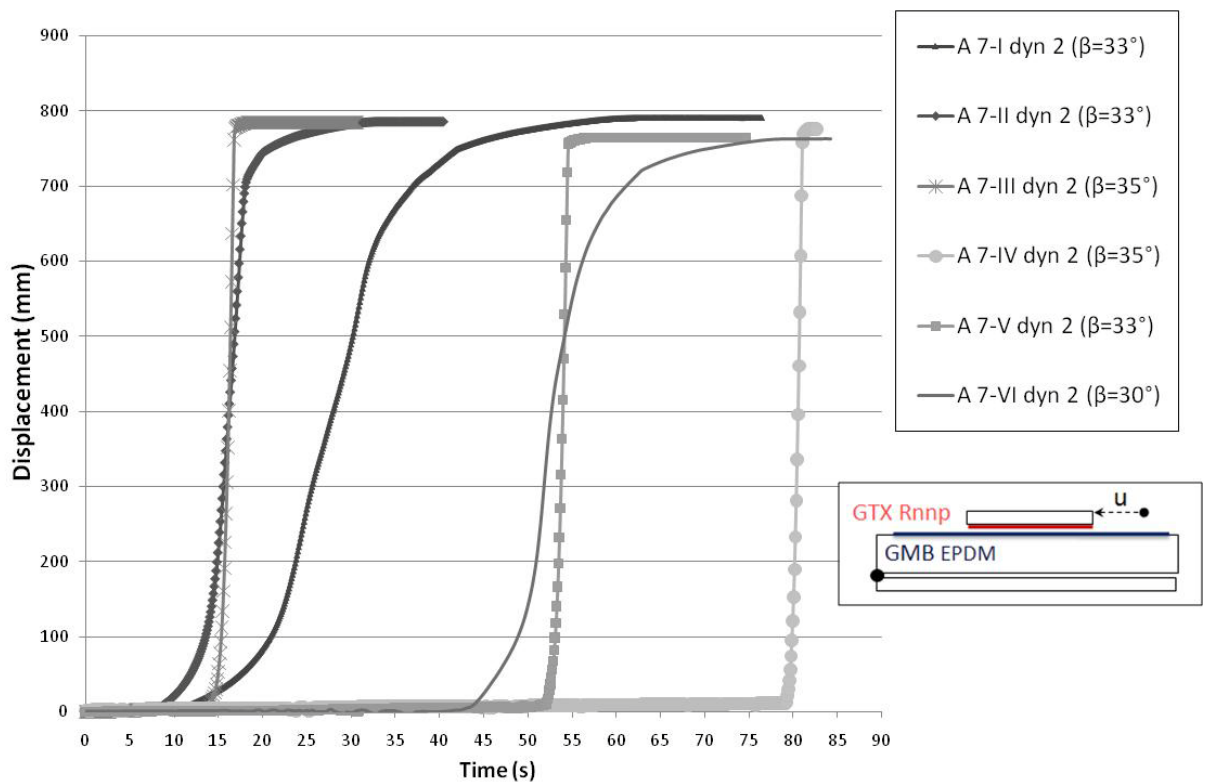
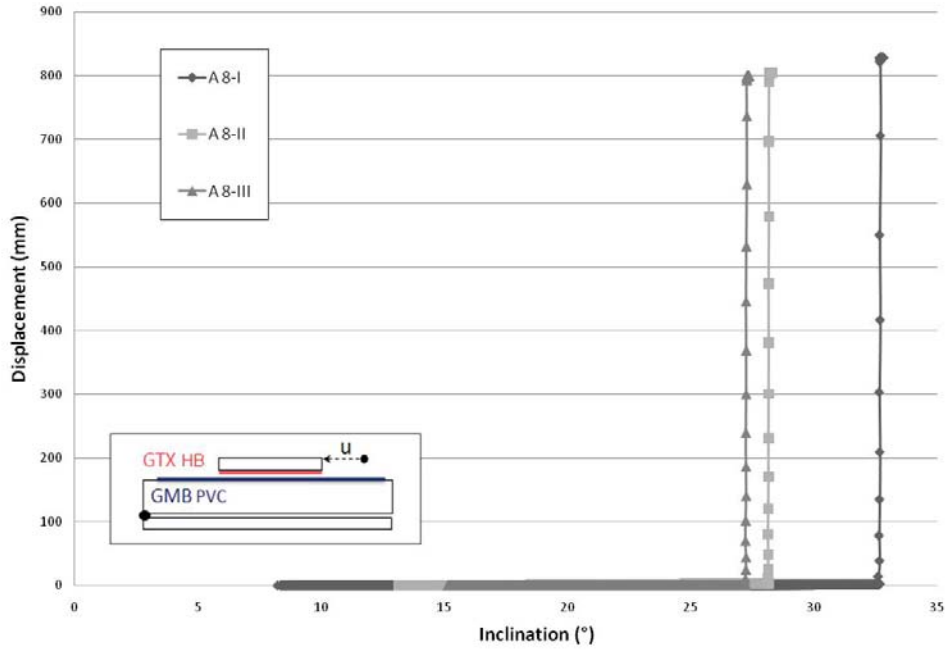


Figure I.7 – Graphic *Displacement vs. Time*

## Series A-8

**Conditions of test:** guidance system  $\alpha$ , new samples of geosynthetics.

**Observation:**  $\beta$  is the inclination of the plane during the entire displacement of the upper box (test dyn2)



**Figure I.8 – Graphic *Displacement vs. Inclination***

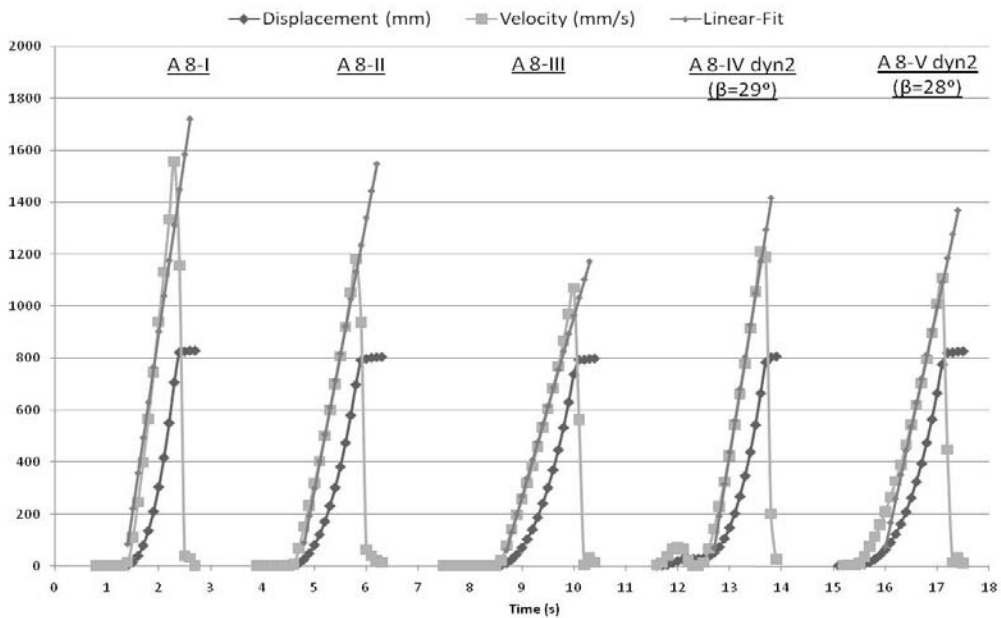


**Figure I.9 – Graphics *Displacement vs. Time, Velocity vs. Time, Acceleration vs. Time***

## Series A-9

**Conditions of test:** guidance system  $\alpha$ , new samples of geosynthetics.

**Observation:**  $\beta$  is the inclination of the plane during the entire displacement of the upper box (test dyn2)

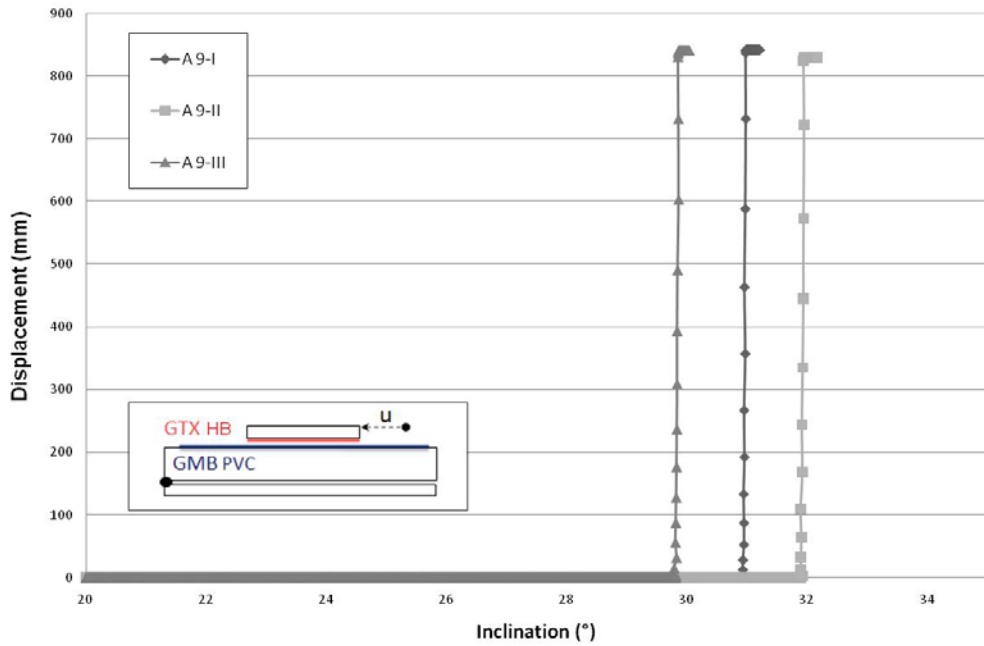


**Figure I.10 – Graphic *Displacement vs. Inclination***

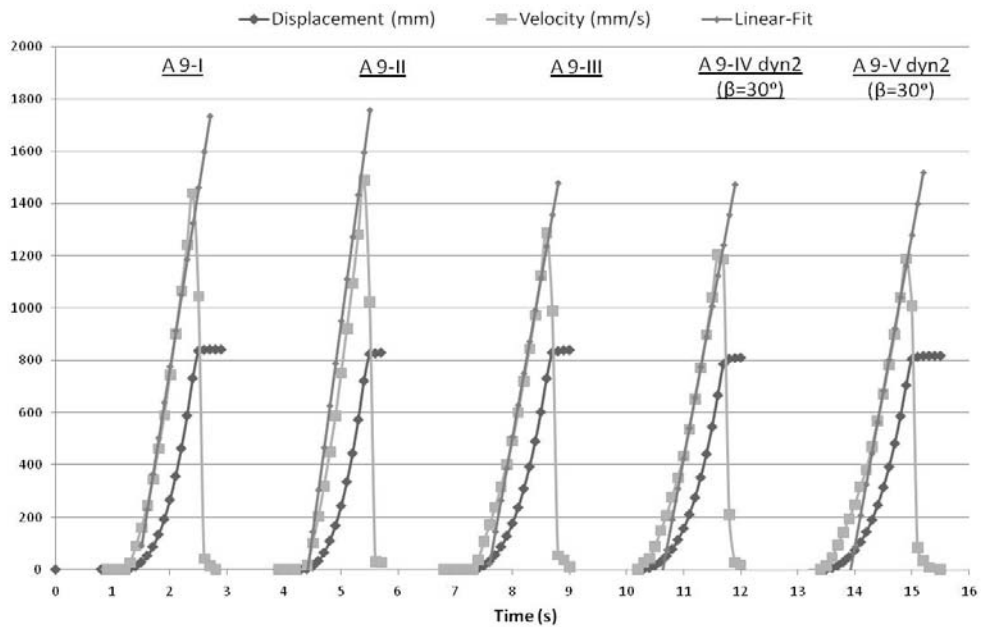


**Figure I.11 – Graphics *Displacement vs. Time, Velocity vs. Time, Acceleration vs. Time***

## Series A-10

**Conditions of test:** guidance system  $\alpha$ , new samples of geosynthetics.

**Observation:** The upper box touched the lateral walls when the displacement was approximately 100 mm.

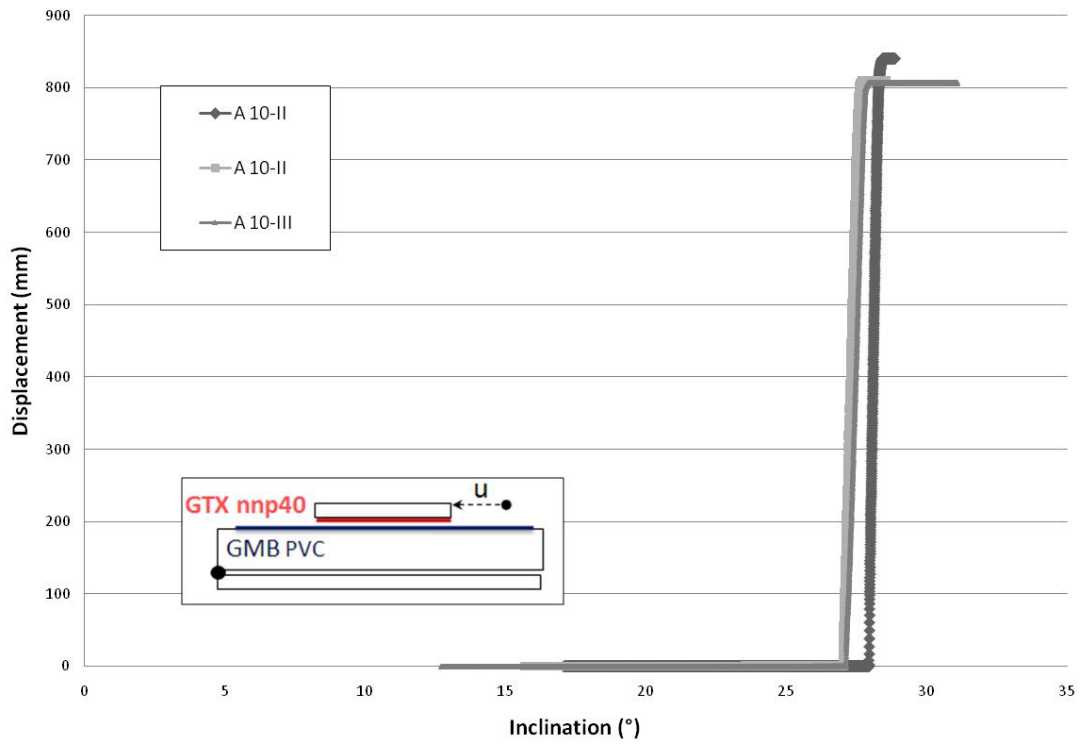


Figure I.12 – Graphic *Displacement vs. Inclination*

## Series A-11

**Conditions of test:** guidance system  $\alpha$ , new samples of geosynthetics.

**Observation:** The upper box touched the lateral walls when the displacement was approximately 100 mm.

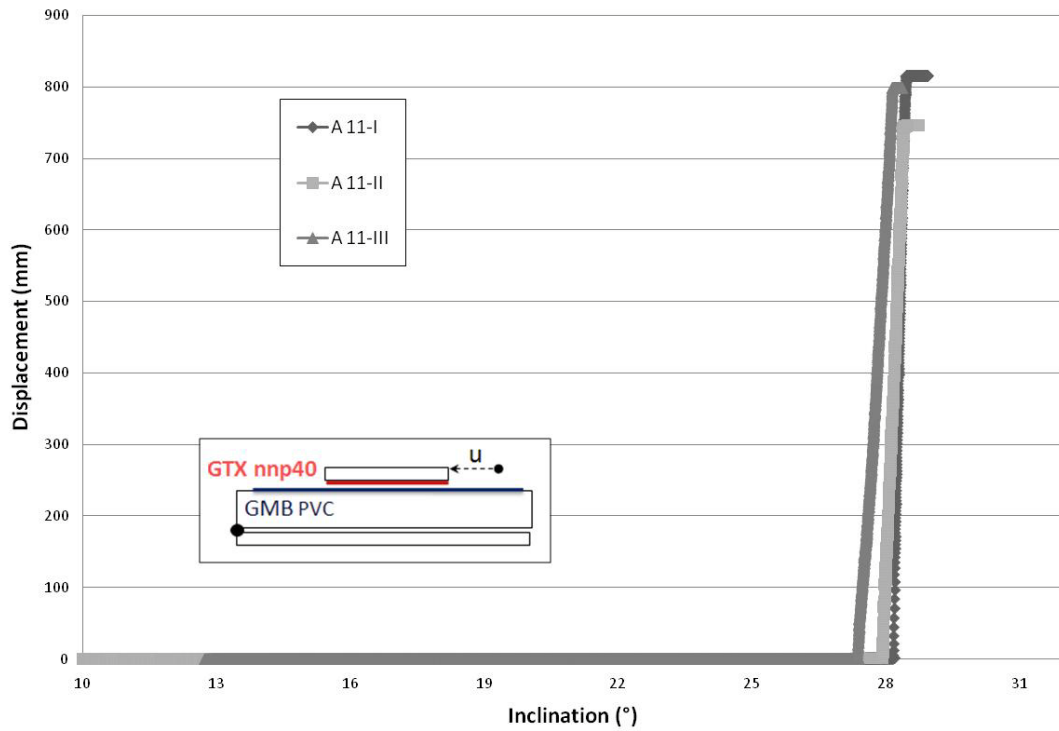


Figure I.13 – Graphic *Displacement vs. Inclination*

## Series A-13

**Conditions of test:** guidance system  $\beta$ , reused sample of PVC.

**Observation:**

- Visually, sample of PVC presented good conditions: no marks of injury or scratches.
- $\beta$  showed in the legend is the inclination of the plane during the entire displacement of the upper box (test dyn2).

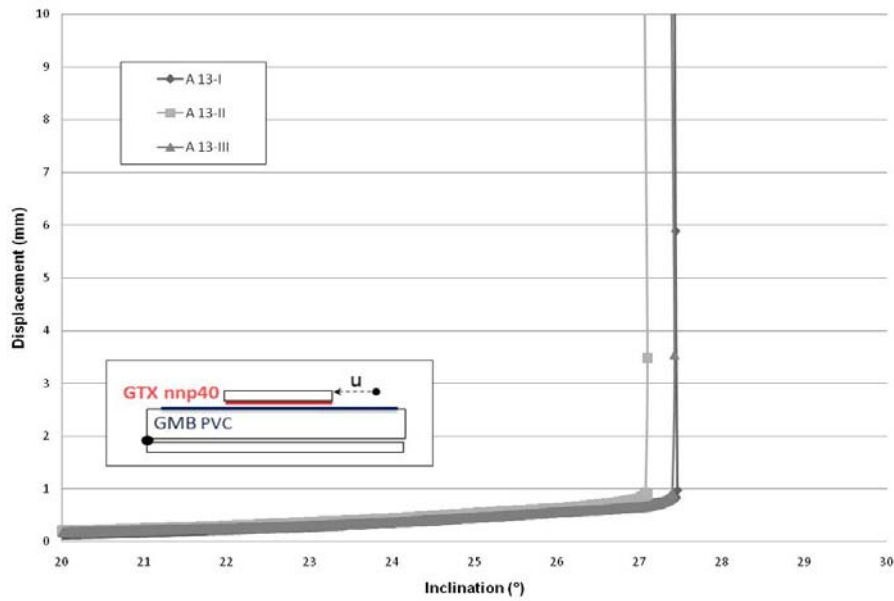


**Figure I.14 – Graphic *Displacement vs. Inclination***

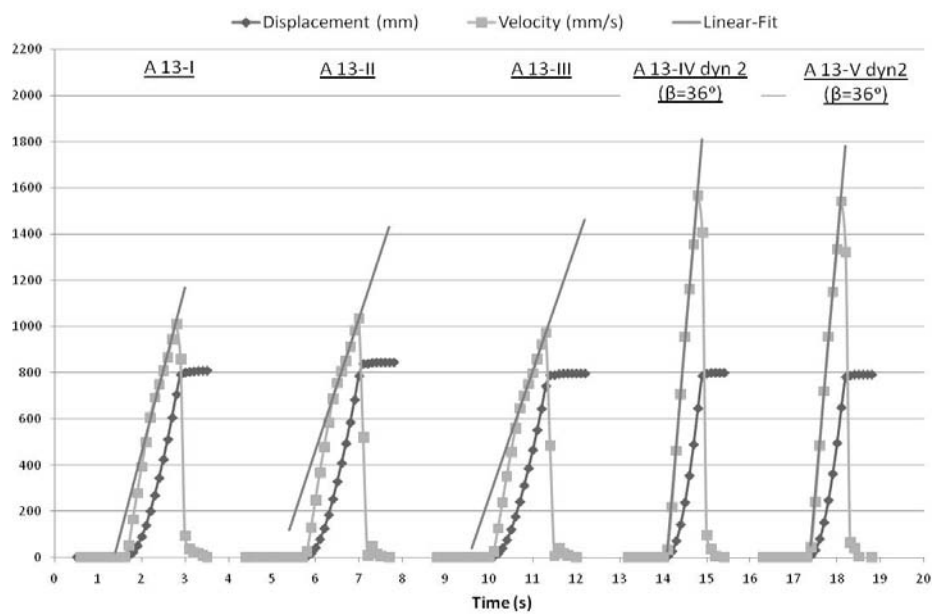


**Figure I.15 – Graphics *Displacement vs. Time, Velocity vs. Time, Acceleration vs. Time***

## Series A-14 & 15

**Conditions of test:** guidance system  $\beta$ , new samples of geosynthetics.

**Observation:** The acceleration was too small to be calculated.

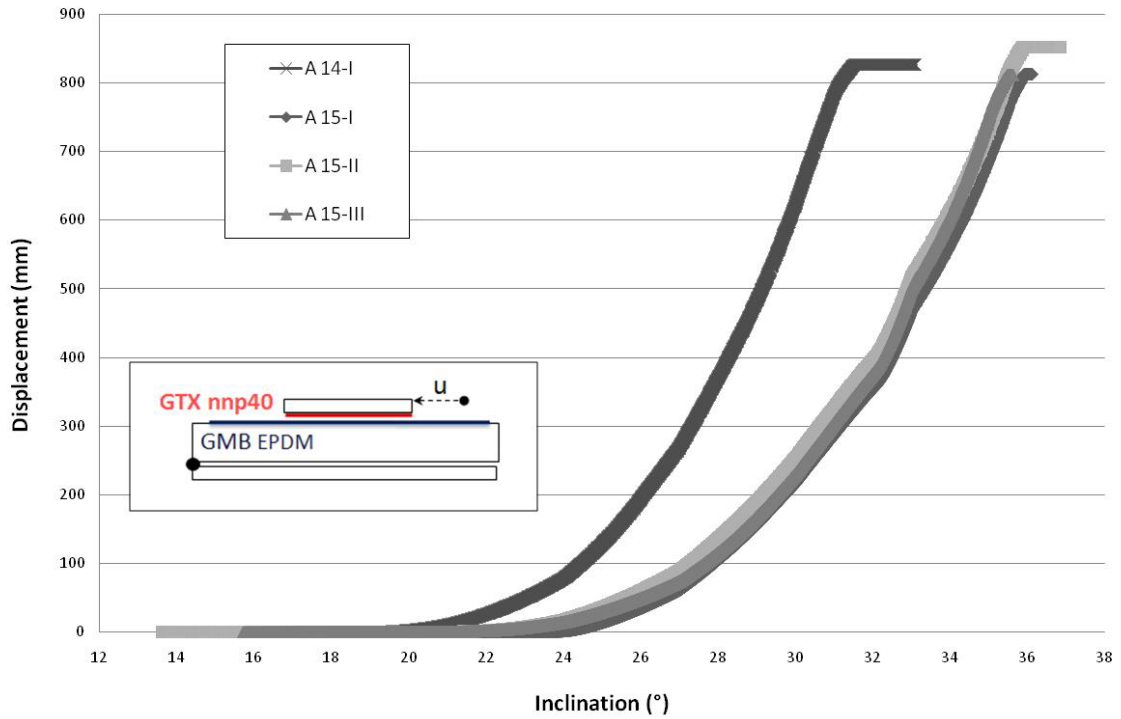


Figure I.16 – Graphic *Displacement vs. Inclination*

## Series A-16

Conditions of test: guidance system  $\beta$ , new samples of geosynthetics.

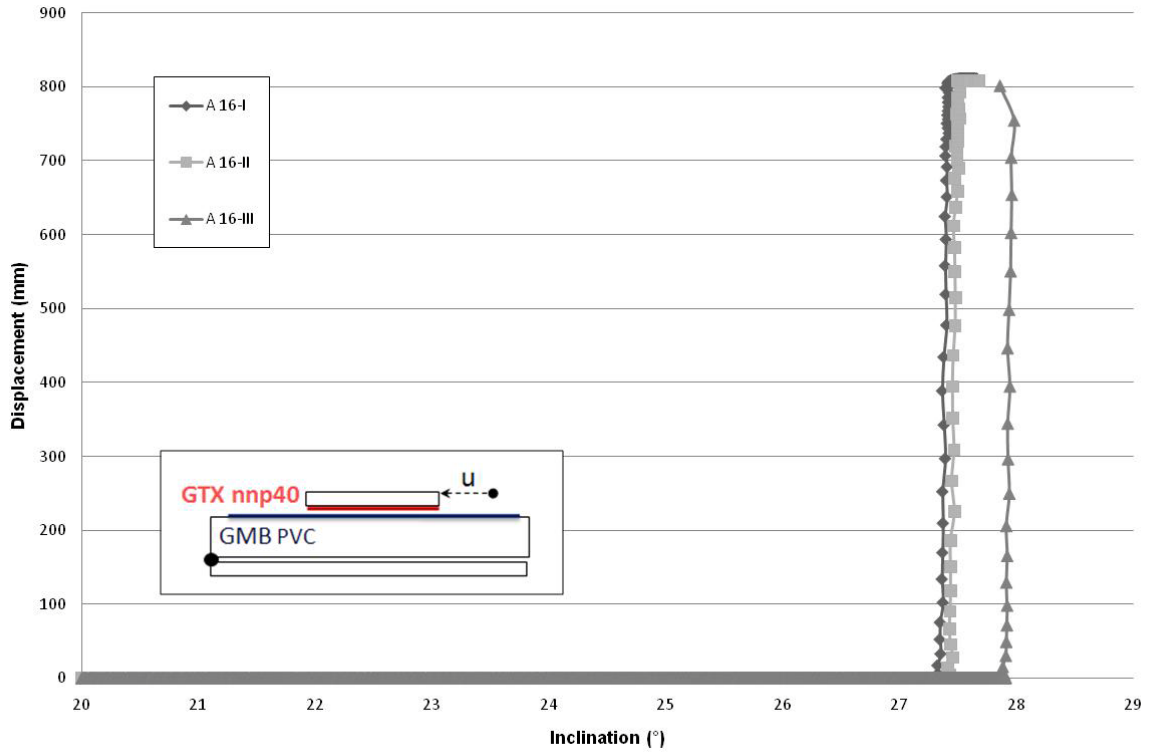


Figure I.17 – Graphic *Displacement vs. Inclination*

## Series A-17

**Conditions of test:** guidance system  $\gamma$ , reused sample of PVC.

**Observation:**

- Visually, sample of PVC presented good conditions: no marks of injury or scratches.
- $\beta$  showed in the legend is the inclination of the plane during the entire displacement of the upper box (test dyn2).

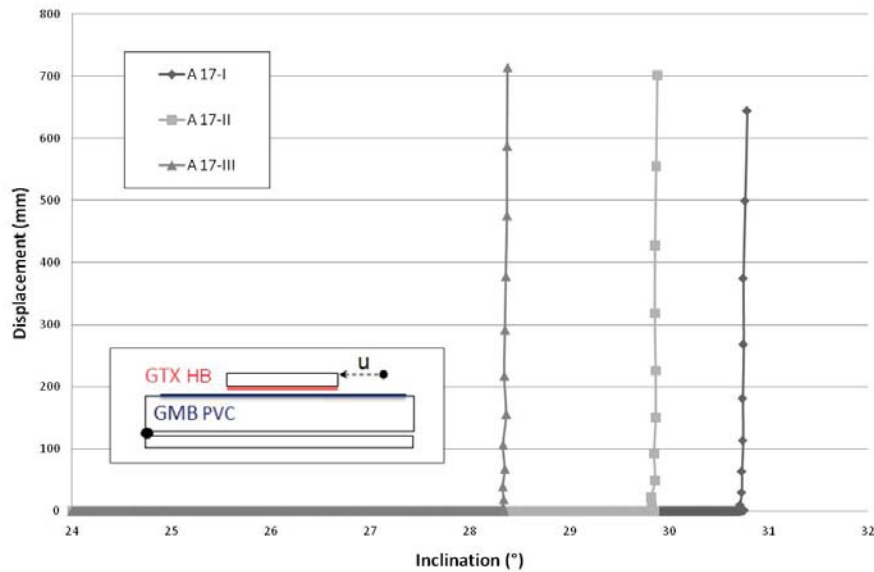


**Figure I.18 – Graphic *Displacement vs. Inclination***

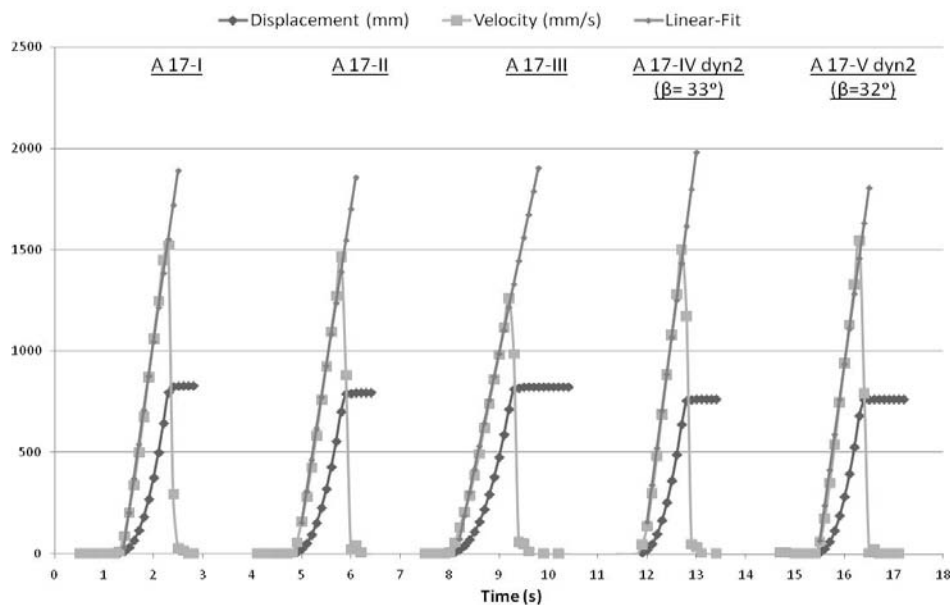


**Figure I.19 – Graphics *Displacement vs. Time, Velocity vs. Time, Acceleration vs. Time***

## Series A-18 & 20

**Conditions of series A18:** guidance system  $\gamma$ , reused sample of PVC.

**Conditions of series A20:** guidance system  $\delta$ , reused sample of PVC.

**Observations:**

- Visually, sample of PVC presented good conditions: no marks of injury or scratches.
- $\beta$  showed in the legend is the inclination of the plane during the entire displacement of the upper box (test dyn2).

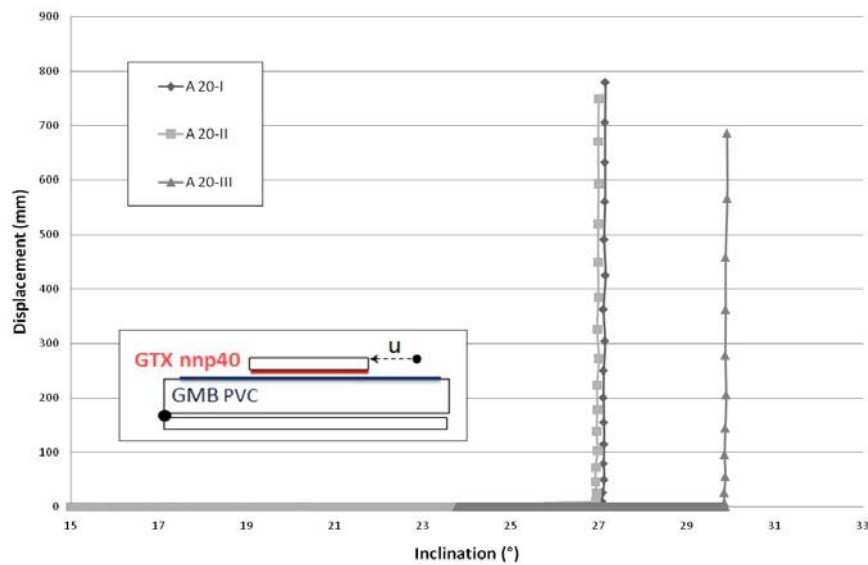


**Figure I.20 – Graphic *Displacement vs. Inclination***

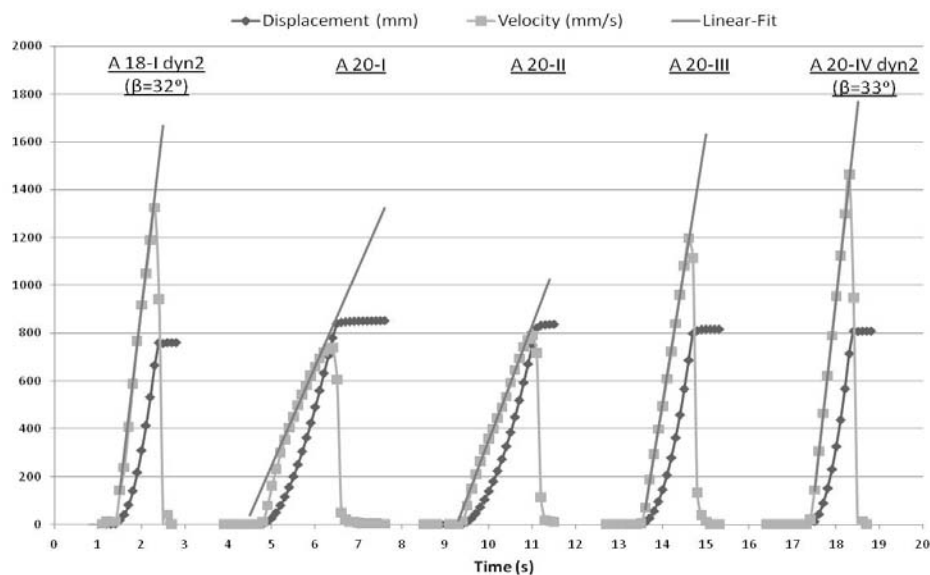


**Figure I.21 – Graphics *Displacement vs. Time, Velocity vs. Time, Acceleration vs. Time***

## Series A-21

**Conditions:** guidance system  $\delta$ , new samples of geosynthetics.

**Observation:**  $\beta$  showed in the legend is the inclination of the plane during the entire displacement of the upper box (test dyn2).

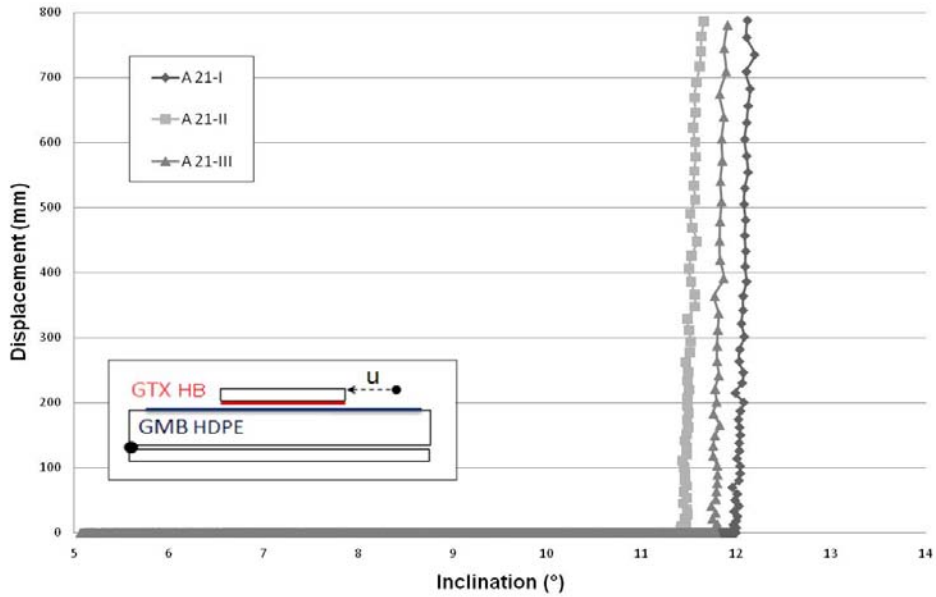


**Figure I.22 – Graphic *Displacement vs. Inclination***

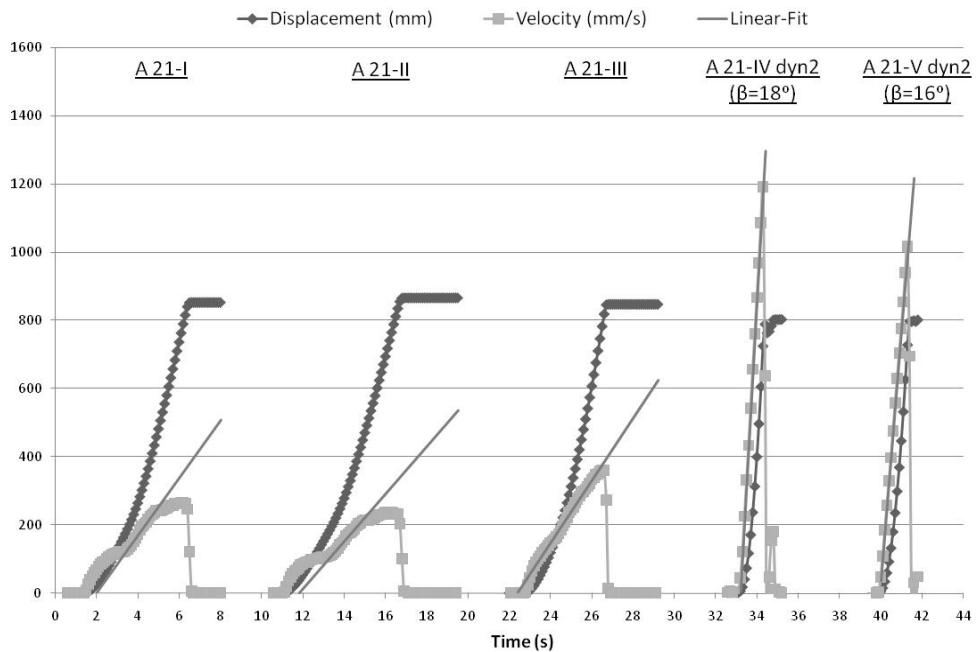


**Figure I.23 – Graphics *Displacement vs. Time, Velocity vs. Time, Acceleration vs. Time***

## Series A-22

**Conditions:** guidance system  $\delta$ , new samples of geosynthetics.

**Observation:**  $\beta$  showed in the legend is the inclination of the plane during the entire displacement of the upper box (test dyn2).

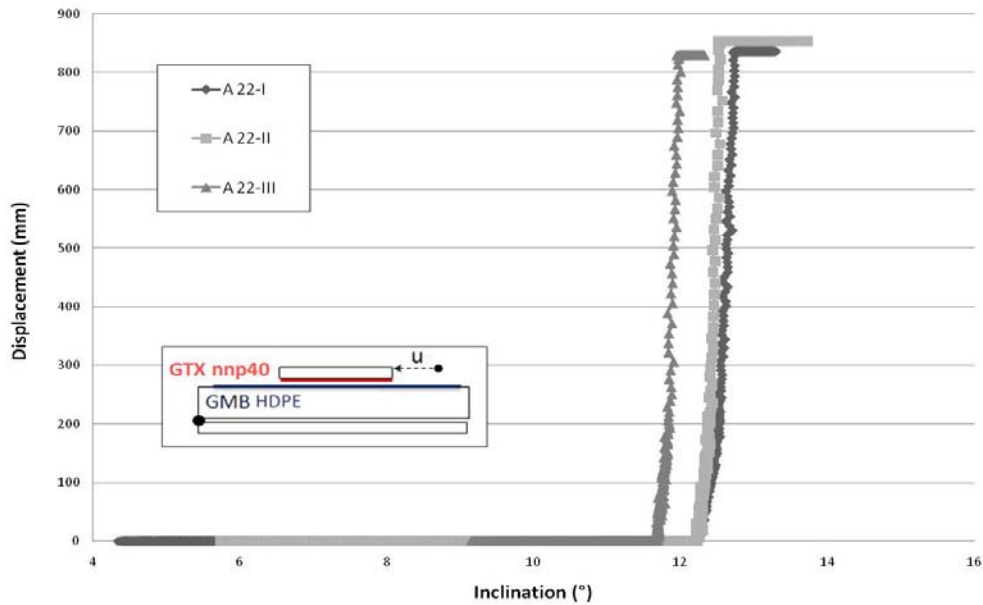


**Figure I.24 – Graphic Displacement vs. Inclination**

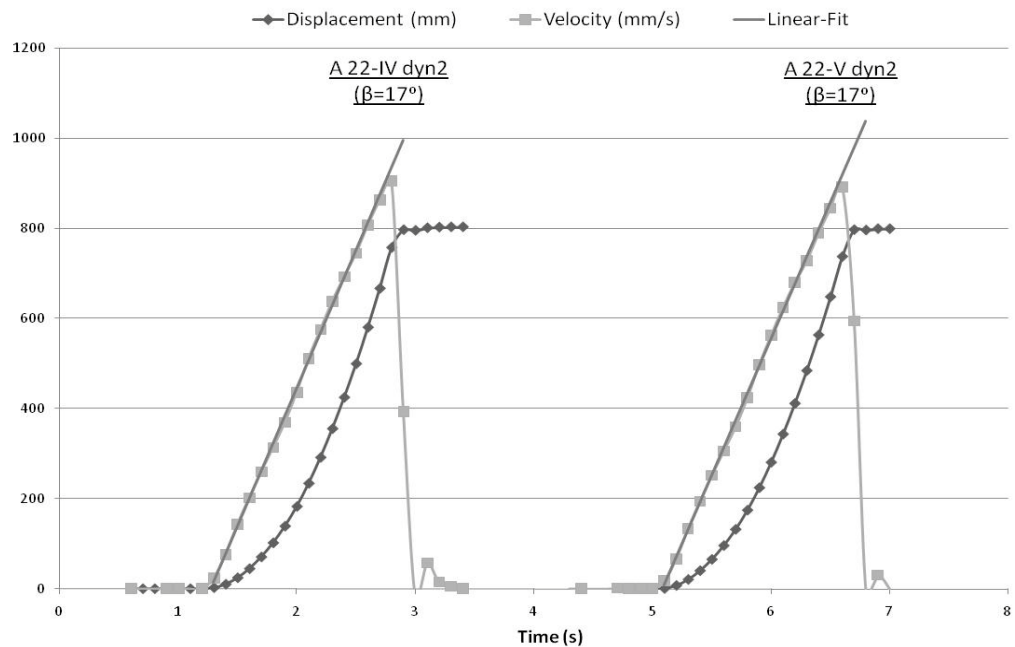


**Figure I.25 – Graphics Displacement vs. Time, Velocity vs. Time, Acceleration vs. Time**

## Series A-23

**Conditions:** guidance system  $\delta$ , new samples of geosynthetics.

**Observation:**  $\beta$  showed in the legend is the inclination of the plane during the entire displacement of the upper box (test dyn2).

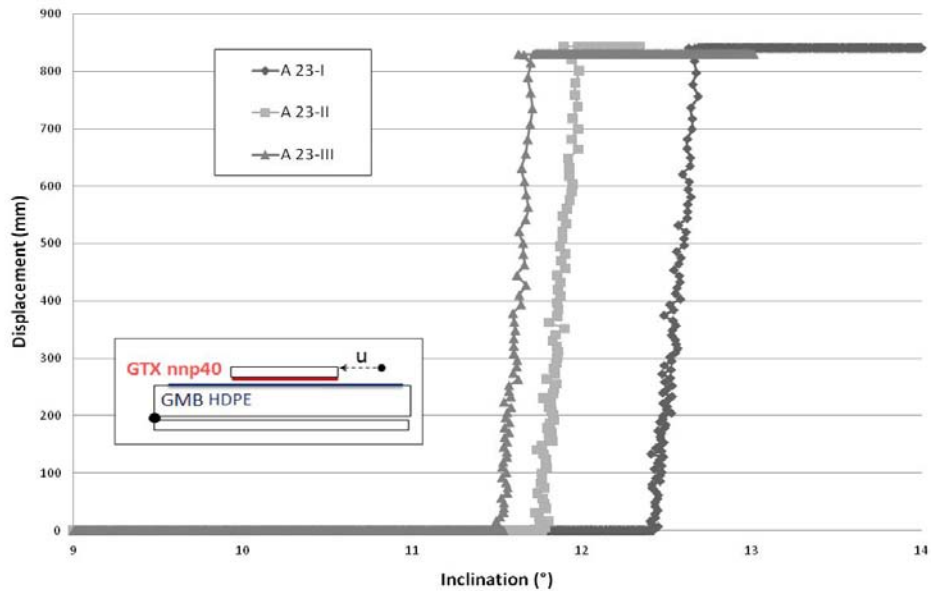


**Figure I.26 – Graphic *Displacement vs. Inclination***

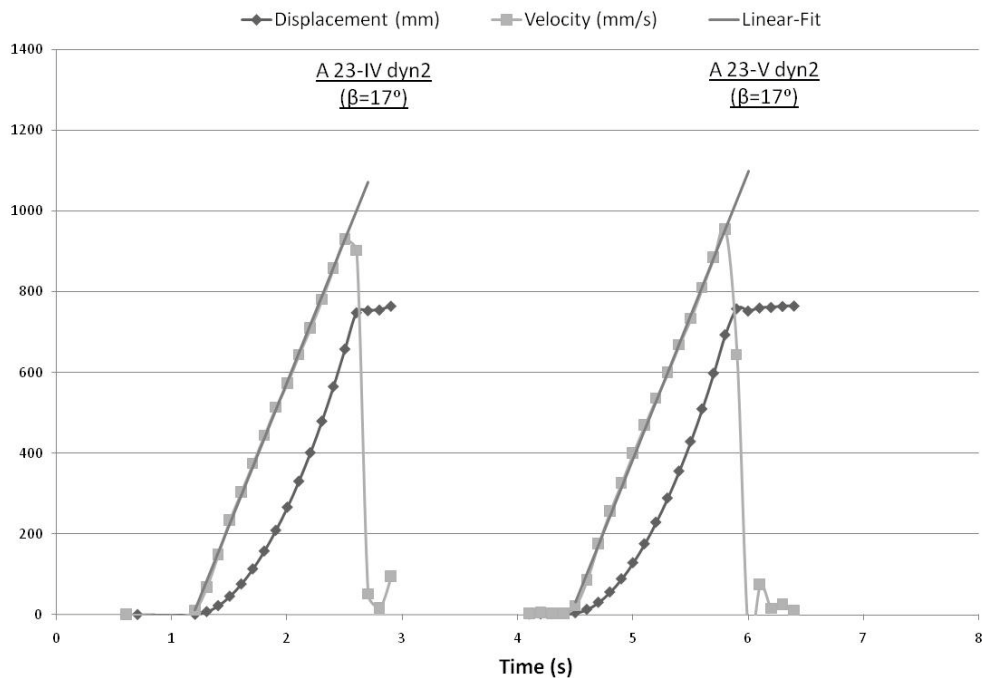


**Figure I.27 – Graphics *Displacement vs. Time, Velocity vs. Time, Acceleration vs. Time***

## Series A-24

**Conditions:** guidance system  $\delta$ , new samples of geosynthetics.

**Observation:**  $\beta$  showed in the legend is the inclination of the plane during the entire displacement of the upper box (test dyn2).

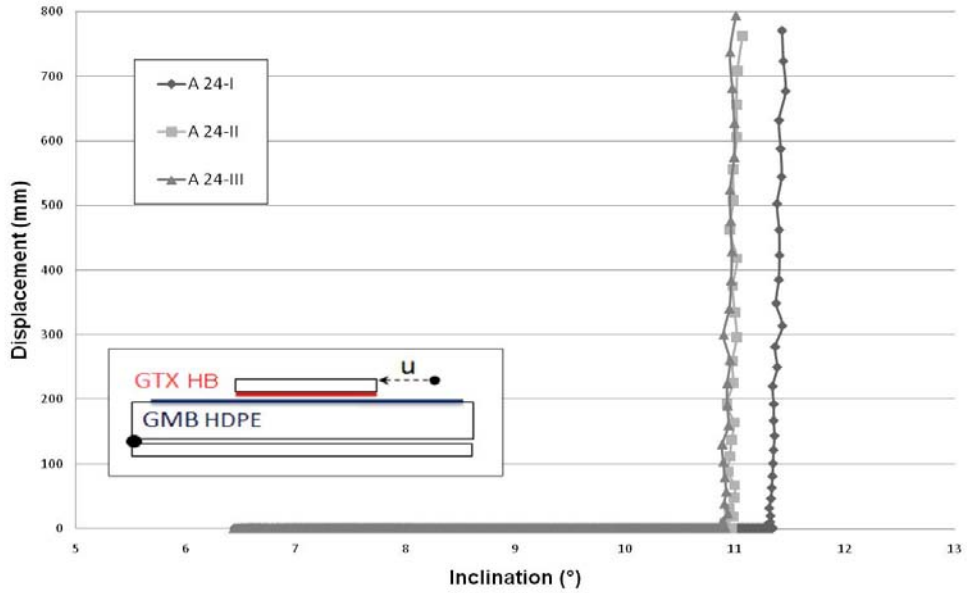


**Figure I.28 – Graphic Displacement vs. Inclination**

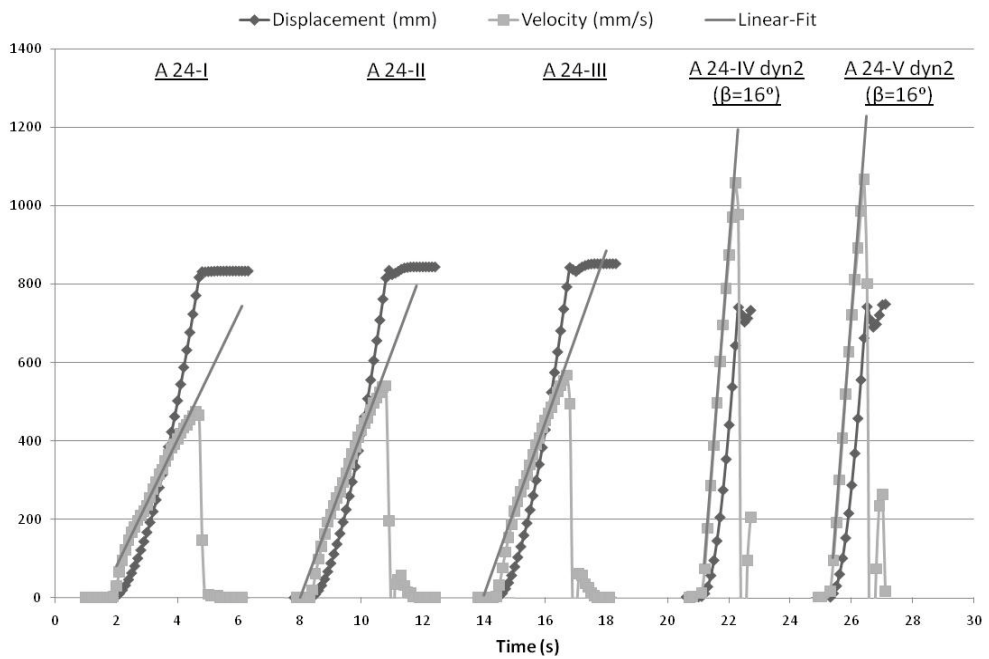


**Figure I.29 – Graphics Displacement vs. Time, Velocity vs. Time, Acceleration vs. Time**

## Series A-25, 26 & 27

**Conditions:** guidance system  $\delta$ , new samples of geosynthetics.

**Observation:**  $\beta$  showed in the legend is the inclination of the plane during the entire displacement of the upper box (test dyn2).

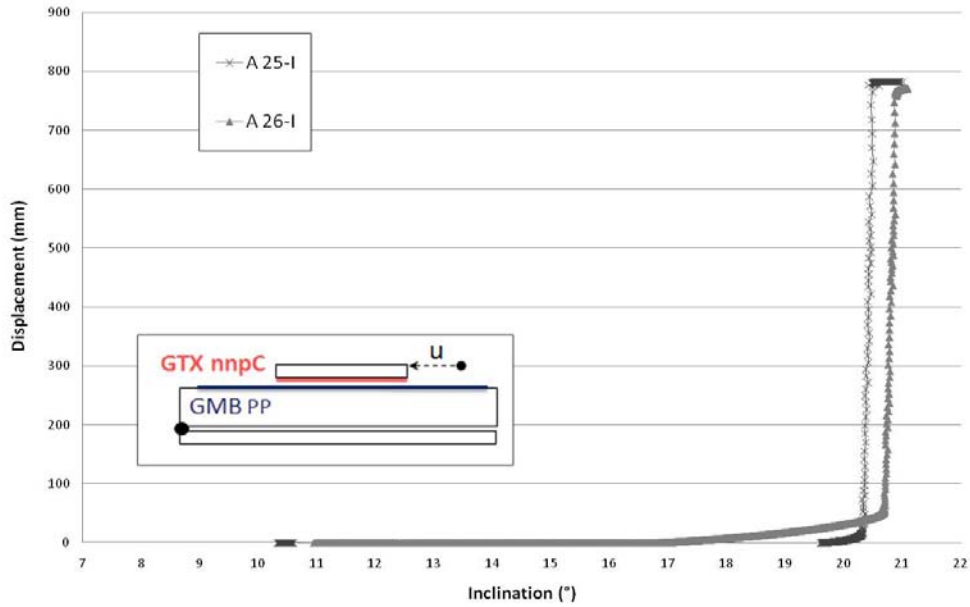


**Figure I.30 – Graphic Displacement vs. Inclination**

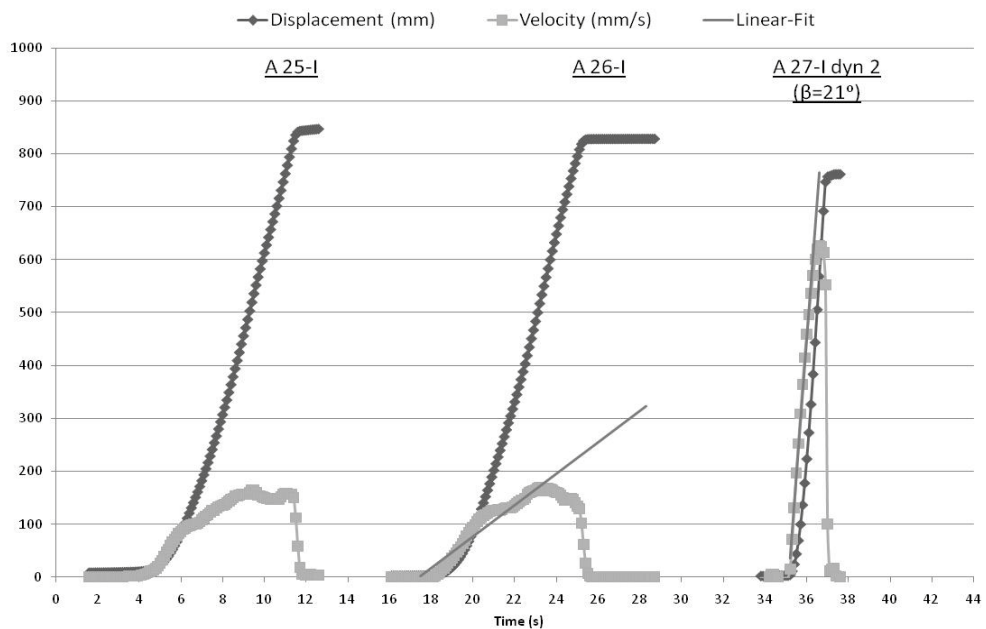


**Figure I.31 – Graphics Displacement vs. Time, Velocity vs. Time, Acceleration vs. Time**

## Series A-28

**Conditions:** guidance system  $\delta$ , new samples of geosynthetics.

**Observation:**  $\beta$  showed in the legend is the inclination of the plane during the entire displacement of the upper box (test dyn2).

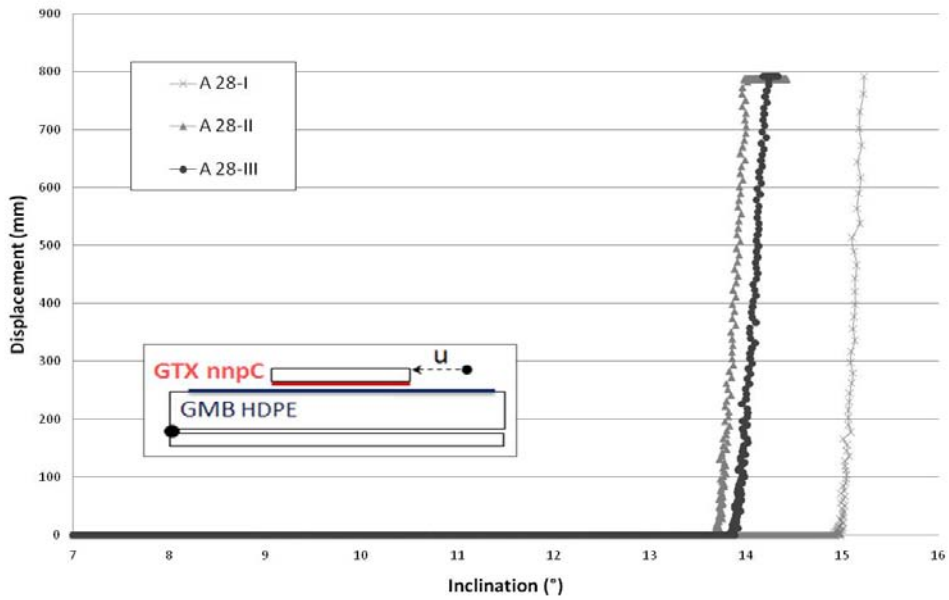


**Figure I.32 – Graphic *Displacement vs. Inclination***

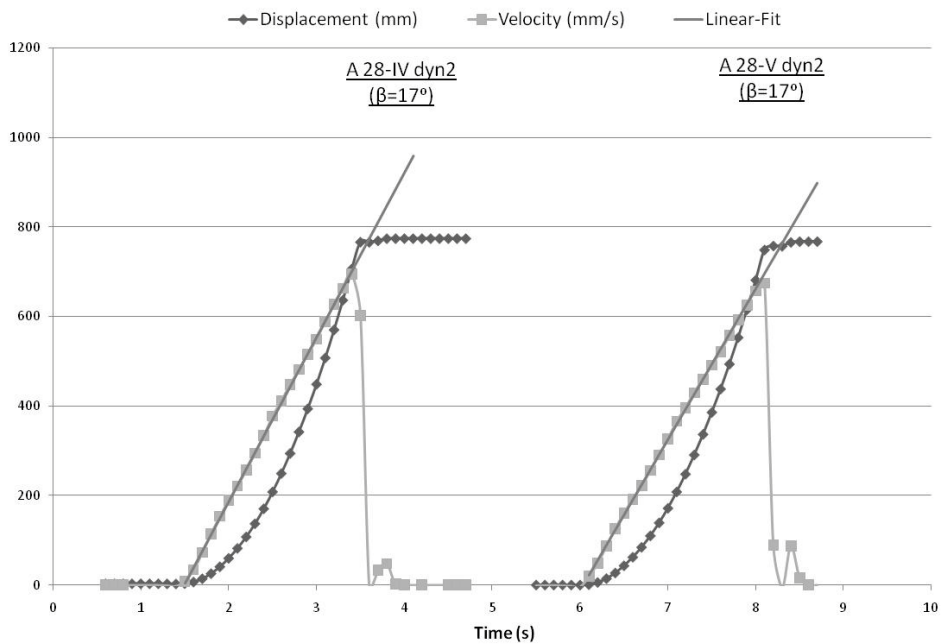


**Figure I.33 – Graphics *Displacement vs. Time, Velocity vs. Time, Acceleration vs. Time***

## Series A-29

**Conditions:** guidance system  $\delta$ , new samples of geosynthetics.

**Observation:**  $\beta$  showed in the legend is the inclination of the plane during the entire displacement of the upper box (test dyn2).

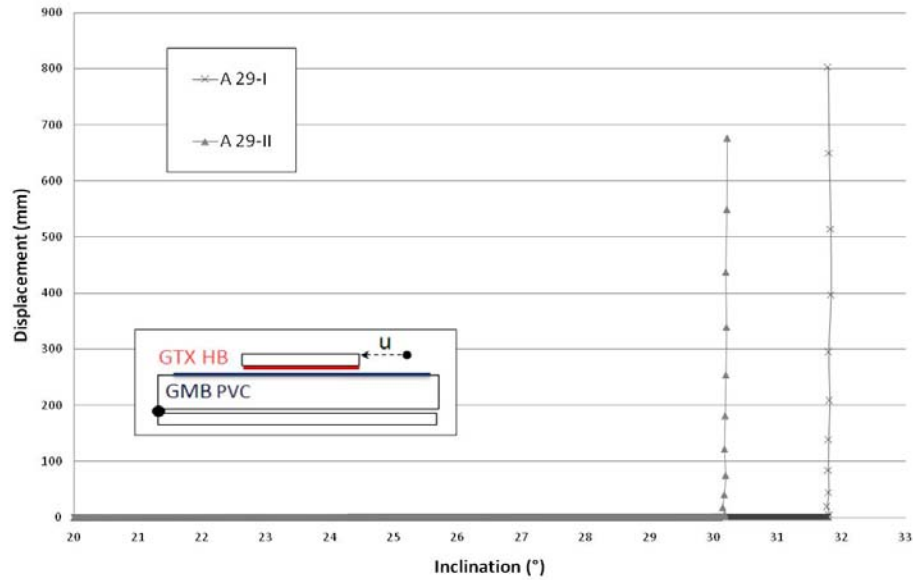


**Figure I.34 – Graphic Displacement vs. Inclination**

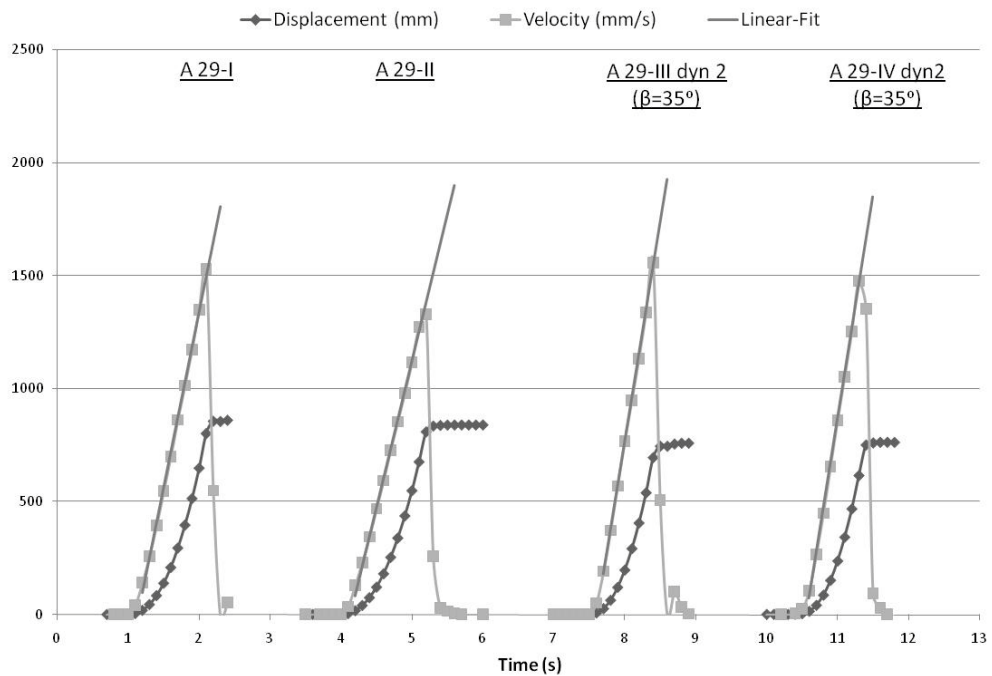


**Figure I.35 – Graphics Displacement vs. Time, Velocity vs. Time, Acceleration vs. Time**

## Series A-30

**Conditions:** guidance system  $\delta$ , new samples of geosynthetics.

**Observation:**  $\beta$  showed in the legend is the inclination of the plane during the entire displacement of the upper box (test dyn2).

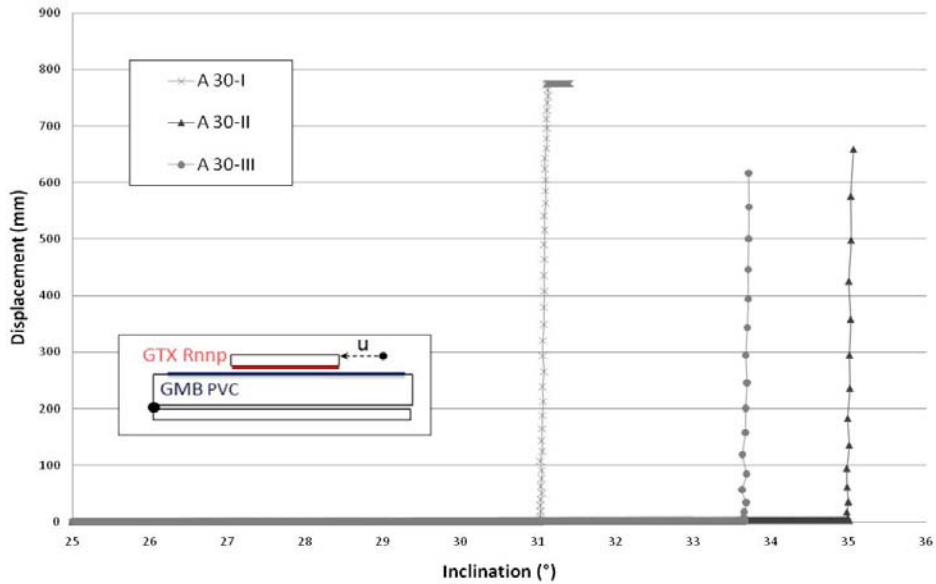


**Figure I.36 – Graphic Displacement vs. Inclination**

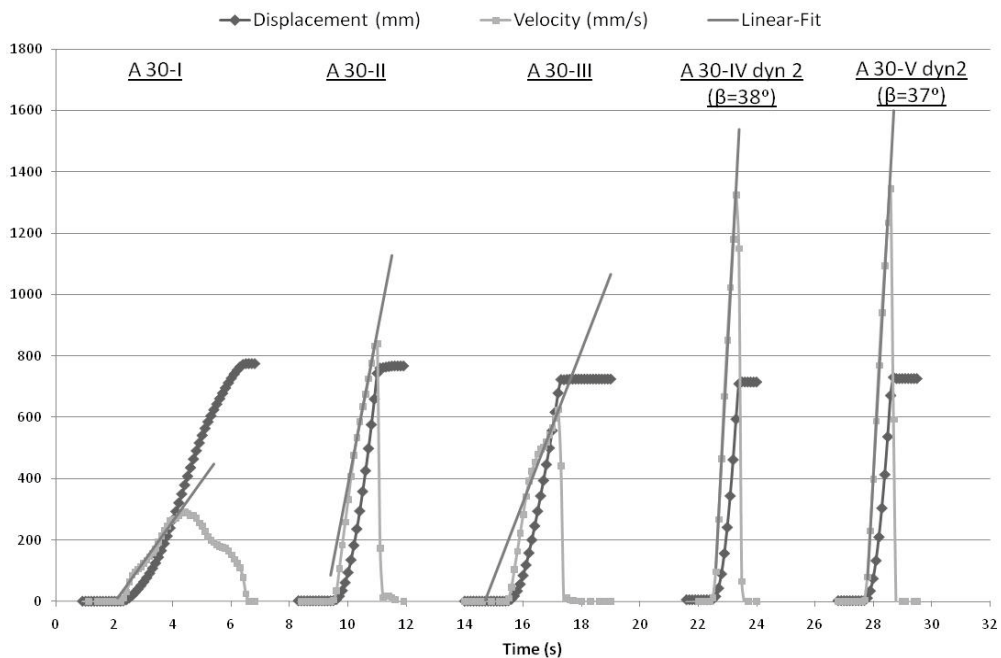


**Figure I.37 – Graphics Displacement vs. Time, Velocity vs. Time, Acceleration vs. Time**

## Series A-31

**Conditions:** guidance system  $\delta$ , new samples of geosynthetics.

**Observation:**  $\beta$  showed in the legend is the inclination of the plane during the entire displacement of the upper box (test dyn2).

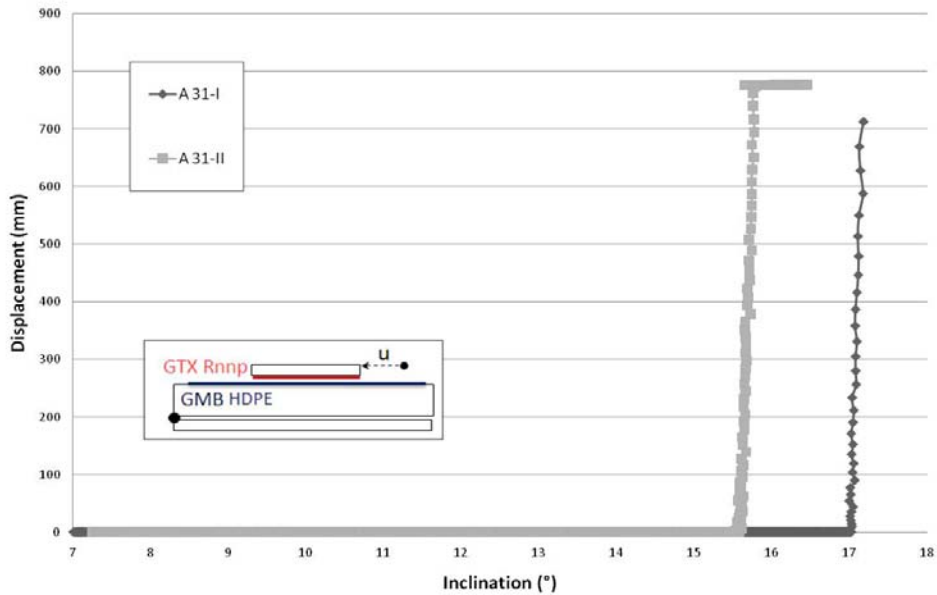


**Figure I.38 – Graphic *Displacement vs. Inclination***

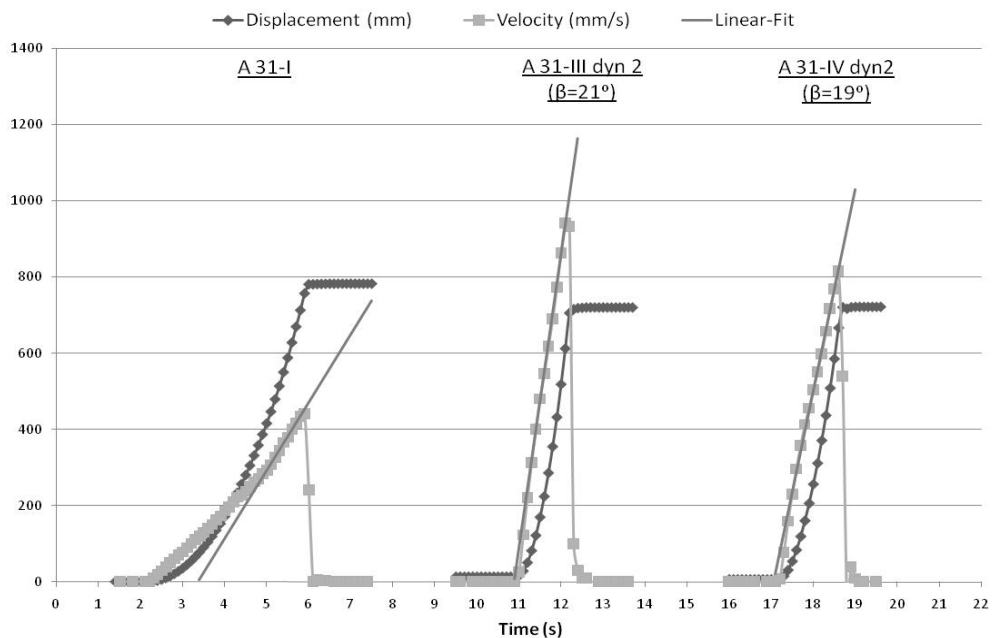


**Figure I.39 – Graphics *Displacement vs. Time, Velocity vs. Time, Acceleration vs. Time***

## Series A-32 & 33

**Conditions:** guidance system  $\delta$ , new samples of geosynthetics.

**Observation:**  $\beta$  showed in the legend is the inclination of the plane during the entire displacement of the upper box (test dyn2).

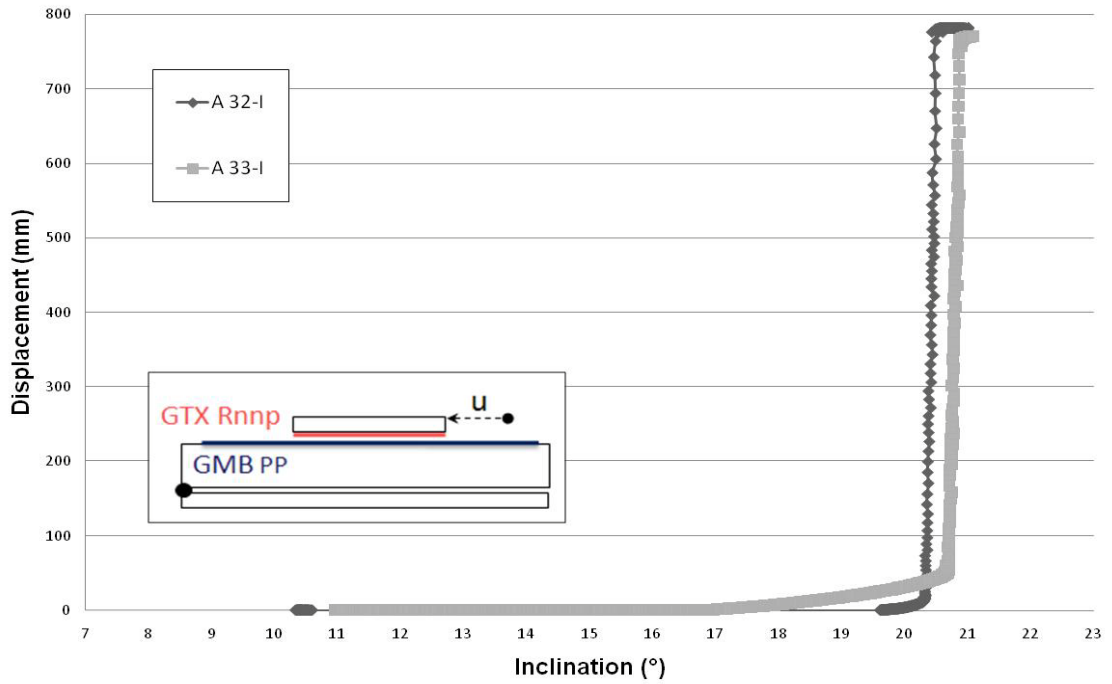
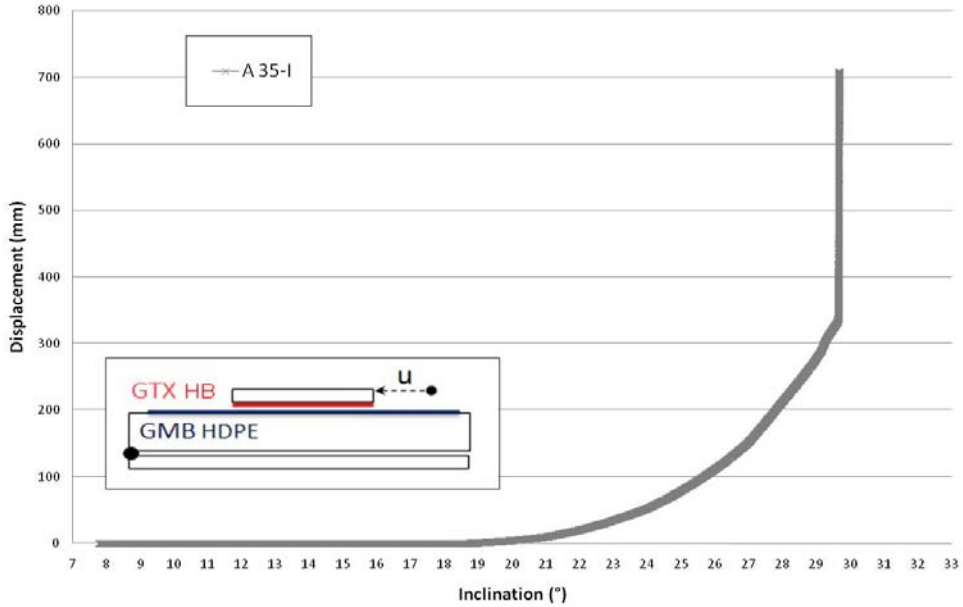


Figure I.40 – Graphic *Displacement vs. Inclination*

## Series A-35 36 & 37

**Conditions:** guidance system  $\delta$ , new samples of geosynthetics.

**Observation:**  $\beta$  showed in the legend is the inclination of the plane during the entire displacement of the upper box (test dyn2).



**Figure I.41 – Graphic *Displacement vs. Inclination***

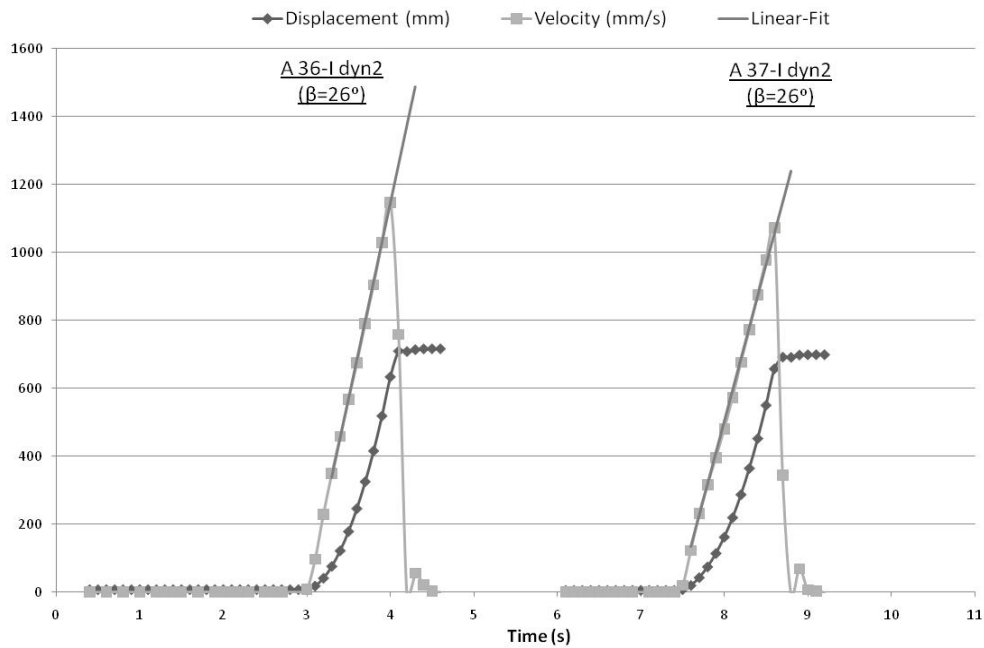


**Figure I.42 – Graphics *Displacement vs. Time, Velocity vs. Time, Acceleration vs. Time***

## **APPENDIX II**

### **Results of trials using inclined plane B**

---

## Series B-40, 41 & 43

**Weight of soil:** 375 kg (B-40), 502 kg (B-41), 518 kg (B43)

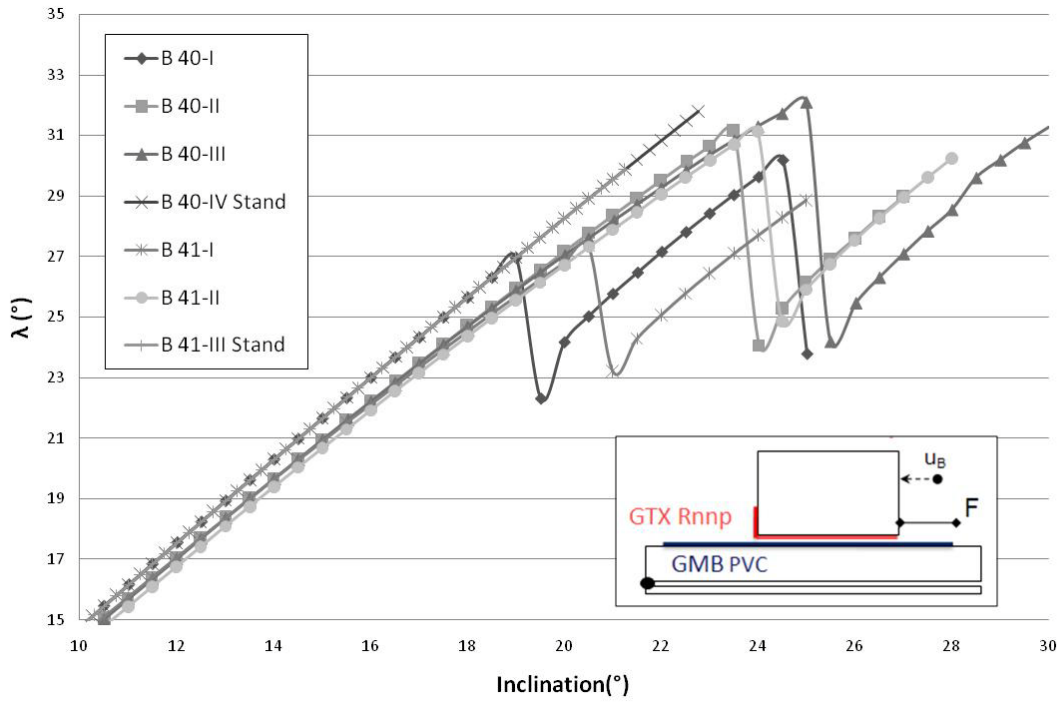


**Figure II.1 – Graphic  $\Lambda$  vs. Inclination**

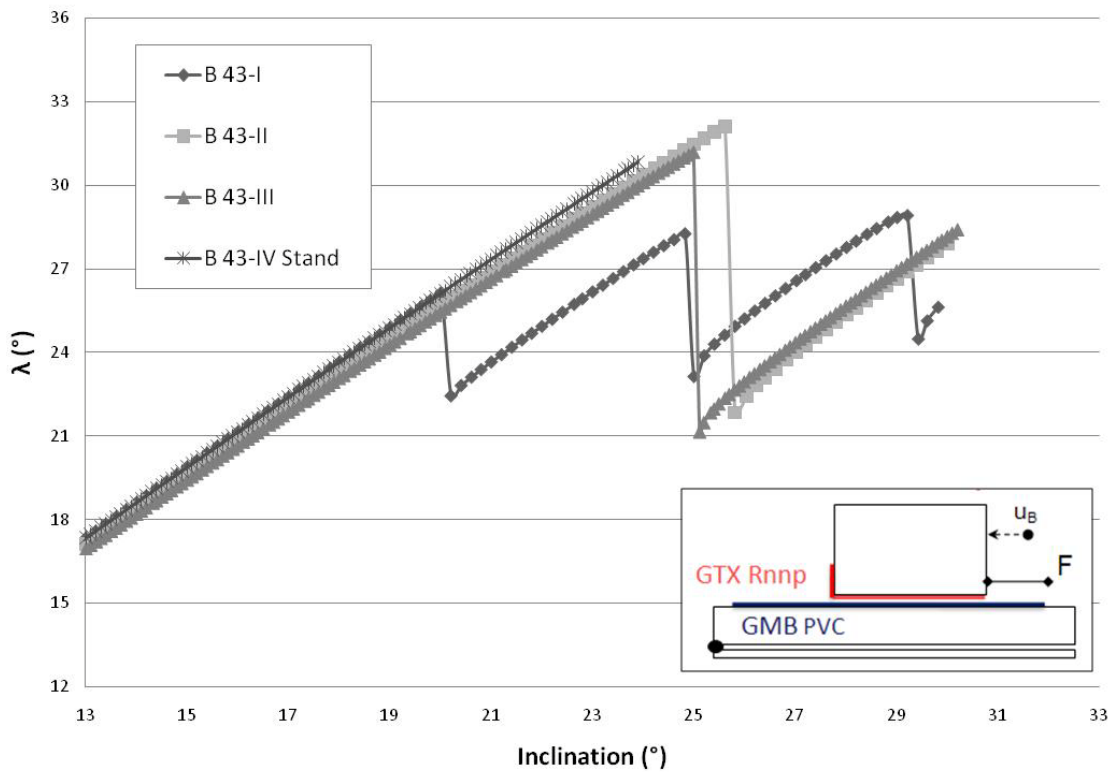


**Figure II.2 – Graphic  $\Lambda$  vs. Inclination**

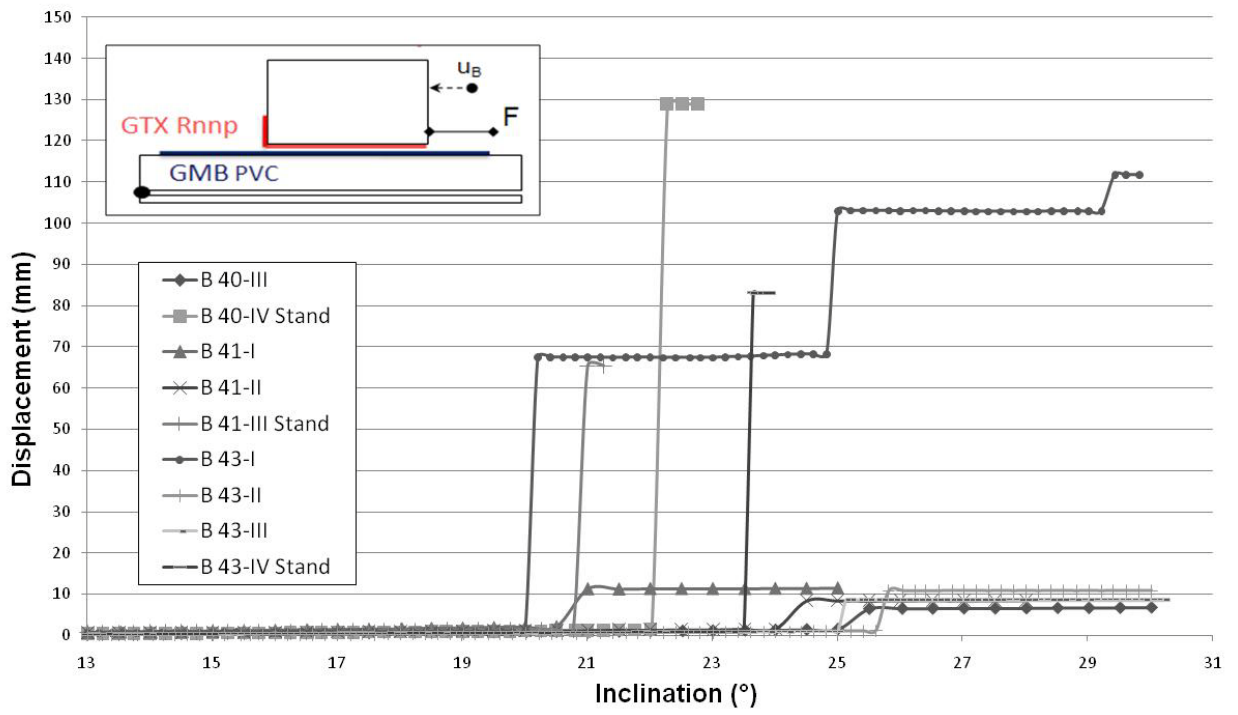
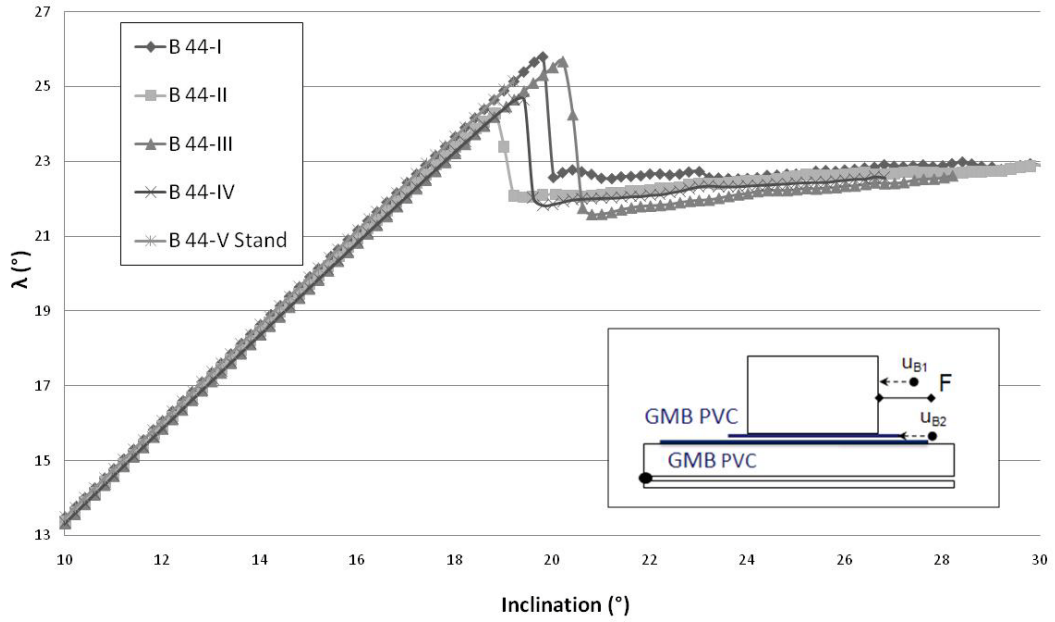


Figure II.3 – Graphic Displacement vs. Inclination

## Series B-44

**Weight of soil: 516 kg**



**Figure II.4 – Graphic  $\lambda$  vs. Inclination**

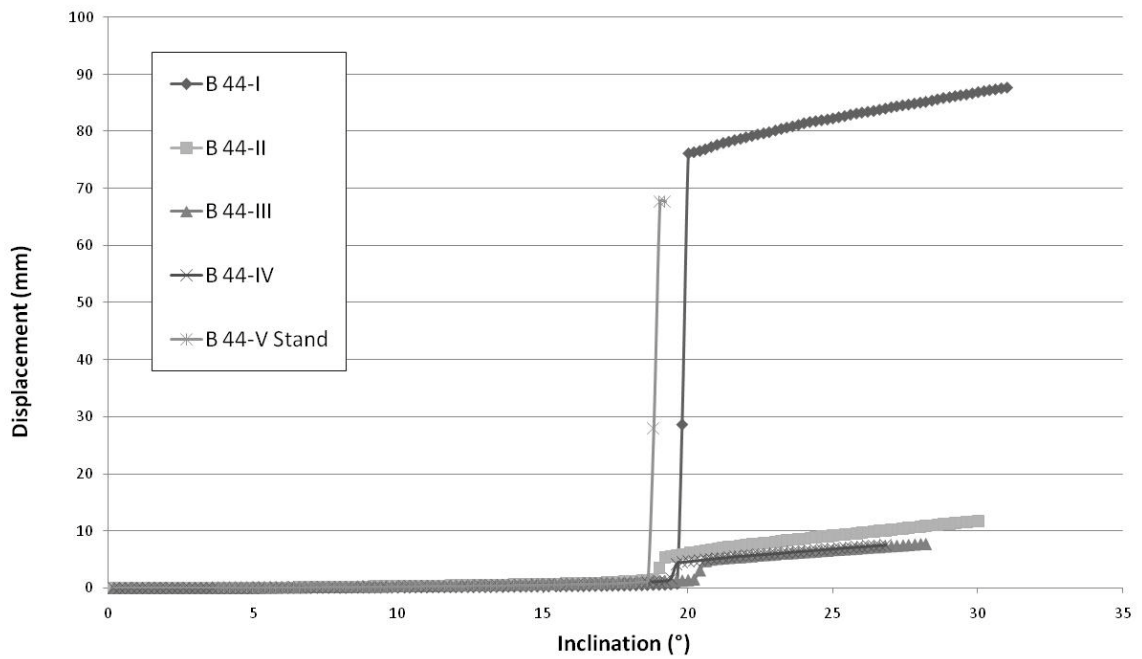


**Figure II.5 – Graphic Displacement vs. Inclination**

## Series B-45

Weight of soil: 519 kg

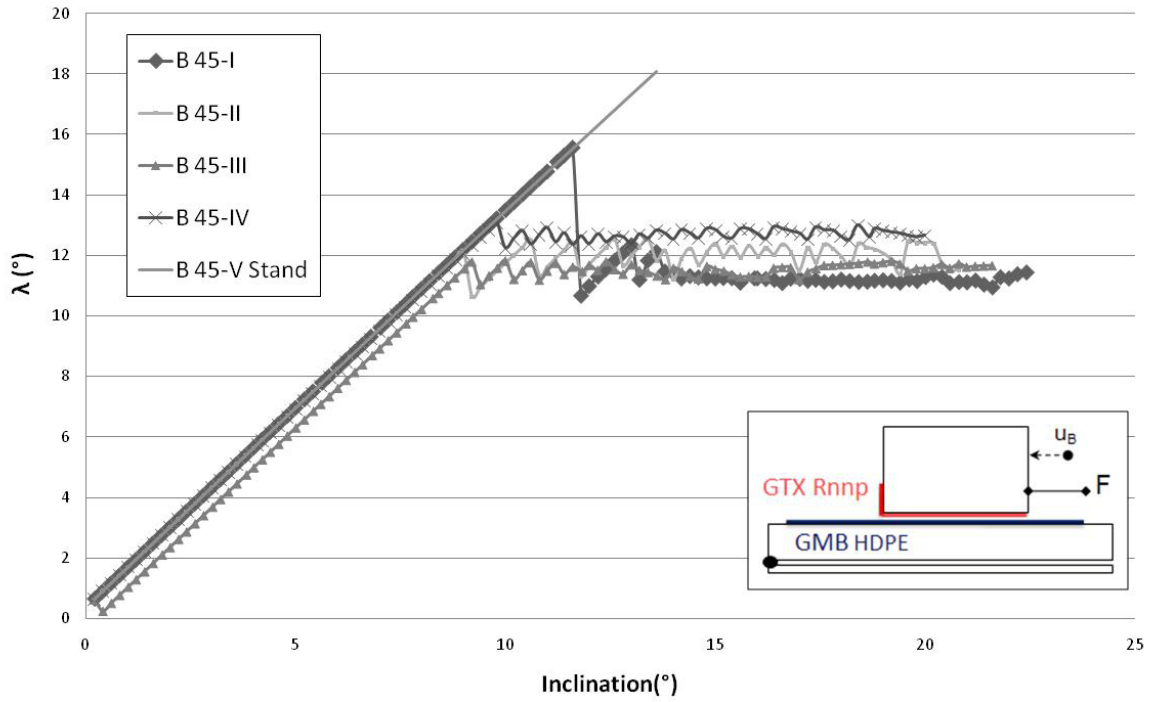


Figure II.6 – Graphic Lambda vs. Inclination

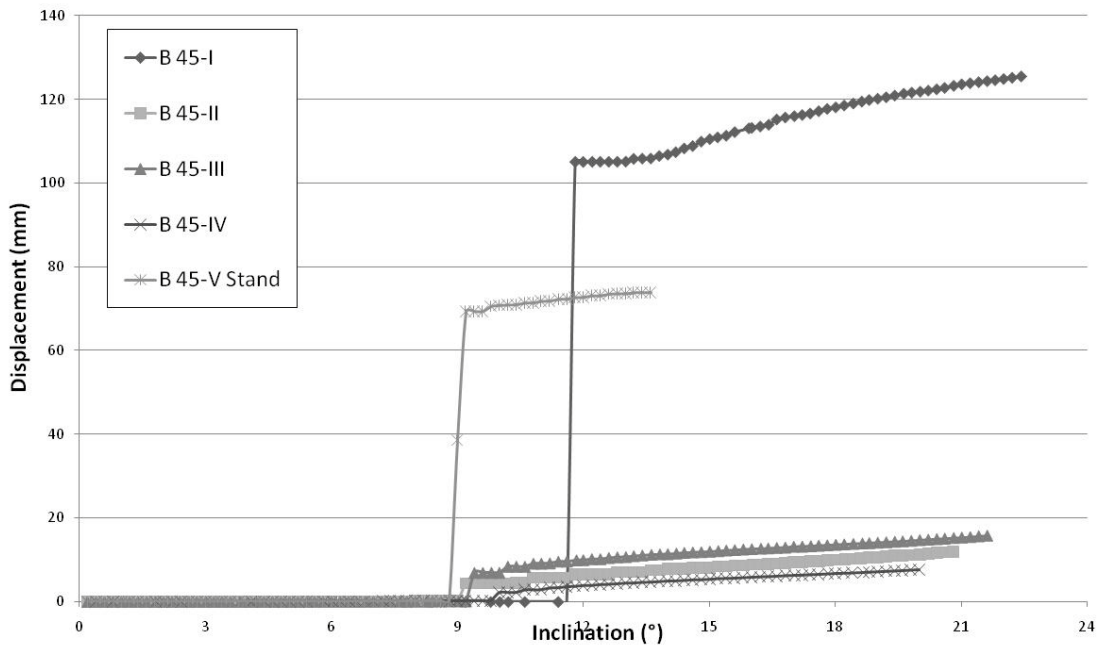
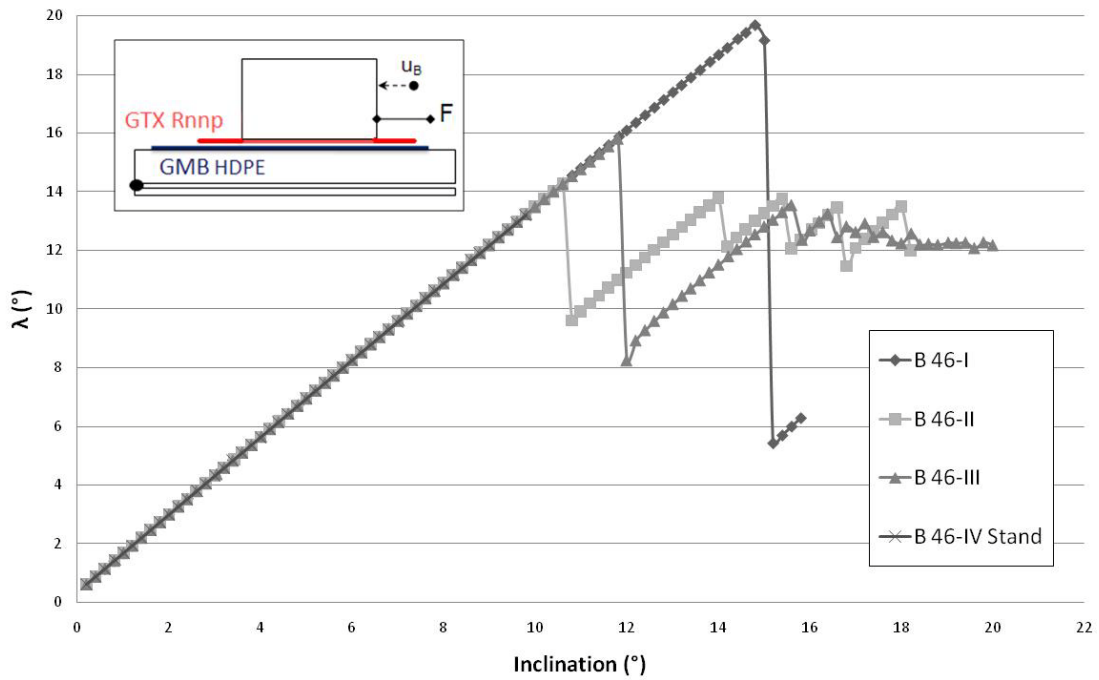


Figure II.7 – Graphic Displacement vs. Inclination

## Series B-46

Weight of soil: 517 kg



**Figure II.8 – Graphic  $\lambda$  vs. Inclination**

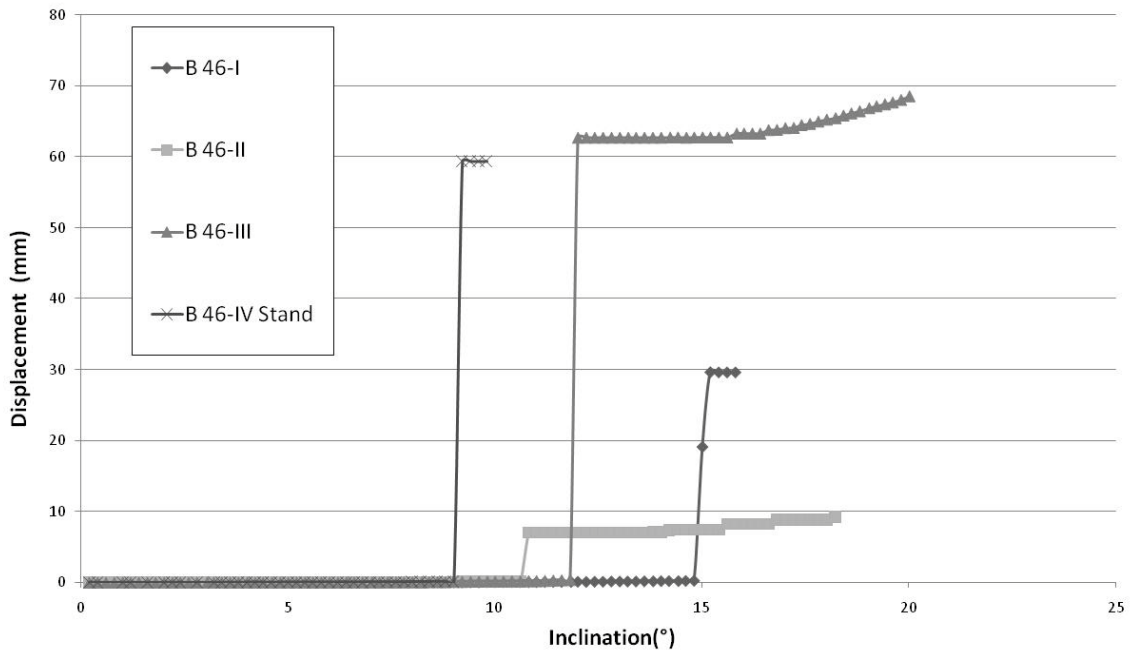


**Figure II.9 – Graphic Displacement vs. Inclination**

## Series B-52 & 53

Weight of soil: 508 kg

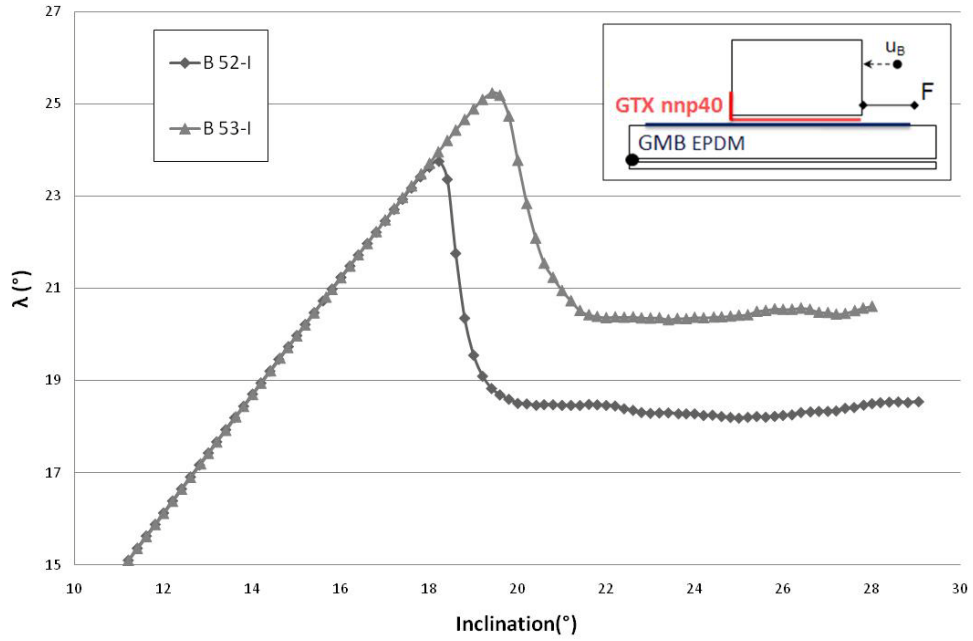


**Figure II.10 – Graphic  $\Lambda$  vs. Inclination**

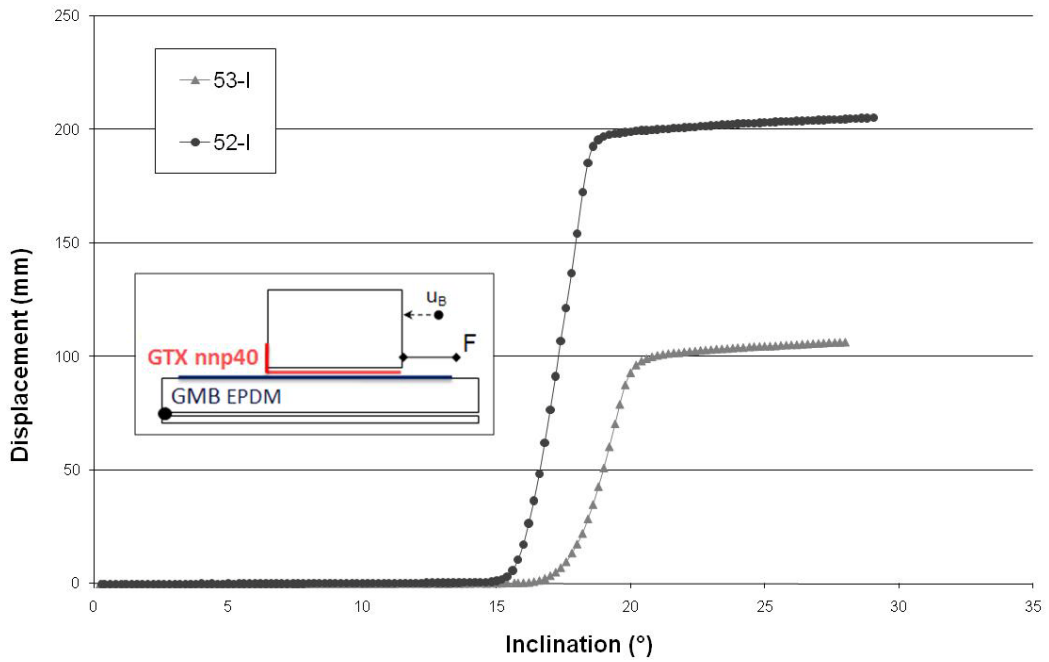


**Figure II.11 – Graphic Displacement vs. Inclination**

## Series B-73

Weight of soil: 484 kg

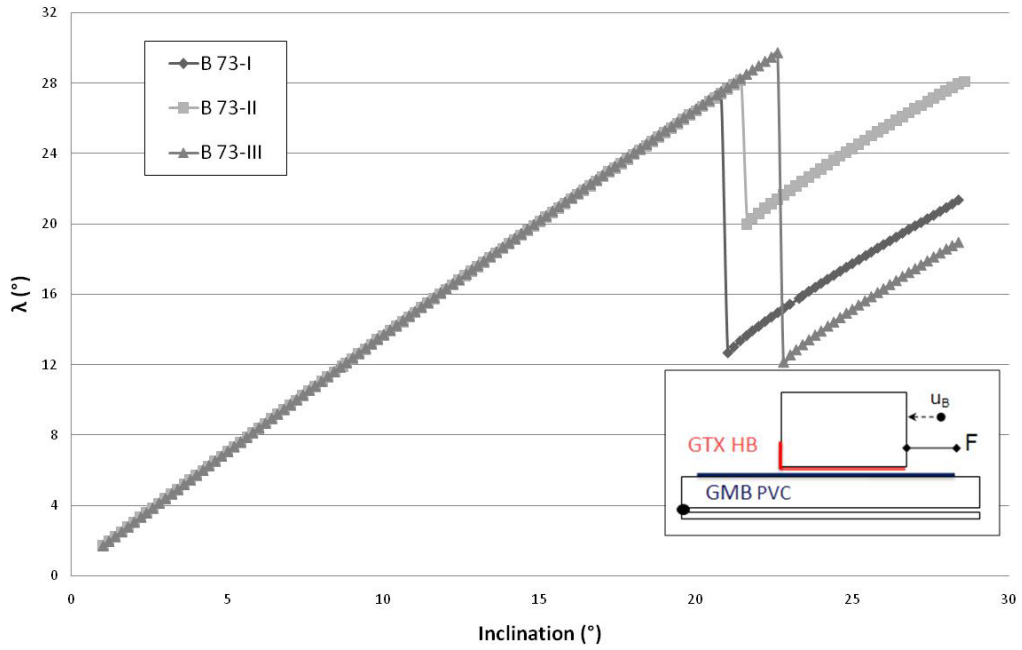


**Figure II.12 – Graphic *Lambda vs. Inclination***

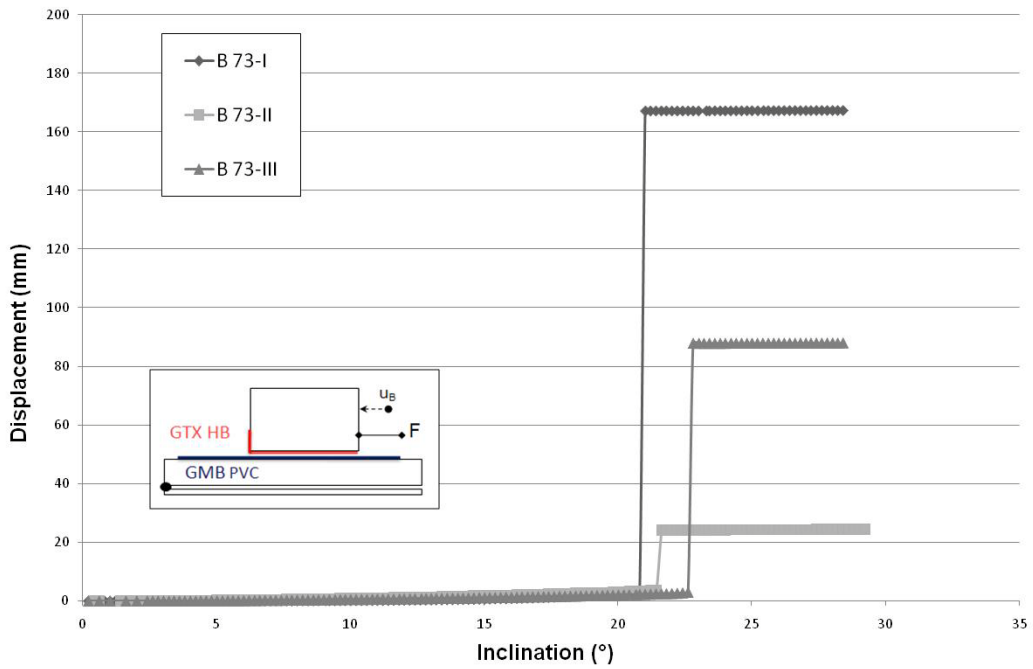


**Figure II.13 – Graphic *Displacement vs. Inclination***

## Series B-74

Weight of soil: 484 kg

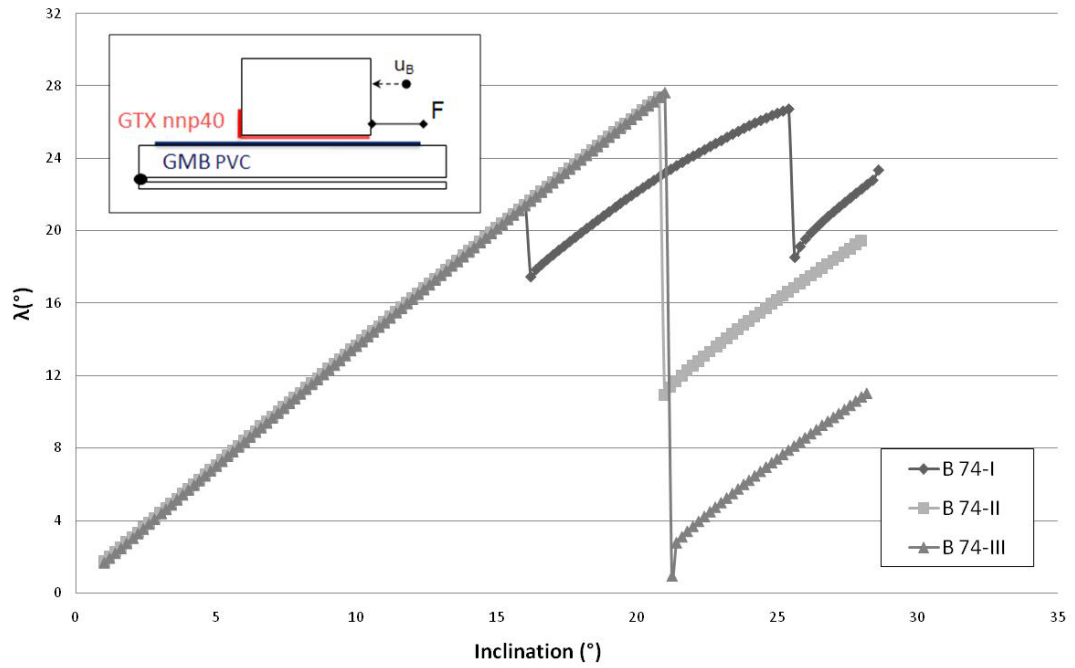


Figure II.14 – Graphic *Lambda vs. Inclination*

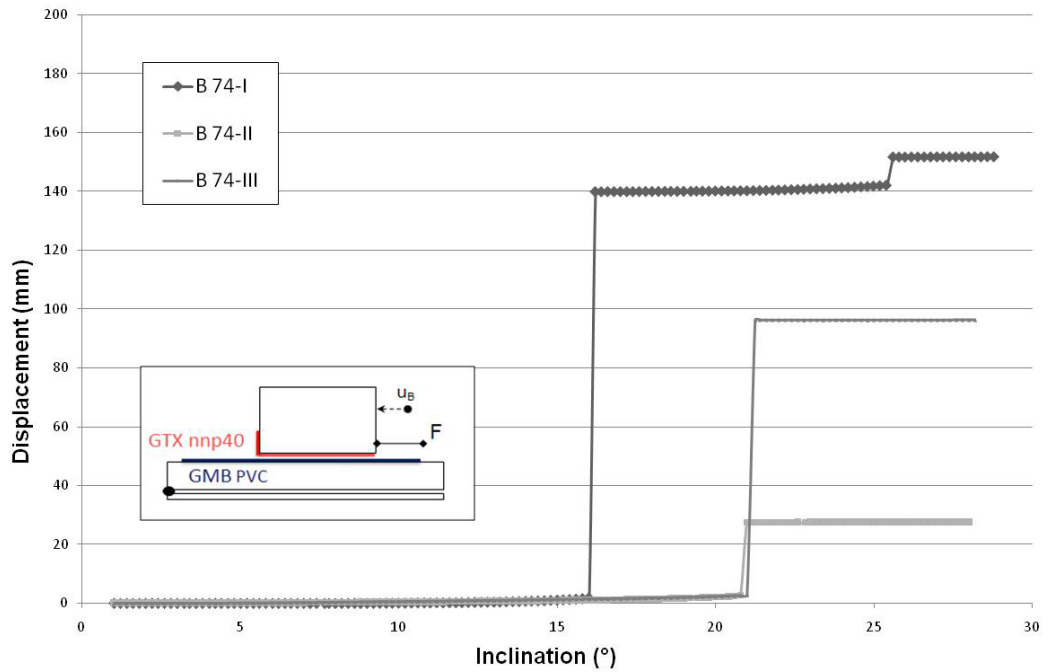
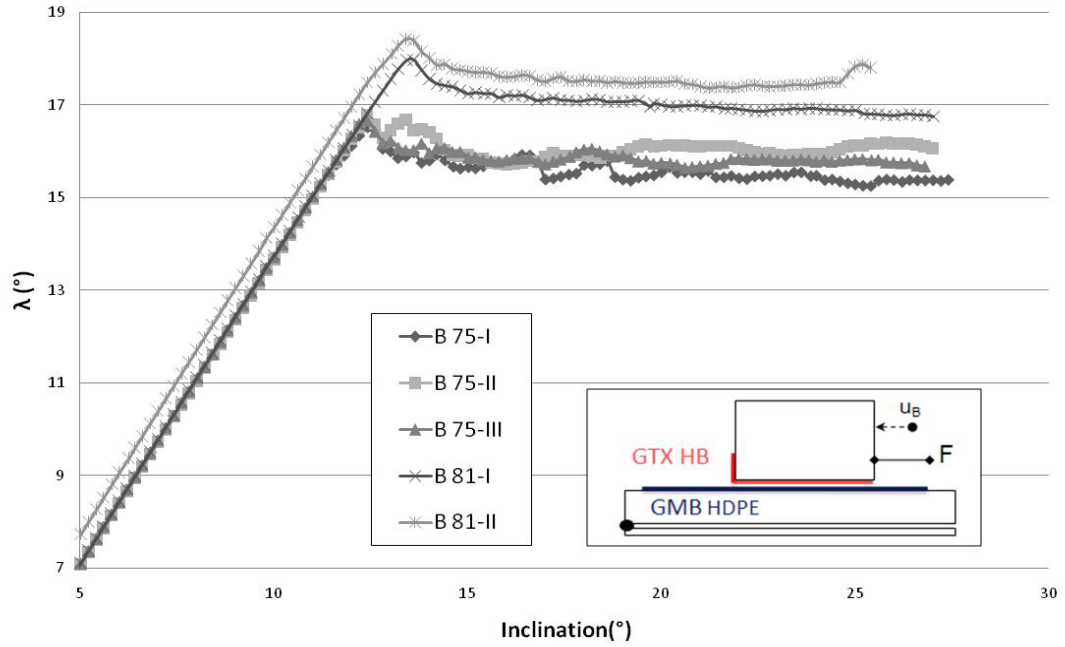


Figure II.15 – Graphic *Displacement vs. Inclination*

## Series B-75 & 81

**Weight of soil:** 482 kg (B-75), 476 kg (B-81)



**Figure II.16 – Graphic *Lambda vs. Inclination***

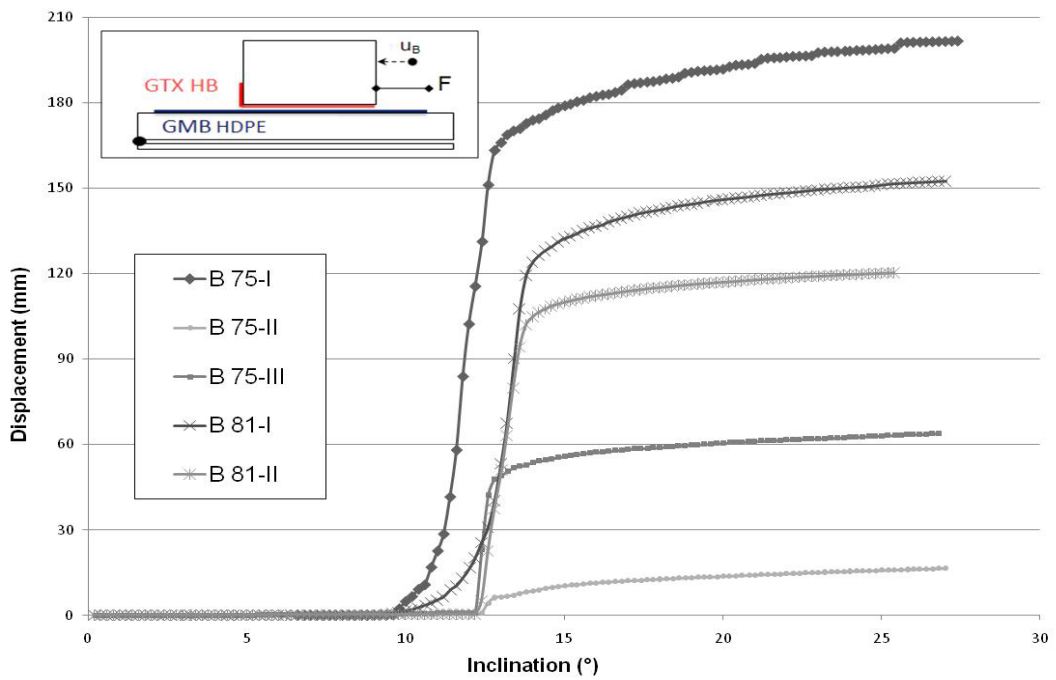


**Figure II.17 – Graphic *Displacement vs. Inclination***

## Series B-80

**Weight of soil: 480 kg**

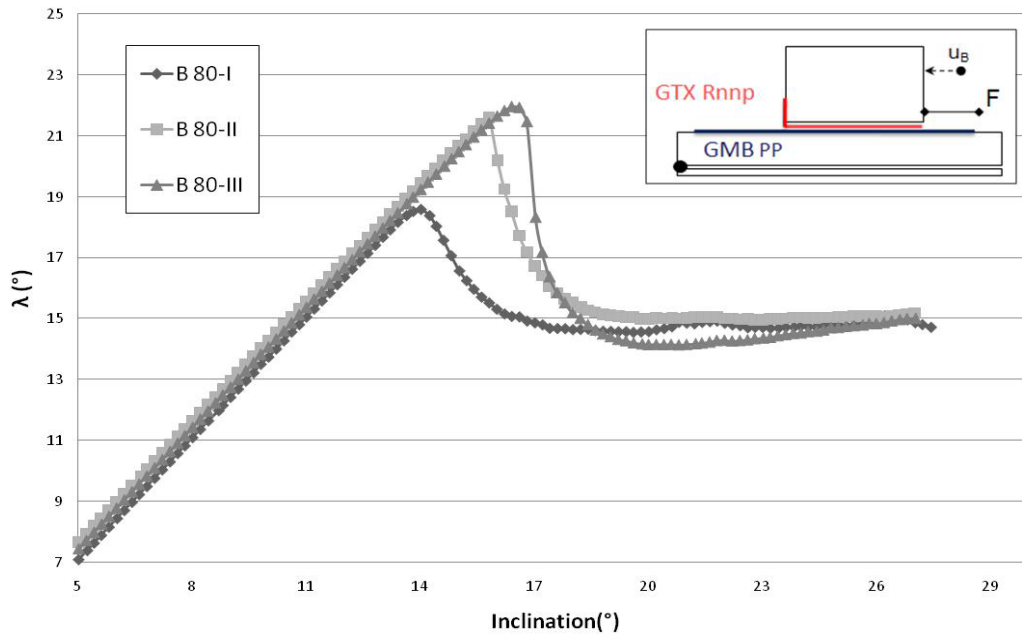


**Figure II.18 – Graphic  $\Lambda$  vs. Inclination**

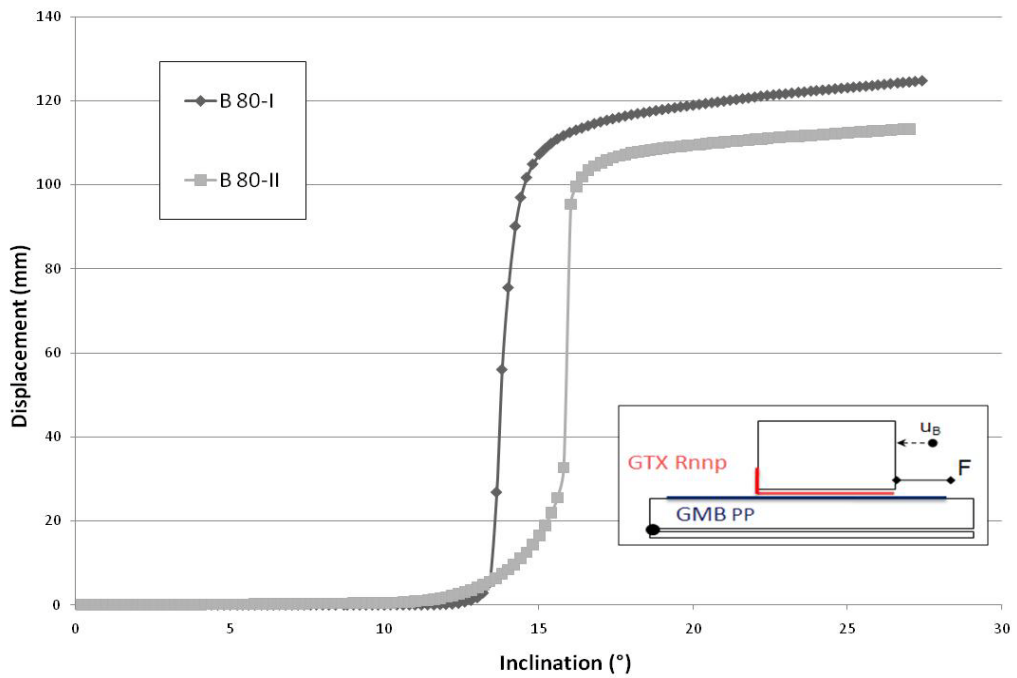


**Figure II.19 – Graphic Displacement vs. Inclination**

## Series B-82

**Weight of soil: 476 kg**

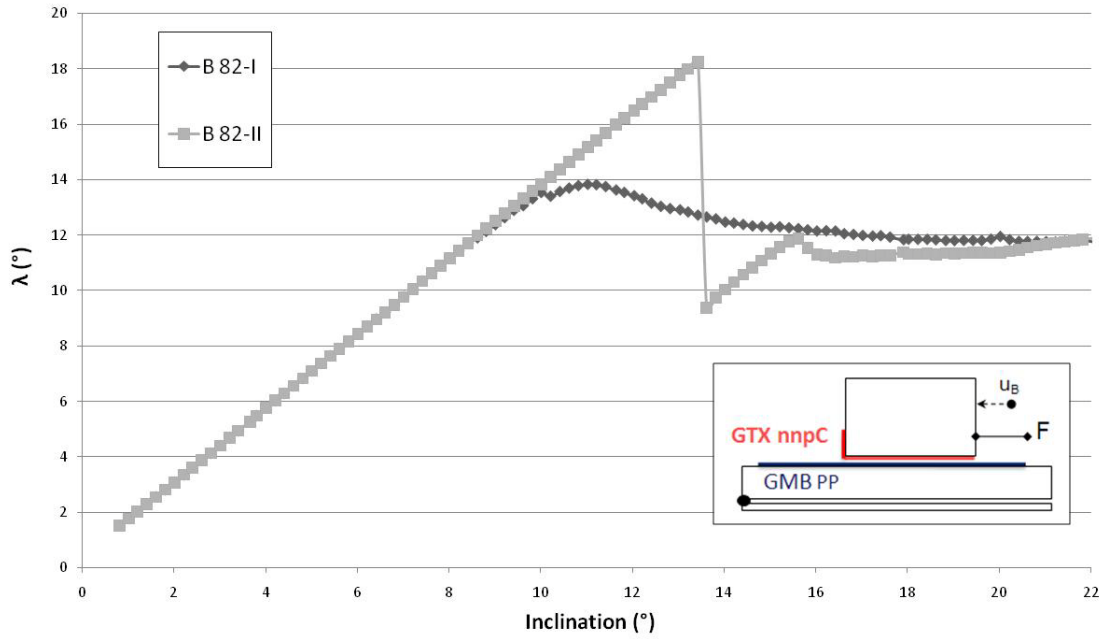


**Figure II.20 – Graphic *Lambda vs. Inclination***

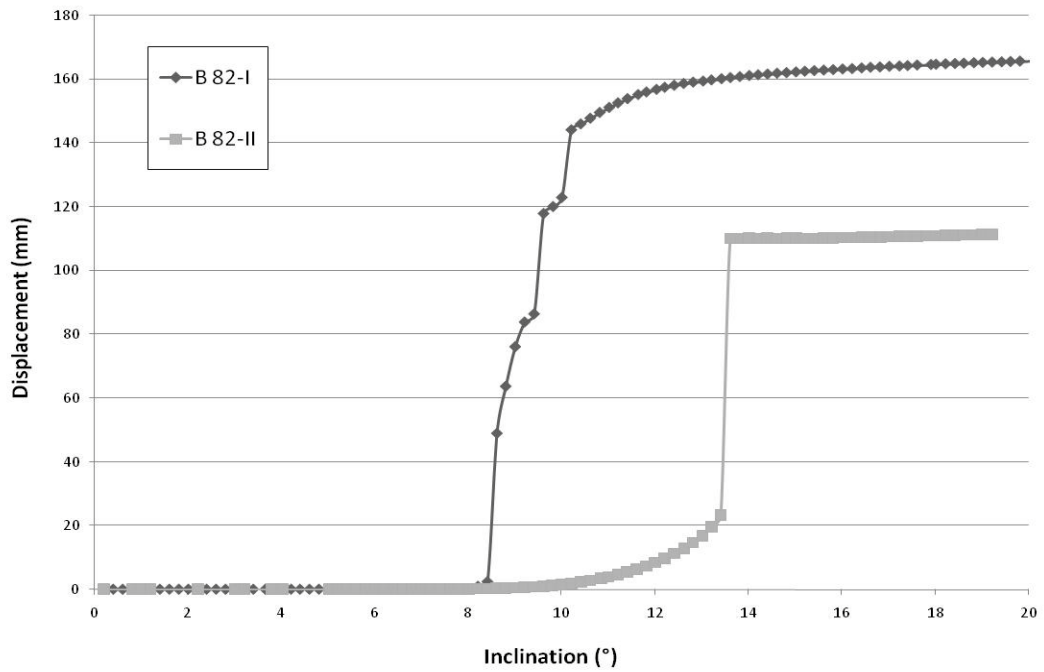


**Figure II.21 – Graphic *Displacement vs. Inclination***

## **ANNEX A**

# Geomembrane PVC

## product

Description: Homogeneous grey/grey-bluish flexible polyvinyl chloride (PVC-P) geomembrane.

To ensure impermeability in:

- Agricultural storage vessels
- Industrial storage vessels
- Lagoon ponds
- Liquid manure pits
- Canals
- Barrages etc.

## characteristics

- Not stabilised with regard to UV radiation, as it is not designed to be permanently exposed to the sun.
- Made solely from virgin resins, without any recycled constituents, thereby ensuring excellent consistency of characteristics and optimum durability.
- Highly impermeable even if permanently deformed.
- Can be successfully used on uneven and deformed substrates
- Highly puncture resistant.
- Root resistant to DIN 4062 part 1.
- Resists swelling, rotting and ageing.
- Not bitumen, oil or tar resistant.
- Not compatible with polystyrene- or polyurethane-based insulants
- Highly weldable using hot air or a heated wedge.

# Alkorplan<sup>®</sup> geomembrane

Type : 35053

hydraulic engineering and environmental protection structures



## options

- Composite geomembrane, thermally combined with a PES fabric of between 150 and 500 g/m<sup>2</sup>
- Geomembrane reinforced with a PES grid.

## storage

Must be stored away from heat and moisture in a dry place, with the rolls lying horizontally and parallel to one another and kept in their original packaging; the storage of rolls in criss-cross layers is prohibited. The storage area must not comprise anything that could damage the geomembrane.

## installation

When installing and welding the geomembrane, please consult the specific instructions in force at the time.

### WELDING

- Prefabricated lengths or sheets are assembled using hot air or heated wedge welding.
  - Weldability and the quality of welds produced on site may be influenced by:
    - atmospheric conditions, e.g. temperature, air humidity
    - the surface condition of the geomembrane, i.e. the cleanliness or the degree of dryness of its surface.
- Welding parameters, e.g. temperature, speed, pressure, preliminary cleaning, must therefore be adapted accordingly.
- High frequency welding may be used for prefabrication purposes in the workshop.

## installation (cont.)

### INSTALLATION

- If the geomembrane is to be installed on top of a rough substrate, a geotextile membrane affording protection from puncturing or a composite protective product (a draining protective system) must be installed first.
- If a layer of gritty sand, gravel or specially selected hard core is to be laid on top of the geomembrane, a geotextile shall, as a rule, be installed.
- If concrete is to be laid on top of the geomembrane, a homogeneous PVC Alkorplan® 35020 protective sheet shall preferably be installed, or failing this, a geotextile.
- The geomembrane may be used on top of a bituminous substrate provided that a suitable geotextile is installed first (e.g. PP or PES fabric of at least 250 g/m<sup>2</sup>).

### FOR FURTHER INFORMATION SEE :

- Specification CCT10 approved by VERITAS: Making ponds, tanks, canals or similar structures impermeable.
- Specification CCT13 approved by VERITAS: Making concrete storage vessels impermeable.

From Design - C2133EX0501

## technical data

Physical characteristics*	Standards	Units	Nominal values (thickness) > 1 mm
Density	ISO 1183-87 DIN 53479 ASTM D 792	g/cm <sup>3</sup>	1.24 ± 0.02
Breaking strength	ISO R 527 NFT 54102	N/mm <sup>2</sup>	≥ 17 L ≥ 17 T
Elongation at break	DIN 53455 ASTM D 882	%	≥ 300 L ≥ 300 T
Tear resistance	NFT 54108 DIN 53363	N/mm	≥ 85 L ≥ 85 T
Static puncturing (resistance)	NFT 84507	N	thickness 1.0 mm : 280 thickness 1.5 mm : 405
Static puncturing (displacement)		mm	thickness 1.0 mm : 25 thickness 1.5 mm : 25
Hardness	ISO 868-85 NFT 54109 DIN 53505	Shore A 10 sec.	79 ± 2
Cold resistance	NFT 54110 DIN 53372	°C	min -20 no cracking
Dimensional stability 6 h/80°C	NFT 54105 DIN 53377	%	≤  1.8
Water permeability	CEMAGREF	m/s	≤ 10 <sup>-14</sup>
Mullen burst test on a diameter of 50 mm	CEMAGREF	kPa	1.0 mm ≥ 600 1.2 mm ≥ 700
Puncturing on quartzite 20/40	CEMAGREF	kPa	1.0 mm ≥ 900 1.0 mm ≥ 1400

\*routinely inspected during production to the DIN Standard.

The results mentioned in the red text are typical mean values based on a representative number of individual results and may not be considered as specifications. We do not assume responsibility for the use of our products, and for the use of non-authorized resellers, legal regulations or local rules.

## packaging

Standard packaging: Supplied in cored rolls on pallets.

GEOMEMBRANE			PALLET				
thickness	width	length	rolls	width	length	height	weight
1.00 mm	2.05 m	50 m	8	1000 mm	2100 mm	700 mm	1060 kg
1.00 mm	2.05 m	200 m	2	1000 mm	2100 mm	700 mm	1040 kg
1.20 mm	2.05 m	50 m	6	1000 mm	2100 mm	750 mm	950 kg
1.20 mm	2.05 m	150 m	2	1000 mm	2100 mm	680 mm	940 kg
1.50 mm	2.05 m	50 m	6	1000 mm	2100 mm	800 mm	1180 kg
2.00 mm	2.05 m	100 m	2	1000 mm	2100 mm	760 mm	1040 kg

Other thicknesses and lengths available on request.

**AlkorDraka**  
geomembranes



a Passion for Progress®

# Geomembrane EPDM

## Technical Information Sheet

### RubberCover™ EPDM membrane

#### 1. Description

The Firestone RubberCover™ EPDM membrane is a 100% cured single-ply roofing membrane made of a synthetic rubber Ethylene-Propylene-Diene Terpolymer.

#### 2. Preparation

Substrates need to be clean, smooth, dry and free of sharp edges, loose or foreign materials, oil, grease and other materials that may damage the membrane. All surface voids greater than 5 mm wide shall be properly filled with an acceptable fill material.

#### 3. Application

Allow the membrane to relax for approximately 30 minutes before adhering it to the substrate. Install the RubberCover™ EPDM membrane in accordance with the installation instructions and details.

#### 4. Coverage

The dimensions of the membrane are calculated to cover the substrate and possible upstands. Provide an additional length (150 mm) at upstands for easy manipulation.

#### 5. Characteristics

Physical	■	Elastomeric membrane with a good combination of high elasticity and tensile strength.		
	■	Excellent resistance to U.V. and ozone.		
	■	Retains its flexibility at low temperature (-45°C).		
	■	Resists to temperature shocks up to 250°C.		
	■	Excellent resistance to alkali rains.		
	■	Less resistant to oil products. Contact with mineral and vegetable oils, petroleum based products, hot bitumen and grease must be avoided.		
Technical	<b>Property</b>	<b>Test Method</b>	<b>Declared value</b>	
	■ Thickness	EN 1849-2	1.0 mm	
	■ Watertightness	EN 1928 (B)	Pass	
	■ Tensile strength (L/T)	EN 12311-2 (B)	≥ 6 N/mm <sup>2</sup>	
	■ Elongation (L/T)	EN 12311-2 (B)	≥ 300 %	
	■ Resistance to impact - hard substrate	EN 12691 (A)	≥ 200 mm	
	■ Resistance to static load - hard substrate	EN 12730 (B)	≥ 25 kg	
	■ Tear resistance (L/T)	EN 12310-2	≥ 30 N	
	■ Dimensional stability	EN 1107-2	≤ 0.5 %	
	■ Foldability at low temperature	EN 495-5	≤ - 45°C	
■ UV exposure	EN 1297	Pass		

Note: As European standards continue to develop, please contact Firestone Technical Services or check Firestone RubberCover™ Website for latest updates on physical properties.

#### 6. Packaging / Storage / Shelf Life

Thickness (mm)	Width (m)	Length (m)	Weight (kg/m <sup>2</sup> )
1.0	3.05 - 4.57 - 6.10	7.62	1.17

Note: Special sizes are available upon request.

**Storage:** Store away from sources of punctures and physical damage. Store away from ignition sources and open flame.

**Shelf Life:** Unlimited.



Rubbercover TIS - Last updated 08-04-09

# Geomembrane HDPE



## Geosynthetic barrier PE - HD

MATERIAL PROPERTIES			
Property	Unit	Test method	Value
Density	g/cm <sup>3</sup>	ISO 1183-87 ASTM D 1505	0.950 +/- 0.01
Melt flow range 190/2,16	g/10min	DIN ISO 1133 ASTM D 1238	0.05 - 0.30
Carbon black content (TGA)	%	ASTM D 1603	2 - 3
Carbon black dispersion	-	ASTM D 5596	A1 - A2

DURABILITY			
Property	Unit	Test method	Value
Oxidative induction time (OIT)	min	ASTM D 3895	> 100
Oxidative induction time (OIT)	-	DIN EN 14575	fulfilled
Stress crack resistance	h	DIN EN 14576	> 200
Stress crack resistance	h	ASTM D 1693	> 2000
Stress crack resistance	h	ASTM D 5397	> 300
Weathering resistance	-	DIN EN 12224	fulfilled
Root resistance	-	DIN EN 14416	fulfilled
Microbiological resistance	-	DIN EN 12225	fulfilled

FUNCTIONAL PROPERTIES			
Property	Unit	Test method	Value
Foldability at low temperatures	°C	DIN EN 495-5	< -40
Water absorption after 7 days	%	DIN ISO 175	< 0.1
Dimensional stability	%	DIN 53377	+/- 1

wepelen PE-HD contains approx 97,5% of high quality polymers and 2,5% of carbon black, antioxidants and heat stabilizers. Certifications such as CE according to EN 13361, EN 13362, EN 13491, EN 13492, EN 13493 und EN 13967; DiBT and ASQUAL made by independent test institutes confirm the quality and versatile application possibilities of our geomembranes. Our films have a 10years warranty and are suitable for worldwide application even in climatically demanding regions.

MECHANICAL PROPERTIES									
Property	Unit	Test method	Value						
Thickness	mm		0,50	0,75	1,00	1,50	2,00	2,50	
Tolerance of thickness	%	DIN 53370	+/- 5						
Tensile strength at yield	Mpa	DIN EN ISO 527 ASTM D 638	> 16	> 16	> 16	> 17	> 17	> 17	
Elongation at yield	%		> 8	> 9	> 9	> 10	> 10	> 10	
Tensile strength at break	Mpa		> 27	> 27	> 27	> 29	> 29	> 29	
Elongation at break	%		> 700	> 700	> 750	> 750	> 750	> 750	
Tear resistance	N/mm	DIN 53515 ASTM D 1004	> 120	> 125	> 130	> 130	> 130	> 130	
Puncture resistance	N	ASTM D 4833	-	> 240	> 320	> 480	> 640	> 800	
Bursting pressure	%	DIN 61551						> 15	
Static puncture	KN	DIN EN ISO 12236						5,00	

**REMARKS**  
This information is no warranty. The company RKW-AG does not take over any liability for the use of this information.

**RKW-AG**  
Rheinische Kunststoffwerke  
Business Unit WERRA  
Industriestrasse 2 - 6  
36269 Philipsthal  
Germany  
RKWDatasheet/0001



Phone +49 6620 78 0  
Fax +49 6620 73 73  
Mail [info@rkw-ag.com](mailto:info@rkw-ag.com)  
Web [www.wepelen.com](http://www.wepelen.com)  
[www.rkw-ag.com](http://www.rkw-ag.com)

01.02.2008

# Geomembrane PP



## Geosynthetic barrier FPP

MATERIAL PROPERTIES			
Property	Unit	Test method	Value
Density	g/cm <sup>3</sup>	ISO 1183-87 ASTM D 1505	0.900 +/-0.01
Melt flow range 190/2,16	g/10min	DIN ISO 1133 ASTM D 1238	0.15 - 1.0
Carbon black content (TGA)	%	ASTM D 1603	2.0 - 3.0
Carbon black dispersion		ASTM D 5596	A1 - A2

DURABILITY			
Property	Unit	Test method	Value
Oxidative induction time (OIT)	min	ASTM D 3895	> 100
Stress crack resistance	h	DIN EN 14576	fulfilled
Stress crack resistance	h	ASTM D 1693	> 2000
Stress crack resistance	h	ASTM D 5397	> 300
Weathering resistance	-	DIN EN 12224	fulfilled
Root resistance	-	DIN EN 14416	fulfilled
Microbiological resistance	-	DIN EN 12225	fulfilled

FUNCTIONAL PROPERTIES			
Property	Unit	Test method	Value
Foldability at low temperatures	°C	DIN EN 495-5	< -40
Water absorption after 7 days	%	DIN ISO 175	< 0.20
Dimensional stability	%	DIN 53377	+/- 2

MECHANICAL PROPERTIES								
Property	Unit	Test method	Value					
Thickness	mm		0,50	0,75	1,00	1,50	2,00	
Tolerance of thickness	%	DIN 53370	+/- 5					
Tensile strength at break	Mpa	DIN EN ISO 527	> 18	> 18	> 18	> 18	> 17	
Elongation at break	%	ASTM D 638	> 750	> 750	> 750	> 750	> 800	
Tear resistance	N/mm	DIN 53515 ASTM D 1004	> 45	> 45	> 45	> 45	> 45	
Puncture resistance	N	FTMS 101C	> 120	> 150	> 170	> 210	> 300	
Resistance to static loading		DIN EN 12730	fulfilled					
Bursting pressure	KN	DIN 61551	> 200					
Static puncture	KN	DIN EN ISO 12236	1,00					

wepelen FPP contains approx 97,5% of high quality polymers and 2,5% of carbon black, antioxidants and heat stabilizers. Certifications such as CE according to EN 13361, EN 13362, EN 13491, EN 13492, EN 13493 und EN 13967; and ASQUAL made by independent test institutes confirm the quality and versatile application possibilities of our geomembranes. Our films have a 10years warranty and are suitable for worldwide application even in climatically demanding regions.

### REMARKS

This information is no warranty. The company RKW-AG does not take over any liability for the use of this information.

**RKW-AG**  
Rheinische Kunststoffwerke  
Business Unit WERRA  
Industriestrasse 2 - 6  
36269 Philippsthal



Phone +49 6620 78 0  
Fax +49 6620 73 73  
Mail [info@rkw-ag.com](mailto:info@rkw-ag.com)  
Web [www.wepelen.com](http://www.wepelen.com)  
[www.rkw-ag.com](http://www.rkw-ag.com)

RKW-AG sheet/0001

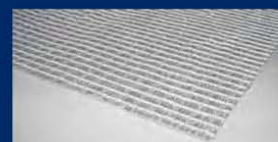
01.02.2008

# Geotextile Rnnp



## Rock PEC - Geocomposites Technical Data

TenCate Polyfelt Rock PEC biaxial geocomposites are engineered materials suitable for subgrade stabilisation and base reinforcement applications. They are composed of high modulus polyester fibres, attached to a continuous filament nonwoven geotextile backing.



TenCate Polyfelt Rock PEC

Properties (Standard)	Unit	PEC 35/35	PEC 55/50	PEC 75/75	PEC 95/95
<b>Mechanical Properties</b>					
Tensile strength [EN ISO 10319]	MD	37	58	79	100
	min	35	55	75	95
	CD	37	53	79	100
	min	35	50	75	95
Elongation at nominal strength [EN ISO 10319]	MD	10	10	10	10
	CD	10	10	10	10
Tensile strength at 2% 3% 5% [EN ISO 10319]	MD & CD	7.5	11.5	16	20
	MD & CD	10	16	22	27
	MD & CD	17	22	37	46
	MD & CD				
<b>Hydraulic Properties</b>					
Water permeability normal to the plane [EN ISO 11058] - Δh = 50 mm	l/m <sup>2</sup> s (mm/s)	55	55	55	55
Water flow capacity in the plane [EN ISO 12958]	20 kPa 10 <sup>-7</sup> m <sup>2</sup> /s	20	20	20	20
Characteristic opening size O <sub>90</sub> [EN ISO 12956]	μm	95	95	95	95
<b>Forms of Supply</b>					
Roll width	m	5.3	5.3	5.3	5.3
Roll length	m	100	100	100	100
Roll weight	kg	201	222	259	296

MD = machine direction / CD = cross direction min: These values are given within the 95% confidence level. Other forms of supply as well as grades, adjusted to the requirements of the project, are available on request.

For information concerning long term design strength, friction behaviour or other product properties please contact Ten Cate Geosynthetics.

The values given are average values obtained in our laboratories and in accredited testing institutes. The information given in this datasheet is to the best of our knowledge true and correct. However new research results and practical experience can make revisions necessary. The right is reserved to make changes without notice at any time. No guarantee or liability can be drawn from the information mentioned herein.

### TENCATE GEOSYNTHETICS AUSTRIA GMBH

Schachermayerstrasse 18 Tel. +43 732 6983 0, Fax +43 732 6983 5353  
A 4021 Linz, Austria service.at@tencate.com, www.tencate.com

#### BelLux

Tel. +31 546 544 911

Tel. +420 2 2425 1843

Tel. +33 1 34 23 53 83

Tel. +49 6074 3751 50

Tel. +39 0382 34 58 11

Tel. +44 2920 562 569

Tel. +48 12 268 8375

Tel. +31 546 544 911

Tel. +420 2 2425 1843

Tel. +33 1 34 23 53 83

Tel. +49 6074 3751 50

Tel. +39 0382 34 58 11

Tel. +44 2920 562 569

Tel. +48 12 268 8375

Tel. +31 546 544 911

Tel. +420 2 2425 1843

Tel. +33 1 34 23 53 83

Tel. +49 6074 3751 50

Tel. +39 0382 34 58 11

Tel. +44 2920 562 569

Tel. +48 12 268 8375

Tel. +31 546 544 911

Tel. +420 2 2425 1843

Tel. +33 1 34 23 53 83

Tel. +49 6074 3751 50

Tel. +39 0382 34 58 11

Tel. +44 2920 562 569

Tel. +48 12 268 8375

Tel. +31 546 544 911

Tel. +420 2 2425 1843

Tel. +33 1 34 23 53 83

Tel. +49 6074 3751 50

Tel. +39 0382 34 58 11

Tel. +44 2920 562 569

Tel. +48 12 268 8375

Tel. +31 546 544 911

Tel. +420 2 2425 1843

Tel. +33 1 34 23 53 83

Tel. +49 6074 3751 50

Tel. +39 0382 34 58 11

Tel. +44 2920 562 569

Tel. +48 12 268 8375

Tel. +31 546 544 911

Tel. +420 2 2425 1843

Tel. +33 1 34 23 53 83

Tel. +49 6074 3751 50

Tel. +39 0382 34 58 11

Tel. +44 2920 562 569

Tel. +48 12 268 8375

service.nl@tencate.com

service.cz@tencate.com

service.fr@tencate.com

service.de@tencate.com

service.it@tencate.com

service.nme@tencate.com

service.pl@tencate.com

#### Romania

Tel. +40 21 322 06 09

Tel. +7 495 739 12 60

Tel. +45 4485 7474

Tel. +34 91 650 6491

Tel. +41 44 318 6590

Tel. +44 1952 588 066

Tel. +40 21 322 06 09

Tel. +7 495 739 12 60

Tel. +45 4485 7474

Tel. +34 91 650 6491

Tel. +41 44 318 6590

Tel. +44 1952 588 066

Tel. +40 21 322 06 09

Tel. +7 495 739 12 60

Tel. +45 4485 7474

Tel. +34 91 650 6491

Tel. +41 44 318 6590

Tel. +44 1952 588 066

Tel. +40 21 322 06 09

Tel. +7 495 739 12 60

Tel. +45 4485 7474

Tel. +34 91 650 6491

Tel. +41 44 318 6590

Tel. +44 1952 588 066

Tel. +40 21 322 06 09

Tel. +7 495 739 12 60

Tel. +45 4485 7474

Tel. +34 91 650 6491

Tel. +41 44 318 6590

Tel. +44 1952 588 066

Tel. +40 21 322 06 09

Tel. +7 495 739 12 60

Tel. +45 4485 7474

Tel. +34 91 650 6491

Tel. +41 44 318 6590

Tel. +44 1952 588 066

Tel. +40 21 322 06 09

Tel. +7 495 739 12 60

Tel. +45 4485 7474

Tel. +34 91 650 6491

Tel. +41 44 318 6590

Tel. +44 1952 588 066

Tel. +40 21 322 06 09

Tel. +7 495 739 12 60

Tel. +45 4485 7474

Tel. +34 91 650 6491

Tel. +41 44 318 6590

Tel. +44 1952 588 066

Tel. +40 21 322 06 09

Tel. +7 495 739 12 60

Tel. +45 4485 7474

Tel. +34 91 650 6491

Tel. +41 44 318 6590

Tel. +44 1952 588 066



502 172 | 04.2007

Protective & Outdoor Fabrics  
Aerospace Composites  
Armour Composites

Geosynthetics  
Industrial Fabrics  
Grass

**TENCATE**  
materials that make a difference

## Rock PEC

### Fiche Technique

Les géocomposites bi-directionnels TenCate Bidim Rock PEC sont conçus pour des applications de renforcement de sol. Ce sont des géotextiles haute résistance associant un non-tissé de filaments continus en polypropylène et un réseau de câbles de renfort en polyester.



TenCate Bidim Rock PEC

Caractéristiques (Norme)	Symbole	Unité	PEC 55/50	PEC 35/35	PEC 75/75	PEC 95/95
<b>Géotextile certifié Asqual</b>						
<b>Valeurs certifiées selon la fonction**</b>	Filtration		✓			
	Séparation		✓			
	Drainage / Filtration		✓			
	Renforcement		✓			
<b>Caractéristiques mécaniques</b>						
Résistance à la traction	SP*	T <sub>max</sub> kN/m	58	37	79	100
(NF EN ISO 10319)	ST*	T <sub>max</sub> kN/m	52,8	37	79	100
Résistance à 5% de déformation	SP*	T <sub>5%</sub> kN/m	22,1	17	37	46
(NF EN ISO 10319)	ST*	T <sub>5%</sub> kN/m	22,1	17	37	46
Déformation à l'effort de traction maximale	SP*	ε <sub>max</sub> %	11,5	11,5	11,5	11,5
	ST*	ε <sub>max</sub> %	11	11	11	11
Perforation dynamique (NF EN 918 ****)		P <sub>d</sub> mm	18	18	18	18
Résistance au poinçonnement (NFC 38019)		P <sub>s</sub> kN	1,3	1,1	1,3	1,3
Rés. au poinçonnement statique CBR (NF EN ISO 12236)		P <sub>CBR</sub> kN	4,25	2,4	5,75	6,6
<b>Caractéristiques hydrauliques</b>						
Perméabilité normale au plan (NF EN ISO 11058) (Δh = 50 mm)		V <sub>H50</sub> m/s	0,055	0,055	0,055	0,055
Ouverture de filtration (NF EN ISO 12956)		O <sub>90,w</sub> μm	95	95	95	95
Capacité de débit dans leur plan (NF EN ISO 12958)	20 kPa	Q / I 10 <sup>7</sup> m <sup>2</sup> /s	20	20	20	20
	100 kPa	Q / I 10 <sup>7</sup> m <sup>2</sup> /s	5	5	5	5
Fluage en compression	à 2 min	%	38			
	à 1 h	%	41			
	à 1008 h	%	45			
<b>Caractéristiques descriptives</b>						
Masse surfacique (NF EN ISO 9864)		μ <sub>GT</sub> g/m <sup>2</sup>	390	340	440	540
Epaisseur sous 2 kPa (NF EN ISO 9863-1)		t <sub>GT</sub> mm	2,5	2,5	2,6	3,0
<b>Caractéristiques spécifiques à la fonction renforcement</b>						
Résistance à la traction à 2%	SP*	T <sub>2%</sub> kN/m	11,5	7,5	16	20
Résistance à la traction à 3%	SP*	T <sub>3%</sub> kN/m	16	10	22	27
<b>Conditionnement ***</b>						
Largeur x Longueur		m	5,3 x 100	5,3 x 100	5,3 x 100	5,3 x 100

\* SP = Sens Production, ST = Sens Travers \*\* Voir tolérances certifiées sur le certificat Asqual \*\*\* Voir conditions générales de ventes TenCate Geosynthetics France S.A.S. \*\*\*\* - NF EN ISO 13433 Attention ! Les valeurs ci-dessus sont celles en vigueur à la date d'édition de la présente fiche et sont susceptibles d'être modifiées à tout moment. Vérifiez que vous disposez bien de la dernière édition.

TENCATE GEOSYNTHETICS FRANCE S.A.S.  
9, rue Marcel Paul B.P. 40080 95673 Bezons, France  
Tel. +33 (0)1 34 23 53 63, Fax +33 (0)1 34 23 53 98  
service.fr@tencate.com, www.tencate.com/geosynthetics



Certification AF AQ n°1997/8666a pour la conception, la fabrication et la vente de géotextiles et produits apparentés

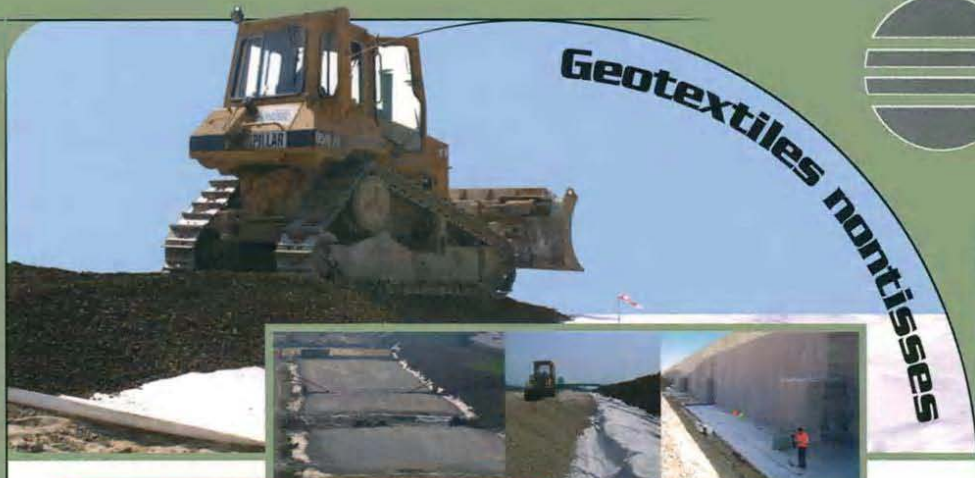
961 142 | 09.2007

Protective & Outdoor Fabrics  
Aerospace Composites  
Armour Composites

Geosynthetics  
Industrial Fabrics  
Grass

**TENCATE**  
materials that make a difference

# Geotextile nnpC



## GEODREN PP/S/T

GEODREN PPST est un geotextile nontissé en polypropylène à haute ténacité à fibre courte de couleur blanche, fabriqué par aiguilletage mécanique et calandrage. Aucun procédé ou additif chimique n'est utilisé pendant la fabrication.



Le procès de production se déroule conformément au système de contrôle ISO 9001/2000.



GEODREN PPST a obtenu le marquage de sécurité CE pour les applications et fonctions suivantes:

<b>UNI EN 13249:2001</b>	Routes	<b>UNI EN 13254:2002</b>	Bassins et barrages
<b>UNI EN 13250:2002</b>	Chemin de fer	<b>UNI EN 13255:2002</b>	Canaux
<b>UNI EN 13251:2002</b>	Fondations	<b>UNI EN 13256:2002</b>	Tunnels et ouvrages souterrains
<b>UNI EN 13252:2002</b>	Systèmes de drainage	<b>UNI EN 13257:2002</b>	Déchets solides
<b>UNI EN 13253:2002</b>	Contrôle de l'érosion	<b>UNI EN 13265:2002</b>	Déchets liquides

FONCTIONS	100	120	130	170	200P	230	280	290	300P	340	350	400P	500P	600P	700P	800P	1000P	1200P	
Filtration	[Bar chart showing filtration performance across all models]																		
Séparation	[Bar chart showing separation performance across all models]																		
Protection	[Bar chart showing protection performance across all models]																		
Drainage	[Bar chart showing drainage performance across all models]																		

Les informations ci-dessus sont totalement indicatives. Pour plus de détails sur l'utilisation des géotextiles adaptés aux types d'ouvrage d'ingénierie civile concerné adressez-Vous aux responsables techniques.

GEODREN PPST est disponible en bobines de laize 200 – 300 – 600 cm et de longueur variable. Dans le tableau ci-dessous on a mentionné les dimensions, les diamètres et les surfaces des différents grammages. Pour tout renseignement complémentaire, notre service commercial est à Votre disposition.

	100	120	130	170	200P	230	280	290	300P	340	350	400P	500P	600P	700P	800P	1000P	1200P
Longueur (m)	170	150	150	120	100	100	90	90	80	80	75	65	50	50	50	40	30	25
Hauteur (cm)	600	600	600	600	600	600	600	600	600	600	600	600	600	600	600	600	450	450
Surface (m <sup>2</sup> )	1020	900	900	720	600	600	540	540	480	480	450	390	300	300	300	240	135	113
Diamètre (cm)	40	40	40	40	40	40	40	40	40	40	40	40	40	45	48	45	45	48
Poids du roul. (Kg)	102	108	117	123	120	138	152	157	144	164	158	156	150	180	210	192	135	136



Contactez novintiss tél. 05.46.51.02.01 fax 05.46.51.18.98 info@novintiss.com

## FICHE TECHNIQUE

Dernière version: 01.01.2004

PROPRIETES		UNITES		VALEURS																		
<b>Masse surfacique</b> (EN ISO 965)		g/m <sup>2</sup>	Pa	100	120	130	170	200P	230	280	290	300P	340	350	400P	500P	600P	700P	800P	1000P	1200P	
<b>Epaisseur</b> (EN ISO 964-1)		a 2kPa	mm	d	0,9	0,95	1,00	1,23	2,40	1,40	1,60	2,00	3,00	2,10	2,50	3,50	4,00	4,60	5,20	5,80	7,00	8,20
CARACTERISTIQUES MECANIQUES																						
<b>Résistance à la traction</b> (EN ISO 10319)	SP	kN/m	T <sub>max</sub>	6,5	8	10	12	13	16	20	20	20	25	25	26	32	37	42	46	54	62	
	ST	kN/m	T <sub>max</sub>	6,5	8	10	12	13	16	20	20	20	25	25	26	32	37	43	50	62	72	
<b>Allongement à la rupture</b> (EN ISO 10319)	SP	%	ε <sub>s</sub>	70	80	80	70	110	80	70	80	110	70	70	110	110	110	115	110	110	110	
	ST	%	ε <sub>s</sub>	90	80	80	80	110	80	80	90	110	80	80	110	110	110	115	110	110	110	
<b>Résistance au poinçonnement statique CBR test</b> (EN ISO 12236)		kN	F <sub>P</sub>	1,1	1,3	1,5	2,0	2,5	3,0	3,3	3,5	4,1	4,2	4,6	5,2	6,5	7,6	8,8	10	11	12,5	
<b>Résistance au poinçonnement statique pyramidal</b> (NF G 39019)		kN	F <sub>P</sub>	0,7	0,7	0,8	0,9	1,5	1,3	1,5	1,7	2,0	1,8	2,1	2,5	3,0	3,5	4,0	4,5	5,0	6,0	
<b>Résistance au poinçonnement dynamique Cone Drop Test</b> (EN 918)		mm	D <sub>C</sub>	24	23	22	17	16	18	12	8	10	10	7	8	4	3	2	0	0	0	
CARACTERISTIQUES HYDRAULIQUES																						
<b>Index de vitesse V<sub>HS0</sub></b> (EN ISO 11068)		mmV/s m/s	v-index	73	70	66	47	57	62	51	28	51	45	26	47	42	37	33	25	20	17	
<b>Débit perpendiculaire au plan</b>		l/m <sup>2</sup> ·s	q <sub>n</sub>	0,073	0,070	0,066	0,047	0,057	0,062	0,057	0,028	0,051	0,045	0,026	0,047	0,042	0,037	0,033	0,025	0,020	0,017	
<b>Permittivité</b>		s-1	ψ	1,5	1,4	1,3	0,9	1,1	1,2	1,0	0,6	1,0	0,9	0,5	0,9	0,8	0,7	0,7	0,5	0,4	0,3	
<b>Coefficient de perméabilité perpendiculaire au plan</b>		10 <sup>-3</sup> m/s	k <sub>n</sub>	1,3	1,3	1,3	1,2	2,7	1,7	1,6	1,1	3,1	1,9	1,3	3,3	3,4	3,4	3,4	2,9	2,8	2,8	
<b>Capacité de débit dans le plan (MD)</b> (EN ISO 12958)		a 20kPa	m <sup>2</sup> /s	q <sub>n</sub>	1,0	1,0	1,0	1,1	8,2	4,3	4,1	5,1	8,2	4,1	5,9	8,2	9,1	9,6	1,0	2,0	4,0	6,0
<b>Ouverture de filtration caract.</b> (EN ISO 12956)		µm	Q <sub>90</sub>	70	65	60	53	70	50	49	49	64	48	47	63	<63	<63	<63	<63	<63	<63	
NOTES DE DURABILITE																						
<b>Résistance aux agents atmosphériques</b> (EN ISO 12224)				A couvrir sous 15 jours après l'exposition																		
<b>Résistance à l'oxydation</b> (EN ISO 13438)				Prévision de durabilité de minimum 25 ans pour toute application, sauf le renforcement, dans des terrains naturels avec 4<pH<9 et températures < 25°C																		

Les valeurs mentionnés ci-dessus correspondent à la moyenne des résultats obtenus dans nos laboratoires et dans des laboratoires indépendants.

Pour avoir des détails supplémentaires sur les tolérances de chaque valeur, calculées avec une PRV de 95%, adressez-Vous aux responsables commerciaux.

Les tolérances sur les caractéristiques hydrauliques résultent de la comparaison parmi différents laboratoires extérieurs.

Edifloor Spa peut apporter à tout moment tout changement sans préavis



Contactez **novintiss** tél. 05.46.51.02.01 fax 05.46.51.18.98 info@novintiss.com

# Geotextile nnp40



## Gamme P Fiche Technique

La gamme Protection TenCate Bidim P se compose de géotextiles non-tissés aiguilletés de filaments continus, 100 % polypropylène. 7 produits certifiés Asqual.



TenCate Bidim P

Caractéristiques (Norme)	Symbole	Unité	P20	P30	P40	P50	P60	P70	P80	P50UV*	P100
<b>Géotextile certifié Asqual</b>											
<b>Valeurs certifiées selon la fonction**</b>											
Protection			✓	✓	✓	✓	✓	✓	✓		
Séparation			✓	✓	✓	✓	✓	✓	✓		
Drainage / Filtration			✓	✓	✓	✓	✓	✓	✓		
Renforcement				✓	✓		✓	✓	✓		
Résistance à la traction	SP*	T <sub>max</sub> kN/m	15	20	25	34	38	42	45	34	55
[NF EN ISO 10319]	ST*	T <sub>max</sub> kN/m	15	20	25	34	38	42	45	34	55
Déformation à l'effort de traction maximale	SP*	ε <sub>max</sub> %	80	80	85	85	95	95	95	85	105
[NF EN ISO 10319]	ST*	ε <sub>max</sub> %	75	75	75	75	78	78	80	75	100
Perforation dynamique	[NF EN ISO 13433]	P <sub>d</sub> mm	21	16	12	9,5	8,5	7,5	7	9,5	6
Résistance au poinçonnement	[NF EN ISO 12958]	P <sub>s</sub> kN	1,1	1,6	2,1	2,5	3,1	3,5	4	2,5	5,6
Résistance au poinçonnement statique CBR	[NF EN ISO 12236]	P <sub>CBR</sub> kN	2,35	3,5	4,3	5,4	6,2	7,2	7,8	5,4	9,6
Perméabilité normale au plan	[NF EN ISO 11058] (dh = 50 mm)	V <sub>h50</sub> m/s	0,08	0,06	0,02	0,015	0,01	0,01	0,01	0,015	0,01
Ouverture de filtration caractéristique	[NF EN ISO 12956]	O <sub>90,w</sub> μm	90	85	85	80	85	80	80	80	75
Capacité de débit dans leur plan	20 kPa [NF EN ISO 12958]	Q / l 10 <sup>2</sup> m <sup>2</sup> /s	15	26	39	55	71	90	110	75	110
	100 kPa	Q / l 10 <sup>2</sup> m <sup>2</sup> /s	4,0	6,6	11	16	23	31	41	25	41
Masse surfacique	[NF EN ISO 9864]	μ <sub>GT</sub> g/m <sup>2</sup>	205	300	400	500	600	700	800	525	1000
Épaisseur sous 2 kPa	[NF EN ISO 9863-1]	t <sub>GT</sub> mm	2,1	2,8	3,4	4,2	4,5	5,7	6	4,2	7,2
<b>Conditionnement ***</b>											
Largeur		m	6	6	6	6	6	6	6	6	5,4
Longueur		m	175	110	100	80	65	55	50	80	40
Surface		m <sup>2</sup>	1050	660	600	480	390	330	300	450	216

\* SP = Sens Production, ST = Sens Travers

\*\* Voir tolérances certifiées sur le certificat Asqual

\* Résistance aux UV (EN 12224) - Résistance résiduelle > 90 %

\*\*\* Voir conditions générales de ventes TenCate Geosynthetics France S.A.S.

Attention ! Les valeurs de certifications ci-dessus sont celles en vigueur à la date d'édition de la présente fiche et sont susceptibles d'être modifiées à tout moment. Vérifiez que vous disposez bien de la dernière édition.

TENCATE GEOSYNTHETICS FRANCE S.A.S.  
9, rue Marcel Paul B.P. 40080 95873 Bezons, France  
Tél. + 33 (0)1 34 23 53 63, Fax + 33 (0)1 34 23 53 98  
service.fr@tencate.com, www.tencate.com/geosynthetics



Certification AF AQ n°13978/0006 pour la conception, la fabrication et la vente de géotextiles et produits apparentés

9681 01 | 033 696

Protective Fabrics  
Outdoor Fabrics  
Aerospace Composites  
Armour Composites

Geosynthetics  
Industrial Fabrics  
Grass

**TENCATE**  
materials that make a difference

# Geotextile HB

DuPont™  
**Typar® SF**  
GEOTEXTILE

## Measured Properties EUROPE

Property	Standard	Unit	SF20	SF27	SF32	SF37	SF40	SF44	SF49	SF56	SF65	SF70	SF77	SF85	SF94	SF111
<b>Descriptive Properties</b>																
Area Weight	EN ISO 9864	g/m <sup>2</sup>	68	90	110	125	136	150	165	190	220	240	260	290	320	375
Thickness under 2kN/m <sup>2</sup>	EN ISO 9863-1	mm	0,35	0,39	0,43	0,45	0,47	0,48	0,49	0,57	0,59	0,65	0,65	0,73	0,74	0,83
Thickness under 200kN/m <sup>2</sup>	EN ISO 9863-1	mm	0,28	0,31	0,35	0,37	0,39	0,40	0,40	0,48	0,53	0,59	0,59	0,69	0,69	0,79
<b>Mechanical Properties</b>																
Energy Absorption	EN ISO 10319	kJ/m <sup>2</sup>	1,0	1,8	3,0	3,6	3,7	4,5	5,8	5,8	7,4	8,2	8,6	9,8	11,4	13,0
Tensile Strength	EN ISO 10319	kN/m	3,4	5,0	7,0	8,5	9,0	10,3	12,6	13,1	16,5	16,7	20,0	21,3	25,0	30,0
Elongation	EN ISO 10319	%	35	40	45	52	52	52	52	52	55	55	55	55	55	55
Strength at 5%	EN ISO 10319	kN/m	1,8	2,6	3,3	3,8	4,0	4,5	5,2	5,7	6,8	7,2	8,2	8,8	10,0	11,5
Puncture CBR*	EN ISO 12236	N	500	750	1000	1200	1250	1575	1800	1850	2350	2400	2900	3150	3500	4250
Dyn. Cone Puncture	EN 918	mm	50	45	35	33	29	27	30	22	25	23	22	16	17	14
Grab Strength	ASTM D4632	N	300	450	625	725	750	900	1050	1100	1400	1450	1680	1750	2050	2350
Tear Strength	ASTM D4533	N	160	220	290	320	370	385	335	460	440	570	450	610	570	600
<b>Hydraulic Properties</b>																
Opening Size O <sub>90Wet</sub>	EN ISO 12956	µm	225	175	140	130	120	100	90	80	80	75	75	70	70	65
Flow Rate at 10 cm WH	BS 6906-3	l/(m <sup>2</sup> ·s)	240	175	110	80	75	70	50	60	35	40	23	30	15	15
Permeability (V <sub>H50</sub> )	EN ISO 11058	10 <sup>-3</sup> m/s	180	100	70	50	50	40	25	35	18	20	12	15	5	5
Permeability at 20 kN/m <sup>2</sup>	DIN 60500-4	10 <sup>-4</sup> m/s	5,2	4,7	4,6	3,2	2,8	2,6	1,7	1,9	1,6	1,8	1,4	1,6	1,1	1,0
Permeability at 200 kN/m <sup>2</sup>	DIN 60500-4	10 <sup>-4</sup> m/s	3,2	3,1	2,9	1,8	2,0	1,8	1,2	1,4	1,2	1,3	1,0	1,2	0,8	0,7

\* Equivalent to DIN 54307 and BS 6906-4

### Durability

Predicted to be durable for a minimum of 100 years in all natural soils

Natural UV light	Good resistance up to several months in direct sunlight, but prolonged exposure, particularly in tropical sunlight, can cause strength losses. Product should be covered after 2 weeks of installation.
------------------	---

Natural occurring acids and alkali	Unaffected
------------------------------------	------------

Oxidation Resistance	prEN ISO 13438	100% retained strength
----------------------	----------------	------------------------

Chemical Resistance	EN 14030	100% retained strength
---------------------	----------	------------------------

Microbiological Resistance	EN 12225	100% retained strength
----------------------------	----------	------------------------

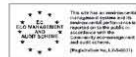
### Product Description

• Polymer	100% Polypropylene UV Stabilised
• Specific gravity	0,91
• Melting Point	165° C
• Type of fiber	continuous filament
• Fiber diameter	40 - 50 micron
• Fiber bonding	Thermal bonding

The values correspond to average results obtained in our laboratories and outside institutes and are indicative. The right is reserved to make changes at any time without notice.

## Typar® SF Packaging Data

Type	width m	length m	area m <sup>2</sup>	diameter cm	weight kg	Max Rolls per full truck 13.6 loading meters
SF20	2.25	250	563	32	44	175
	4.50	200	900	28	72	144
	5.20	400	2080	38	154	48
SF27	2.10	200	420	29	43	288
	4.50	200	900	29	92	144
	5.20	200	1040	29	107	96
SF32	2.00	200	400	30	49	210
	4.50	200	900	30	110	105
	5.20	200	1040	30	127	70
SF37	2.10	150	315	29	45	288
	4.50	150	675	29	96	144
	5.20	150	780	29	111	96
SF40	2.10	150	315	30	48	288
	4.50	150	675	30	103	144
	5.20	150	780	30	119	96
SF44	4.50	150	675	31	113	105
	5.20	150	780	31	130	70
SF49	4.50	100	450	26	86	162
	5.20	100	520	26	99	108
SF56	4.50	100	450	29	97	144
	5.20	100	520	29	112	96
SF65	4.50	100	450	30	110	144
	5.20	100	520	30	127	96
SF70	4.50	100	450	31	119	105
	5.20	100	520	31	138	70
SF77	4.50	100	450	32	128	105
	5.20	100	520	32	148	70
SF85	4.50	100	450	33	142	105
	5.20	100	520	33	164	70
SF94	4.50	100	450	35	155	105
	5.20	100	520	35	179	70
SF111	4.50	100	450	37	180	105
	5.20	100	520	37	208	70



DuPont de Nemours (Luxembourg) S.à.r.l.  
 Rue Général Patton  
 L-2984 Luxembourg  
 Tél: +352 3666 5779  
 Fax: +352 3666 5021  
 www.typargeo.com

This information corresponds to our current knowledge on the subject. It is offered solely to provide possible suggestions for your own experimentations. It is not intended, however, to substitute for any testing you may need to conduct to determine for yourself the suitability of our products for your particular purposes. This information may be subject to revision as new knowledge and experience becomes available. Since we cannot anticipate all variations in actual end-use conditions, DuPont makes no warranties and assumes no liabilities in connection with any use of this information. Nothing in this publication is to be considered as a license to operate under or a recommendation to infringe any patent right.



The miracles of science™

L-1810 - 07/2006 Copyright © 2006 DuPont. All rights reserved. The DuPont Oval Logo, DuPont™, The miracles of science™ and TYPAR® are registered trademarks or trademarks of E. I. du Pont de Nemours and Company or its affiliates.

FOLHA DE REGISTRO DO DOCUMENTO

1. CLASSIFICAÇÃO/TIPO TC	2. DATA 18 de novembro de 2009	3. REGISTRO N° CTA/ITA/TC-140/2009	4. N° DE PÁGINAS 165
5. TÍTULO E SUBTÍTULO: Friction characterization of geosynthetic interfaces through inclined plane experiment			
6. AUTOR(ES): <b>Fernanda Muzzio Almirão</b>			
7. INSTITUIÇÃO(ÕES)/ÓRGÃO(S) INTERNO(S)/DIVISÃO(ÕES): Instituto Tecnológico de Aeronáutica - ITA			
8. PALAVRAS-CHAVE SUGERIDAS PELO AUTOR: Inclined plane experiment, friction angles, geosynthetic, dynamic analysis, force analysis, lining systems			
9. PALAVRAS-CHAVE RESULTANTES DE INDEXAÇÃO: Coeficientes de atrito; Geossintéticos; Revestimento; Talude; Pesquisa experimental; Engenharia civil; Engenharia geotécnica			
10. APRESENTAÇÃO: <b>Nacional</b> <b>X Internacional</b> ITA, São José dos Campos. Curso de Graduação em Engenharia Civil-Aeronáutica. Orientadora: Profa. Dra. Delma Vidal. Co-orientador: Jean-Pierre Gourc. Publicado em 2009.			
11. RESUMO: The purpose of this research is to compare the test results found with two inclined plane apparatus. The first plane tested was developed according to ISO12957-2: 2005 and, besides the analysis prescribed by this standard, it was performed the force and combined analyses. In force analysis, it is measured the force required to hold the upper box during the inclination of the plane. The combined analysis includes both standard and force analysis. The second plane to be tested has smaller dimensions than the ones prescribed by the standard however it enables the study of the dynamic behavior of interfaces. The parameters obtained in this test are the static friction angles ( $\Phi_0$ and $\Phi_{50}$ ) and the dynamic friction angle ( $\Phi^{lim}$ ). The focus of the work is to evaluate whether both planes provide equivalent parameters to characterize the geosynthetic-geosynthetic interfaces.			
12. GRAU DE SIGILO: <b>(X) OSTENSIVO</b> ( ) RESERVADO ( ) CONFIDENCIAL ( ) SECRETO			